Synthesis of Copper-free Stable Single-Chain Nanoparticles

Author: Agustín Blázquez Martín

Supervisors: Prof. José A. Pomposo and Dr. María Ester Verde

Donostia –San Sebastián, 2023

eman ta zabal zazu

Universidad del País Vasco

Euskal Herriko Unibertsitatea

(cc)2024 AGUSTIN BLAZQUEZ MARTIN (cc by 4.0)

Contents

Resumen

Esta tesis presenta dos nuevos métodos de síntesis de nanopartículas poliméricas unimoleculares conocidas en inglés como “single-chain nanoparticles” (SCNPs). Estas partículas nanométricas blandas se forman al colapsar una cadena polimérica mediante enlaces químicos entre distintas partes de la cadena, obteniendo una morfología más colapsada. Como existe un gran número de monómeros y se pueden combinar entre ellos, con un diseño inteligente se pueden sintetizar polímeros y SCNPs con propiedades fisicoquímicas específicas. Además, gracias a su reducido tamaño y a su gran relación superficie/volumen, las SCNPs son aptas para una gran variedad de aplicaciones como sensores, catalizadores químicos o para el transporte de medicamentos. Aunque ya existen diferentes métodos de síntesis de SCNPs muchos precisan de catalizadores metálicos que terminan siendo indivisibles del producto, de modo que las nanopartículas ven mermadas sus aplicaciones por la presencia de esos metales que suelen tener efectos adversos para la salud. Por otro lado, muchos métodos actuales dan buenos resultados sólo en disolución, ya que al pasar a estado sólido las nanopartículas se agregan de forma irreversible, impidiendo su redisolución. Los nuevos métodos de síntesis de SCNPs que se presentan en esta Tesis son libres de metales y permiten sintetizar las nanopartículas a partir de diferentes polímeros, quedan libres de problemas de agregación y aptas para ser almacenadas en sólido y redisolverse. Además, también se presenta una aplicación concreta de uno de los métodos para revalorizar policloruro de vinilo (PVC), usándolo para crear SCNPs catalíticas reutilizables.

Esta tesis está estructurada de la siguiente forma:

En el capítulo 1 se introducen los distintos conceptos teóricos que se consideran necesarios para entender correctamente los resultados de los capítulos 4 a 6. Se presentan los conceptos básicos de las SCNPs, como su síntesis, morfología y caracterización. También se ilustran distintos tipos de aplicaciones que tienen estas nanopartículas.

En el capítulo 2 se resumen los objetivos de esta tesis.

En el capítulo 3 se presentan las técnicas experimentales usadas durante esta tesis, con una breve descripción de sus principios físicos, así como los equipos concretos usados. Se han empleado técnicas para caracterizar el tamaño de las muestras (como la cromatografía de exclusión por tamaño o la difracción de rayos X a bajo ángulo) para comprobar la reducción de tamaño esperada tras la síntesis de SCNPs; técnicas de caracterización elemental (como la resonancia magnética nuclear o el análisis elemental) para comprobar la correcta realización de

las distintas reacciones químicas y técnicas de caracterización térmicas (análisis termogravimétrico y la calorimetría diferencial de barrido) para comprobar los cambios de las temperaturas de transición vítrea y de degradación. También se han usado la espectroscopia ultravioleta-visible y otras espectroscopias para caracterizar las nanopartículas catalíticas sintetizadas y los productos de las reacciones en las que se ha probado.

En el capítulo 4 se presenta el primer método de síntesis de SCNPs desarrollado. Este método necesita de un monómero particular, 4-azido-2,3,5,6-tetrafluoroestireno (ATFS); pero es rápido, libre de catalizadores y no precisa de co-monómeros para evitar agregaciones. Además, se ha ideado un método para romper los enlaces de los puntos de entrecruzamiento y devolver la nanopartícula a su forma previa de polímero lineal. Este método se basa en la reacción de Staudinger, reacción en la que un grupo azida y un grupo fosfato se unen formando un iminofosforano, que en condiciones normales se hidroliza rápidamente. Pero en el caso particular de los iminofosforanos formados a partir de ATFS funcionalizado con grupos azida, los átomos de flúor protegen el enlace evitando de su hidrolización y volviéndolo estable. De modo que un copolímero de ATFS colapsaría en presencia de moléculas entrecruzantes que tengan dos grupos fosfano.

Para probar este método se ha polimerizado un copolímero de estireno y 2,3,4,5,6-pentafluoroestireno (P(S-*co*-PFS)). Con la caracterización de análisis elemental se comprobó que el copolímero final constaba de un 68 % de monómeros de estireno y 32 % de 2,3,4,5,6-pentafluoroestireno. Dicho copolímero se modificó con una reacción de azidación con azida sódica en *N,N*-dimetilformamida (DMF) para conseguir una sustitución parcial de los átomos de flúor en la posición 4 por grupos azida, obteniendo un 11 % de monómeros azidados en el polímero. Para sintetizar las SCNPs se han disuelto el copolímero por un lado y el entrecruzante por otro. Se han usado dos entrecruzantes distintos, 1,3-bis(difenilfosfino)propano (DPPP) y 1,4-bis(difenilfosfino)butano (DPPB) para comprobar la diferencia entre ellos, llegando a la conclusión de que ambos actúan de la misma forma y con resultados similares. El copolímero disuelto se ha inyectado en la otra disolución, para evitar agregados, y la mezcla se ha agitado durante 24 horas. Tras la reacción el producto se ha precipitado en hexano para recuperar las nanopartículas y eliminar el entrecruzante sobrante. Las nanopartículas sintetizadas mediante este método han mostrado una reducción de tamaño en la caracterización, así como una desaparición del pico característico de las azidas en la espectroscopia infrarroja y la aparición de picos relacionados con el entrecruzante en los espectros de resonancia magnética nuclear.

Tras comprobar la formación de nanopartículas, estas han sido redisueltas y expuestas a distintas condiciones para comprobar su estabilidad y buscando la rotura "a medida" de los grupos entrecruzantes, tales como un calentamiento en baño de silicona a 120ºC durante 3 días, un calentamiento mediante microondas durante 1 hora, o ser expuestas durante 3 días a un exceso de sulfuro de carbono (CS_2), ácido trifluoroacético (TFA) o trimetilsilanol (TMS). Tras estas exposiciones, las muestras fueron secadas, limpiadas con hexano y caracterizadas por NMR, donde se podía observar el pico correspondiente al entrecruzante en el espectro 31P, salvo la muestra expuesta a TMS que no mostraba pico alguno. Al caracterizar por GPC esta muestra se observó que su tamaño había aumentado hasta el del polímero precursor, por lo que se puede asegurar que efectivamente se ha conseguido romper el enlace entrecruzante, devolviendo el copolímero a su forma de cadena.

Mediante técnicas de espectros de difusión (DOSY) y de correlación protón-silicio (HETCOR) se ha podido comprobar que un grupo compuesto por un átomo de silicio unido a tres metilos ha quedado anclado a la cadena polimérica. Observar en la cadena este grupo, proveniente del TMS, nos da una primera idea de cómo es el mecanismo de ruptura del enlace, por lo que se presenta una propuesta del mecanismo de ruptura del iminofosforano.

Resumiendo, este método de síntesis de SCNPs libre de metales ha demostrado ser eficaz. A pesar de necesitar de un monómero particular, puede usarse con diferentes entrecruzantes, sin añadir ningún otro producto durante la reacción. Además, se ha demostrado que es fácilmente reversible a su estado de cadena polimérica, siendo esta reversibilidad interesante para posibles aplicaciones.

En el capítulo 5 se presenta el segundo método de síntesis de SCNPs de la Tesis. Este método se basa en la química click, es decir, en reacciones rápidas, eficientes y de fácil purificación. La química click ya se ha usado anteriormente en la síntesis de SCNPs, como por ejemplo la "cicloadición de azidas y alquinos catalizada con cobre (I)", conocida por sus siglas en inglés como CuAAC. En esta reacción un grupo azida, compuesto por tres átomos de nitrógeno, reacciona en presencia del catalizador de cobre (I) con un enlace triple creando un grupo triazol. Esta reacción click es una forma eficiente de sintetizar SCNPs usando polímeros azidados y moléculas con varios grupos alquino como entrecruzantes, pero tiene la pega de que el cobre usado como catalizador termina siendo inseparable de las nanopartículas. Para evitar el uso de éste catalizador metálico se ha desarrollado un método de síntesis que se basa en la "cicloadición de azidas y alquinos promovida por tensión", conocida también como SPAAC nuevamente por sus siglas en inglés. Esta reacción es igual que la CuAAC, pero no necesita

catalizador porque el triple enlace está tensionado, de modo que es más reactivo y puede combinarse con la azida sin necesidad de un catalizador. Al basarse en esta reacción, el método de síntesis no necesita catalizadores; pero, a cambio, solo es factible con alquinos tensionados, típicos en moléculas cíclicas. Por lo tanto, se ha seleccionado la molécula "sym-dibenzo-1,5-cyclooctadiene-3,7-diyne", o DIBOD, como entrecruzante. Esta molécula tiene dos enlaces triples tensionados gracias a su estructura, de modo que es un entrecruzante perfecto que puede reaccionar con dos grupos azida de una misma cadena polimérica para colapsarla.

Para comprobar la eficacia de este método se ha polimerizado un copolímero de estireno y clorometil estireno (P(S-*co*-CMS)) mediante una polimerización por adición, fragmentación y transferencia de cadena (RAFT). Mediante la caracterización por resonancia magnética nuclear (NMR) se comprobó que el copolímero consistía en un 73 % de monómeros de estireno y 27 % de monómeros de clorometil estireno. Dicho copolímero se modificó con una reacción de azidación con azida sódica en *N,N*-dimetilformamida (DMF) para sustituir todos los átomos de cloro por grupos azida, tal y como se puedo comprobar por NMR. Con el copolímero azidado se pasó a optimizar las condiciones de síntesis de SCNPs. Para evitar los agregados se tomaron tres medidas: síntesis en condiciones muy diluidas, inyección lenta y la adición de bencil azida, para forzar a reaccionar al entrecruzante sobrante. Llegando así a las condiciones optimizadas: el copolímero azidado y el DIBOD se disolvieron en tetrahidrofurano (THF) en distintos matraces y la disolución del polímero se inyectó durante 12 horas en el otro matraz. Tras 24 horas de reacción se inyectó becil azida para evitar las agregaciones y se dejó agitando otras 24 horas. Después, las SCNPs se recuperaron precipitándolas en etanol para eliminar el DIBOD sobrante. Se pudo comprobar la reducción de tamaño esperado gracias a las técnicas de cromatografía de permeación de gel (GPC), difracción dinámica de luz (DLS) y difracción de rayos X a bajo ángulo (SAXS). Con la técnica de SAXS, además, se obtuvo el factor de forma (v), que está relacionado como la forma de la muestra, de modo que se pudo comprobar que las SCNPs tenían una forma más globular que el precursor.

Para comprobar la estabilidad a lo largo del tiempo de las SCNPs se almacenaron en sólido y disueltas durante 2 meses. Tras el almacenamiento se volvieron a caracterizar para comprobar si se habían creado agregados durante el almacenamiento. La caracterización por SAXS confirma que las nanopartículas almacenadas en solución no sufrieron ningún tipo de agregación, mientras que las que se almacenaron en solido estaban ligeramente agregadas, pero sin llegar al tamaño del precursor.

Por lo tanto, este nuevo método desarrollado ha demostrado no sólo ser un sustituto eficiente y libre de catalizadores metálicos a los actuales métodos de síntesis; sino que, además, produce nanopartículas muy estables en el tiempo, abriendo la puerta a la posibilidad de comercializar SCNPs ya sintetizadas. Este método ha sido probado para un copolímero particular, pero como sólo necesita de grupos azidas es potencialmente útil para cualquier polímero que pueda ser azidable.

En el capítulo 6 se utiliza el método mostrado en el capítulo 5 para sintetizar nanopartículas de policloruro de vinilo (PVC) revalorizado. Para ello, primero, se usó PVC comercial que pasó por el mismo proceso que el copolímero P(S-*co*-CMS): azidación y síntesis de SCNPs. Las nanopartículas se sintetizaron correctamente y fueron caracterizadas, almacenadas y caracterizadas de nuevo del mismo modo que las nanopartículas de P(S-*co*-CMS), obteniendo unos resultados similares. Las SCNPs mostraban una reducción de tamaño y una estabilidad al almacenamiento durante 2 meses tal y como se esperaba.

A continuación, se buscó unas condiciones de química verde, filosofía que busca transformar este campo en uno más ecológico mediante la reducción del impacto medioambiental y del impacto sobre la salud humana. Para ello se buscó disolventes que tengan un impacto menor y que puedan sustituir los disolventes usados, THF y DMF, que son altamente contaminantes. Para buscar dicho substituto se repitió la reacción de azidación en distintos disolventes verdes para comparar el porcentaje de azidación con el obtenido en esa misma reacción con DMF. Tras esta prueba, y su correspondiente caracterización por espectroscopia infrarroja, se eligió el disolvente 1-butilpirrolidin-2-ona (NBP), que obtuvo un resultado similar al DMF.

Para comprobar si era posible usar este método para revalorizar PVC se seleccionaron dos tubos de PVC, uno flexible y otro rígido. Parte de estos tubos fue cortado en pedazos y purificados tres veces disolviéndolos en NBP y precipitándolos en agua. Tras estas purificaciones se había conseguido retirar los aditivos presentes, obteniendo un PVC indistinguible del comercial tal y como se comprobó por NMR. Este PVC revalorizado (vPVC) pasó por el mismo proceso que el comercial, usando solo NBP, agua y etanol como disolventes. Nuevamente, los resultados fueron similares a los anteriores, de forma que se demostró que se pueden sintetizar SCNPs a partir de PVC revalorizado usando este método de síntesis libre de metales.

Para dar valor añadido a estas nanopartículas, se demostró que son útiles para la aplicación de catálisis. Se preparó un complejo de vPVC y cobre (II) con intención de usarlo de catalizador. El cobre reacciona uniéndose a los grupos triazol, creando nanopartículas catalíticas, y con una caracterización por DLS se pudo comprobar que en este proceso no se creaban agregados. Para

comprobar la eficiencia de las nanopartículas catalíticas se usaron en tres tipos diferentes de reacciones que necesitan cobre (II) como catalizador.

- Reacciones de homoacoplamiento de alquinos. Esta reacción se probó para tres moléculas distintas: acetato de propargilo, propionato de propargilo y 1-etinil-4-fluorobenceno. Con los tres precursores funcionó la reacción, con rendimientos de alrededor del 90 %. Las reacciones modelo hechas con cloruro de cobre (II) obtuvieron rendimientos similares, pero la SCNPs demostraron ser reutilizables hasta 3 veces. Tras 3 repeticiones el rendimiento cae drásticamente. La razón de esta caída de rendimiento es la agregación de las nanopartículas. Un seguimiento en DLS tras cada reacción mostró cómo se van agregando tras cada reacción, hasta el punto de ser parcialmente insolubles.

- Síntesis de benzaldehído. Esta reacción se obtuvo un rendimiento considerablemente superior usando las SCNPs catalíticas que con el cloruro de cobre (II), siendo superior al 60 % frente al 30 % de la reacción modelo.

- Síntesis de 3,5-di-*t*-butil-o-quinona. Esta reacción fue monitorizada mediante espectroscopia ultravioleta-visible (UV-Vis) y se comprobó que la reacción era más rápida con las SCNPs catalíticas que con el catalizador modelo. Para comparar correctamente las reacciones se repitieron las reacciones con distintas concentraciones del sustrato para modelizar la reacción usando el modelo Michaels-Menten, llegando a la conclusión de que la reacción es aproximadamente 3 veces más rápida con las nanopartículas catalíticas que con el cloruro de cobre (II).

En conclusión, se ha demostrado que tal y como se pensaba el método de síntesis presentado en el capítulo anterior es eficaz con distintos tipos de polímeros siempre que sea posible azidarlo. Además, se ha probado que con este método es posible obtener SCNPs a partir de materiales revalorizados como restos de tubos de PVC. Por último, se ha comprobado que es una herramienta útil para la química verde, ya que no solo puede seguirse todo el proceso usando únicamente disolventes verdes, sino que puede usarse para fabricar nanopartículas catalíticas reutilizables.

Por último, en el capítulo 7 se exponen las conclusiones globales de esta tesis. Las cuales se resumen en el desarrollo de dos métodos de síntesis de SCNPs libres de catalizadores metálicos y en la aplicación de uno de estos métodos, en el campo de la química verde, para revalorizar polímeros y crear catalizadores reutilizables.

Summary

In this thesis two new synthesis methods for single-chain nanoparticles (SCNPs) are presented. This type of soft nanoparticles is formed by a single-chain of a polymer that is folded and collapsed by intra-chain chemical bonds. With a smart election and combination of different monomers, SCNPs with specific physical and chemical properties can be designed and synthesized. In addition, their small size and their high ratio between surface and volume allows the use of SCNPs in different applications, such as sensing, chemical catalyst or drug delivery. Currently, some synthesis methods are reported, but almost all of them need metallic catalyst to be carried out correctly. Those catalyst are extremely difficult to remove from the final SCNPs and their properties, as for example toxicity, make impossible some applications of the nanoparticles. On the other hand, some methods only have good results in dissolution, since, when the SCNPs are dried to solid state they aggregate, making impossible their redissolution. The new synthesis methods presented in this thesis did not use any catalyst, works for different polymers and can be stored in solid form without any presence of aggregates. In addition, one of the methods have been used to synthesize reusable catalytic SCNPs from valorized polyvinyl chloride (PVC).

This thesis is structured as follows:

In the first chapter are gathered the main theorical concept that are necessary for the correct interpretation of the results that are reported in the chapters 4, 5 and 6. The basic concepts of SCNPs, their synthesis, morphology, characterization and applications are presented.

In the chapter 2 are summarized the goals of this thesis.

In the chapter 3 are collected the experimental techniques that were been used for this thesis. The physic principles, functionalization and the used specific equipment are presented for each experimental technique. Size characterization techniques (as Size Exclusion Chromatography or Small Angle X-ray Scattering) have been used to check the reduction of size from the polymer chain to SCNPs. The correct performance of the chemical reactions has been checked by elemental characterization techniques (as Nuclear Magnetic Resonance or Elemental Analysis). The thermal behavior of the samples was characterized by Thermogravimetric Analysis and Differential Scanning Calorimetry techniques. In addition, Ultraviolet-Visible Light Spectroscopy and Mas Spectroscopy have been used to characterize the catalytic SCNPs and the products of the catalytic reactions.

In chapter 4 the first SCNPs synthesis method is presented. This method requires a particular monomer, named 4-azido-2,3,5,6-tetrafluorostyrene (ATFS). Nonetheless, it is a fast method, free of catalysts and does not require any product to avoid aggregations. Additionally, a method has been devised to break the intra-chain bond and return the polymer to its previous shape. This method is based on the Staudinger reaction, a reaction in which an azide group and a phosphane group join to form an iminophosphorane, which under normal conditions is rapidly hydrolyzed. But in the particular case of ATFS, the fluorine atoms protect the bond, preventing it from hydrolyzing and making it stable. So, an ATFS copolymer would collapse in the presence of cross-linking molecules that have two phosphane groups.

To check this method, a copolymer of styrene and 2,3,4,5,6-pentafluorostyrene (P(S-*co*-PFS)) has been polymerized. With elemental analysis characterization, it was found that the final copolymer was composed by 68% of styrene monomers and 32% of 2,3,4,5,6-pentafluorostyrene monomers. The copolymer was modified with an azidation reaction with sodium azide in N,N-dimethylformamide (DMF) to replace some of the fluorine atoms in the 4^{th} position with azide groups has been carried out, obtaining 11% of azided monomers. To synthesize the SCNPs, the copolymer was dissolved in one flask and the cross-linker in another one. Two different cross-linkers have been used, 1,3-bis(diphenylphosphino)propane (DPPP) and 1,4-bis(diphenylphosphino)butane (DPPB), and no differences were observed between them in the results. The dissolved copolymer has been injected into the cross-linker solution to avoid aggregates and the mixture has been stirred for 24 hours. After the reaction, the product was precipitated in hexane to recover the nanoparticles and eliminate the excess cross-linker. The expected reduction of size in the SCNPs were observed in the characterization, as well as a disappearance of the characteristic peak of azides in infrared spectroscopy and the appearance of peaks related to the cross-linker in the Nuclear Magnetic Resonance spectra.

After checking the formation of nanoparticles, they have been redissolved and exposed to different conditions to check their stability. The SCNPs were exposed to a heating in a silicone bath at 120ºC for 3 days, heating by microwave for 1 hour, or being exposed for 3 days to an excess of carbon sulfide (CS_2), trifluoroacetic acid (TFA) or trimethylsilanol (TMS). After these exposures, the nanoparticles were dried, cleaned with hexane and characterized by NMR, where the peak corresponding to the cross-linker could be observed in the ^{31}P spectrum in all the case except the sample exposed to TMS, which does not show any peak. The characterization of this sample by GPC shows that the size had increased to the size of the azided precursor polymer. So, can be concluded that the cross-linking bond has been broken, returning the copolymer to its chain form.

The Diffusion-Ordered Spectroscopy (DOSY) and proton-silicon correlation spectroscopy (HETCOR) techniques were used to characterize the opened SCNPs. According to the characterization, a group of a silicon atom linked to three methyl groups has been linked to the polymer chain. The presence of this group of the TMS in the chain gives us a first idea of the bond breaking mechanism, so a proposal for the iminophosphorane breaking mechanism is presented.

In conclusion, this metal-free SCNPs synthesis method has proven to be effective. Despite requiring a particular monomer, it can be used with different crosslinkers, without adding any other product during the reaction. Furthermore, it has been reported that it is easily reversible to its polymer chain state, being this reversibility interesting for possible applications.

In chapter 5 the second method of SCNPs synthesis is presented. This method is based on some fast, efficient and easily purifiable reactions, named click-reactions. Click-chemistry has already been used previously for the synthesis of SCNPs, such as the Copper (I)-catalyzed Azide-Alkyne Cycloaddition" (CuAAC). In this reaction an azide group, composed of three nitrogen atoms, reacts in the presence of the copper (I) catalyst with a triple bond creating a triazole group. This click reaction is an efficient way to synthesize SCNPs using azided polymers and cross-linkers with some alkynes. But this method has the drawback that the copper used as a catalyst is inseparable from the nanoparticles. To avoid the catalyst, a synthesis method has been developed based on the "Stress-Promoted Azide-Alkyne Cycloaddition" (SPAAC). This reaction is the very similar to the CuAAC, but does not need a catalyst. The stressed triple bonds are more reactive and can combine with the azides without aby catalyst. Consequently, this method needs stressed alkynes, such as the ones of the cyclic molecules. Therefore, the molecule "sym-dibenzo-1,5-cyclooctadiene-3,7-diyne", or DIBOD, has been selected as a cross-linker. This molecule has two stressed triple bonds thanks to its structure, so it is a perfect cross-linker that can react with two azide groups of the same polymer chain to collapse it.

To check the effectiveness of this method, a copolymer of styrene and chloromethyl styrene (P(S-*co*-CMS)) has been polymerized by Reverse Addition Fragmentation Chain Transfer polymerization (RAFT). Through Nuclear Magnetic Resonance (NMR) characterization, it was checked that the copolymer consisted of 73% of styrene monomers and 27% of chloromethyl styrene monomers. The copolymer was modified with an azidation reaction with sodium azide in N,N-dimethylformamide (DMF) to replace all chloride atoms with azide groups, as can be verified by NMR. To prevent the aggregation in the synthesis of SCNPs three precautions were taken: synthesis at very dilute conditions, slow injection and the addition of benzyl azide, to

force the excess cross-linker to react. The azided copolymer and DIBOD were dissolved in tetrahydrofuran (THF) in different flasks and the polymer solution is injected for 12 hours in the other flask. After 24 hours of reaction, benzyl azide is injected to avoid aggregations and it is left stirring for another 24 hours. Afterwards, the SCNPs are recovered by precipitating them in ethanol to eliminate the excess DIBOD. The expected size reduction could be verified thanks to the techniques of gel permeation chromatography (GPC), dynamic light diffraction (DLS) and low-angle X-ray diffraction (SAXS). With the SAXS technique, the shape factor (ν) was also obtained, which is related to the shape of the sample, so that it was possible to verify that the SCNPs had a more globular shape than the precursor.

To check the stability the SCNPs were stored in solid form and dissolved for 2 months. After storage they were re-characterized to check if aggregates had been created during storage. The characterization by SAXS confirms that the nanoparticles stored in solution did not suffer any aggregation, while those stored in solid were slightly aggregated, but without reaching the size of the precursor.

Therefore, this new method presented has proven to be an efficient and metal catalyst-free substitute for current synthesis methods. In addition, the nanoparticles are very stable over time, creating the possibility of commercializing already synthesized SCNPs. This method has been tested for a particular copolymer, but since it only requires azide groups it is potentially useful for any polymer that can be azidable.

In chapter 6, valorized polyvinyl chloride (PVC) catalytic SCNPs were synthesized using the method reported in the chapter 5 . First, commercial PVC was subjected to the same process as the P(S-*co*-CMS) copolymer: azidation and synthesis of SCNPs. The nanoparticles were successfully synthesized and were characterized, stored and re-characterized in the same way as the P(S-*co*-CMS) nanoparticles, obtaining similar results. The SCNPs showed size reduction and storage stability for 2 months as expected.

Next, with the objective of reduce the environmental impact and the impact on human health of the method, green chemistry conditions were sought. Azidation reaction was repeated with different green solvents to obtain a green substitute for the THF and DMF used in the synthesis method. After this test, and its corresponding characterization by Infrared spectroscopy, the solvent 1-butylpyrrolidin-2-one (NBP) was chosen, which obtained a result similar to DMF.

One flexible PVC pipe and another rigid one were obtained, cut into pieces and purified three times by dissolving in NBP and precipitating in water. After the purifications, the additives present in the pipes had been removed, obtaining a PVC indistinguishable from the commercial

one, as verified by NMR. This revalued PVC (vPVC) went through the same process as the commercial one, using only NBP, water and ethanol as solvents. The results were similar to the previous ones, so it was demonstrated that SCNPs can be synthesized from revalued PVC using this metal-free synthesis method.

In addition, a complex of vPVC and copper (II) was prepared to obtain a SCNP catalyst. The copper reacts by joining the triazole groups without any aggregation, as has been checked by DLS characterization. To test the efficiency of the catalytic nanoparticles, they were used in three different types of reactions that require copper (II) as a catalyst.

- Alkyne homocoupling reactions. This reaction was tested for three different molecules: propargyl acetate, propargyl propionate, and 1-ethynyl-4-fluorobenzene. The reaction worked with the three precursors, with yields of around 90%. The model reactions made with copper(II) chloride obtained similar yields, but the SCNPs proved to be reusable up to 3 times. After 3 repetitions performance drops drastically. The reason for this drop is the aggregation of the nanoparticles. A DLS follow-up after each reaction shows how they aggregate after each reaction, to the point of being partially insoluble.

- Benzaldehyde synthesis. This reaction obtained a considerably higher yield using the catalytic SCNPs than with copper (II) chloride, being greater than 60% compared to 30% for the model reaction.

- 3,5-di-t-butyl-o-quinone synthesis. This reaction was monitored using ultraviolet-visible (UV-Vis) spectroscopy and it was found that the reaction was faster with the catalytic SCNPs than with the model catalyst. To correctly compare the reactions, the reactions were repeated with different concentrations of the substrate to model the reaction using the Michaels-Menten model, reaching the conclusion that the reaction is approximately 3 times faster with the catalytic nanoparticles than with copper chloride (II).

In conclusion, it has been shown that, the synthesis method presented in the previous chapter is effective with different types of polymers as long as it is possible to azide it. Furthermore, it has been proven that with this method it is possible to obtain SCNPs, from revalued materials such as remains of PVC pipes. Finally, it has been proven to be a useful tool for green chemistry, since not only can the entire process be followed using only green solvents, but it can also be used to manufacture reusable catalytic nanoparticles.

Finally, chapter 7 presents the global conclusions of this thesis. Which are summarized in the development of two methods for the synthesis of SCNPs free of metal catalysts and in the application of one of these methods, in the field of green chemistry, to revalue polymers and create reusable catalysts.

1. Introduction

This section assesses the status of single chain nanoparticle synthesis, analysis and potential applications, and therefore highlights the relevance of the presented thesis.

1.1. Single-chain nanoparticles

In the field of polymer chemistry and materials science, the approach to create nanoscale polymeric structures by the folding of individual polymer chains has been demonstrated success [1]. Through the synthesis polymer chains incorporating functionality via either functional side groups or direct integration into the polymer backbone, individual polymer chains can fold onto themselves using a diverse range of covalent and non-covalent interactions in dilute solution (typically <1 mg mL^{-1}), as is shown schematically in Figure 1. These resulting compact, nano-sized objects (in the size range of proteins around 1-20 nm) called Single Chain Nanoparticles (SCNPs), can find applications across a wide range of functions and practical uses such as cell targeting, catalysis or sensing [2].

Particularly, the size of the nanoparticles (NP) is directly influenced by the length of the precursor polymer, a parameter easily controlled through polymerization techniques developed over the last decades [3]. The crosslinking density employed also plays a role in determining NP size. The first intramolecular crosslinking of polymers dates back to 1962 [4], but it was not until 2002 that the process became well-controlled on larger scales [5]. Since then, various methods have been developed for intramolecularly crosslinking precursor polymer chains to create functional SCNPs [6]. Furthermore, to achieve effectiveness in the desired application, the SCNPs need to be carefully tuned. Particularly, this thesis is focused on the development of various new synthesis method using currently available functionalization methods aimed at incorporating diverse functional groups into SCNPs. With the new methods, we contemplate the next steps for advancing the field of SCNPs, focusing on achieving more stable and versatile SCNPs in a simple way.

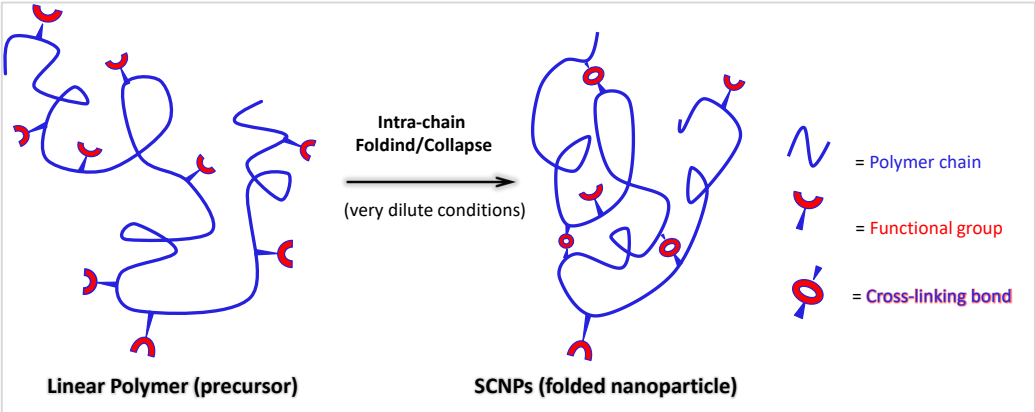

Figure 1. Schematic illustration of a linear polymer precursor and a single-chain nanoparticle (SCNP) obtained through intra-chain folding/collapse.

1.1.1. Design and synthesis of SCNPs

Various synthetic methodologies have been employed in the creation of SCNPs. Typically, this involves the synthesis of appropriately functional polymers, followed by post-polymerization transformation in a dilute solution (usually ≤1 mg mL^{-1}) to facilitate intra-chain cross-linking. Consequently, the chemical reactions that are used must meet the criteria of any effective post-polymerization functionalization reaction: they must be efficient and produce no side products.

Custom SCNPs can be synthesize in three steps: (i) polymer synthesis, (ii) polymer functionalization and (iii) intra-chain folding or collapse (see Figure 2) [7].

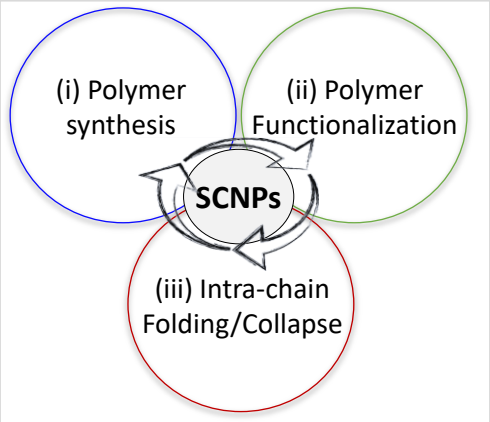

Figure 2. Different steps involved in the construction of single-chain nanoparticles. (i) Polymer synthesis, (ii) polymer functionalization, and (iii) intra-chain folding/collapse of individual polymer chains.

(i) Polymer synthesis

Over time, numerous techniques have been devised for synthesizing (co)polymers with a narrow molecular weight distribution ($Đ \rightarrow 1$), including anionic, cationic, and controlled radical polymerization methods. Among these, the most valuable, versatile, and user-friendly technique is reversible addition-fragmentation chain transfer (RAFT) polymerization [8].

This controlled polymerization technique allows for the precise control of polymer chain length and structure, resulting in polymers with well-defined characteristics. The key feature of RAFT polymerization is the use of a reversible chain transfer agent (CTA). This CTA can reversibly control the polymerization process by mediating the transfer of active polymerization species, such as radicals, between the growing polymer chains. The reversibility of this process enables the control of polymerization kinetics and the ability to halt and restart polymerization [9]. One of the major advantages of RAFT polymerization is its versatility in polymer design. It enables the synthesis of well-defined polymers with controlled molecular weights, low dispersity, and desired end-group functionality.

The RAFT process involves six steps, showed in the Figure 3. The first step is the initiation, where the initiator (in the figure it is decomposed in two reactive fragments *i*) reacts with the monomer (*M*) creating a radical (P_1 because is of length 1). Next, the radical reacts with more monomer molecules, growing the length of the polymer chain (from P_n to P_{n+1}), and a process called propagation. In the third step a pre-equilibrium state is reached when the created polymer chain reacts with the CTA, releasing the radical (*R*) and therefore stopping the grow. This allows the released radical, in the next step, to re-initiate the reaction with other monomers, creating a new polymer chain. At some point the real equilibrium is reached; since, thanks to the CTA, the radicals are interchanged between different chains, allowing equal opportunities of growth for all the chains. The termination is the last step, where two radicals of the active chains react, causing that the chains cannot react further (D_{n+m} or D_n and D_m).

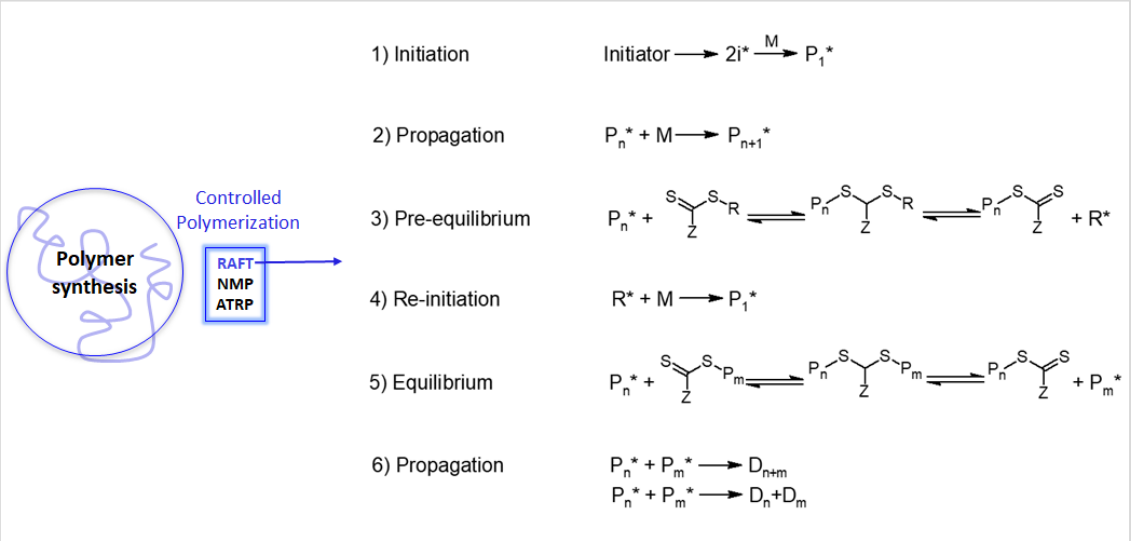

Figure 3. General mechanism of reversible addition-fragmentation chain transfer (RAFT) polymerization.

(ii) Polymer Functionalization

After the synthesis of the polymeric precursor, a functionalization reaction is carried out. The objective of this reaction is to create some factionalized groups along the chain that will be used to create the cross-links that will fold the chain. Nevertheless, with a good design of the polymer, this step can be avoided if the chain has been polymerized with already reactive groups.

Some strategies are based in supramolecular interactions, as the use of hydrophobic interactions, which is a prevalent strategy for the formation of SCNPs. Hydrophobic moieties or blocks within the polymer chain can drive the folding of the chain into a compact structure in aqueous environments, where the hydrophobic segments minimize contact with water. For example, Terashima et al. synthesize amphiphilic random methacrylate copolymer with poly(ethylene glycol) and alkyl pendent groups that collapse reversibly into SCNPs in water [10].

Aromatic moieties with π-electron systems, such as benzene rings, can engage in π-π stacking interactions that contribute to the folding and stabilization of the polymer chain, as the SCNPs prepared by Lu et al. from poly(styrene)-b-poly(dimethylacryl amide)-b-poly(2,3,4,5,6-pentafluorostyrene) triblock copolymer [11]. Incorporating hydrogen-bonding groups, such as amide (N-H) or urea functionalities, can lead to intramolecular hydrogen bonding too, facilitating the folding of the polymer chain. Meijer et al. developed a system to synthesize SCNPs based in 2-ureidopyrimidinone units that form four hydrogen bonds between each other [12]. Other strategy is the formation of coordination bonds with metal ions to stabilize SCNPs. Metal coordination involves the interaction of metal ions with specific functional groups, such as imidazole or carboxylic acid groups. Those complexes have been used to form SCNPs as, for example, the nanoparticles produced by the complexation of poly(methyl methacrylate-*co*-2-(acetoacetoxy)ethyl methacrylate) copolymer with copper(II) reported by Pomposo et al [13]. Inclusion of host-guest interactions, such as cyclodextrin inclusion complexes or cucurbituril binding, can induce folding and stabilize SCNPs. Appel et al. reported a method to synthesize metastable SCNPs by the reversible intramolecular crosslinking of a single polymer chain of poly(N-hydroxyethylacrylamide) functionalized with viologen and naphthalene, two complementary guests for cucurbit[8]uril [14]. Electrostatic interactions, such as those between positively and negatively charged groups, can be used to induce folding and stabilize the nanostructure. This strategy is used by Lambert et al. to synthesize SCNPs from a copolymer of styrene, grafted poly(ethylene oxide) chains, and antagonist benzimidazol- and chlorobenzyl-based units, that react together to spark the folding process, creating imidazolium-based cross-link points [15].

On the other hand, incorporating reactive groups that can undergo covalent crosslinking reactions, such as Michael addition or “click” chemistry, can be used to stabilize the SCNPs through intramolecular bond formation. Different approaches have been made to the covalent bond strategy. Davankov et al. create polystyrene SCNPs by the self-crosslinking of chloromethylene groups via thin(IV) chloride catalyst [16]. Mecerreyes et al. carried out the production of different polymers nanoparticles thanks to the intermolecular interaction of suspended acylate functionalities in the presence of a radical initiator [17]. But “click” reactions in general [18, 19], and specifically copper(I)-catalyzed azide-alkyne cycloaddition (CuAAC) [20-22], are one of the most used methods to collapse the chain thanks to their selectivity and efficiency; making the azide functional group one of the most used one.

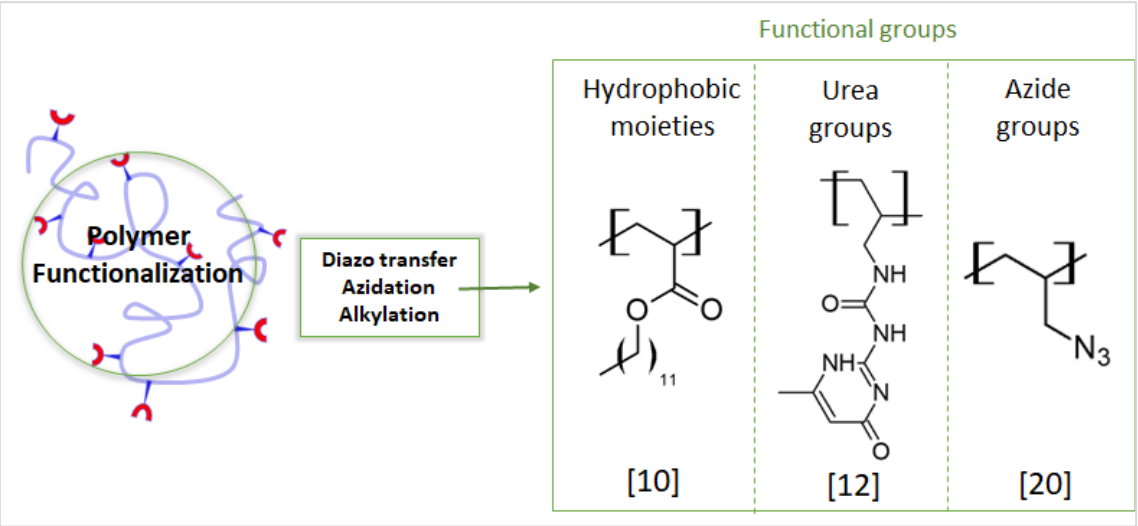

Figure 4. Scheme of the functionalization step with some functionalization reaction and some typical functional groups used in the collapse of the SCNPs.

(iii) Intra-chain folding or collapse

Nature takes advantage of many different orthogonal covalent cross-links (e.g. disulfides) and non-covalent interactions (e.g. hydrogen bonding, metal ligation) as well as well as dynamic covalent chemistry (e.g., acetal formation) in folded biomacromolecules. Taking this as inspiration, SCNP synthesis incorporates similar principles. This section categorizes the discussion of intra-chain cross-linking chemistry into three main groups: covalent, dynamic covalent, and non-covalent (see Figure 5).

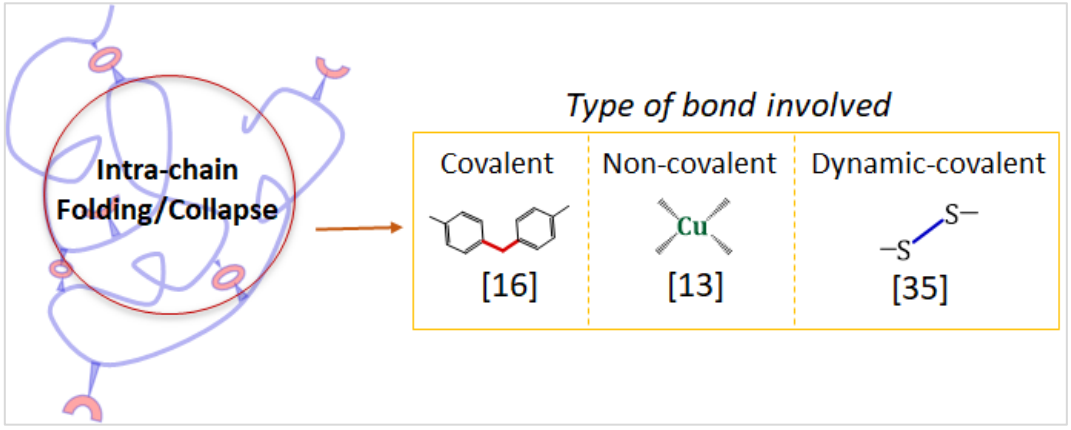

Figure 5. Scheme of different types of bonds involved in the intra-chain folding of the SCNPs.

- *Covalent chemistry*

Covalent bonds are the strongest and therefore the most stable chemical bonds. The covalent nature of the bonds within the polymer chain contributes to the structural integrity of the nanoparticle. These covalent single-chain nanoparticles are typically designed with specific monomers and synthetic strategies to achieve controlled and well-defined structures at the

nanoscale. These nanoparticles may exhibit unique characteristics, such as high stability, well-defined shapes, and tunable functionalities. The covalent nature of the bonds provides durability and robustness to the nanoparticle, which can be advantageous in applications like drug delivery, where stability and controlled release are crucial. Additionally, covalent single-chain nanoparticles can be engineered to have specific chemical groups or functional moieties for targeted interactions in various fields, including materials science, nanomedicine, and catalysis.

One of the first SCNPs synthesize method use the coupling reaction of benzocyclobutene units, that dimerize at 250°C [5]. Hawker et al. developed this method to synthesize SCNPs from a random copolymer of 4-vinylbenzocyclobutene and vinyl monomers. They use a continuous addition method, adding the polymer solution to heated solvent, to avoid the intermolecular coupling without using ultra-diluted conditions. Subsequently, Hawker et al. reported an alternative vinylbenzosulfone monomer that have a similar crosslinking characteristic that the benzocyclobutene groups, but with simpler synthesis and purifications [23].

Nevertheless, some since then they have developed some synthesize method that can be carried out at room temperature, amidation reaction [24], urea formation [25] or thiol-Michael reaction [26-28].

Thanks to the high efficiency, high functional group tolerance and mild reaction conditions “click” reactions are wide used to collapse the polymer chain creatin covalent intra-chain bonds. copper(I)-catalyzed azide-alkyne cycloaddition (CuAAC) [19-21], thiol-ene addition [29, 30], and amine-isocyanate addition [31] have been used already to synthesize SCNPs. Tetrazine-norbornene reaction, despite is not considered a “click” reaction, have been used by O’Reilly et al. to collapse the polymer chain [32], and is fast and have a good conversion at room temperature.

- *Dynamic covalent chemistry*

The synthesis of SCNPs using dynamic covalent bonds represents an intriguing pathway to create adaptable and responsive nanostructures. Under specific conditions, these bonds exhibit reversibility and can be kinetically fixed or cleaved in response to changes in environmental conditions, such as pH, oxidation, or temperature.

Fulton and colleagues employed dynamic covalent acylhydrazone bonds to craft SCNPs with reversible characteristics [33]. In their approach, a bis(hydrazide) crosslinker was continuously introduced to aldehyde-functionalized polystyrene, followed by catalytic trifluoroacetic acid (TFA). To kinetically trap the hydrazone bonds and ensure the integrity of SCNPs upon isolation,

the TFA was quenched with triethylamine. The cross-linking density of the nanoparticles was modulated by adjusting the amount of cross-linker added. Notably, no collapse was observed at higher cross-linking densities in these studies. The dynamic nature of the acylhydrazone bond was validated by the formation of SCNPs through an exchange reaction of bis(hydrazide) crosslinker with copolymers decorated with monohydrazide. In a subsequent publication, Fulton et al. reported a similar system functionalized with oligo(ethylene glycol) side chains, introducing thermoresponsive behavior [34]. At low pH, a solution of nanoparticles was kinetically trapped; however, exposure to acid and heat led to nanoparticle precipitation, followed by hydrogel formation. This process was reversed upon cooling.

Pomposo, Fulton, and colleagues synthesized SCNPs capable of reversibly undergoing a coil-to-globule transition via enamine bond formation, which is reversible under acidic conditions [24]. Linear polymers functionalized with beta-keto ester groups were synthesized and condensed with butylamine. SCNPs were created through an enamine exchange reaction with ethylene diamine under dilute conditions. The cross-links were cleaved upon the addition of phosphoric acid and reformed with additional ethylene diamine, illustrating the reversible nature of the process.

Disulfides, noteworthy for their presence in biological systems and sensitivity to redox chemistry, were investigated. Berda et al. reported the synthesis of anhydride-functionalized linear polymers, where intramolecular disulfide linkages were installed by adding 4-aminophenyl disulfide [35]. The disulfides were reversibly cleaved and reformed in dilute solution through treatment with dithiothreitol (reducing) and iron(III) chloride (oxidative), respectively.

- *Non-covalent chemistry*

Supramolecular interactions, such as H-bonding and π–π interactions, constitute the primary intra-chain linkages in folded biopolymers. Similar chemistry has been explored in the synthesis of SCNPs by various research groups. Frequently, monomers are functionalized with hydrogen bonding units, which are protected to prevent polymer aggregation during synthesis. This approach is exemplified in several publications by Meijer and colleagues, specifically in the context of 2-ureidopyrimidinone (UPy) dimerization [12]. Deprotection in dilute solutions enables the formation of intra-chain quadruple hydrogen bonds, facilitating chain folding. The resulting SCNPs are referred to as "metastable" because, when cast into a film, they remain soluble in chloroform; however, upon heating, the SCNPs uncoil, and the UPy moieties form inter-chain linkages, resulting in an insoluble supramolecular network.

The use of UPy dimerization has been instrumental in studying the impact of various variables on SCNP formation. The rigidity of the polymer backbone, the placement of additional hydrogen bonding sites in the UPy linker, and the molecular weight of the polymer were found to have little effect on the ability of a polymer to form supramolecular SCNPs, while the solvent played a crucial role in disrupting or facilitating H-bond formation.

Benzene-1,3,5-tricarboxamide (BTA), known for its ability to form helical assemblies via hydrogen bonding in supramolecular chemistry, has also been employed in SCNP synthesis. In one approach, a photoprotected BTA-containing monomer prevents aggregation during polymer synthesis [36]. In subsequent publications, this protection strategy proved unnecessary; BTA-containing monomers were polymerized directly in a solvent capable of disrupting H-bonds [37]. Alternatively, the BTA unit can be attached to a polymer via azide–alkyne "click" chemistry [38].

Cucurbit[n]urils form host–guest complexes with various aromatic molecules without requiring protection chemistry. In work by Scherman et al., methyl viologen and naphthyl-functionalized polymers were combined with cucurbit[n]urils in dilute solution to form ternary host–guest complexes, resulting in SCNPs [14]. Notably, the polymers had to be studied at very low concentrations, as significant aggregation occurred above 0.1 mg mL^{-1}.

To date, the use of metal coordination to form intramolecular cross-links in SCNPs is relatively limited. The approaches have been relatively straightforward; a metal complex is introduced to a ligand-bearing polymer in dilute solution, and a ligand exchange reaction occurs, with the high local concentration of polymer-bound ligand driving SCNP formation forward. Examples include rhodium binding with polycyclooctadiene [39], which contains 1,5-dienes, and acac-functionalized polymers containing copper(II) as a bridging metal for catalytic purposes [13].

1.1.2. Morphology of SCNPs

Single-chain nanoparticles (SCNPs) can exhibit a variety of morphologies that can vary based on the type of polymer, the method of synthesis, and environmental conditions. It's important to note that the specific morphology of single-chain nanoparticles can be fine-tuned by adjusting parameters during synthesis, such as the choice of polymer, solvent conditions, and temperature. In this sense there are two different precursors copolymers that collapse into different types of morphologies [40]: block copolymers and random copolymers, as can see in the Figure 6. Block copolymers can collapse to form Janus SCNPs, with very differentiable regions, and tend to exhibit a self-assembly behavior that create a bigger and more complicate multimolecular structures as micelles or lamellae. On the other hand, random copolymers

collapse to form sparse or globular morphologies, which do not have the self-assembly behavior. The ability to control and understand the morphology of single-chain nanoparticles is crucial for tailoring their properties for diverse applications, including drug delivery, sensing, and nanomaterials development.

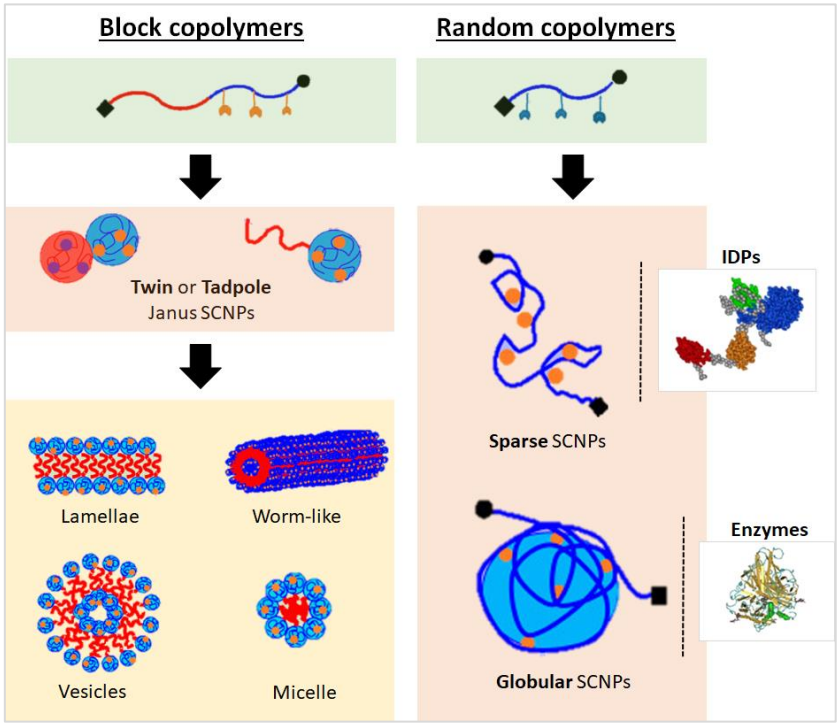

Figure 6. Scheme of the different morphologies of SCNPs from block copolymer precursor and from random copolymer precursor. It showed some self-assembly structures formed by janus SCNPs and the similarity of morphology between sparse SCNPs and intrinsically disordered proteins (IDPs), and globular SCNPs and enzymes.

In order to accurately design a SCNP, it is necessary to correctly understand the properties of the precursor polymer in order to predict, among other properties, the final morphology. As mentioned before, there are mainly two types of precursors:

I. Block copolymer

A block copolymer is a type of polymer that consists of two or more chemically distinct polymer blocks covalently bonded to each other. These blocks can vary in terms of their chemical composition, structure, and properties. The key feature of block copolymers is the presence of distinct blocks with different characteristics within the same polymer chain. Block copolymers often undergo phase separation, forming microdomains of each block.

Due to the different regions, this type of polymer collapse into Janus SCNPs. The term "Janus" is used to describe a particle or structure with two distinct faces or regions that have different properties or compositions. In the context of single-chain nanoparticles, the Janus morphology

involves the segregation of different segments or blocks, within a single polymer chain, resulting in a particle with two chemically distinct regions. This heterogeneous morphology is caused by the independent collapse of each region of the precursor block copolymer. If all the different blocks collapse correctly into a nanoparticle-like shape Twin Janus SCNP will be form [41]. On the other hand, if not all the regions collapse Tadpole Janus SCNP will be form [42].

Thanks to their self-assembly behavior, those Janus SCNPs can lead to unique morphologies, such as micelles, lamellae, or vesicles, depending on the specific characteristics of the blocks [43].

II. Random Copolymers

A random copolymer is a type of copolymer in which two or more different monomers are polymerized together in a random sequence along the polymer chain. Unlike block copolymers, random copolymers exhibit a statistical distribution of monomers along the polymer chain. The arrangement of monomers is not predetermined or ordered in specific blocks, and the sequence of monomers appears at random intervals.

The properties of random copolymers can be tuned by adjusting the ratio of the different monomers used in their synthesis. The incorporation of different monomers introduces variations in chemical and physical properties, such as melting point, solubility, and mechanical strength. This versatility makes random copolymers useful in a range of applications, including the production of plastics, elastomers, adhesives, and coatings.

With random copolymer precursor, two different limiting conformations of SCNPs can be obtained: sparse and globular. The Figure 6 represents the morphology of sparse SCNPs and his similarity to the morphology of Intrinsically Disordered Proteins (IDP), and the morphology of globular SCNPs compared to the morphology of enzymes.

Sparse single-chain nanoparticles are obtained when the nanoparticle is collapse in a good solvent (that solvents that promote the swelling and expansion of polymer chains, allowing them to separate) [45]. As molecular dynamics simulations show, the self-avoiding character of the chain avoid the cross-linking of functional groups separated by long distances. Despite so efficient is the intra-chain cross-linking technique, the nature of the polymer favors reaction of bonds between closer functional groups, creating short-range loops. Therefore, a non-globular and non-compact morphology is obtained, with almost linear chain sections and sections that are more compact are interspersed [46, 47].

Curiously, some biomacromolecules, in particular intrinsically disordered proteins, have a very similar morphology to the spare SCNPs [48], as can see in the Figure 6. Additionally, in the same way that the SCNPs, intrinsically disordered proteins are intrinsically polydisperse in size and topology [45, 46, 49, 50]. Those proteins, that are vital for some biological system, depends on its morphology for the correct function correctly. Therefore, the capacity to control precisely the morphology of the SCNPs open the door to different applications [51].

On the other hand, globular single-chain nanoparticle is obtained be collapsing the SCNPs by more complex synthesis routes. This a global core-shell morphology is more homogeneous, presenting a single locally compact section. Native proteins, as enzymes, have a similar morphology that the globular SCNPs (see Figure 6).

Different approximations have been studied to obtain globular single-chain nanoparticles. The use of relatively long cross-linkers, in combination with bifunctional groups in the precursor, increase the probability of form long-range loops to obtain a better compaction, as have been proved by both, simulations and experimentally [52]. Other approaches are based in the self-assembly nature of the amphiphilic random copolymers [19, 53-55].

1.1.3. Characterization

The corroboration of data provided by multiple techniques is often required to characterize SCNP formation. The identification of functional groups participating in cross-linking chemistry, as well as alterations in the size and morphology of the polymer structure, can be discerned through the methodologies outlined in this section. Importantly, it is often necessary to use techniques that are sensitive enough to detect small concentrations of aggregates that may be formed by intermolecular cross-linking to prove the single molecule nature of these nanostructures.

To characterize the length of the polymer chain or the SCNPs two different values are used: the radius of gyration and the hydrodynamic radius [56]. The “radius of gyration” (R_g) of a polymer is the average distance from the center of mass to any point of the chain, as is showed in Figure 7 a). This value is dependent of the solvent too, because the polymer chains have the tendency to shrink or to swell in function of the interactions with the solvent. The “hydrodynamic radius” (R_h) of a polymer in one solvent is the radius of a hard sphere that diffuses at the same speed in this same solvent, as is showed in Figure 7 b). This radius takes in account the size of the chain and the interaction between the solute and the solvent.

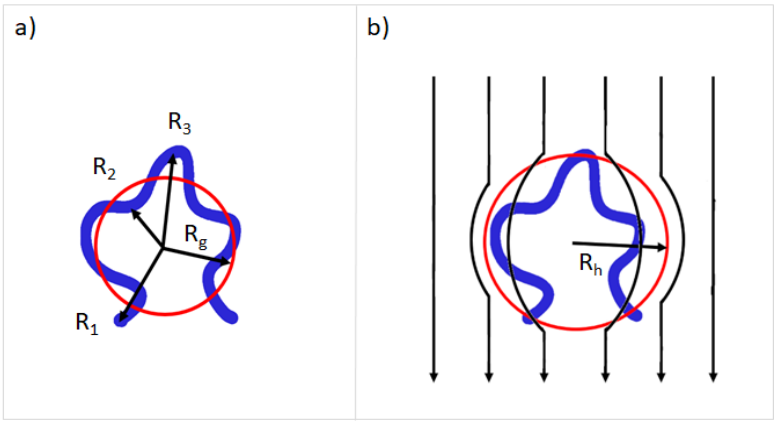

Figure 7. *Schematic illustration of a) radius of gyration and b) hydrodynamic radius of a polymer.*

The reduction the radius, and therefore, the correct folding of the polymeric chain can be monitored by different characterization techniques, which used in combination can prove the formation of the single-chain nanoparticle. The most commonly used characterization techniques in the SCNPs field are the size exclusion chromatography (SEC), dynamic light scattering (DLS) and nuclear magnetic resonance spectroscopy (NMR).

Due to the availability and ease of use, SEC techniques in general, and the gel permeation chromatography (GPC) in particular, are one of the most used analytical tools in polymer science and also in the SCNPs field. Although the morphology of the nanoparticle can be very different from the employed linear calibration standards, the reduction of the hydrodynamic radius can be observed by the shift to higher retention times [57] (see Figure 8). Moreover, with a good detectors election, GPC technique can obtain the absolute molecular weight and the radius of gyration of the sample, allowing to observe a reduction of the size while the mass is constant, a proof that the sample has been compacted.

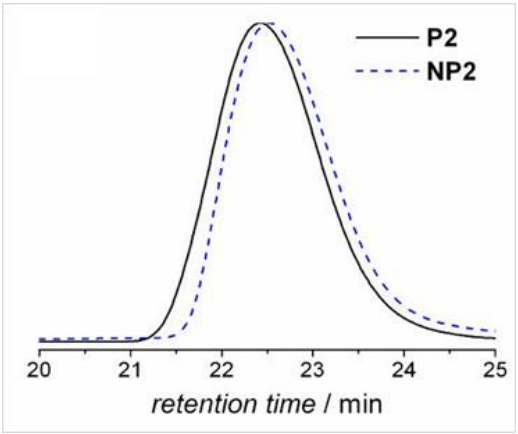

Figure 8. GPC chromatogram showing the size reduction of the SCNPs (NP2) from the polymer precursor (P2) [57].

Likewise, DLS technique measure the light scattering of the sample to determine the diffusion coefficient in solution, and from this the hydrodynamic radius. The radius is presented as an intensity percentage in function of the size of the sample, being able to differentiate samples of very different sizes. So, in this case, the SCNPs formation can be checked by the displacement of the signal to the left, to smaller sizes, as can see in the Figure 9 [57]. However, as the intensity is proportional to the sixth power of the particle diameter, the scattering intensity is heavily weighted towards large particles. Furthermore, the measurement can be difficult with samples that interact with the light, such as the colored and fluorescent samples.

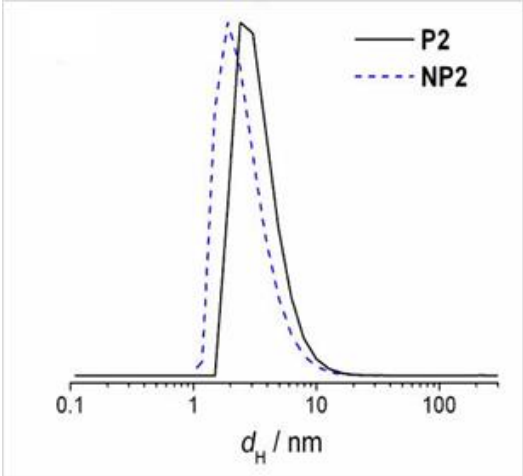

Figure 9. DLS result showing the size reduction of the SCNPs (NP2) from the polymer precursor (P2) [57].

NMR spectroscopy can be used to monitor the chain folding reaction, observing the disappearance or shift of peaks associated with the cross-linking moieties, confirming that the compaction reaction is carried out correctly. Furthermore, with diffusion-ordered NMR techniques the diffusion coefficient, and therefore, the hydrodynamic radius can be obtained [58, 59].

Moreover, the small angle scattering techniques, as neutron scattering (SANS) or x-ray scattering (SAXS), can be used to determine the form factor of the sample in solution [46, 47, 60, 61]. These techniques are used to obtain the radius of gyration and the form factor, allowing to check not only the size reduction, but also the compaction of the polymer chain to a more globular-like shape. In the Figure 10 is shown a result of SAXS experiment reported by ter Huume et al. with the comparison of SCNPs of hydrophilic polymers grafted with chiral units of 3,3'-bis(acylamino)-2,2'-bipyridine-substituted benzene-1,3,5-tricarboxamides at different solvent composition (mixtures of THF and water with volume fraction of ϕ_{THF} = 0.1, ϕ_{THF} = 0.4, and ϕ_{THF} = 1.0) [62]. This polymer is insoluble in pure water, so as expected, have a more compact conformation in the THF/water mixtures than the in the pure THF. That can be observe by the steeper slope in

ϕ_{THF} = 0.1 and ϕ_{THF} = 0.4 cases than the ϕ_{THF} = 1.0 case. In this sense, in a comparison between a SCNP and his precursor polymer a steeper slope is expected for the nanoparticle.

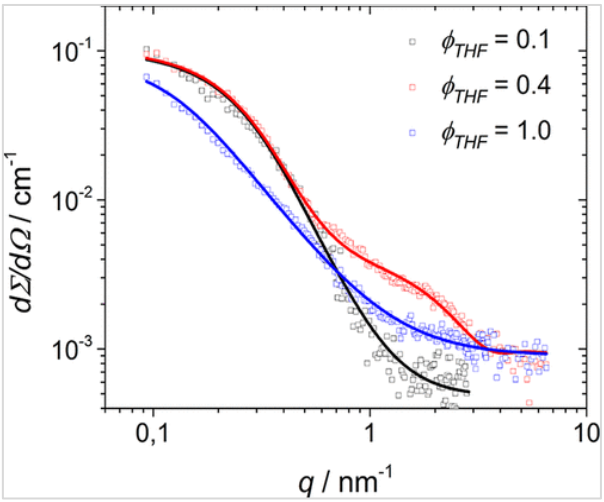

Figure 10. SAXS results in various solvent compositions, showing the compaction differences in function of the solvent [62]. As ϕ_{THF} = 0.1 and ϕ_{THF} = 0.4 are not good solvent for the sample the result shows a compaction in these cases.

Another characterization techniques, as the Infra-Red Spectroscopy (IR) or Elemental Analysis (EA), are used to check the carrying out of the reactions. Just like NMR, the appearance or disappearance of absorption peaks in the IR spectroscopy allows to check the elemental changes in the sample [63]. Moreover, with the Elemental Analysis (EA), quantitative mass percentage of some elements (hydrogen, carbon, oxygen and nitrogen) can be obtained [64].

Additionally, thermal characterizations, such as Thermogravimetric Analysis (TGA) and Differential Scanning Calorimetry (DSC), are useful tools in the SCNPs field. TGA is useful for studying the thermal stability and decomposition behavior of single-chain nanoparticles, that differs from the precursor's properties due to the compaction and the presence of the intra-chain bonds [65]. DSC is a widely used technique in the polymer field to measure the heat flow associated with phase transitions in materials. It can provide information about the thermal transitions, such as melting or crystallization, which can be important for understanding the stability and behavior of single-chain nanoparticles [66]. DSC technique is very used to obtain the glass-transition temperature (T_g), that is a critical temperature at which the polymer undergoes a transition from a rigid, glassy state to a more flexible, rubbery state.

1.1.4. Potential applications of SCNPs

The potential applications of SCNPs include catalysis, sensors and nanomedicine, as are showed in the Figure 11. The advantageous features of SCNP technology in these domains are largely attributed to the nanoparticles' small size and their adaptability to specific purposes. While the

research on SCNPs has predominantly been of a fundamental nature, these materials have found practical applications. By design, the interior of the particle offers a useful chemical environment. The environment can be hydrophobic or hydrophilic, and the size can be controlled by varying the amount of intra-chain cross-linking and the molecular weight of the precursor polymer. Additionally, controlled polymerization techniques and post-polymerization modification techniques allow the incorporation of selective sites for desired function. The following section summarizes recent applied research involving SCNPs.

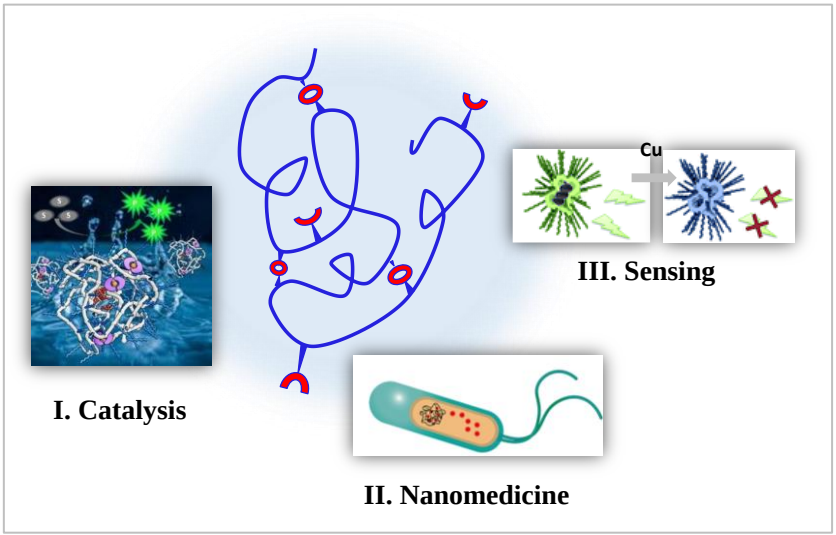

Figure 11. Illustration of some examples of potential applications of SCNPs: I) Caralysis, II) Nanomedicine and III) Sensing.

I. Catalysis

The SCNPs similarity with the proteins, because of the folding, propose one of the applications: the catalysis systems. Enzymes are proteins that accelerate the cellular biological chemical reactions enormously. As other catalyst, enzymes can low the activation energy to increase the reaction rate and are more specific that other catalyst. Is well know that the structure of the enzymes is important for their function, so there are many studies of the nature and characteristics of the enzymes [67, 68]. Due to the efficiency of these reactions, there are research to mimic the function of enzymes to synthesize different molecules, as polymers [69]. There are attempts to imitate this effect with synthetic structures; as the nanoreactors, nanosized vessels systems with catalyst inside that provide to the reaction a different environment that protect the catalyst and have a high surface area and volume ratio that favors the reactions. There are different proposals as yolk-shell system with metallic catalyst as nucleus and silica or polymeric coatings [70, 71], protein cages [72], core-shell microgels [73] or polymersome (polymeric vessels) [74-80]. Of course, SCNPs are too a good candidate for these systems thanks to their properties [81-83].

II. Sensing

SCNPs can be used in sensor technologies for detecting various analytes. Their size and surface properties make them suitable for sensing applications in fields such as environmental monitoring and medical diagnostics. In addition, the reversibility of the SCNPs allows using as responsive materials that can open and close, changing from chain form to particle form in a specific condition. Therefore, can be used to detect that condition that allows opening or closing. Using a group that only is detectable when the nanoparticle is opened or closed, as an aggregation induced emission molecules, the form of the SCNPs can be detected, and therefore, the environmental conditions of them.

SCNPs can be functionalized to create biosensors that can be used for the detection of specific biomolecules, pathogens, or other biological markers, as such the detection of zein protein reported by Pomposo et al. [84]. SCNPs can be tailored too to detect specific chemical analytes. Functionalizing the surface of SCNPs with ligands or receptors that selectively interact with target molecules enables the development of chemical sensors with high selectivity and sensitivity. Palmans et al. reported a method to synthesize SCNPs for sensor of metal ions [85]. Nanoparticles have been investigated for gas sensing applications too. Their small size and high surface-to-volume ratio make them suitable for detecting gases through interactions at the nanoparticle surface, as for example, the carbon dioxide-responsive SCNPs reported by Fan et al. [86]. Gas sensors based on SCNPs can be used for environmental monitoring, industrial safety, and healthcare applications.

On the other hand, environmental conditions as pH [87] or temperature [58] can be detected by SCNPs. This can be particularly valuable in biomedical and environmental monitoring where pH or temperature variations are relevant indicators.

III. Nanomedicine

Nanomedice is the application of the nanotechnology in the medicine field, using a nanometric objects to protect human health [6]. The size of the SCNPs allows their use inside the human body, but should be biocompatible to avoid the creation of new health problems. Several cytotoxicity studies have already shown the non-toxic character of several SCNPs [88-90]. In this sense, SCNPs are promising candidates for different nanomedicine applications. Mainly, there are two applications for SCNPs: drug delivery and imaging.

Because of them reduce size SCNPs can encapsulate and deliver small quantities of drugs, using the reversibility to open and releasing them. The control of this delivery allows increasing the

effectivity, reducing the quantities of drugs and it contact with the healthy cells. Therefore, the toxicity of the treatment can be reduced radically [91]. For example, Cheng et al. presents stimuli-responsive single-chain nanoparticle that reside stably in tumor-like microenvironments, providing new insight for drugs-deliver by SCNPs [92].

On the other hand, encapsulating contrast compounds, SCNP can be used as contrast agent or luminescent markers, reducing the toxicity of these molecules. The use of single-chain nanoparticles has been studied as image contrast for Pump–probe Photoacoustic Imaging [93] Magnetic Resonance Imaging [94, 95], using metal-complexed SCNPs, and as gamma emitters for single photon emission computerized tomography [90]. Additionally, fluorescent SCNPs, which can be used for medical imaging, have been synthesized [85, 89, 95-100].

IV. Other applications

Although the three mentioned above are the most common applications, there are other uses of single chain-nanoparticles. SCNPs have potential applications in the development of advanced materials with tailored properties. By manipulating the polymer chain structure, researchers can create materials with specific mechanical, thermal, or electrical properties, making them suitable for various applications, including coatings and advanced composites. Despite being more particular applications that are still in development, the use of nanoparticles has been investigated for the engineering of nanostructures [101], the enhanced oil recovery [102] or the fabrication of plasmonic nanoparticles [103], hydrophobic coating [104] and resistant hydrophobic cotton [105, 106].

References

[1] W. Hu, The physics of polymer chain-folding, *Physics Reports* **2018**, 747, 1-50.

[2] C. K. Lyon, A. Prasher, A. M. Hanlon, B. T. Tuten, C. A. Tooley, P. G. Frank, E. B. Berda, A Brief User's Guide to Single-Chain Nanoparticles. *Polymer Chemistry* **2015**, 6, 181-197.

[3] C. Liu, C.-Y. Hong, C.-Y. Pan, Polymerization techniques in polymerization-induced self-assembly (PISA), *Polymer Chemistry* **2020**, 11, 3673-3689.

[4] K. W. Scott, An experimental verification of gel network formation theories, *Journal of Polymer Science* **1962**, 58, 517-532.

[5] E. Harth, B. Van Horn, V. Y. Lee, D. S. Germack, C. P. Gonzales, R. D. Miller, C. J. Hawker, A facile approach to architecturally defined nanoparticles via intramolecular chain collapse, *Journal of the American Chemical Society* **2002**, 124, 8653–8660.

[6] N. M. Hamelmann, J. M. J. Paulusse, Single-chain polymer nanoparticles in biomedical applications. *Journal of Controlled Release* **2023**, 356, 26-42.

[7] Y. Yang, X. Liu, X. Li, J. Zhao, S. Bai, J. Liu, Q. Yang, A Yolk-Shell Nanoreactor with a Basic Core and an Acidic Shell for Cascade Reactions. *Angewandte Chemie International Edition* **2012**, 51, 9164-9168.

[8] S. Perrier, 50th Anniversary Perspective: RAFT Polymerization—A User Guide, *Macromolecules* **2017**, 50, 7433-7447.

[9] G. Moad, J. Chiefari, Y.K. Chong, J. Krstina, R.T.A. Mayadunne, A. Postma, E. Rizzardo, S.H. Thang, Living free radical polymerization with reversible addition – fragmentation chain transfer (the life of RAFT), *Polymer International* **2000**, 49, 993-1001.

[10] T. Terashima, T. Sugita, K. Fukae, M. Sawamoto, Synthesis and Single-Chain Folding of Amphiphilic Random Copolymers in Water, *Macromolecules* **2014**, 47, 2, 589–600.

[11] J. Lu , N. ten Brummelhuis, M. Weck, Intramolecular folding of triblock copolymers via quadrupole interactions between poly(styrene) and poly(pentafluorostyrene) blocks, *Chemical Communications* **2014**, 50, 6225-6227.

[12] E. B. Berda, E. J. Foster, E. W. Meijer, Toward Controlling Folding in Synthetic Polymers: Fabricating and Characterizing Supramolecular Single-Chain Nanoparticles. *Macromolecules* **2010**, 43, 1430-1437.

[13] A. Sanchez-Sanchez, A. Arbe, J. Colmenero, J. A. Pomposo, Metallo-Folded Single-Chain Nanoparticles with Catalytic Selectivity, *ACS Macro Letters* **2014**, 3, 5, 439–443.

[14] E. A. Appel, J. Dyson, J. del Barrio, Z. Walsh, O. A. Scherman, Formation of Single-Chain Polymer Nanoparticles in Water through Host–Guest Interactions, *Angewandte Chemie International Edition* **2012**, 51, 17, 4185-4189.

[15] R. Lambert, A.-L. Wirotius, D. Taton, Intramolecular Quaternization as Folding Strategy for the Synthesis of Catalytically Active Imidazolium-Based Single Chain Nanoparticles, *ACS Macro Letters* **2017**, 6, 5, 489–494.

[16] V.A. Davankov, M.M. Ilyin, M.P. Tsyurupa, G.I. Timofeeva, L. V. Dubrovina, From a dissolved polystyrene coil to an intramolecularly-hyper-cross-linked "Nanosponge", *Macromolecules* **1996**, 29, 8398–8403.

[17] D. Mecerreyes, V. Lee, C.J. Hawker, J.L. Hedrick, A. Wursch, W. Volksen, T. Magbitang, E. Huang, R.D. Miller, A Novel Approach to Functionalized Nanoparticles: Self-Crosslinking of Macromolecules in Ultradilute Solution, *Advanced Materials* **2001**, 13 204-208.

[18] R.K. Iha, K.L. Wooley, A.M. Nyström, D.J. Burke, M.J. Kade, C.J. Hawker, Applications of orthogonal "Click" chemistries in the synthesis of functional soft materials. *Chemical Reviews* **2009**, 109, 5620–5686.

[19] J.B. Beck, K.L. Killops, T. Kang, K. Sivanandan, A. Bayles, M.E. Mackay, K. L. Wooley, C. J. Hawker, Facile preparation of nanoparticles by intramolecular cross-linking of isocyanate functionalized copolymers. *Macromolecules* **2009**, 42, 5629–5635.

[20] A. R. de Luzuriaga, N. Ormategui, H. J. Grande, I. Odriozola, J. A. Pomposo, I. Loinaz, Intramolecular Click Cycloaddition: An Efficient Room-Temperature Route towards Bioconjugable Polymeric Nanoparticles. *Macromolecular Rapid Communications* **2008**, 29, 1156-1160.

[21] L. Oria, R. Aguado, J.A. Pomposo, J. Colmenero, A versatile "Click" chemistry precursor of functional polystyrene nanoparticles. *Advanced Materials* **2010**, 22, 3038–3041.

[22] A. Ruiz de Luzuriaga, I. Perez-Baena, S. Montes, I. Loinaz, I. Odriozola, I. García, J.A. Pomposo (2010) New route to polymeric nanoparticles by click chemistry using bifunctional crosslinkers. *Macromolecular Symposia* **2010**, 296, 303–310.

[23] T. A. Croce, S. K. Hamilton, M. L. Chen, H. Muchalski, E. Harth, Alternative o-Quinodimethane Cross-Linking Precursors for Intramolecular Chain Collapse Nanoparticles, *Macromolecules*, **2007**, 40, 6028–6031.

[24] A. Sanchez-Sanchez, D.A. Fulton, J.A. Pomposo, pH-responsive single-chain polymer nanoparticles utilising dynamic covalent enamine bonds, *Chemical Communications* **2014**, 50, 15, 1871-1874.

[25] J.B. Beck, K.L. Killops, T. Kang, K. Sivanandan, A. Bayles, M.E. Mackay, K.L. Wooley, C.J. Hawker, Facile preparation of nanoparticles by intramolecular cross-linking of isocyanate functionalized copolymers, *Macromolecules* **2009**, 42, 15, 5629-5635.

[26] A.P.P. Kröger, R.J.E.A. Boonen, J.M.J. Paulusse Well-defined single-chain polymer nanoparticles via thiol-Michael addition, *Polymer* **2017**, 120, 119-128.

[27] A.P.P. Kröger, N.M. Hamelmann, A. Juan, S. Lindhoud, J.M.J. Paulusse Biocompatible single-chain polymer nanoparticles for drug delivery—a dual approach, *ACS Applied Materials & Interfaces* **2018**, 10, 37, 30946-30951.

[28] A.P.P. Kröger, J.-W.D. Paats, R.J.E.A. Boonen, N.M. Hamelmann, J.M.J. Paulusse Pentafluorophenyl-based single-chain polymer nanoparticles as a versatile platform towards protein mimicry, *Polymer Chemistry* **2020**, 11, 37, 6056-6065.

[29] D. M. Stevens, S. Tempelaar, A. P. Dove and E. Harth, Nanosponge formation from organocatalytically-synthesized poly(carbonate) copoplymers, *ACS Macro Letters* **2012**, 1, 915–918.

[30] D. Chao, X. Jia, B. Tuten, C. Wang, E. B. Berda, Controlled folding of a novel electroactive polyolefin via multiple sequential orthogonal intra-chain interactions, *Chemical Communications* **2013**, 49, 4178–4180.

[31] J. B. Beck, K. L. Killops, T. Kang, K. Sivanandan, A. Bayles, M. E. Mackay, K. L. Wooley, C. J. Hawker, Facile Preparation of Nanoparticles by Intramolecular Crosslinking of Isocyanate Functionalized Copolymers, *Macromolecules* **2009**, 42, 5629–5635.

[32] C. F. Hansell, A. Lu, J. P. Patterson, R. K. O'Reilly, Exploiting the tetrazine–norbornene reaction for single polymer chain collapse, *Nanoscale* **2014**, 6, 4102–4107.

[33] B. S. Murray, D. A. Fulton, Dynamic Covalent Single-Chain Polymer Nanoparticles, *Macromolecules* **2011**, 44, 18, 7242–7252.

[34] B. S. Murray, A. W. Jackson, C. S. Mahon, D. A. Fulton, Reactive thermoresponsive copolymer scaffolds, *Chemical Communications* **2010**, 46, 8651-8653.

[35] B. T. Tuten, D. Chao, C. K. Lyonb, E. B. Berda, Single-chain polymer nanoparticles *via* reversible disulfide bridges, *Polymer Chemistry* **2012**, 3, 3068-3071.

[36] T. Mes, R. van der Weegen, A. R. A. Palmans, E. W. Meijer, Single-Chain Polymeric Nanoparticles by Stepwise Folding. *Angewandte Chemie International Edition* **2011**, 50, 5085–5089.

[37] P. J. M. Stals, M. A. J. Gillissen, T. F. E. Paffen, T. F. A. de Greef, P. Lindner, E. W. Meijer, A. R. A. Palmans, I. K. Voets, Folding Polymers with Pendant Hydrogen Bonding Motifs in Water: The Effect of Polymer Length and Concentration on the Shape and Size of Single-Chain Polymeric Nanoparticles, *Macromolecules* **2014**, 47, 9, 2947–2954.

[38] N. Hosono, L. M. Pitet, A. R. A. Palmans, E. W. Meijer, The effect of pendant benzene-1,3,5-tricarboxamides in the middle block of ABA triblock copolymers: synthesis and mechanical properties, *Polymer Chemistry* **2014**, 5, 1463-1470.

[39] V. Kobernik, R. S. Phatake, J. Tzadikov, O. Reany, N. G. Lemcoff, Organometallic single-chain polymer nanoparticles *via* intra-chain cross-linking with dinuclear μ-halo(diene)Rh(I) complexes, *Reactive and Functional Polymers* **2021**, 165, 104971.

[40] A. Nitti, R. Carfora, G. Assanelli, M. Notari, D. Pasini, Single-Chain Polymer Nanoparticles for Addressing Morphologies and Functions at the Nanoscale: A Review. *ACS Applied Nano Materials* **2022**, 5, 13985-13997.

[41] X. Ji, Y. Zhang, H. Zhao, Amphiphilic Janus Twin Single-Chain Nanoparticles, *Chemistry – A European Journal* **2018**, 24, 3005.

[42] E. Harth, B. Van Horn, V. Y. Lee, D. S. Germack, C. P. Gonzales, R. D. Miller, C. J. Hawker, A Facile Approach to Architecturally Defined Nanoparticles via Intramolecular Chain Collapse, *Journal of the American Chemical Society* **2002**, 124, 29, 8653–8660.

[43] G. M. ter Huurne, A. R. A. Palmans, E. W. Meijer, Supramolecular Single-Chain Polymeric Nanoparticles, *CCS Chemistry* **2019**, 1, 1, 64-82.

[44] P. Wang, H. Pu, J. Ge, M. Jin, H. Pan, Z. Chang, D. Wan, Fluorescence-labeled hydrophilic nanoparticles via single-chain folding, *Materials Letters* **2014**, 132, 102-105.

[45] J. A. Pomposo, I. Perez-Baena, F. Lo Verso, A. J. Moreno, A. Arbe, J. Colmenero, How Far Are Single-Chain Polymer Nanoparticles in Solution from the Globular State?, *ACS Macro Letters* **2014**, 3, 767-772.

[46] A. J. Moreno, F. Lo Verso, A. Sanchez-Sanchez, A. Arbe, J. Colmenero, J. A. Pomposo, Advantages of Orthogonal Folding of Single Polymer Chains to Soft Nanoparticles, *Macromolecules* **2013**, 46, 9748-9759.

[47] A. Sanchez-Sanchez, S. Akbari, A. Etxeberria, A. Arbe, U. Gasser, A. J. Moreno, J. Colmenero, J. A. Pomposo, "Michael" Nanocarriers Mimicking Transient-Binding Disordered Proteins, *ACS Macro Letters* **2013**, 2, 491-495.

[48] A. M. Stadler, L. Stingaciu, A. Radulescu, O. Holderer, M. Monkenbusch, R. Biehl, D. Richter, Internal Nanosecond Dynamics in the Intrinsically Disordered Myelin Basic Protein, *Journal of the American Chemical Society* **2014**, 136, 6987-6994.

[49] F. Lo Verso, J. A. Pomposo, J. Colmenero, A. J. Moreno, Simulation guided design of globular single-chain nanoparticles by tuning the solvent quality, *Soft Matter* **2015**, 11, 1369-1375.

[50] F. Lo Verso, J. A. Pomposo, J. Colmenero, A. J. Moreno, Multi-orthogonal folding of single polymer chains into soft nanoparticles, *Soft Matter* **2014**, 10, 4813-4821.

[51] M. Vert, Y. Doi, K.-H. Hellwich, M. Hess, P. Hodge, P. Kubisa, M. Rinaudo, F. Schué, Terminology for biorelated polymers and applications (IUPAC Recommendations 2012), *Pure and Applied Chemistry* **2012**, 84, 377-410.

[52] I. Perez-Baena, I. Asenjo-Sanz, A. Arbe, A. J. Moreno, F. Lo Verso, J. Colmenero, J. A. Pomposo, Efficient Route to Compact Single-Chain Nanoparticles: Photoactivated Synthesis via Thiol–Yne Coupling Reaction, *Macromolecules* **2014**, 47, 8270-8280.

[53] T. Terashima, T. Sugita, K. Fukae, M. Sawamoto, Synthesis and Single-Chain Folding of Amphiphilic Random Copolymers in Water, *Macromolecules* **2014**, 47, 589-600.

[54] T. Akagi, P. Piyapakorn, M. Akashi, Formation of Unimer Nanoparticles by Controlling the Self-Association of Hydrophobically Modified Poly(amino acid)s, *Langmuir* **2012**, 28, 5249-5256.

[55] M. Chen, C. J. Riddles, M. R. Van De Mark, Electroviscous Contribution to the Rheology of Colloidal Unimolecular Polymer (CUP) Particles in Water, *Langmuir* **2013**, 29, 14034-14043.

[56] A. M. Hanlon, K. J. Rodriguez, R. Chen, E. Bright, E. B. Berda, Characterization of Single-Chain Polymer Nanoparticles: Analytical Techniques. *Single-Chain Polymer Nanoparticles: Synthesis, Characterization, Simulations, and Applications*; J. A. Pomposo, Ed.; John Wiley & Sons: Weinheim, Germany **2017**.

[57] E. H. H. Wong, S. Jie Lam, E. Nam, and G. G. Qiao, Biocompatible Single-Chain Polymeric Nanoparticles via Organo-Catalyzed Ring-Opening Polymerization, *ACS Macro Letters* **2014**, 3, 6, 524–528.

[58] N. Ormategui, I. García, D. Padro, G. Cabañero, H. J. Grande, I. Loinaz, Synthesis of single chain thermoresponsive polymer nanoparticles, *Soft Matter* **2012**, 8, 734-740.

[59] C. Heiler, J. T. Offenloch, E. Blasco, C. Barner-Kowollik, Photochemically Induced Folding of Single Chain Polymer Nanoparticles in Water, *ACS Macro Letters* **2017**, 6, 1, 56–61.

[60] N. Hosono, M. A. J. Gillissen, Y. Li, S. S. Sheiko, A. R. A. Palmans, E. W. Meijer, Orthogonal Self-Assembly in Folding Block Copolymers, *Journal of the American Chemical Society* **2013**, 135, 1, 501–510.

[61] I. Perez-Baena, F. Barroso-Bujans, U. Gasser, A. Arbe, A. J. Moreno, J. Colmenero, J. A. Pomposo, Endowing Single-Chain Polymer Nanoparticles with Enzyme-Mimetic Activity. *ACS Macro Letters* **2013**, 2, 775–779.

[62] G. M. ter Huurne, M. A. J. Gillissen, A. R. A. Palmans, I. K. Voets, E. W. Meijer, The Coil-to-Globule Transition of Single-Chain Polymeric Nanoparticles with a Chiral Internal Secondary Structure, *Macromolecules* **2015**, 48, 12, 3949–3956.

[63] O. Altintas, C. Barner-Kowollik, Single-Chain Folding of Synthetic Polymers: A Critical Update. *Macromolecule rapid communication* **2016**, 37, 29–46.

[64] A. Sanchez-Sanchez, J. A. Pomposo, Efficient Synthesis of Single-Chain Polymer Nanoparticles *via* Amide Formation, *Journal of Nanomaterials* **2015**, 2015, 723492.

[65] D. Xiang, B. Jiang, F. Liang, L. Yan, Z. Yang, Single-Chain Janus Nanoparticle by Metallic Complexation, *Macromolecules* **2020**, 53, 3, 1063–1069.

[66] A. Arbe, J. Rubio-Cervilla, A. Alegría, A. J. Moreno, J. A. Pomposo, B. Robles-Hernández, P. Malo de Molina, P. Fouquet, F. Juranyi, J. Colmenero, Mesoscale Dynamics in Melts of Single-Chain Polymeric Nanoparticles, *Macromolecules* **2019**, 52, 18, 6935–6942.

[67] P. A. Fitzpatrick, A. C. U. Steinmetz, D. Ringe, A. M. Klibanov, Enzyme Crystal Structure In A Neat Organic Solvent. *Proceedings of the National Academy of Sciences of the United States of America* **1993**, 90, 8653.

[68] R. Callender, R. B. Dyer, The Dynamical Nature of Enzymatic Catalysis. *Accounts of Chemical Research* **2015**, 48, 407-413

[69] J. Kadokawa, S. Kobayashi, Polymer synthesis by enzymatic catalysis. *Current Opinion in Chemical Biology* **2010**, 14, 145-153

[70] J. Liu, S. Z. Qiao, J. S. Chen, X. W. (David) Lou, X. Xing, G. Q. (Max) Lu, Yolk/shell nanoparticles: new platforms for nanoreactors, drug delivery and lithium-ion batteries. *Chemical Communications* **2011**, 47, 12578-12591

[71] J. Lee, J. C. Park, H. Song, A Nanoreactor Framework of a Au@SiO2 Yolk/Shell Structure for Catalytic Reduction of p-Nitrophenol. *Advanced Materials* **2008**, 20, 1523-1528.

[72] A. de la Escosura, R. J. M. Nolte, J. J. L. M. Cornelissen, Viruses and protein cages as nanocontainers and nanoreactors. *Journal of Materials Chemistry* **2009**, 19, 2274-2278.

[73] Y. Lu, M. Ballauff, Thermosensitive core–shell microgels: From colloidal model systems to nanoreactors. *Progress in Polymer Science* **2011**, 36, 767-792.

[74] H. Che, J. C. M. van Hest, Stimuli-responsive polymersomes and nanoreactors. *Journal of materials chemistry. B, Materials for Biology and Medicine* **2016**, 4, 4632-4647.

[75] K. Renggli, P. Baumann, K. Langowska, O. Onaca, N. Bruns, W. Meier, Selective and Responsive Nanoreactors. *Advanced Functional Materials* **2011**, 21, 1241-1259.

[76] M. Spulber, A. Najer, K. Winkelbach, O. Glaied, M. Waser, U. Pieles, W. Meier, N. Bruns, Photoreaction of a Hydroxyalkyphenone with the Membrane of Polymersomes: A Versatile Method To Generate Semipermeable Nanoreactors. *Journal of the American Chemical Society* **2013**, 135, 9204-9212.

[77] I. Louzao, J. C. M. van Hest, Permeability Effects on the Efficiency of Antioxidant Nanoreactors. *Biomacromolecules* **2013**, 14, 2364-2372.

[78] M. Grzelakowski, O. Onaca, P. Rigler, M. Kumar, W. Meier, Immobilized Protein-Polymer Nanoreactors. *Small* **2009**, 5, 2545-2548.

[79] K. T. Kim, J. J. L. M. Cornelissen, R. J. M. Nolte, J. C. M. van Hest, A Polymersome Nanoreactor with Controllable Permeability Induced by Stimuli-Responsive Block Copolymers. *Advanced Materials* **2009**, 21, 2787-2791.

[80] Z. Wei, C.-H. Liu, Q. Luo, S. Thanneeru, A. M. Angeles-Boza, M.-P. Nieh, J. He, Hydrophobic pockets built in polymer micelles enhance the reactivity of Cu^{2+} ions, *Materials Chemistry Frontiers* **2023**, 7, 2038-2048.

[81] J. Chen, K. Li, S. E. Bonson, S. C. Zimmerman, A Bioorthogonal Small Molecule Selective Polymeric "Clickase". *Journal of the American Chemical Society* **2020**, 142, 13966-13973.

[82] J.A. Pomposo, Bioinspired single-chain polymer nanoparticles, *Polymer International* **2014**, 63 589-592.

[83] J. Rubio-Cervilla, E. González, J.A. Pomposo, Advances in Single-Chain Nanoparticles for Catalysis Applications, *Nanomaterials* **2017**, 7, 341.

[84] A. Latorre-Sanchez, J.A. Pomposo, A simple, fast and highly sensitive colorimetric detection of zein in aqueous ethanol via zein–pyridine–gold interactions, *Chemical Communications* **2015**, 51, 15736-15738.

[85] M.A.J. Gillissen, I.K. Voets, E.W. Meijer, A.R.A. Palmans, Single chain polymeric nanoparticles as compartmentalised sensors for metal ions, *Polymer Chemistry* **2012**, 3, 3166-3174.

[86] W. Fan, X. Tong, F. Farnia, B. Yu, Y. Zhao, CO_2-Responsive Polymer Single-Chain Nanoparticles and Self-Assembly for Gas-Tunable Nanoreactors, *Chemistry of Materials* **2017**, 29, 13, 5693–5701.

[87] Z. Zhang, K. Bando, K. Mochizuki, A. Taguchi, K. Fujita, S. Kawata, Quantitative Evaluation of Surface-Enhanced Raman Scattering Nanoparticles for Intracellular pH Sensing at a Single Particle Level, *Analytical Chemistry* **2019**, 91, 5, 3254–3262.

[88] E. H. H. Wong, S. J. Lam, E. Nam, G. G. Qiao, Biocompatible Single-Chain Polymeric Nanoparticles via Organo-Catalyzed Ring-Opening Polymerization, *ACS Macro Letters* **2014**, 3, 524-528.

[89] Y. Bai, H. Xing, G. A. Vincil, J. Lee, E. J. Henderson, Y. Lu, N. G. Lemcoff, S. C. Zimmerman, Practical synthesis of water-soluble organic nanoparticles with a single reactive group and a functional carrier scaffold, *Chemical Science* **2014**, 5, 2862-2868.

[90] A. B. Benito, M. K. Aiertza, M. Marradi, L. Gil-Iceta, T. Shekhter Zahavi, B. Szczupak, M. Jimenez-Gonzalez, T. Reese, E. Scanziani, L. Passoni, M. Matteoli, M. De Maglie, A. Orenstein, M. Oron-Herman, G. Kostenich, L. Buzhansky, E. Gazit, H. J. Grande, V. Gomez-Vallejo, J. Llop, I. Loinaz, Functional Single-Chain Polymer Nanoparticles: Targeting and Imaging Pancreatic Tumors in Vivo, *Biomacromolecules* **2016**, 17, 3213-3221.

[91] J. Rubio-Cervilla, E. González, J.A. Pomposo, Applications of Single-Chain Polymer Nanoparticles, *Wiley-VCH* **2017**, 341-400.

[92] C. Cheng, D. Lee, Z. Liao, J. Huang, Stimuli-responsive single-chain polymeric nanoparticles towards the development of efficient drug delivery systems. *Polymer Chemistry* **2016**, 7, 6164-6169.

[93] J. F. Thümmler, A. H. Roos, J. Krüger, D. Hinderberger, F.-J. Schmitt, G. Tang, F. Ghane Golmohamadi, J. Laufer, W. H. Binder, Tuning the Internal Compartmentation of Single-Chain Nanoparticles as Fluorescent Contrast Agents, *Macromolecular Rapid Communications* **2023**, 44, 2200618.

[94] I. Perez-Baena, I. Loinaz, D. Padro, I. García, H.J. Grande, I. Odriozola, Single-chain polyacrylic nanoparticles with multiple Gd(iii) centres as potential MRI contrast agents, *Journal of Materials Chemistry* **2010**, 20, 6916-6922.

[95] C. T. Adkins, J. N. Dobish, S. Brown, E. Harth, Water-Soluble Semiconducting Nanoparticles for Imaging, *ACS Macro Letters* **2013**, 2, 710-714.

[96] C. Song, L. Li, L. Dai, S. Thayumanavan, Responsive single-chain polymer nanoparticles with host–guest features, *Polymer Chemistry* **2015**, 6, 4828-4834.

[97] G. Qian, B. Zhu, Y. Wang, S. Deng, A. Hu, Size-Tunable Polymeric Nanoreactors for One-Pot Synthesis and Encapsulation of Quantum Dots, *Macromolecular Rapid Communications* **2012**, 33, 1393-1398.

[98] C. K. Lyon, E. O. Hill, E. B. Berda, Zipping Polymers into Nanoparticles via Intrachain Alternating Radical Copolymerization, *Macromolecular Chemistry and Physics* **2016**, 217, 501-508.

[99] C. T. Adkins, H. Muchalski, E. Harth, Nanoparticles with Individual Site-Isolated Semiconducting Polymers from Intramolecular Chain Collapse Processes, *Macromolecules* **2009**, 42, 5786-5792.

[100] G. Li, F. Tao, L. Wang, Y. Li, R. Bai, A facile strategy for preparation of single-chain polymeric nanoparticles by intramolecular photo-crosslinking of azide polymers, *Polymer* **2014**, 55, 3696-3702.

[101] H. He, X. Shen, Z. Nie, Engineering interactions between nanoparticles using polymers, *Progress in Polymer Science* **2023**, 143, 101710.

[102] C. A. Paternina, H. Quintero, R. Mercado, Improving the interfacial performance and the adsorption inhibition of an extended-surfactant mixture for enhanced oil recovery using different hydrophobicity nanoparticles, *Fuel* **2023**, 350, 128760.

[103] M. Distaso, W. Peukert, A biphasic batch and continuous flow synthesis of hydrophobic gold and silver nanoparticles, *Reaction Chemistry & Engineering* **2023**, 8, 1855-1867.

[104] B. Yu, H. Liu, H. Chen, W. Li, L. Zhu, W. Liang, A wear and heat-resistant hydrophobic fluoride-free coating based on modified nanoparticles and waterborne-modified polyacrylic resin, *RSC Advances* **2023**, 13, 4542-4552.

[105] S. Zhang, K. Fang, X. Liu, M. Cheng, D. Liu, X. Qiao, J. Wang, Polymethylhydrosiloxane and ZIF-8/color nanoparticles enhanced the UV-resistance, antibacterial and hydrophobicity performance of cotton fabrics, *Progress in Organic Coatings* **2023**, 182, 107702.

[106] S. Zhang, K. Fang, X. Liu, D. Liu, X. Qiao, J. Wang, F. Sun, Enhanced hydrophobicity and UV resistance of cotton fabrics through the synergistic effect of raspberry-shaped colored nanoparticles and polymethylhydrosiloxane, *Applied Surface Science* **2023**, 637, 157849.

2. Motivation and goals

The motivation of this thesis is to explore metal-free synthetic methods for single-chain nanoparticles (SCNPs). While several SCNP synthetic methods have been reported, many exhibit significant drawbacks. Numerous methods rely on a metallic catalyst to form the intra-chain bond, but these catalysts often become inseparable from the nanoparticles themselves.

On one hand, the challenges in removing metals from the nanoparticles hinder the use of SCNPs in certain applications, primarily due to the interaction of the remaining catalyst. For instance, SCNPs containing toxic metal components are unsuitable for medical applications. The catalyst compound tends to create aggregates, limiting the use of many current SCNP synthetic methods to diluted conditions. These nanoparticles are not very stable over time and are challenging to store, thus limiting their potential applications.

To address these issues, we seek alternative synthetic methods capable of producing stable SCNPs without the need for a catalyst. In Chapter 4, we attempt to develop a synthesis method based on the "Staudinger" reaction, cross-linking the chain with stable azaylide (-N=P-) moieties. Under normal conditions, the azaylide bond formed in the "Staudinger" reaction hydrolyzes quickly. However, when the reaction is conducted with p-azido-tetrafluorophenyl moieties, the bond becomes stable, making it a promising candidate for the intra-chain bond in SCNPs.

In Chapter 5, we adopt a different approach by employing the strain-promoted azide-alkyne cycloaddition (SPAAC) "click" reaction. While SCNPs synthesized via "click" chemistry, such as Cu(I)-catalyzed azide–alkyne cycloaddition (CuAAC), are widely reported, the metal-free equivalent reaction is a suitable candidate for synthesizing SCNPs without a catalyst.

In Chapter 6, we explore the application of the SPAAC synthesis method to produce SCNPs from out-of-use pieces of polymers, aiming to "valorize" them. Additionally, we deviate from traditional solvents and opt for less-contaminant solvents to synthesize "valorized" PVC single-chain nanoparticles in environmentally friendly "green" media.

3. Experimental Techniques

3.1. Gel permeation chromatography

Gel Permeation Chromatography (GPC) (Figure 12) is a type of Size Exclusion Chromatography (SEC). All SEC are chromatographic technique that separate the sample according to the size. GPC, specifically, separate the sample according to their hydrodynamic radius.

A solution of the sample is injected in the continuous flux of the solvent and pass through one or more chromatographic column that have pores with different sizes. The molecules that are bigger than the pores cannot get in, so they are retained less time. Small molecules need more time to elute because they get in pores, increasing their retention time. Then different detectors measure the proprieties of the sample, as molecular weight and concentration. As result, different chromatographs are generated, showing the detectors signal intensity at different retention times. There are different configurations of GPC, changing the number and type of detectors. In the configuration used in this thesis, consist in a multi-angle light scattering (MALS) detector, a viscometer (VI) and a refractive index (RI) detector.

RI detector measures continuously the refractive index of the solution, detecting the changes caused by the concentration of the sample. Therefore, concertation can be easily measured for each retention time. The intensity of the detector signal (I_{RI}) is proportional to the concentration (c) and to $\frac{dn}{dc}$ value. This value, the variation of the reflective index (n) with the concentration, depends on the material, solvent and temperature. Therefore, as the GPC has a temperature control, this value is constant for all retentions time of the same sample and there are recoded for most polymers.

(Equation 1)

$$I_{RI} \propto \frac{dn}{dc} * c$$

One very used method to measure the molar mass of a sample is to create a calibration curve with a monodisperse standard of known molecular weight. Retention time can be related with the weight to interpolate the weight for others samples. Despite being a widely used method cannot be used for SCNP, because is based in the hypothesis that the heaviest molecules have bigger size; but SCNP have the same weight, or higher because the cross-linker, but smaller size.

To obtain the absolute molecular weight MALS detector can be used. This detector uses two or more laser that scatters with the sample. Signal intensity (I_{LS}) depends on the molecular weight (M_w), concentration (c) and the $\frac{dn}{dc}$ value. Therefore, the signal of the RI detector is necessary to obtain the molecular mass.

(Equation 2)

$$I_{LS} \propto \left(\frac{dn}{dc}\right)^2 * c * M_w$$

With this detector, size can be calculated from the difference between the signals of different angles. Partial Zimm plot shows the anisotropic scattering, plotting the inverse of the intensity of the detector signal for different angles. From the slope of this plot radius of gyration can be determinate. Nevertheless, it must be taken into account that samples smaller than 10 nm have an isotropic scattering, being impossible to determinate the gyration radius with this method.

With the viscometer, the hydrodynamic radius can be obtained. The signal intensity (I_{VI}) is proportional to the concentration (c) and the intrinsic viscosity (η) of the sample. Using the Einstein's model [1] for the viscosity of a solution of spherical particles hydrodynamic radius can be determinate, being N_A the Avogadro's number.

(Equation 3)

$$I_{VI} = c * \eta$$

$$\eta * M_w = \frac{10\pi}{3} * N_A * {R_h}^3$$

In addition to obtain measurements of size and weight, this technique can be used to monitoring the formation of SCNP. As a reduction in the size is related with an increase of the retention time, injecting a SCNP synthesis reaction at different times, the evolution of the reaction can be observed. SCNP, as are more compact, have smaller radius than the precursor polymer, having bigger retention times [2].

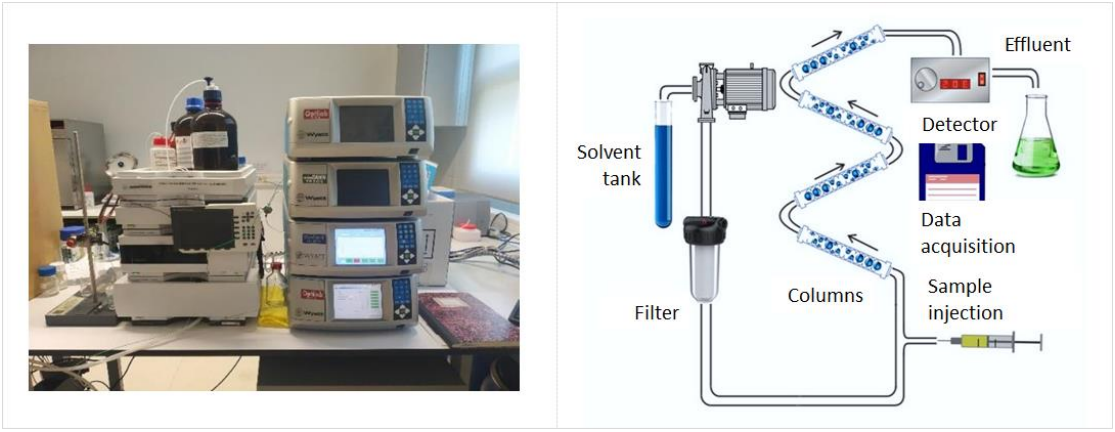

Figure 12. Picture of the GPC equipment used in this work (left) and a scheme of the equipment's functionalization (right).

3.2. Dynamic light scattering

Dynamic light scattering (DLS) (Figure 13) is a characterization technique that determinate the distribution of sizes of polymers in solution or small particles in suspension. To measure, a laser beam is scattered and collected by a detector at a fixed angle. The light is diffracted in all directions, creating interface patterns. Due to the Brownian motion of the sample in the solvent, the diffraction vary with time, giving information about the time scale of movement of the scatters. A correlation function is created with the comparison of the intensity at each point over the time. While small particles cause fluctuation of the light intensity at shorter time-scales, larger particles change the intensity at larger time-scales, so different sizes of particles can be distinguished for same sample [3]. Diffusion coefficient (D) is calculated for each time, and with this value, the radius of the particles (R) can be calculated with the Stokes-Einstein equation [4].

(Equation 4)

$$D = \frac{k_B T}{6\pi\eta R}$$

Where k_B is the Boltzmann's constant, T is the temperature in Kelvins and η is the viscosity.

This is a good technique to obtain a measurement of the size of the SCNP, so the reduction of radius can be observed with respect to the precursor.

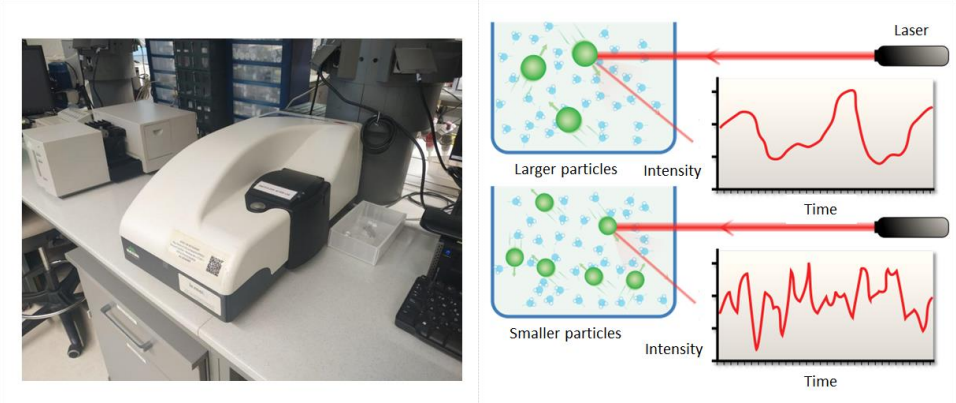

Figure 13. Picture of the DLS equipment used in this work (left) and a scheme of the equipment's functionalization (right).

3.3. Small-angle X-ray scattering

Small-angle X-ray (SAXS) (Figure 14) characterization technique is an X-ray scattering technique that measure the size and form of the nano-metric samples. Some characterization techniques use the X-ray scattering to study the properties of materials because the beam is scattered by the electronic cloud of the atoms, giving information of the sample. The different angles of the scattered beam provide information of different length scales, and small angles (0.1-10º) correspond to nanometer scale [5].

In SAXS characterization a monochromatic X-ray beam goes though the sample dissolved. A detector is located behind the sample with a stopper in order to detect the scattered beams but ignore the original one. The signal of the detector forms a 2D scattering pattern that can be reduced to an expression of the intensity in function of the scattering vector q [6]. This vector is related with the wavelength of the x-rays, λ, and with the scattering angle, 2θ, as:

(Equation 5)

$$q = \frac{4\pi * sin\,(\theta)}{\lambda}$$

The intensity, I(q), of the scattered beams is the product of two factors: the form factor, P(q), and the structure factor, S(q). The structure factor depends on the interaction between particles; and the form factor depends on the size and shape of the particles. Therefore, information about size, shape and distribution of nanoparticles can be obtained [7].

This technique is very useful to characterize SCNP, because, in addition of the radius of gyration, the scaling exponent can be obtained. GPC and DLS techniques can measure the size too, but the scaling exponent gives information about the shape of the samples. Precursors are polymer chains, and their form factor is approximately $v = 3/5 = 0.6$; while SCNP have a smaller scaling exponent $v = 0.4{\sim}0.5$, which is related with their more compact sphere-like shape.

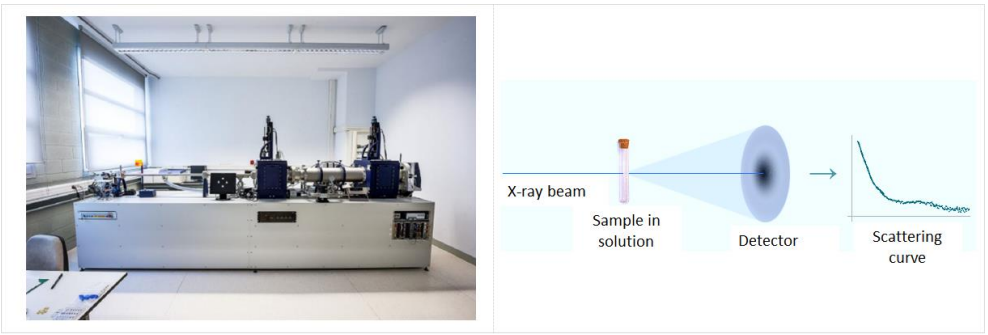

Figure 14. Picture of the SAXS equipment used in this work (left) and a scheme of the equipment's functionalization (right).

3.4. Nuclear magnetic resonance

Nuclear magnetic resonance (NMR) (Figure 15) is a spectroscopic technique used to characterize the composition of the molecules. The sample, dissolved in a deuterated solvent, is exposed to a strong magnetic field that is perturbed by an oscillating weak field. This perturbation produces an electromagnetic signal that depends of the magnetic field of the nucleus of the sample.

The protons and neutrons have a physical property named spin. When the number of particles of the nucleus is even the spins are canceled two by two; but when it is odd the nucleus has an overall spin. In the presence of a magnetic field, the spin states aligned with this field have less energy that anti-aligned states. The difference of the energy is proportional to the intensity of the magnetic field. The oscillating magnetic field induce the transition between the energy levels, and the frequency is proportional to the magnetic field around the nuclei. Therefore, we obtain information of the environment of the nuclei with this technique.

As the resonant frequency changes with the intensity of the applied magnetic field, a reference sample. This reference is tetramethyl silane and all the others frequency are expressed as the difference from tetramethyl silane's one. The chemical shift (δ) is calculated form the resonant frequency (f) and the reference frequency (f_0) as:

(Equation 6)

$$\delta = \frac{f - f_0}{f_0}$$

In this thesis ^{1}H, ^{13}C, ^{19}F and ^{31}P NMR spectroscopy were used to characterize the composition of the samples and to check if the reactions were carried out correctly. For more specialized characterization ^{29}Si-^{1}H Heteronuclear Correlation Spectroscopy (HETCOR), to check the presence of silicon, and Diffusion-Ordered Spectroscopy (DOSY), to check the signals that are related with the studied sample. HETCOR experiment shows, in a two-dimension spectrum, signals related with the coupling between nuclei of two different types, silicon and hydrogen in this case. On the other hand, in the DOSY experiment a series of ^{1}H NMR spectra are collected with different pulsed field gradient strengths, showing a decay of signal between spectra. Analyzing the decay, a two-dimension diffusion domain is created, where the peaks of the ^{1}H NMR spectra presents different diffusion coefficient. This diffusion domain allows to distinguish between different substances present in the sample, if these substances have different diffusion coefficient.

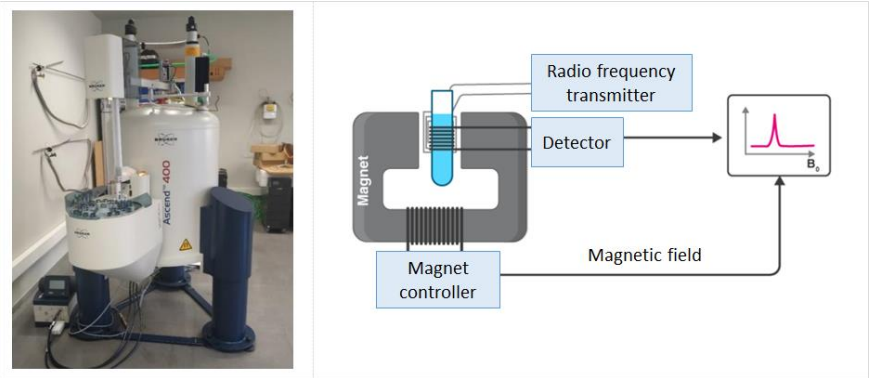

Figure 15. Picture of the NMR equipment used in this work (left) and a scheme of the equipment' functionalization (right).

3.5. Fourier transform infrared spectroscopy

Infrared spectroscopy (IR) (Figure 16) is a characterization technique that measure the absorption by the sample of the infrared light. This absorption is related with the different vibrational energy levels of the sample, and the frequencies of the vibrations are related to the strength of the bound and the mass of the atoms present in that bond. Therefore, this technique characterizes the composition of the sample.

Fourier transform infrared spectroscopy (FTIR) is a technique for obtain the IR spectra faster. The sample is irradiated simultaneously with the entire range of frequencies and the light is collected into an interferometer. A beam-splitter separate the light into two, those are reflected by two mirrors and are directed to the detector. An interferogram is produced changing the optical path length moving one of the mirrors. The equipment detects a different spectrum each moment and coverts them into the IR spectrum through a Fourier transform [8].

The sample can be pressing into pellet mixed with potassium bromide to be crossed by the light beam; or can be use the attenuated total reflection (ATR) where the sample is placed in contact with a crystal that the light will pass through, reflecting on the sample and producing evanescent waves that goes into the sample.

This technique is very powerful to characterize the chemical bonds present in the samples. Specifically, in this thesis was used to check the presence of azide group that have a very characteristic signal.

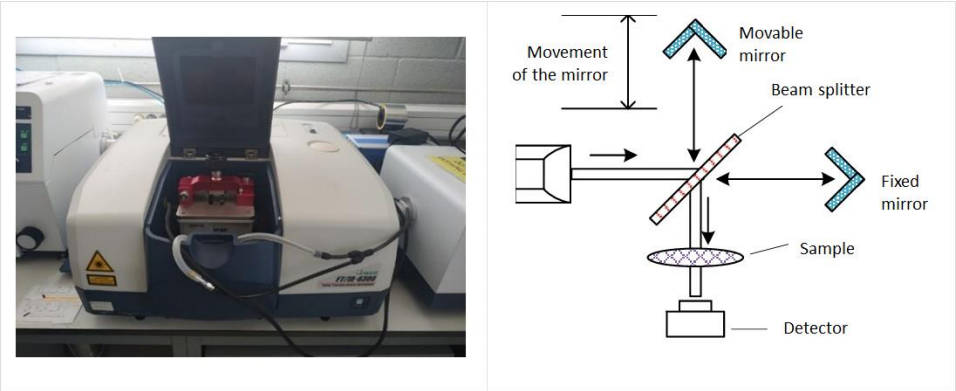

Figure 16. Picture of the FTIR equipment used in this work (left) and a scheme of the equipment's functionalization (right).

3.6. Elemental analysis

Elemental analysis (EA) (Figure 17) is a series of characterization techniques that can quantify the proportions of the elements of the sample. The most common type of EA is the CHNS analysis, named that way because determinate the quantities of carbon, hydrogen, nitrogen and sulphur. In this technique, the sample is burned; liberating carbon dioxide, water, nitrogen oxide and sulphur dioxide gases. Weighting these products, the proportions of those elements can be easily obtained.

This technique was used to characterize the composition of the samples and to check if the reactions were carried out correctly.

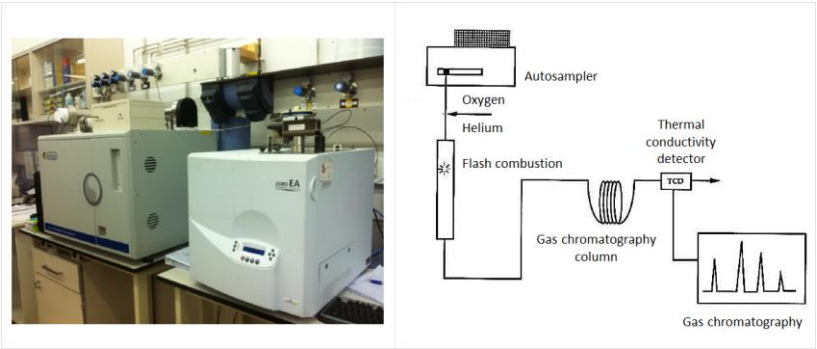

Figure 17. Picture of the EA equipment used in this work (left) and a scheme of the equipment's functionalization (right).

3.7. Thermogravimetric analysis

Thermogravimetric analysis (TGA) (Figure 18) is a characterization technique that analyze the thermal degradation. Sample, in solid state, is weight in a balance inside an oven that heat the sample to high temperatures so the equipment measures the mass loss. This procedure can be do in presence of air, to measure the effect of the oxidation, or under inert atmosphere. With

this technique, the degradation temperature is determinate, what is the temperature until the sample is stable.

This technique was used to characterize thermally the materials, obtaining the degradation temperature of each sample.

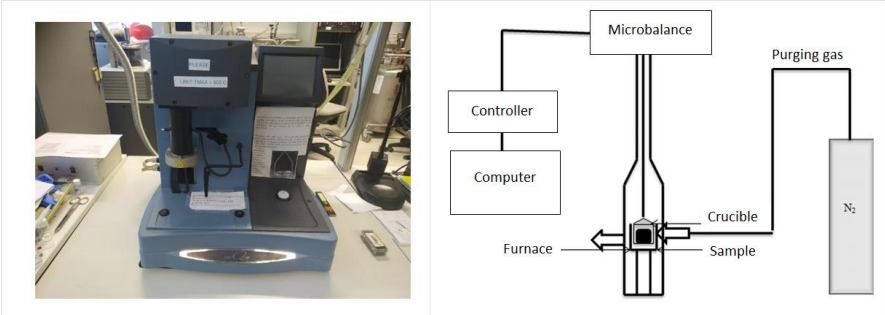

Figure 18. Picture of the TGA equipment used in this work (left) and a scheme of the equipment's functionalization (right).

3.8. Differential scanning calorimetry

Differential scanning calorimetry (DSC) (Figure 19) is a thermal characterization technique that analyze the heat capacity of the sample at different temperatures. The sample and a standard used as reference are exposed to some heating-cooling cycles while is measured the heat capacity, the amount of energy needed to change one grade the temperature of the material. The sample is heated bellow the degradation temperature to avoid damaging it, and with the first heating solvent residues are removed. This technique is used to determinate the glass-transition temperature of the material, because in this temperature a change of heat capacity is observed because of the structure change.

This technique was used to obtain the glass-transition temperature of the sample, and see how the compaction of the SCNP affect to the mobility of the material.

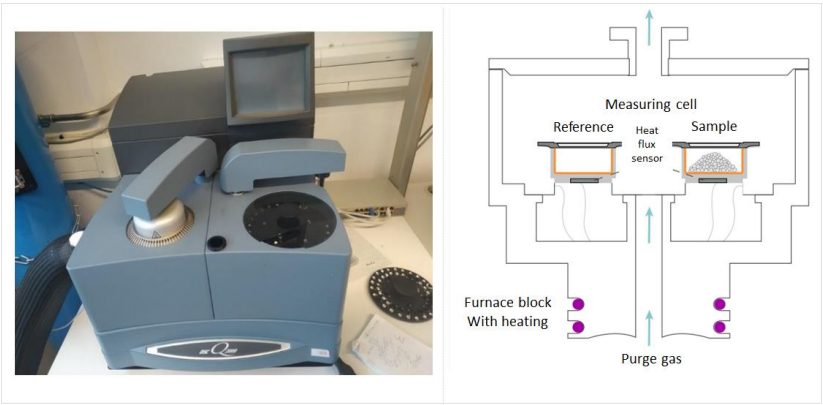

Figure 19. Picture of the DSC equipment used in this work (left) and a scheme of the equipment's functionalization (right).

3.9. Ultraviolet-visible spectroscopy

Ultraviolet-visible spectroscopy (UV-Vis) (Figure 20) is a characterization technique that measures the light absorption. The sample is irradiated with visible, near ultraviolet and near infrared light and the absorption is measured by the change of the detector signal of the blank and the sample. This absorption is related with the electronic transition from the low energy atomic and molecular orbitals to higher energy ones. To excite the electron form the Highest Occupied Molecular Orbital (HOMO) to the Lowest Unoccupied Molecular Orbital (LUMO) energy equal to the gap between them must be irradiated. Therefore, the absorption at long wavelength is related with small energy gaps.

For absorption values of A < 1 Beer-Lambert law relates the absorption with the intensity of the incident light (I_0), the intensity of the transmitted light (I), the concentration of the sample (c), the path length (L) and an intrinsic property of the sample named extinction coefficient (ε).

(Equation 7)

$$A = log\ (I_0/I)\ = \varepsilon cL$$

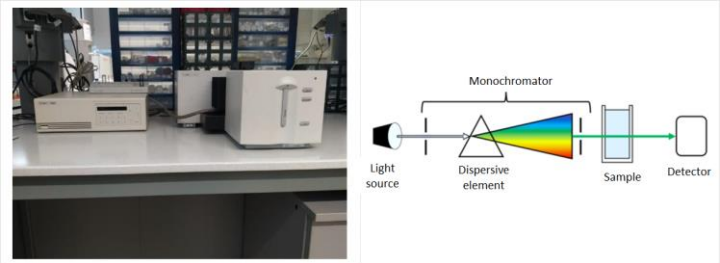

Figure 20. Picture of the V-Vis equipment used in this work (left) and a scheme of the equipment's functionalization (right).

3.10. Inductively coupled plasma mass spectrometry

Mass spectrometry (MS) (Figure 21) is a family of different analytical techniques where the sample is ionized and separate according to the mass-to-charge ratio. In the inductively couple plasma mass spectrometry (ICP-MS) technique an inductively coupled plasma is used to ionize the sample and those ions are detected by a detector.

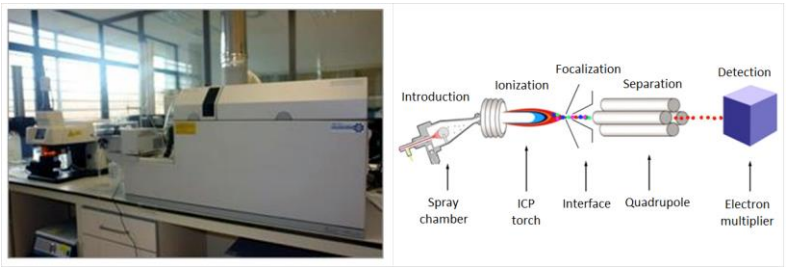

Figure 21. Picture of the ICP-MS equipment used in this work (left) and a scheme of the equipment's functionalization (right).

References

[1] M.P.J. Dohmen, A.M. Pereira, J.M.K. Timmer, N.E. Benes, J.T.F. Keurentjes, Hydrodynamic Radii of Polyethylene Glycols in Different Solvents Determined from Viscosity Measurements, *Journal of Chemical & Engineering Data* **2008**, 53, 63-65.

[2] A. Latorre-Sánchez, A. Alegría, F. Lo Verso, A.J. Moreno, A. Arbe, J. Colmenero, J.A. Pomposo, A Useful Methodology for Determining the Compaction Degree of Single-Chain Nanoparticles by Conventional SEC, *Particle & Particle Systems Characterization* **2016**, 33, 373-381.

[3] W.I. Goldburg, Dynamic light scattering, *American Journal of Physics* **1999**, 67, 1152-1160.

[4] M. Sartor, Dynamic light scattering to determine the radius of small beads in Brownian motion in a solution, *University of California San Diego* **2003**, pp. 1-21.

[5] T. Li, A.J. Senesi, B. Lee, Small Angle X-ray Scattering for Nanoparticle Research, *Chemical Reviews*, **2016**, 116, 11128-11180.

[6] B. Hammouda, Small-Angle Scattering From Branched Polymers, *Macromolecular Theory and Simulations*, **2012**, 21, 372-381.

[7] B. Chu, B.S. Hsiao, Small-Angle X-ray Scattering of Polymers, *Chemical Reviews* **2001**, 101, 1727-1762.

[8] O. Faix, Fourier Transform Infrared Spectroscopy, in: S.Y. Lin, C.W. Dence (Eds.) Methods in Lignin Chemistry, *Springer Berlin Heidelberg* **1992**, pp. 83-109.

4. Unfolding of Robust "Staudinger" Single-Chain Nanoparticles

4.1. Motivation

Single-chain polymer nanoparticles (SCNPs) obtained through intrachain folding of discrete synthetic polymer chains are emerging soft nano-objects with potential application in catalysis, nanomedicine, and sensing. The unfolding of SCNPs involving reversible interactions triggered by a variety of external stimuli or substances is well known. Conversely, methods for unfolding (i.e., intrachain disassembly) of SCNPs with covalent interactions are scarce. In this Chapter, we report a method to construct robust “Staudinger” SCNPs with stable azaylide (-N=P-) moieties as intrachain cross-linking units and, moreover, a breakthrough, unique and selective reagent for the on-demand unfolding of these –otherwise– highly stable SCNPs.

4.2. Introduction

Intrachain folding of isolated, discrete synthetic polymer chains gives to single-chain nanoparticles (SCNPs) [1-7]. SCNPs are promising nano-objects for the development of new enzyme-mimetic catalysts, improved sensing nano-materials, innovative drug delivery vehicles, and so on [8]. For instance, Barner-Kowollik et al. [9] reported SCNPs capable of catalyzing the photo-oxidation of nonpolar alkenes under green light up to three times more efficiently than an equivalent small-molecule photosensitizer at an identical concentration. Binder et al. [10] developed near infra-red (NIR)-fluorescent SCNPs that change their photophysical behavior upon heating and generate a fluctuating photo-acoustic (PA) signal which can be used as a novel effect for PA imaging. Moreover, Paulusse et al. [11] showed rapid up-take by HeLa cancer cells of SCNPs via polyplex formation and cytosolic delivery of doxorubicin from the SCNPs acting as nanocarriers. Those and other examples a sample of the full range of possibilities SCNPs offer in different applications [12-21].

When the intrachain folding process in a synthetic polymer chain is induced through reversible interactions, unfolding of the resulting SCNPs, intrachain disassembly, is possible under certain conditions [22]. For instance, SCNPs folded through hydrogen bonding (HB) interactions were found to unfold upon acidification [23], by addition of a competitive HB compound [24-26], anion [27], solvent [28], or by increasing temperature [28,29]. Additionally, reversible SCNPs have been unfolded triggered by addition of a base [30], under interrupted illumination (dark conditions) [31], by losing CO_2 molecules [32,33] or upon external voltage stimuli [34]. Complementary, SCNPs folded through dynamic covalent bonds like disulfide [35,36] or enamine bonds [37] went back to their linear precursor chains in the presence of reducing agents or by lowering the pH, respectively. The decrease in activity of some catalytic SCNPs in

vivo was attributed to the spontaneous unfolding of these reversible SCNPs in these complex media [38].

Conversely, robust SCNPs result when the intrachain folding process involves the generation of stronger covalent interactions [39]. Unfolding of robust SCNPs could be a useful method to modulate SCNPs activity/functionality. However, only a few examples of unfolding of robust SCNPs have been reported. In a pioneering work, Temel et al. [40] synthesized SCNPs through intrachain cross-linking with Michler’s ketone units via Menschutkin chemistry that unfold to the linear precursor upon photoirradiation at a wavelength of λ = 365 nm. Barner-Kowollik et al. [41] reported the unfolding triggered by meta-chloroperbenzoic acid (mCPBA) of fluorescent SCNPs photo-crosslinked at λ = 320 nm. The same group disclosed the chemiluminescent self-reported unfolding of peroxyoxalate-containing SCNPs triggered by hydrogen peroxide [42] and, more recently, SCNPs containing fluorescent bimane moieties as cross-linking units that can be fully unfolded using visible light (λ = 415 nm) [43]. Previously, Studer et al. [44] demonstrated λ-orthogonal folding (at λ = 415 nm) and unfolding (at λ = 254 nm) of SCNPs based on the photo-click reaction of acylsilanes with indoles. Critically, the development of new methods for unfolding robust SCNPs is still a challenging task. We report on the folding of linear precursor chains containing p-azido-tetrafluorophenyl moieties to robust “Staudinger” SCNPs with exceptional stability, and their unfolding triggered selectively by Me_3SiOH.

The Staudinger reaction, schemed in the Figure 22, is the coupling of an azide group and a tertiary phosphine group to create an iminophosphorane (i.e., azaylide) releasing N_2 [45]. The created bond hydrolyzes, in presence of water, giving a primary amine and phosphine oxide. This reaction, which proceeds in nearly full conversion without the need for any catalyst, has found broad application in organic synthesis and, as pioneered by Bertozzi and coworkers [46], in chemical biology.

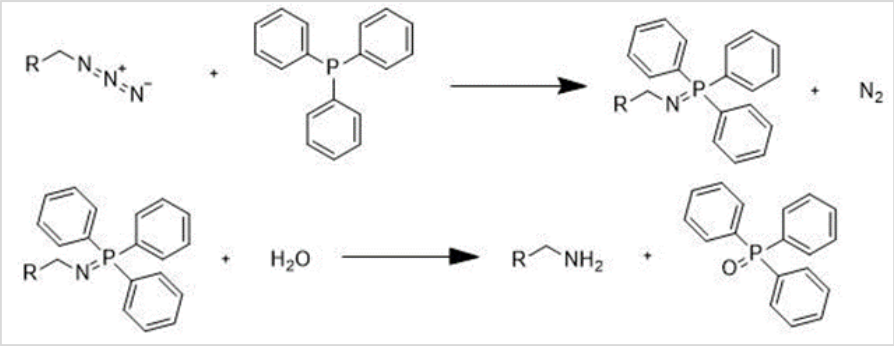

Figure 22. Scheme of the Staudinger reaction’s mechanism.

Recently, several strategies to stabilize the azaylide intermediate of the Staudinger reaction against hydrolysis, oxidation and aza-Wittig reactions have been reported. Hence, Ramström, Yan and coworkers [47] discovered that the use of perfluoroaryl azides in the Staudinger reaction leads to the rapid formation of stable iminophosphoranes in high yield, as is showed in the Figure 23. Similarly, Yi et al. reported a fast non-hydrolysis Staudinger reaction based on the use of o,o´-difluorinated aromatic azides [48] that becomes a very fast reaction when tetrafluorinated aromatic azides are employed [49]. Additionally, the formation of robust, water- and air-stable azaylides through the Staudinger reaction between electron-deficient aromatic azides such as o,o´-dichlorophenyl azide and triarylphosphines was reported by Yoshida, Hosoya and coworkers [50]. In the case of organic compounds with *p*-azido-tetrafluorophenyl moieties, the azaylides investigated were so stable over time that they did not hydrolyze in the presence of water and did not react when mixed for 35 days with an excess of CS_2, a standard reagent for azaylides [47]. Moreover, the synthesis of polyphosphazenes with high thermal stability by the fast non-hydrolysis Staudinger reaction between a bis-perfluoroaryl azide and a bis-phosphine was additionally reported by Yan and coworkers [51]. Intrigued by the high stability of the azaylides resulting from *p*-azido-tetrafluorophenyl moieties, we envisioned the construction of single-chain nanoparticles (SCNPs) with robust azaylide moieties as intra-chain cross-linking units, that we will name as “Staudinger” SCNPs. Herein, we report the synthesis of robust “Staudinger” SCNPs and, moreover, a breakthrough, unique and selective reagent for the on-demand unfolding of these, otherwise, highly stable SCNPs.

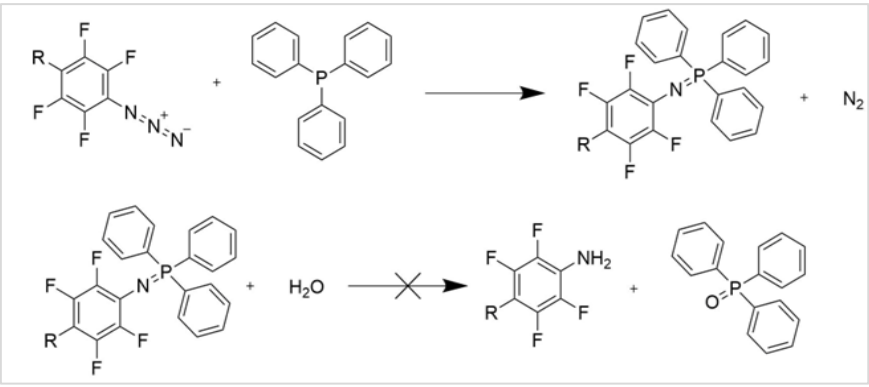

Figure 23. Schem of the frustrated Staudinger reaction, avoiding the hydrolyzation of the azaylide bond.

In this chapter, a new metal-free method to synthesize SCNP is presented using the frustrated Staudinger reaction. To illustrate the utility of this method for the synthesis of metal-free SCNPs, a poly(styrene-*co*-2,3,4,5,6-pentafluorostyrene) (P(S-*co*-PFS)) copolymer has been synthesized through radical addition fragmentation chain-transfer (RAFT) polymerization. Since the monomer reactivity ratios of S and PFS are reported [52] to be r_S = 0.43 and r_{PFS} = 0.22, the

copolymer is expected to show a moderate alternating behavior as a consequence of the relatively low value of $r_S \times r_{PFS} = 0.095$.

Initial precursor copolymer was functionalized through the azide–para-fluoro substitution. This reaction, originally developed for photoaffinity labeling by Keana and Cai [53], was recently implemented for efficient sequential post-polymerization modification by Roth and coworkers [54].

To create the stable azaylide intra-chain bonds that fold the functionalized copolymer chain into SCNPs 1,3-Bis(diphenylphosphino)propane (DPPP) and 1,4-Bis(diphenylphosphino)butane (DPPB) (Figure 24) molecules were used as external bifunctional cross-linkers.

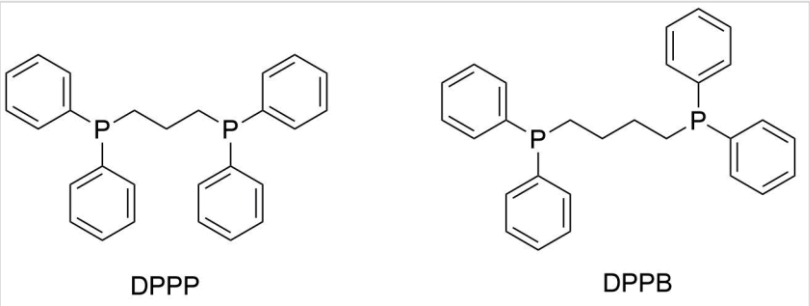

Figure 24. Structure of the selected diphenylphosphino molecules (cross-linkers) to form the intra-chain bond of the SCNPs.

After the synthesis of the SCNPs, the stability of the intra-chain bonds was studied. To investigate how robust are the cross-linking N=P bonds against oxidation, hydrolysis, and aza-Wittig reactions, we carried out several experiments. We investigated the stability of the SCNPs in solution, 5 mg/mL, under different conditions and re-agents through ^{31}P NMR spectroscopy. The SCNPs were exposed to a traditional heating and microwave heating. Also were exposed for 3 days to an excess of trifluoroacetic acid (TFA), carbon disulfide (CS_2) and trimethylsilanol (TMS). We choose TFA, to check the stability against acids, and CS_2, for be standard reagent for azaylides. TMS was selected for presenting high affinity towards both the iminophosphorane linkage and C_6F_4 ring while also exhibiting a nucleophilic character against the former. Silicon-based compounds become an attractive option not only because of the known affinity between Si and F but also because of their ability to be activated by phosphazene structures (iminophosphoranes) [55]. We hypothesized that trimethylsilanol containing the “electropositive” silicon atom and having weak acidity (pKa = 11) could be a good candidate [56]. To check the stability, we observe the ^{31}P NMR spectrum of the resulting material to observe the disappearance of the peak corresponding to the N=P cross-linking.

4.3. Experimental procedures

4.3.1. Materials

Styrene (S, ≥99%), sodium azide (NaN_3, ≥99%), N,N-dimethylformamide (DMF, ≥99.9%), cyanomethyl dodecyl carbonotrithioate (CMDTC, 98%)), hexane (≥97%), carbon disulphide (CS_2, ≥99.9%) and trifluoroacetic acid (TFA, ≥98%) were purchased from Sigma-Aldrich (Madrid, Spain). 1,3-Bis(diphenylphosphino)propane (DPPP, >98%) and 1,4-Bis(diphenylphosphino)butane (DPPB, >98%) were supplied by TCI. Tetrahydrofuran (THF, GPC grade) was purchased from Scharlau (Barcelona, Spain). 2,2’-Azobis(2-methylpropionitrile) (AIBN, ≥97%) was purchased from Honeywell Fluka (North Carolina, United States of America). 2,3,4,5,6-pentafluorostyrene (PFS, 98%) and trimethylsilanol (TMS, 96.85%) were purchased from BLDpharm (Kaiserslautern, Germany). Deuterated chloroform ($CDCl_3$, 99.50%, 0.03% TMS v/v) and deuterated tetrahydrofuran (THF-d8) (99.50% D, water < 0.05%) were purchased from Eurisotop (Saint-Aubin, France). Unless otherwise specified, all reagents were used as received without further purification. To remove the inhibitor, S and PFS were purified by being passed through a column packed with activated basic alumina.

4.3.2. Techniques

- *Gel permeation chromatography (GPC)*

GPC measurements were performed at 25 ºC on an Agilent 1200 system equipped with PLgel 5 µm Guard and PLgel 5 µm MIXED-C columns, and triple detection: a differential refractive index (RI) detector (Optilab Rex, Wyatt, Toulouse, France), a multi-angle laser light scattering (MALS) detector (MiniDawn Treos, Wyatt, Toulouse, France), and a viscosimetric (VIS) detector (ViscoStar-II, Wyatt, Toulouse, France). Data analysis was performed using ASTRA Software (version 6.1) from Wyatt. THF was used as an eluent at a flow rate of 1 mL/min. A value of dn/dc = 0.100 was used for P(S-*co*-PFS), P(S-*co*-ATFS) and P(S-*co*-PFS)-SCNPs.

- *Dynamic light scattering (DLS)*

DLS measurements (number distribution) were taken at room temperature on a Malvern Zetasizer Nano ZS (Cambridge, United Kingdom) apparatus.

- *Small-angle X-ray scattering (SAXS)*

SAXS experiments were conducted on the Rigaku (Barcelona, Spain) 3-pinhole PSAXSL equipment of the Materials Physics Center, operating at 45 kV and 0.88 mA. The MicroMax-002+ X-ray Generator System is composed of a microfocus sealed tube source module and an

integrated X-ray generator unit, which produces CuK transition photons of wavelength λ = 1.54 Å. The flight path and the sample chamber in this equipment are under vacuum. The scattered X-rays are detected on a two-dimensional multiwire X-ray Detector (Gabriel (Barcelona, Spain) design, 2D-200X) and converted to one-dimensional scattering curves by radial averaging. This gas-filled proportional type detector offers a 200 mm diameter active area with ca. 200-micron resolution. After radial integration, the scattered intensities were obtained as a function of momentum transfer $Q = 4\pi\lambda^{-1} sin\,\theta$, where θ is half the scattering angle. Reciprocal space calibration was performed using silver behenate as standard. The sample-to-detector distance was 2 m, covering a Q-range between 0.008 and 0.20 $Å^{-1}$. The measurements were taken at r.t. on the THF solutions in boron-rich capillaries of 2 mm thickness, with counting times of 1 h. The concentration was 1 mg/mL in order to avoid interference effects between different macromolecules. The data were carefully corrected for background scattering (due to the capillary and solvent) and measured for each sample on the same capillary for the same time. Scattering cross-sections were obtained in absolute units using water as the calibration standard. The generalized Gaussian coil function was employed for a precise determination of the values of the radius of gyration, R_g, and scaling exponent, ν.

- *Nuclear magnetic resonance (NMR)*

^{1}H, ^{13}C, ^{19}F, and ^{31}P NMR spectra were recorded at r.t. on a Bruker AscendTM spectrometer operating at 400 MHz. $CDCl_3$ was used as solvent for the characterization of the precursor copolymer (P(S-*co*-PFS)), functionalized copolymer (P(S-*co*-ATFS)) and the nanoparticles (P(S-*co*-PFS)-SCNPs). THF-d_8 was used as solvent after the unfolding experiments. DOSY and HETCOR experiments were recorded at r.t. on a two-bay Bruker AvanceTM spectrometer operating at 500 MHz, using THF-d_8 as solvent.

- *Fourier transform infrared spectroscopy (FTIR)*

FTIR spectra were recorded using ATR in a FT-IR JASCO 6360 (130-400K) infrared spectrometer at room temperature.

- *Elemental analysis (EA)*

The samples of this thesis were measured in an EA3000 elemental analyzer (CHNS).

- *Thermogravimetric analysis (TGA)*

TGA measurements were performed on a Q500-TA Instruments (Cerdanyola del Valles, Spain) apparatus at a heating rate of 10ºC/min under a nitrogen atmosphere.

- *Differential scanning calorimetry (DSC)*

The DSC measurements were carried out in a DSC Q2000 TMDSC instrument heating and cooling rate of 20ºC/min. The results are presented in “exo down” mode.

4.3.3. Procedures

- *Synthesis of Poly(S-co-PFS)*

P(S-*co*-CMS) was prepared by RAFT polymerization in bulk. S (1 mL, 8.7 mmol, 1 eq.), PFS (0.5 mL, 3.7 mmol, 0.43 eq.), AIBN as the initiators (1.4 mg, 9.5 x 10^{-4} eq.), and CMDTC (2.6 mg, 9.5 x 10^{-4} eq.) as the RAFT agent were added to a 50 mL round bottom flask (Figure 25). The reaction was stirred at 65 ºC for 15 h. P(S-*co*-PFS) was obtained by precipitation in cold water, isolated by filtration, and finally dried in a vacuum oven at 35 ºC overnight. Its parameter values were: yield = 61%; PFS content (EA) = 32 mol%; M_w (SEC/MALS) = 42.6 kDa; Đ (SEC) = 1.08; and R_g (SEC/MALS) = 6.2 nm.

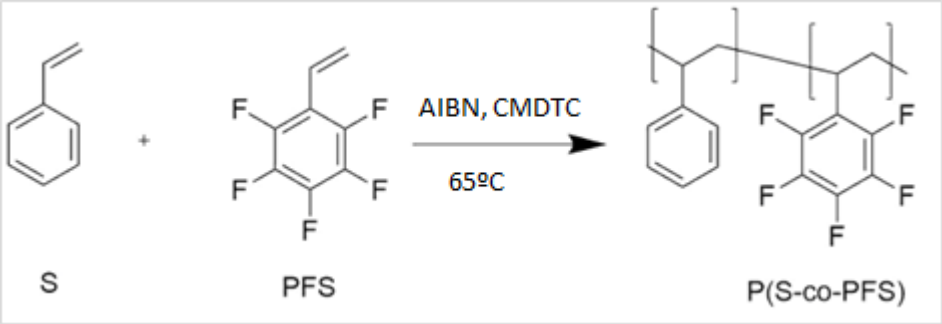

Figure 25. Synthetic scheme of the synthesis of P(S-co-PFS).

- *Synthesis of Poly(S-co-ATFS)*

P(S-*co*-PFS) (0.5 g, 1.2 mmol of *p*-F, 1 eq.) and NaN_3 (0.17 g, 2.6 mmol, 2.2 eq.) were dissolved in DMF (25 mL) in a 100 mL round-bottom flask and the resulting mixture was stirred at 80 ºC for 24 h (Figure 26). P(S-*co*-ATFS) was recovered by precipitation in cold water and then filtered and dried at 35 ºC under vacuum overnight. Yield = 88%; azide content (^{19}F NMR) = 10.5 mol%; M_w (SEC/MALS) = 50.9 kDa; Đ (SEC) = 1.13; and R_g (SEC/MALS) = 5.5 nm.

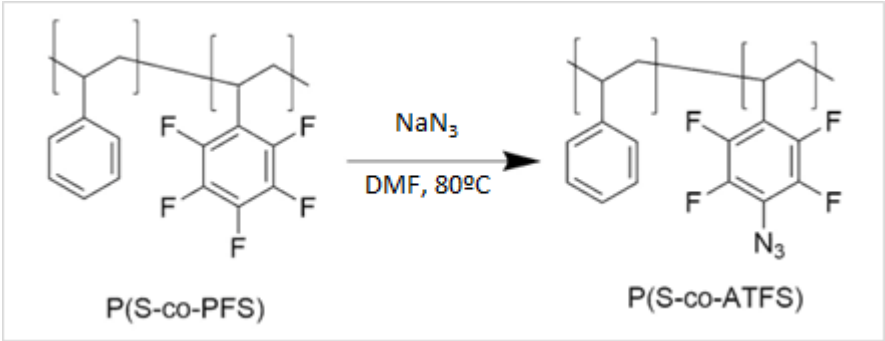

Figure 26. Synthetic scheme of the synthesis of P(S-co-ATFS).

- *Synthesis of Metal-Free P(S-co-PFS)-SCNPs*

P(S-*co*-ATFS) (100 mg, 0.08 mmol of N_3 groups, 1 eq.) was dissolved in THF (25 mL) in a flask that was sealed and degassed. In a second flask that was also sealed, degassed, and protected from light with aluminum foil, DPPP (20 mg, 0.05 mmol, 0.59 eq.) or DPPP (20 mg, 0.05 mmol, 0.59 eq.) was dissolved in 175 mL of THF. The solution containing P (S-*co*-PFS) was injected into the DPPP solution (both at r.t.) using an infusion pump at an addition rate of 30 mL/h (Figure 27). After 24 h, the product was precipitated in cold hexane, filtrated, and dried at 35 ºC under vacuum overnight. Its parameter values were yield = 94.4%; M_w (SEC/MALS) = 61.4 kDa; Đ (SEC) = 1.04; and R_g (SEC/MAL) = 4.3 nm.

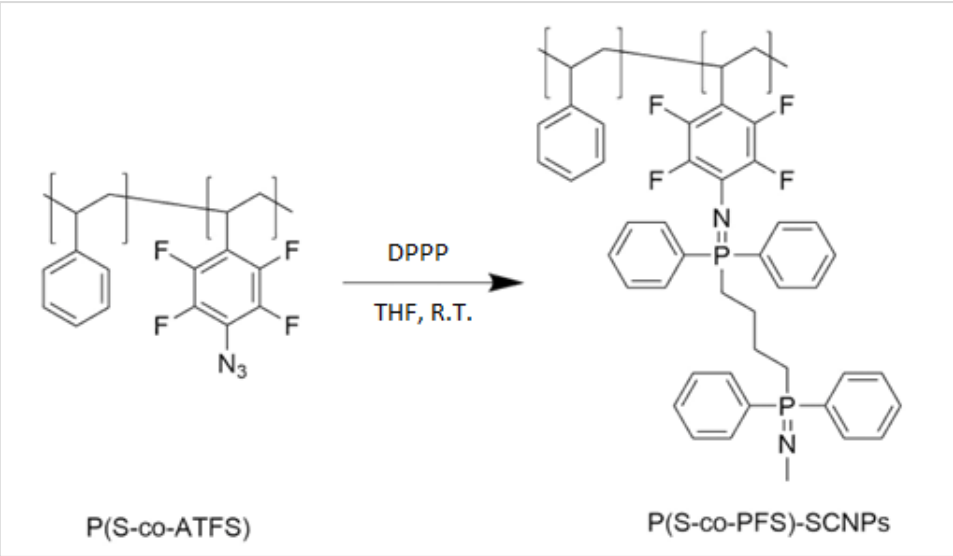

Figure 27. Synthetic scheme of the synthesis of P(S-co-PFS)-SCNPs.

- *Stability study*

In several 10 mL-vials, P(S-*co*-PFS)-SCNPs (10 mg, 0.008 mmol of N=P bonds) was dissolved in 2 mL of solvent (DMF or THF). Several experiments were carried out:

- SCNPs in DMF were heated to 120ºC for 3 days.
- SCNPs in DMF were exposed to microwave irradiation for 1 h (CEM Discover SP System, 25 W, 120 ºC).
- SCNPs in THF and an excess of TFA (2 ml, 18.0 mmol) were stirred at r.t. for 3 days.
- SCNPs in THF and an excess of CS_2 (2 ml, 33.2 mmol) were stirred at r.t. for 3 days.
- SCNPs in THF and an excess of TMS (2 ml, 26.1 mmol) was stirred at r.t. for 3 days.

After the experiment the solvent were removed by evaporating and the samples were cleaned with hexane and dried at 35 ºC under vacuum overnight. Samples were characterized by ^{31}P NMR spectroscopy.

4.4. Results and discussion

4.4.1. Synthesis of P(S-*co*-PFS)

The synthesized P(S-*co*-PFS) copolymer that contains 32 mol % of CMS units, calculated by elemental analysis (Table 1), was synthesized with a 61 % yield. The sample was characterized by ^{1}H NMR (Figure 28), ^{19}F NMR (Figure 29) and GPC techniques (Figure 30); obtaining a weight-average molecular weight (M_w) of 42.6 kDa, polydispersity (Đ) of 1.08 and a hydrodynamic radius (R_g (MALS)) in DMF of 6.2 nm.

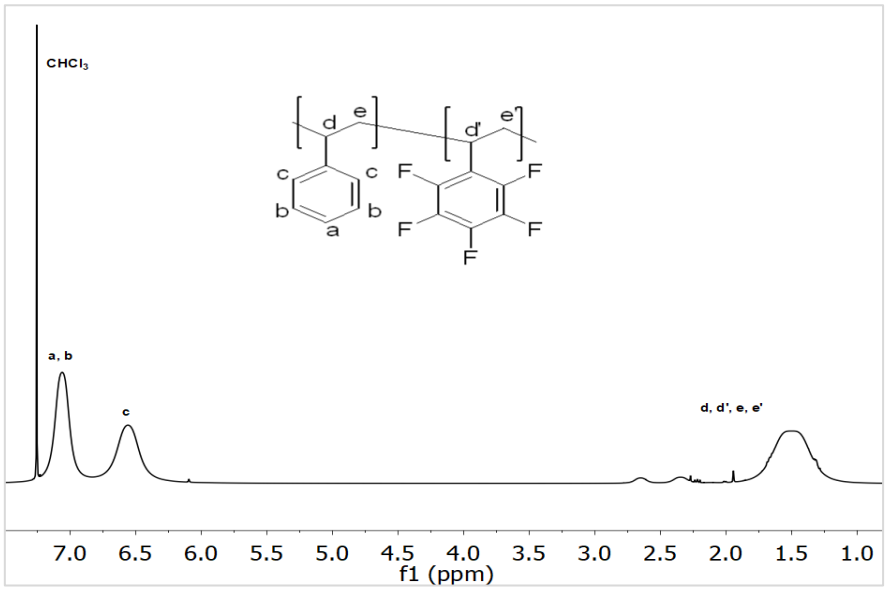

Figure 28. ^{1}H NMR spectra of P(S-co-PFS).

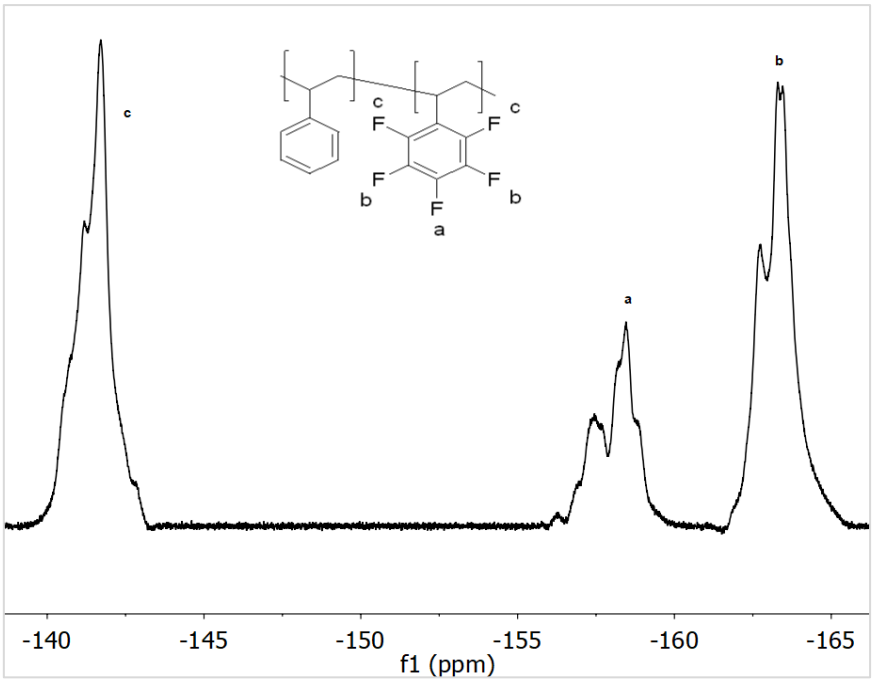

Figure 29. ^{19}F NMR spectra of P(S-co-PFS).

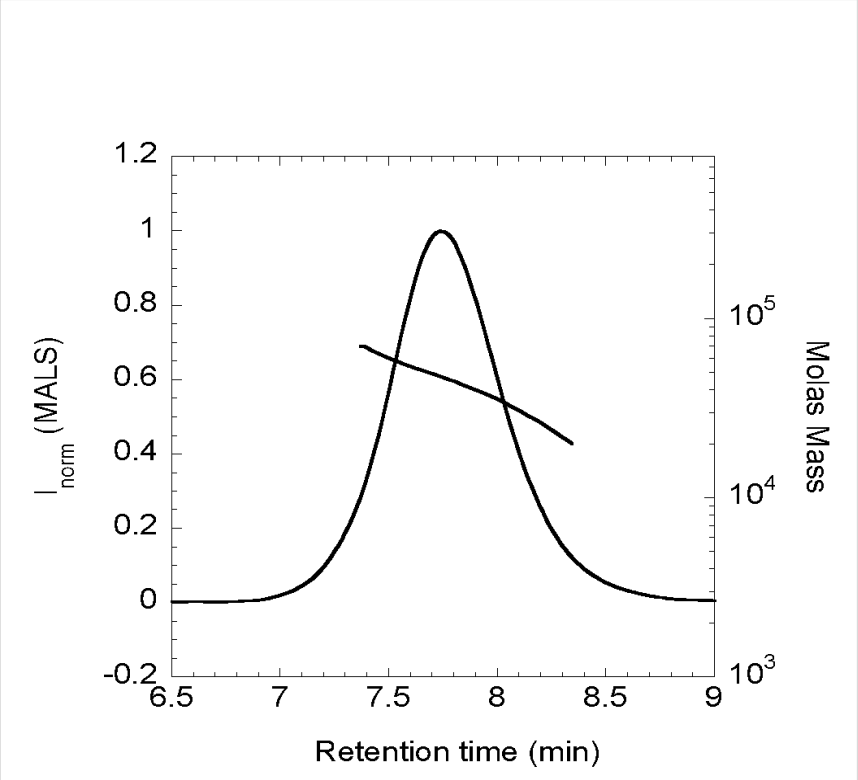

Figure 30. GPC chromatograph of P(S-co-PFS) (LS signal).

Table 1. EA of the P(S-co-PFS), P(S-co-ATFS) and P(S-co-PFS)-SCNPs.

EA P(S-*co*-PFS)					
Theoretical			Experimental		
P(S-*co*-PFS) [S=68%, PFS=32%]	C%	72.92	P(S-*co*-PFS)	C%	71.49
	H%	4.82		H%	5.24
	N%	-		N%	<1.6
P(S-*co*-ATFS) [S=68%, PFS=21%, ATFS=11%]	C%	70.94	P(S-*co*-ATFS)	C%	69.01
	H%	4.73		H%	4.98
	N%	3.41		N%	3.27
P(S-*co*-PFS)-SCNPs [100% of reaction of azide groups]	C%	73.47	P(S-*co*-PFS)-SCNPs	C%	70.83
	H%	5.05		H%	7.79
	N%	0.99		N%	<1.6

4.4.2. Azidation of P(S-*co*-PFS)

The azidation of the P(S-*co*-PFS), 88 % of yield, was checked by FTIR, observing the characteristic peaks of the azide group at 2135 cm^{-1}, corresponding to the asymmetric N=N=N stretching vibration of the azide group, and at 1225 cm^{-1}, from the symmetric stretching vibration (Figure 31). The azidation percentage, 11 mol%, of the sample was calculated by EA and was checked

by ^{19}F NMR spectroscopy, where can see a new peak related with the signal of the two fluorine atoms near the azide groups (Figure 32). Integration of the areas corresponding to the new peak ($A_{b'}$) and the remainder peak (A_b) allows one to estimate the molar content of *p*-azido-tetrafluorophenyl units as $[A_{b'}/(A_{b'} + A_b)] \times 100$. The azidation degree estimated from ^{19}F NMR was in very good agreement with that obtained from EA data.

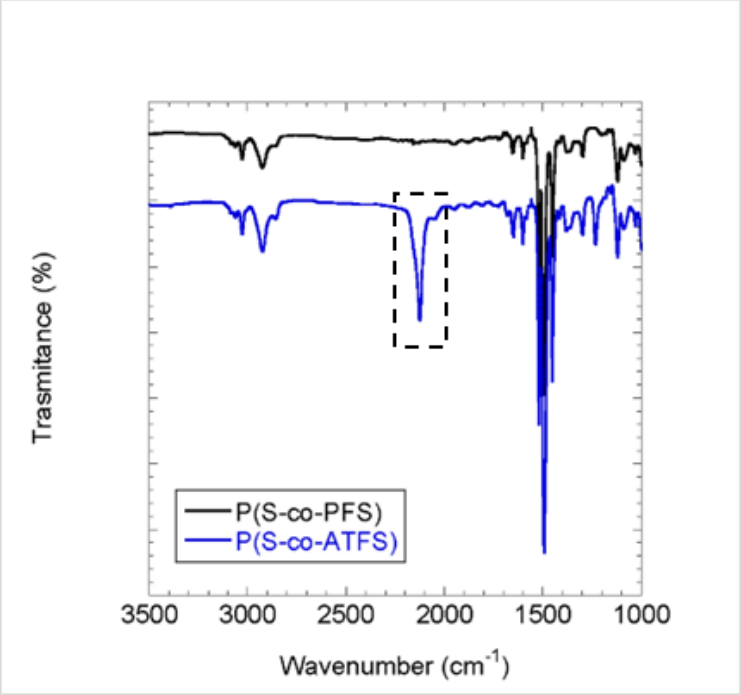

Figure 31. FTIR spectra of P(S-co-PFS) (black) and P(S-co-ATFS) (blue). In the black box is resalted the peak that is related with the azide group.

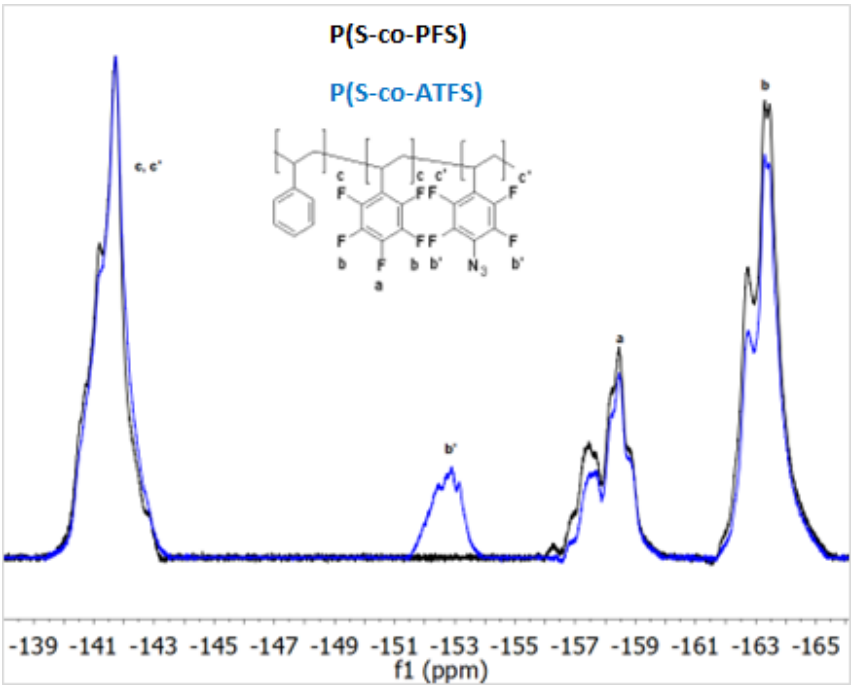

Figure 32. ^{19}F NMR spectra of P(S-co-PFS) (black) and P(S-co-ATFS) (blue). The displacement form b to b’ correspond to the azided monomers.

As can check in the GPC and DLS (Figure 33 and 34), the azidation did not affect much to the polymer size, but an increase of the molecular weight is observed (M_w (P(S-*co*-PFS)) = 42.6 kDa and M_w (P(S-*co*-ATFS)) = 50.9 kDa).

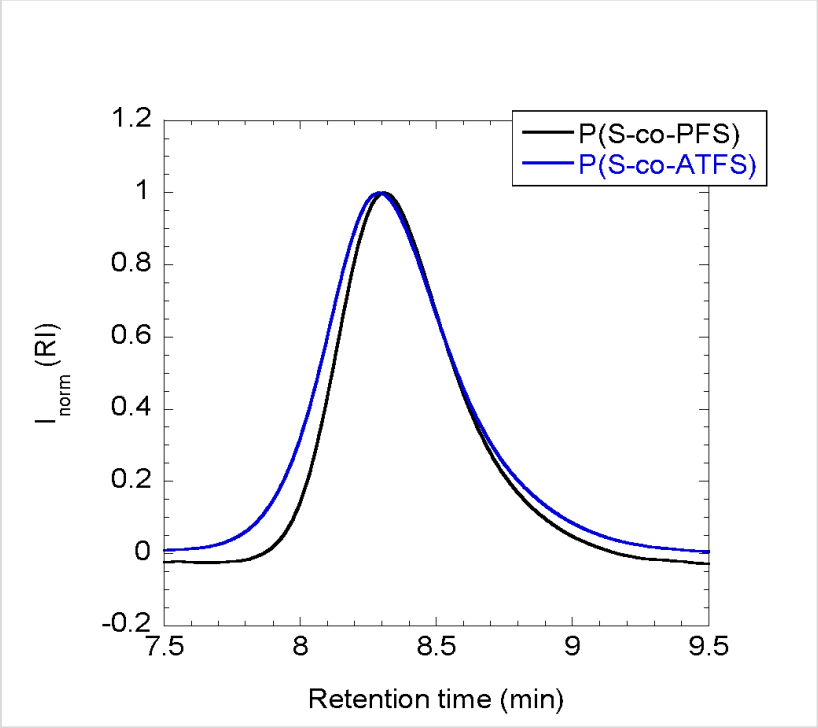

Figure 33. GPC chromatogram (RI detector) and of P(S-co-PFS) (black) and P(S-co-ATFS) (blue) (RI signal).

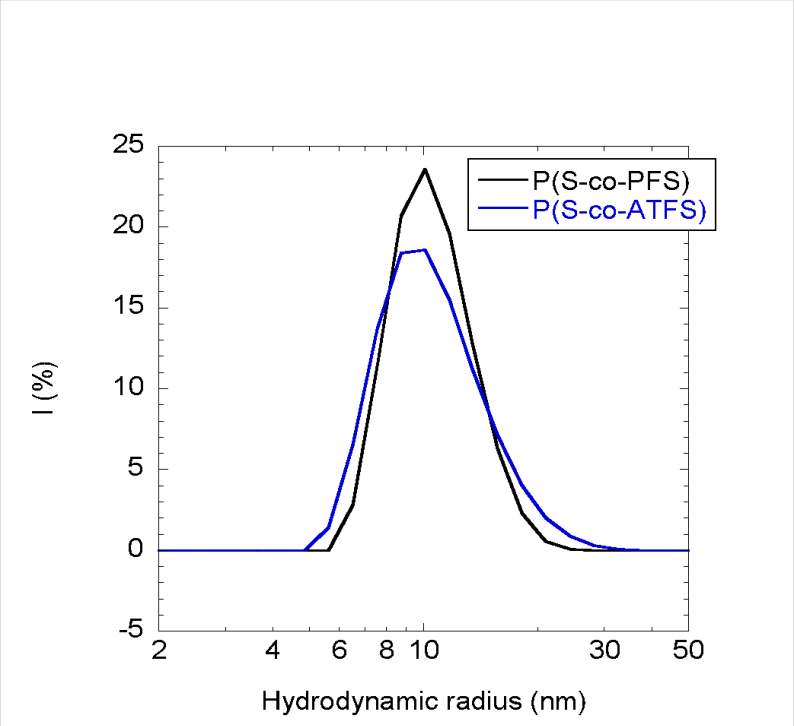

Figure 34. DLS size distribution in THF of P(S-co-PFS) (black) and P(S-co-ATFS) (blue).

The azide-para-fluoro substitution reaction was found to have a profound effect on the thermal behavior of the functionalized precursor, as illustrated in (Figure 35 and Figure 36). On one hand, partial azidation of the initial precursor increase the glass transition temperature (T_g) from 95 °C to 105 °C probably due to dipolar interactions between the residual pentafluophenyl and the new *p*-azido-tetrafluorophenyl moieties reducing the segmental mobility of P(S-*co*-ATFS). On the other hand, azidation of P(S-*co*-PFS) leads to a significant decrease in thermal stability as observed in (Figure 35). The functionalized precursor is thermally stable up to 150 °C so above this temperature loss of dinitrogen takes place due to the thermally labile nature of the *p*-azido-tetrafluorophenyl moieties [54]. All the above results support the successful preparation of an appropriate styrenic precursor of “Staudinger” SCNPs with 11 mol% of *p*-azido-tetrafluorophenyl pendants. It is worth of mention that SCNPs are typically synthesized from precursors containing between 10 and 30 mol% of functional groups.

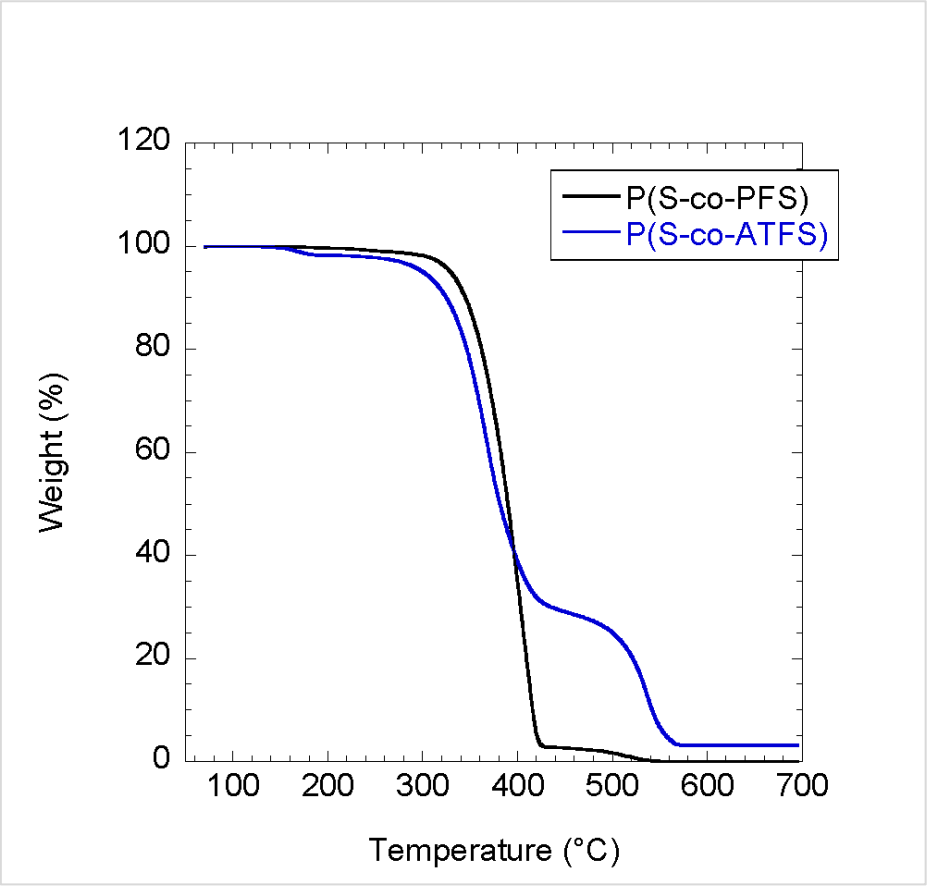

Figure 35. TGA of P(S-co-PFS) (black) and P(S-co-ATFS) (blue). The first small degradation correspond to the azide groups.

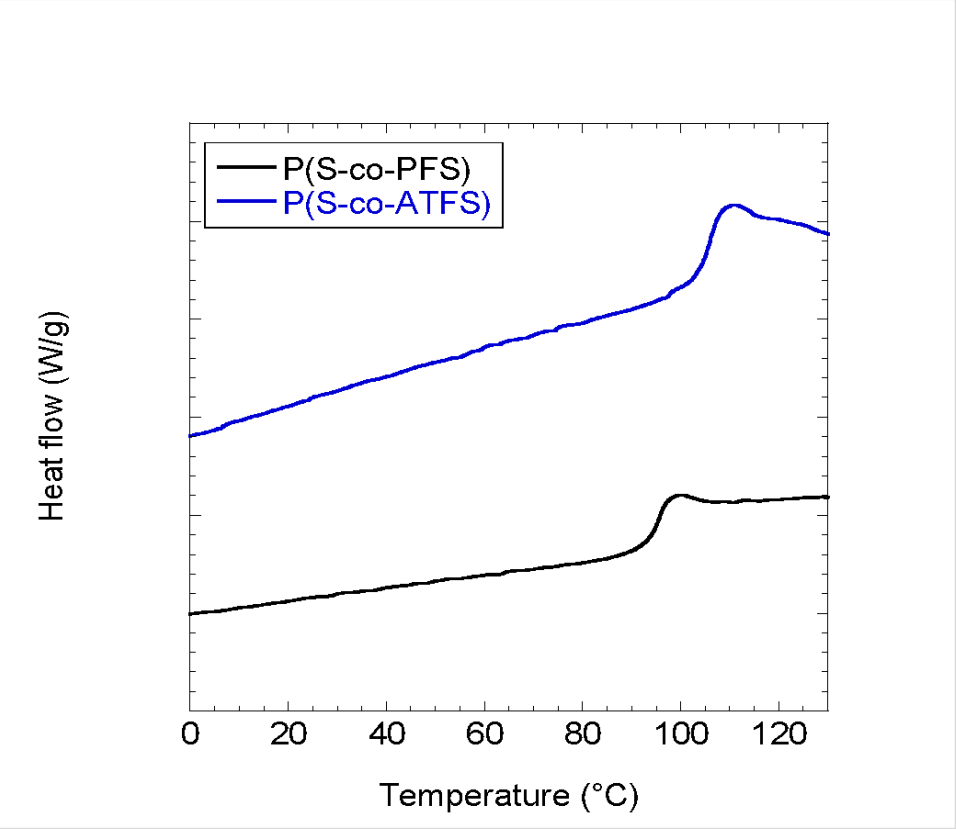

Figure 36. DSC of P(S-co-PFS) (black) and P(S-co-ATFS) (blue). After the azidation the T_g is increased due to the dipolar interaction between pentafluophenyl and the new p-azido-tetrafluorophenyl moieties.

4.4.3. Synthesis of P(S-*co*-PFS)-SCNPs

The P(S-*co*-PFS)-SCNPs were synthesized with a yield of 94.4 %. As illustrated in Figure 37 and Figure 38, results from size exclusion chromatography (SEC) and dynamic light scattering (DLS) supported the successful single-chain nanoparticle formation. A shift toward longer retention time and, hence, smaller hydrodynamic radius (R_h) was observed by SEC (Figure 37) [8]. Molar mass obtained from GPC is increased because of the incorporation of the cross-linker (M_w (P(S-*co*-ATFS)) = 50.9 kDa and M_w (P(S-*co*-PFS)-SCNPs) = 61.4 kDa). DLS measurements confirmed a reduction in average hydrodynamic size from R_h(P(S-*co*-ATFS)) = 9.4 nm to R_h(P(S-*co*-PFS)-SCNPs) = 6.3 nm. No differences were observed between SCNPs synthesized with DPPP and DPPB as cross-linker (Figure 39).

Confirmation of the quantitative consumption of *p*-azido-tetrafluorophenyl units in P(S-*co*-ATFS) to give stable azaylide-based cross-linking points in the SCNPs was obtained from IR, ^{19}F and ^{31}P NMR spectroscopy. Figure 40 illustrates the complete disappearance of the asymmetric N=N=N stretching vibration band at 2135 cm^{-1} upon formation of the “Staudinger” SCNPs, and the appearance of a new band in the IR spectrum centered at 1175 cm^{-1} corresponding to the N=P stretching vibration. Similarly, the ^{19}F NMR band at d = -152.9 ppm corresponding to two fluorine

atoms near the azide moiety in each p-azido-tetrafluorophenyl unit of P(S-*co*-ATFS) was found to completely disappear upon formation of SCNPs (Figure 41 b)). Instead, the ^{19}F NMR spectrum of SCNPs showed two new peaks centered at d = -155.2 ppm and d = -147.1 ppm arising from F atoms at orto- and meta-positions with respect to azaylide groups respectively. Moreover, the ^{31}P NMR spectrum of P(S-*co*-PFS)-SCNPs) revealed an intense peak centered at d = 32.9 ppm arising from the N=P cross-linking points. No sign of unreacted bis-phosphine (d = -16.9 ppm) was found in the ^{31}P NMR spectrum of the “Staudinger” SCNPs (Figure 41 c)). Taken together, the above results confirm the successful folding of functionalized precursor to “Staudinger” SCNPs via azaylide intrachain formation.

Thermally the SCNP have similar degradation temperature that the azidated polymer but with bigger weight loss, doe to the break of the cross-linkers, as can see in the TGA (Figure 42). While, no glass transition temperature was observed in the DSC characterization (Figure 43).

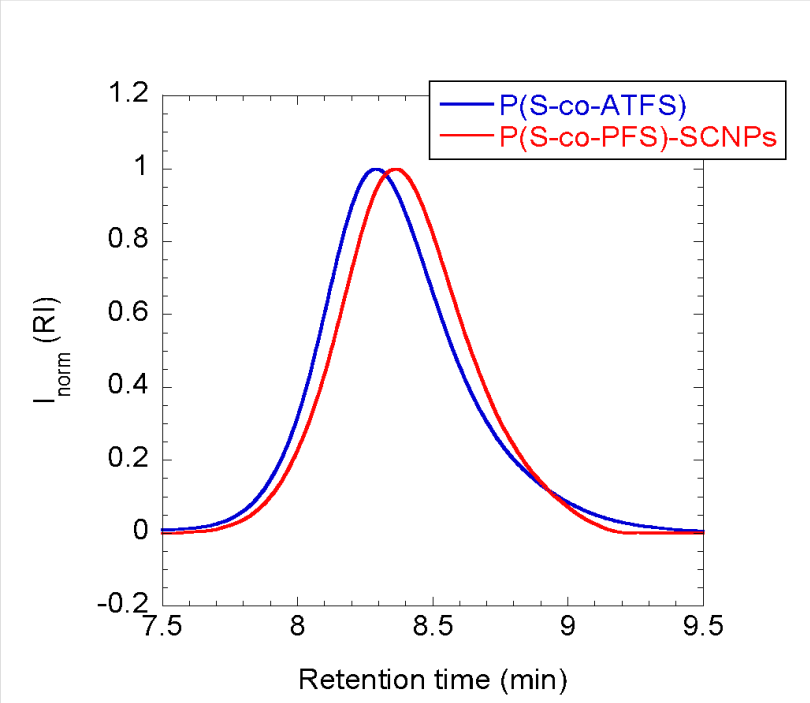

Figure 37. GPC chromatogram (RI detector) of P(S-co-ATFS) (blue) and P(S-co-PFS)-SCNPs (red) (RI signal). The displacement to higher retention times correspond to the expected reduction of size of the SCNPs.

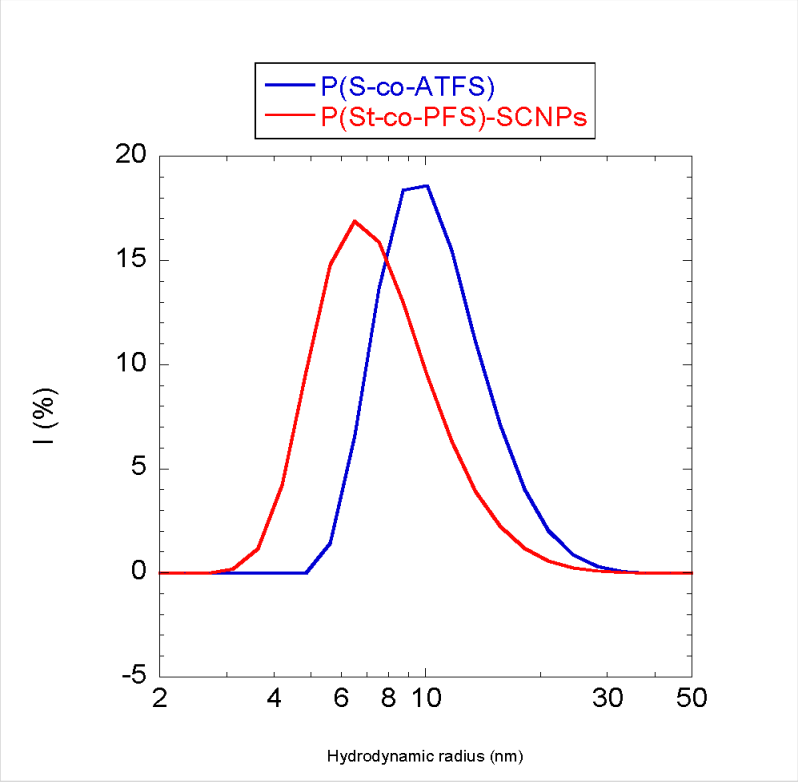

Figure 38. DLS size distribution in THF of P(S-co-ATFS) (blue) and P(S-co-PFS)-SCNPs (red). As expected the SCNPs have a smaller size than the precursor.

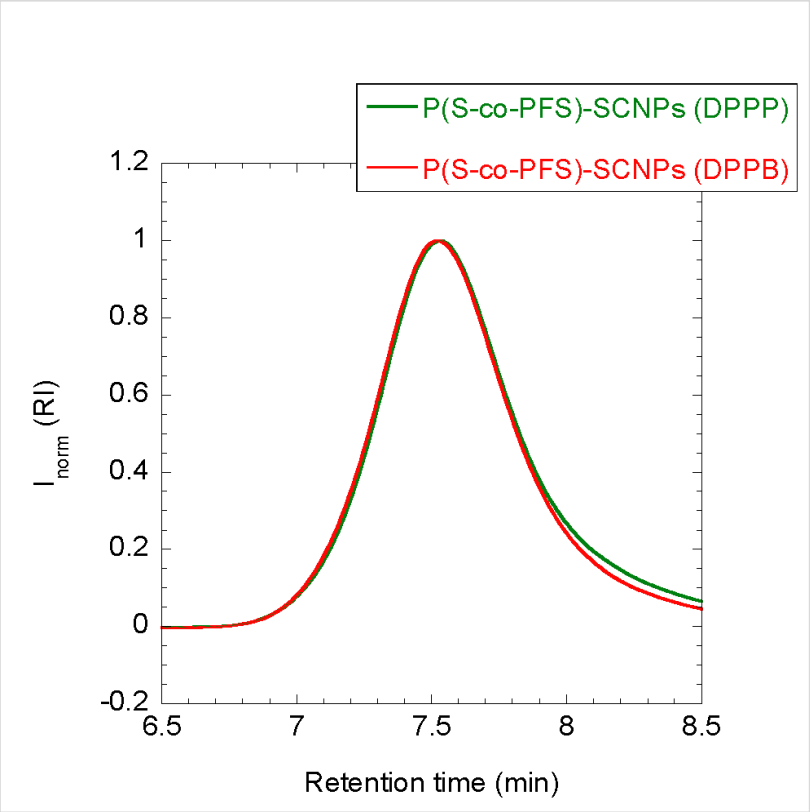

Figure 39. DLS size distribution in THF of P(S-co-ATFS) (blue) and P(S-co-PFS)-SCNPs (red). No differences are observed with the different cross-linkers.

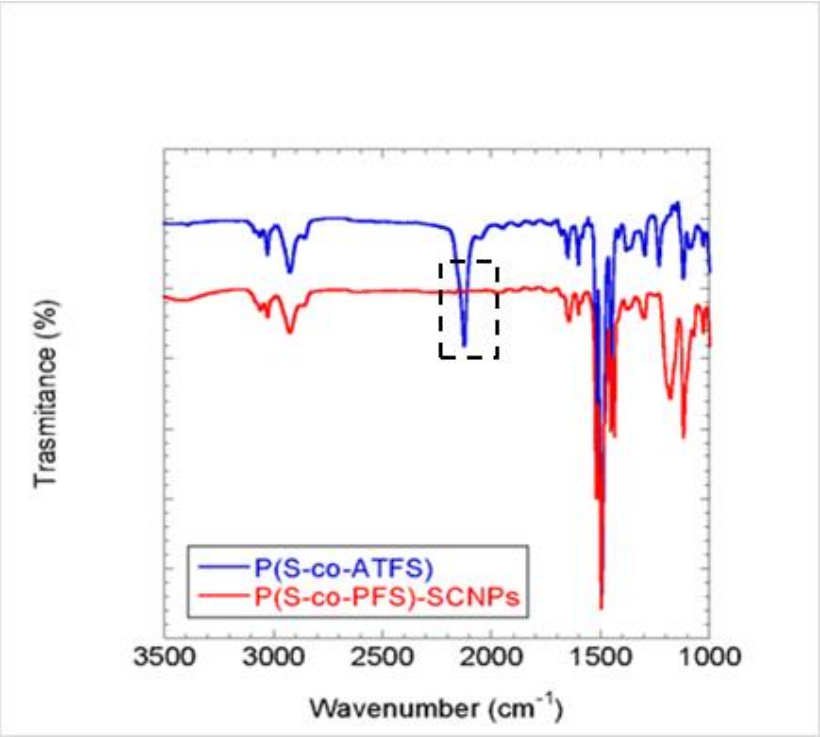

Figure 40. FTIR spectra of P(S-co-ATFS) (blue) and P(S-co-PFS)-SCNPs (red). The disappearance of the signal related to the azide groups confirm the total reaction of those groups.

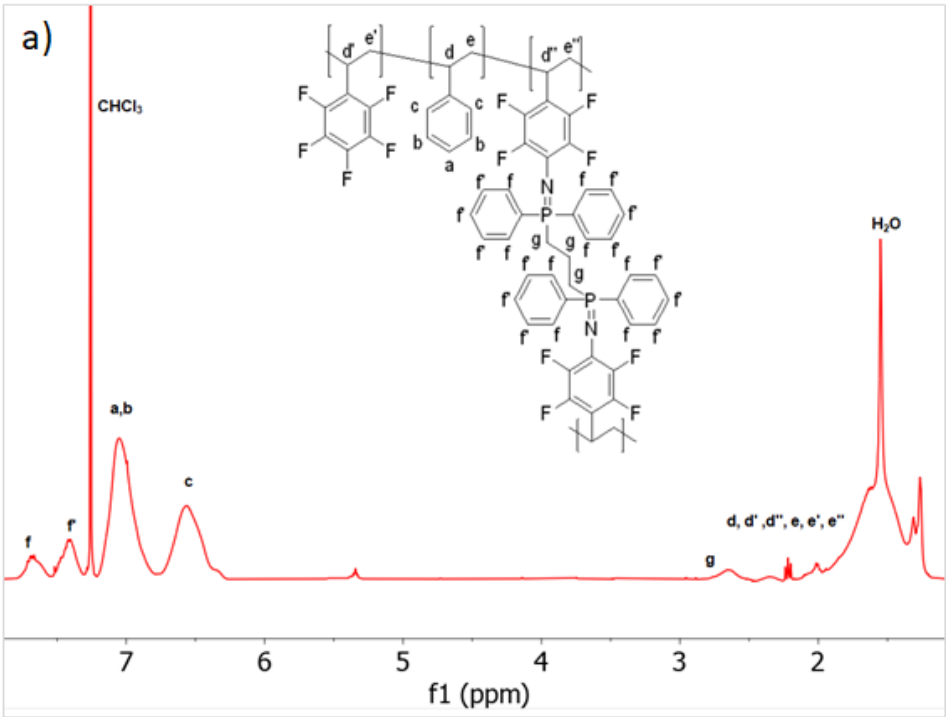

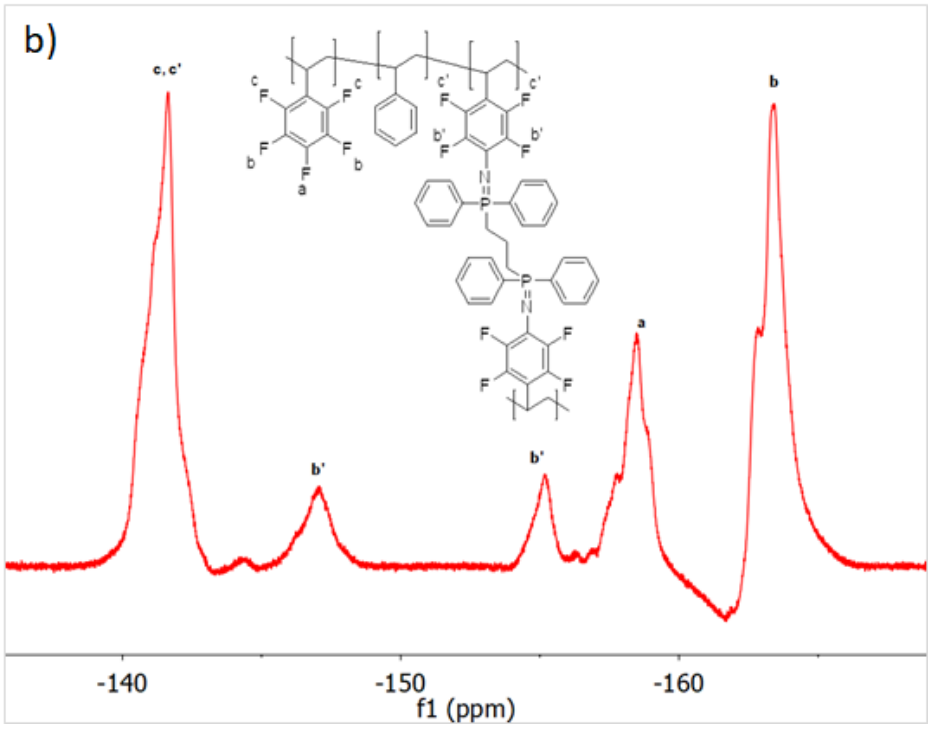
b)
c, c'
b'
b'
a
b
-140
-150
-160
f1 (ppm)

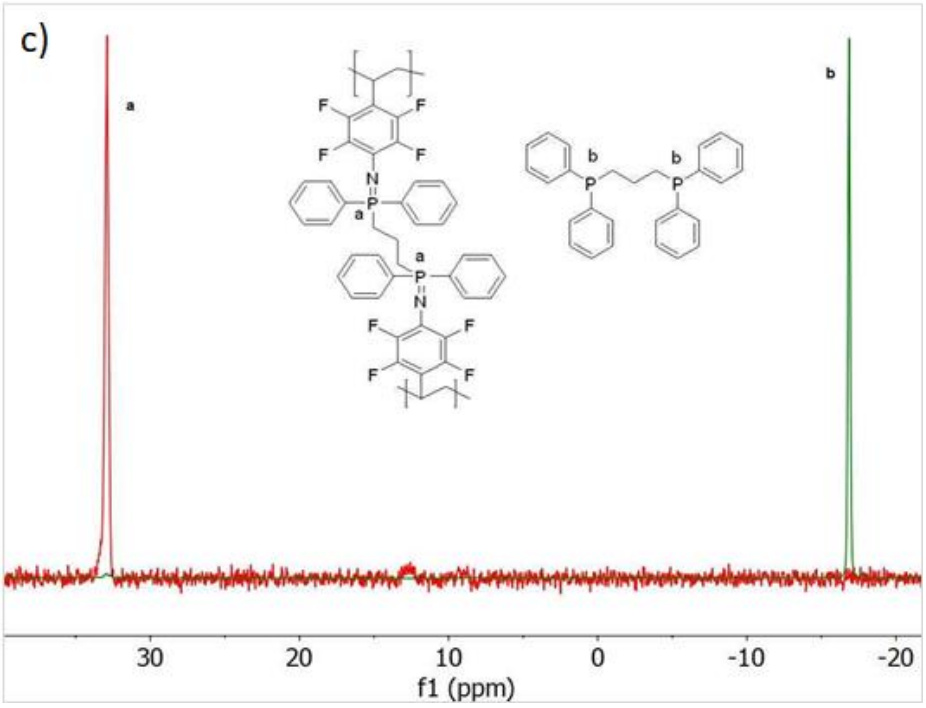
c)
a
b
30
20
10
0
-10
-20
f1 (ppm)

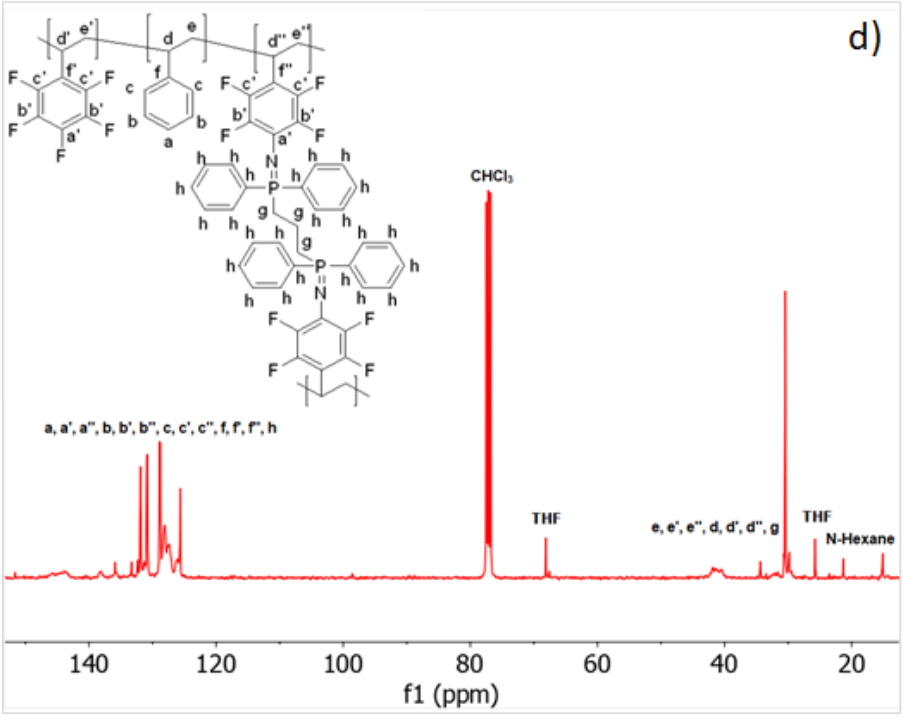

Figure 41. NMR spectra of P(S-co-PFS)-SCNPs (red) and DPPP (green). a) ^{1}H NMR, showing the new peaks f and g related with the cross-linker. b) ^{19}F NMR showing the unfolding of the peak b’ into two different peaks. c) ^{31}P NMR, showing the shift of the peak of the cross-linker before and after the reaction. d) ^{13}C NMR, showing the new peaks g and h related with the cross-linker.

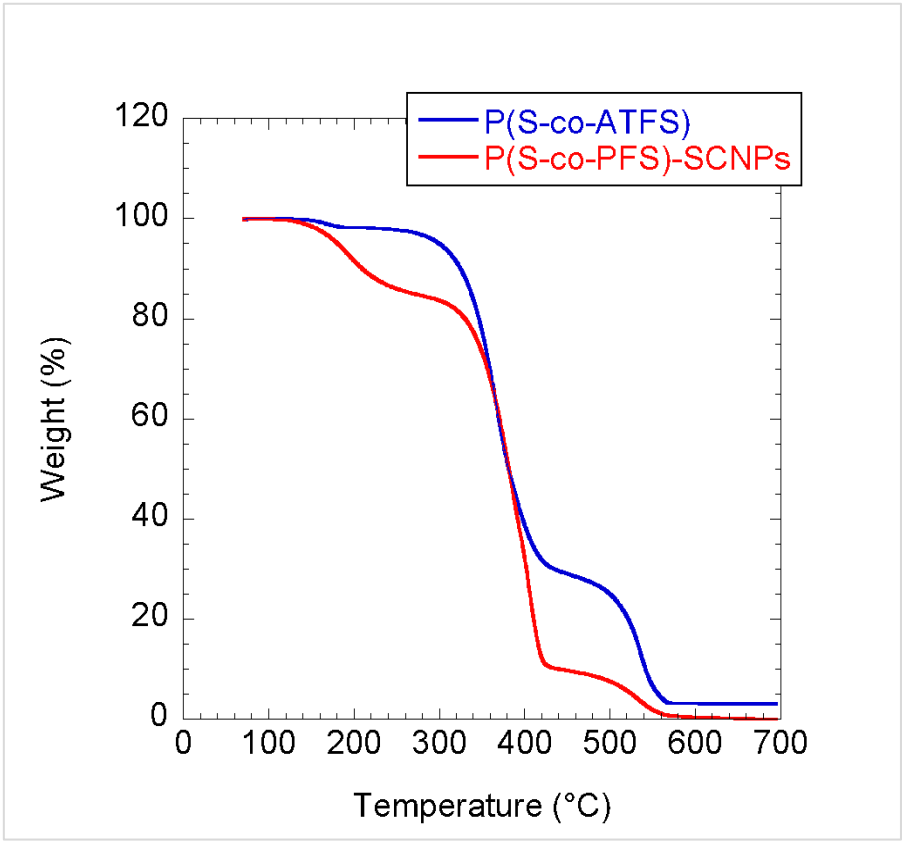

Figure 42. TGA results of P(S-co-ATFS) (blue) and P(S-co-PFS)-SCNPs (red).

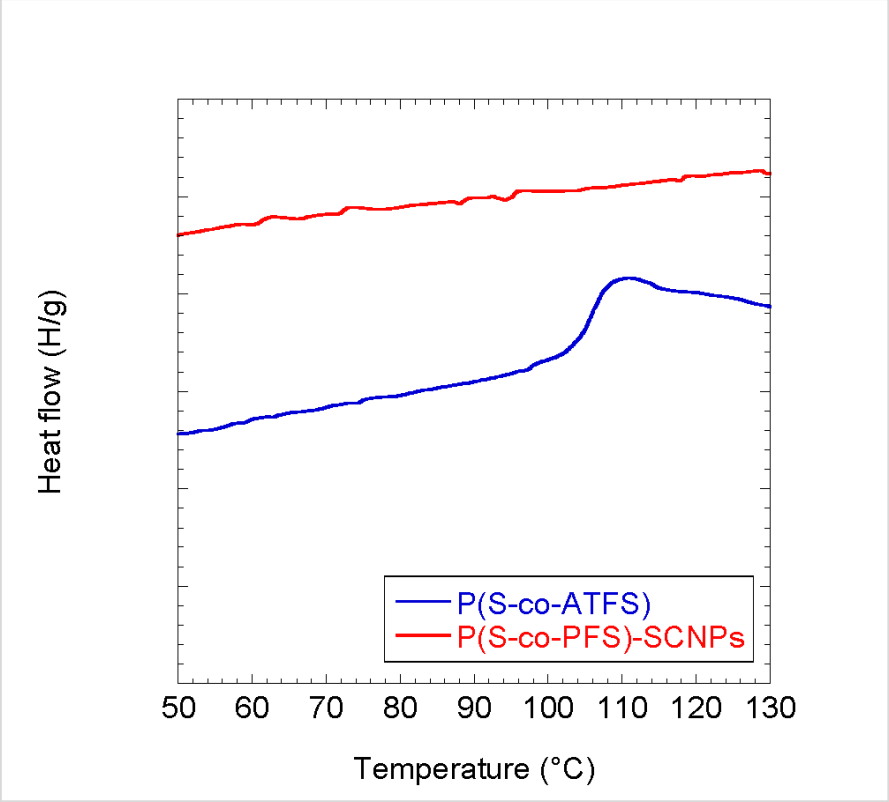

Figure 43. DSC results of P(S-co-ATFS) (blue) and P(S-co-PFS)-SCNPs (red).

4.4.4. Stability of P(S-*co*-PFS)-SCNPs

First, TGA results in air atmosphere revealed that the P(S-*co*-PFS)-SCNPs are thermally stable up to 150 ºC (Figure 42). As illustrated in Figure 44, no changes in the peak position corresponding to the N=P cross-linking points was observed when the SCNPs were heated at 120 °C for 3 days or when are heated by microwave at 120ºC for 1h, both in dimethylformamide (DMF). Moreover, P(S-*co*-PFS)-SCNPs in THF solution were found to be stable in the presence of an excess of either trifluoroacetic acid (TFA) or carbon disulfide (CS_2) at r.t. for 3 days. At this stage, we realize that to break the robust N=P bonds in the nanoparticles.

When we treated a THF solution of P(S-*co*-PFS)-SCNPs with an excess of trimethylsilanol (TMS) for 3 days at r.t. we observed the complete disappearance of the peak corresponding to the N=P cross-linking points in the ^{31}P NMR spectrum of the resulting material (Figure 44). Additionally, GPC results showed a shift toward shorter retention time and, hence, larger R_h (Figure 45 a)). In fact, the GPC retention time at the peak maximum of unfolded nanoparticles, P(S-*co*-NTFS), and the functionalized precursor, P(S-*co*-ATFS), were found to be nearly identical. Additional characterization of unfolded nanoparticles was carried out by combining a variety of techniques including IR and (^1H, ^{19}F) NMR spectroscopy.

The IR spectrum of P(S-*co*-NTFS) showed the complete disappearance of the N=P stretching vibration at 1175 cm^{-1} and the appearance of new bands that can be assigned to vibrations of $-CH_3$ groups (see Figure 46 a)). On one hand, the ^{19}F NMR spectrum of P(S-*co*-NTFS) confirmed the complete disappearance of the two peaks coming from -F atoms at *orto*- (δ = -155.2 ppm) and *meta*- (δ = -147.1 ppm) position with respect to azaylide groups (Figure 46 b)). On the other hand, the ^{1}H NMR spectrum of P(S-*co*-NTFS) showed a new band centered at δ = 0.11 ppm that can be assigned to protons of $-CH_3$ groups, whereas in neat TMS the band of the protons from $-CH_3$ groups was located at δ = 0.03 ppm (Figure 47 a)). Moreover, a DOSY NMR experiment [57] confirmed the $-CH_3$ groups, having the same diffusion coefficient as main chain $-CH_2-$ and -CH- protons, belong to the polymer structure of P(S-*co*-NTFS) (see Figure 47 b)). Consequently, all the above results support that that trimethylsilanol is a break-through, unique and selective reagent for the efficient on-demand unfolding of the highly stable “Staudinger” SCNPs. Figure 48 shows a tentative mechanism of the trimethylsilanol triggered stable azaylide rupture reaction.

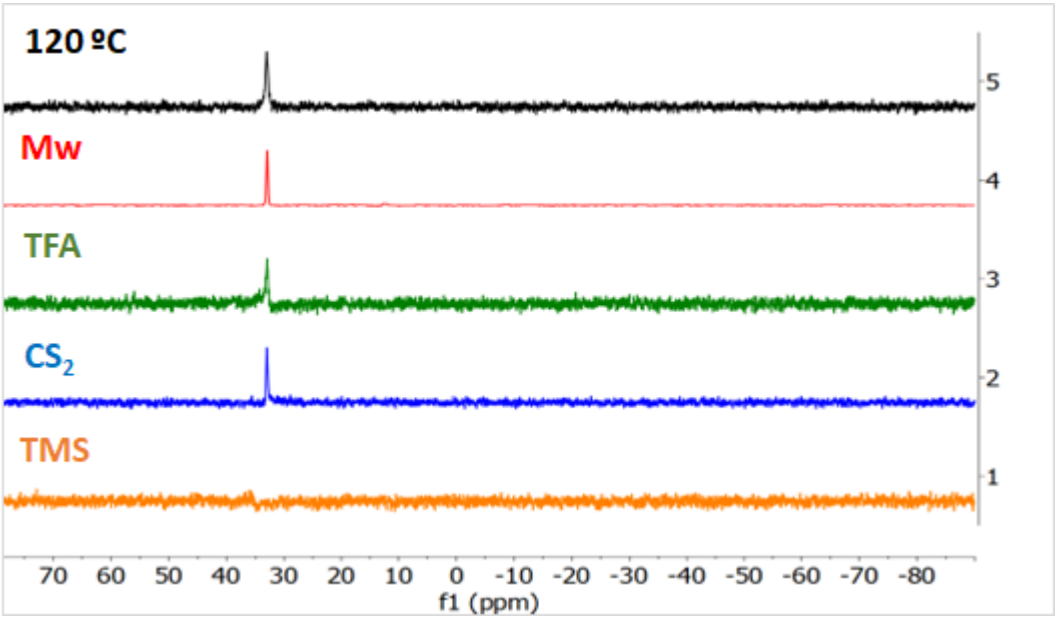

Figure 44. a) ^{31}P NMR of P(S-co-PFS)-SCNPs after been exposed to 3 days of conventional thermal heating at 120 ºC in DMF (black),microwave heating at 120 ºC for 1 h in DMF (red), 3 days in THF at r.t. in the presence of an excess of TFA (green), 3 days in THF at r.t. in the presence of an excess of CS_2 (blue) and 3 days in THF at r.t. in the presence of an excess of TMA (orange).

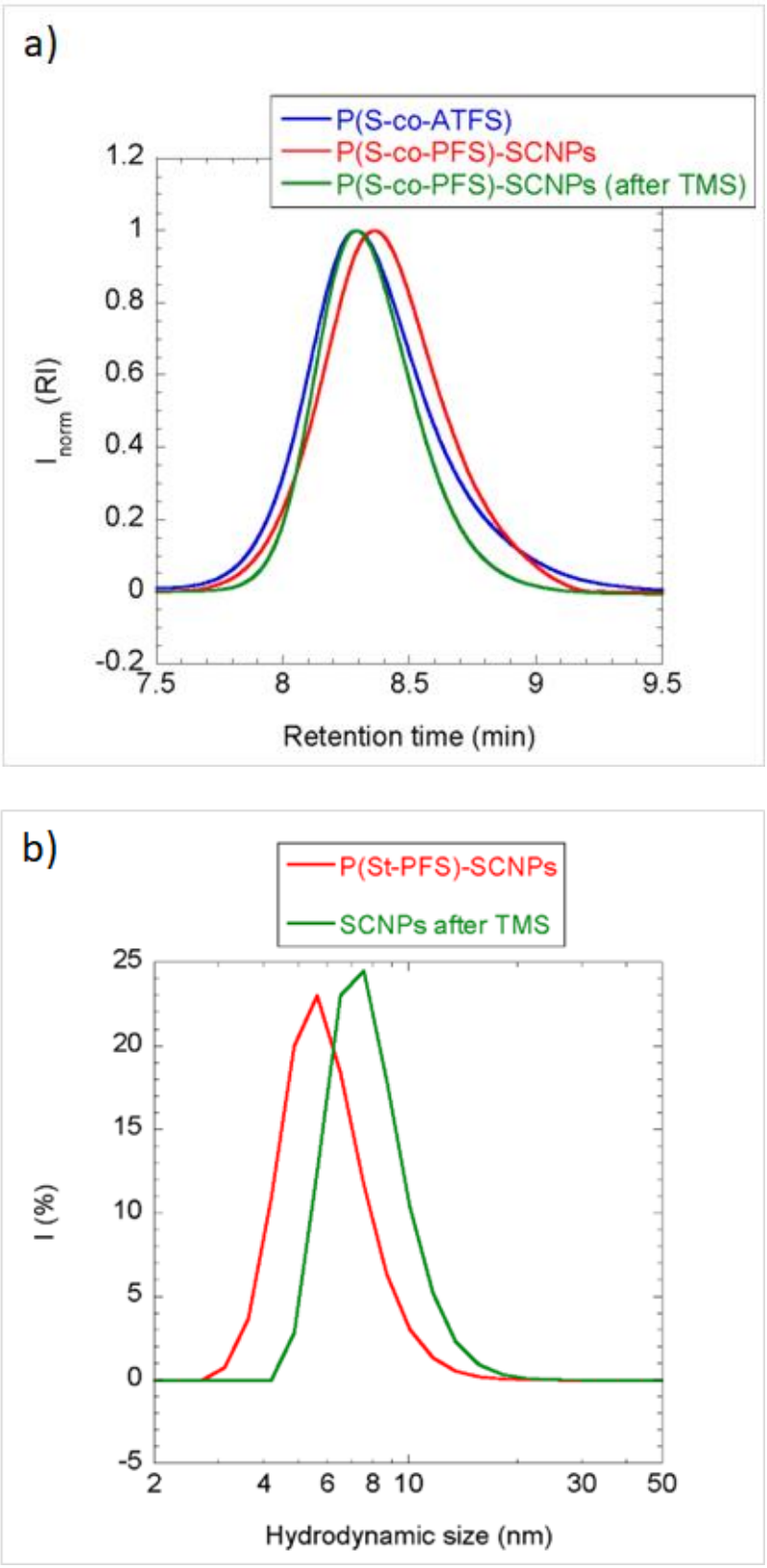

Figure 45. a) GPC chromatogram (RI detector) and b) DLS size distribution in THF of P(S-co-ATFS) (blue), P(S-co-PFS)-SCNPs (red) and P(S-co-PFS)-SCNPs after been exposed to TMS for 3 days. As expected, after break the intra-chain bonds the size is increased.

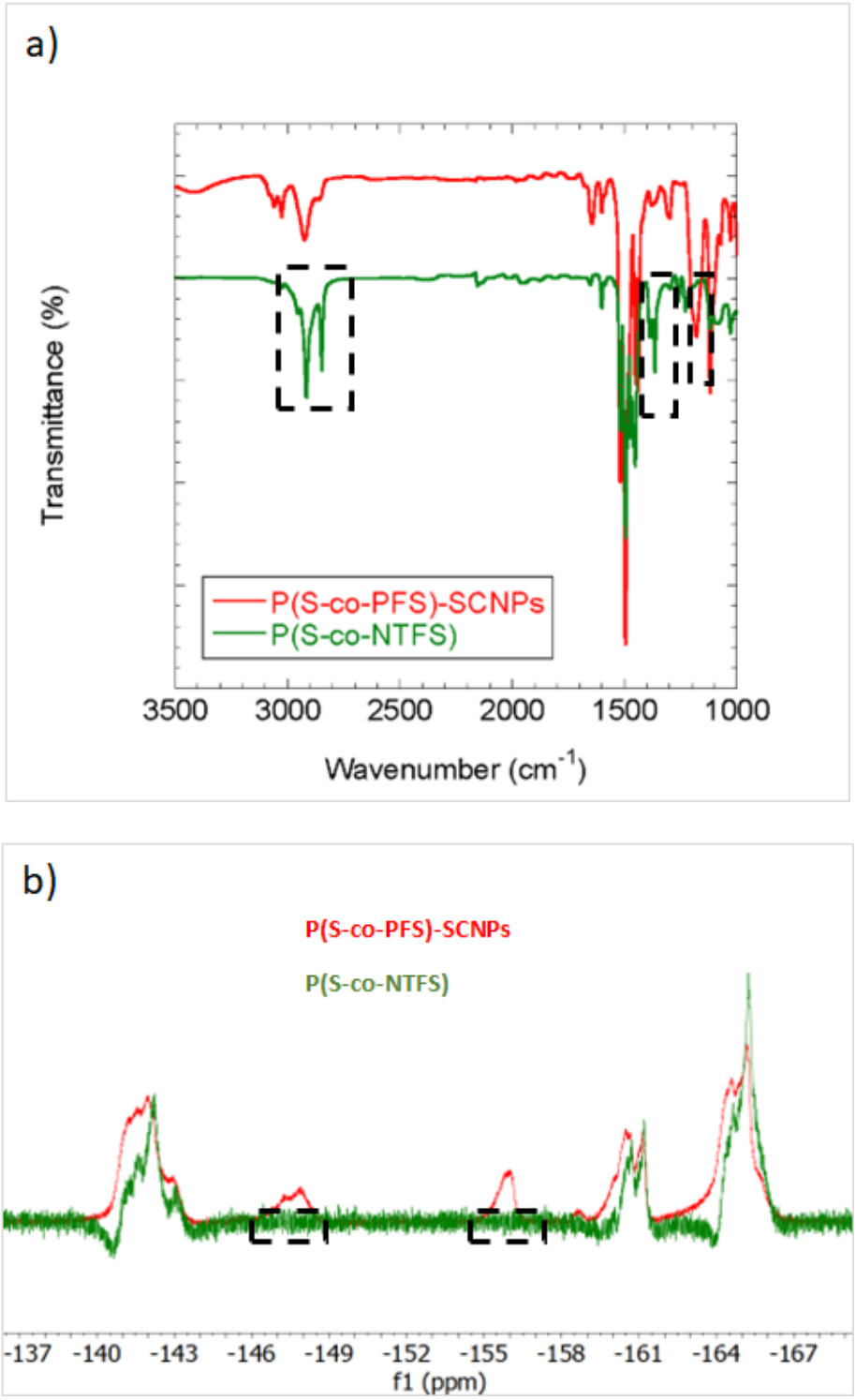

Figure 46. a) FTIR spectra of P(S-co-PFS)-SCNPs (red) and P(S-co-NTFS) (green) showing the disappearance of the N=P stretching vibration band centered at 1175 cm^{-1} and new bands that can be assigned to vibrations of $–CH_3$ groups. b) ^{19}F spectra of P(S-co-PFS)-SCNPs (red) and P(S-co-NTFS) (green) showing the complete disappearance of the bands coming from -F atoms at orto- and meta-position with respect to azaylide groups.

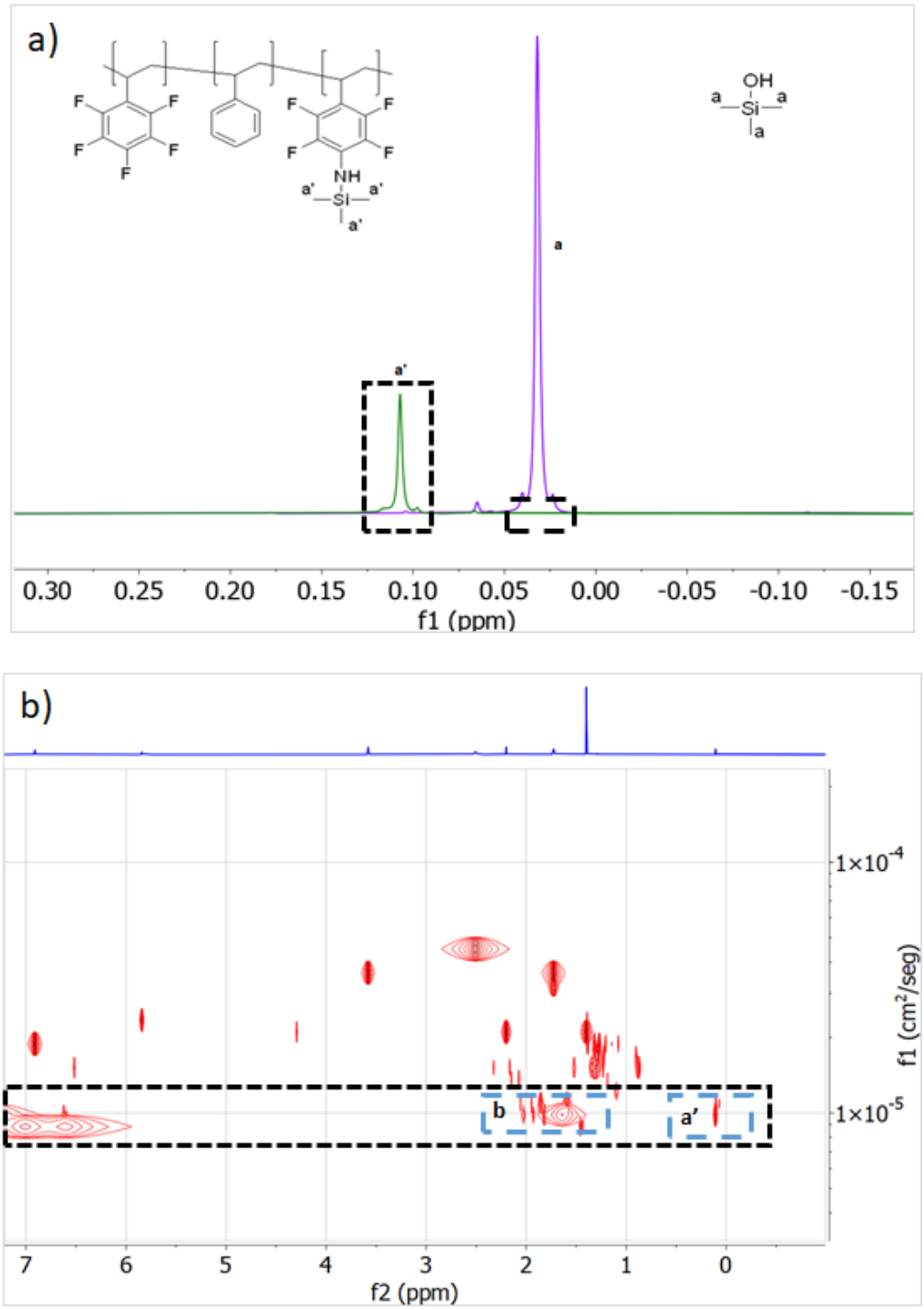

Figure 47. a) ^{1}H NMR spectra of TMS (purple) and P(S-co-NTFS) showing the region in which protons from -CH_3 groups bonded to the silicon atom appear. b) DOSY NMR experiment confirming that the -CH_3 groups (denoted as a´) having the same diffusion coefficient as main chain -CH_2- and -CH- protons (denoted as b)- belong to the polymer structure of P(S-co-NTFS).

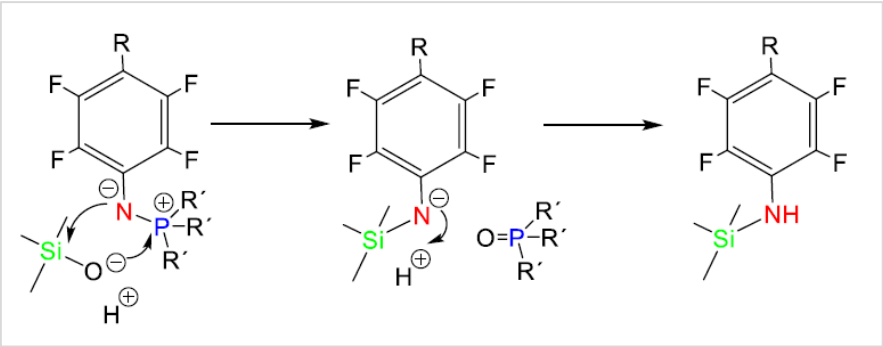

Figure 48. Scheme of the Tentative mechanism of the TMS triggered stable azaylide rupture reaction.

4.5. Conclusion

In conclusion, we have enlarged the toolbox of methods for unfolding covalent-bonded SCNPs by developing the trimethylsilanol triggered selective unfolding of robust “Staudinger” SCNPs. We report on a new platform for the synthesis of stable, inert, dispersible, metal-free single-chain nanoparticles (SCNPs) via intramolecular Staudinger reaction. Doe to the 4-azido-2,3,5,6-tetrafluorostyrene monomer the created bonds are stables and cannot hydrolyze by water. Therefore, using a biphosphino molecule, as 1,3-bis(diphenylphosphino)propane, strong intra-chain bonds can be created with a simple and metal-free reaction at room temperature. We highlight the possibilities of this new synthesis technique by preparing polystyrene-2,3,4,5,6-pentafluorostyrene copolymer (P(S-*co*-PFS)) SCNPs from a copolymer containing 32 mol% of 2,3,4,5,6-pentafluorostyrene monomers. This copolymer was azided with a simple reaction with sodium azide, obtaining an 11 mol%. Compared with the method presented in the chapter 5, this method needs a particular monomer, but can be carried out with different cross-linkers, is faster and do not need for slow injector or additional products to avoid the aggregation. The successful formation of metal-free P(S-*co*-PFS)-SCNPs was confirmed through a powerful combination of techniques, including SEC with triple detection (RI, MALS, and VIS), ^{1}H, ^{19}F, ^{31}P and ^{13}C NMR spectroscopy, DLS, FTIR and TGA measurements. “Staudinger” SCNPs are thermally stable up to 150 °C and their cross-linking N=P bonds are robust against strong acids like TFA (pKa = 0.23) and standard reagents for azaylides like CS_2. However, their cross-linking N=P bonds react with a reagent containing the “electropositive” silicon atom and having weak acidity like TMS allowing the efficient on-demand unfolding of these, otherwise, robust SCNPs.

References

[1] A. Nitti, R. Carfora, G. Assanelli, M. Notari, D. Pasini, Single-Chain Polymer Nanoparticles for Addressing Morphologies and Functions at the Nanoscale: A Review. *ACS Applied Nano Materials* **2022**, 5, 13985-13997.

[2] M. A. M. Alqarni, C. Waldron, G. Yilmaz, C. R. Becer, Synthetic Routes to Single Chain Polymer Nanoparticles (SCNPs): Current Status and Perspectives. *Macromolecular Rapid Communications* **2021**, 42, 2100035.

[3] S. Mavila, O. Eivgi, I. Berkovich, N. G. Lemcoff, Intramolecular Cross-Linking Methodologies for the Synthesis of Polymer Nanoparticles. *Chemical Reviews* **2016**, 116, 878-961.

[4] C. K. Lyon, A. Prasher, A. M. Hanlon, B. T. Tuten, C. A. Tooley, P. G. Frank, E. B. Berda, A Brief User’s Guide to Single-Chain Nanoparticles. *Polymer Chemistry* **2015**, 6, 181-197.

[5] O. Altintas, C. Barner-Kowollik, Single Chain Folding of Synthetic Polymers by Covalent and Non-Covalent Interactions: Current Status and Future Perspectives. *Macromolecular Rapid Communications* **2012**, 33, 958-971.

[6] E. B. Berda, E. J. Foster, E. W. Meijer, Toward Controlling Folding in Synthetic Polymers: Fabricating and Characterizing Supramolecular Single-Chain Nanoparticles. *Macromolecules* **2010**, 43, 1430-1437.

[7] E. Harth, B. V. Horn, V. Y. Lee, D. S. Germack, C. P. Gonzales, R. D. Miller, C. J. Hawker, A Facile Approach to Architecturally Defined Nanoparticles via Intramolecular Chain Collapse. *Journal of the American Chemical Society* **2002**, 124, 8653-8660.

[8] *Single-Chain Polymer Nanoparticles: Synthesis, Characterization, Simulations, and Applications*; J. A. Pomposo, Ed.; John Wiley & Sons: Weinheim, Germany **2017**.

[9] K. Mundsinger, B. T. Tuten, L. Wang, K. Neubauer, C. Kropf, M. L. O'Mara, C. Barner-Kowollik, Visible-Light-Reactive Single-Chain Nanoparticles. *Angewandte Chemie International Edition* **2023**, 62, e2023029.

[10] N. M. Hamelmann, S. Uijttewaal, S. D. Hujaya, J. M. J. Paulusse, Enhancing Cellular Internalization of Single-Chain Polymer Nano-particles via Polyplex Formation. *Biomacromolecules* **2022**, 23, 5036-5042.

[11] J. F. Thuemmler, R. Maragani, F. J. Schmitt, G. Tang, S. M. Rahmanlou, J. Laufer, H. Lucas, K. Maeder, W. H. Binder, Thermoresponsive swelling of photoacoustic single-chain nanoparticles. *Chemical Communications* **2023**, 59, 11373-11376.

[12] N. M. Hamelmann, J. M. J. Paulusse, Single-chain polymer nanoparticles in biomedical applications. *Journal of Controlled Release* **2023**, 356, 26-42.

[13] Y. Shao, Z. Yang, Progress in polymer single-chain based hybrid nanoparticles. *Progress in Polymer Science* **2022**, 133, 101593.

[14] M. H. Barbee, Z. M. Wright, B. P. Allen, H. F. Taylor, E. F. Patteson, A. S. Knight, Protein-Mimetic Self-Assembly with Synthetic Macromolecules. *Macromolecules* **2021**, 54, 3585-3612.

[15] R. Chen, E. B. Berda, 100th Anniversary of Macromolecular Science Viewpoint: Reexamining Single-Chain Nanoparticles. *Angewandte Chemie International Edition* **2020**, 9, 1836-1843.

[16] A. R. A. Palmans. Chap. 25 - Single-chain polymeric nanoparticles: Toward in vivo imaging and catalysis in complex media, in *Self-assembling Biomaterials*. H. S. Azevedo, R. M. P. da Silva, Eds.; Woodhead Publishing, 2018.

[17] E. Verde-Sesto, A. Arbe, A. J. Moreno, D. Cangialosi, A. Alegria, J. Colmenero, J. A. Pomposo, Single-chain nanoparticles: opportunities provided by internal and external confinement. *Materials Horizons* **2020**, 7, 2292-2313.

[18] J. Chen, E. S. Garcia, S. C. Zimmerman, Intramolecularly Cross-Linked Polymers: From Structure to Function with Applications as Artificial Antibodies and Artificial Enzymes. *Accounts of Chemical Research* **2020**, 53, 1244-1256.

[19] H. Rothfuss, N. D. Knofel, P. W. Roesky, C. Barner-Kowollik, Single-Chain Nanoparticles as Catalytic Nanoreactors. *Journal of the American Chemical Society* **2018**, 140, 5875-5881.

[20] A. P. P. Kroger, J. M. J. Paulusse, Single-Chain Polymer Nano-particles in Controlled Drug Delivery and Targeted Imaging. *Journal of Controlled Release* **2018**, 286, 326-347.

[21] J. Rubio-Cervilla, E. González, J. A. Pomposo, Advances in Single-Chain Nanoparticles for Catalysis Applications. *Nanomaterials* **2017**, 7, 341-360.

[22] A. Sanchez-Sanchez, J. A. Pomposo, Single-Chain Polymer Nanoparticles via Non-Covalent and Dynamic Covalent Bonds. *Particle & Particle Systems Characterization* **2014**, 31, 11-23.

[23] E. J. Foster, E. B. Berda, E. W. Meijer, Metastable Supramolecular Polymer Nanoparticles via Intramolecular Collapse of Single Polymer Chains. *Journal of the American Chemical Society* **2009**, 131, 6964-6966.

[24] T. S. Fischer, D. Schulze-Sunninghausen, B. Luy, O. Altintas, C. Barner-Kowollik, Stepwise Unfolding of Single-Chain Nanoparticles by Chemically Triggered Gates. *Angewandte Chemie International Edition* **2016**, 55, 11276-11280.

[25] N. Wedler-Jasinski, T. Lueckerath, H. Mutlu, A. S. Goldmann, A. Walther, M. H. Stenzel, C. Barner-Kowollik, Dynamic covalent single chain nanoparticles based on hetero Diels–Alder chemistry. *Chemical Communications* **2017**, 53, 157-160.

[26] F. Wang, H. T. Pu, Y. Ding, R. Lin, H. Y. Pan, Z. H. Chang, M. Jin, Single-chain folding of amphiphilic copolymers in water via intramolecular hydrophobic interaction and unfolding triggered by cyclodextrin. *Polymer* **2018**, 141, 86-92.

[27] X. F. Ji, C. X. Guo, X. S. Ke, X. D. Chi, J. L. Sessler, Using anion recognition to control the folding and unfolding of a single chain phosphorescent polymer. *Chemical Communications* **2017**, 53, 8774-8777.

[28] T. Mes, R. van der Weegen, A. R. A. Palmans, E. W. Meijer, Single-Chain Polymeric Nanoparticles by Stepwise Folding. *Angewandte Chemie International Edition* **2011**, 50, 5085-5089.

[29] E. Huerta, P. J. M. Stals, E. W. Meijer, A. R. A. Palmans, Consequences of Folding a Water-Soluble Polymer Around an Organocatalyst. *Angewandte Chemie International Edition* **2013**, 52, 2906-2910.

[30] F. Wang, H. T. Pu, M. Jin, D. C. Wan, Supramolecular Nano-particles via Single-Chain Folding Driven by Ferrous Ions. *Macromol. Rapid Communication* **2016**, 37, 330-336.

[31] D. Kodura, H. A. Houck, F. R. Bloesser, A. S. Goldmann, F. E. Du Prez, H. Frisch, C. Barner-Kowollik, Light-fueled dynamic covalent crosslinking of single polymer chains in non-equilibrium states. *Chemical Science* **2021**, 12, 1302-1310.

[32] R. Zeng, L. Chen, Q. Yan, CO_2-Folded Single-Chain Nanoparticles as Recyclable, Improved Carboxylase Mimics. *Angewandte Chemie International Edition* **2020**, 59, 18418-18422.

[33] W. Z. Fan, X. Tong, F. Farnia, B. Yu, Y. Zhao, CO_2-Responsive Polymer Single-Chain Nanoparticles and Self-Assembly for Gas-Tunable Nanoreactors. *Chemistry of Materials* **2017**, 29, 5693-5701.

[34] F. Wang, H. Pu, X. Che, Voltage-responsive single-chain polymer nanoparticles via host–guest interaction. *Chemical Communications* **2016**, 52, 3516-3519.

[35] H. Kalmer, F. Sbordone H. Frisch, Peptide based folding and function of single polymer chains. *Polymer Chemistry* **2022**, 13, 5458-5462.

[36] B. T. Tuten, D. M. Chao, C. K. Lyon, E. B. Berda, Single-chain polymer nanoparticles via reversible disulfide bridges. *Polymer Chemistry* **2012**, 3, 3068-3071.

[37] A. Sanchez-Sanchez, D. A. Fulton, J. A. Pomposo, pH-responsive single-chain polymer nanoparticles utilising dynamic covalent enamine bonds. *Chemical Communications* **2014**, 50, 1871-1874.

[38] S. Wijker, R. Monnink, L. Rijnders, L. L. Deng, A. R. A. Palmans, Simultaneously controlling conformational and operational stability of single-chain polymeric nanoparticles in complex media. *Chemical Communications* **2023**, 59, 5407-5410.

[39] A. Sanchez-Sanchez, I. Pérez-Baena, J. A. Pomposo, Advances in Click Chemistry for Single-Chain Nanoparticle Construction. *Molecules* **2013**, 18, 3339-3355.

[40] S. Babaoglu, D. K. Balta, G. Temel, Synthesis of Photoactive Single-Chain Folded Polymeric Nanoparticles via Combination of Radical Polymerization Techniques and Menschutkin Click Chemistry. *Journal of Polymer Science Part A: Polymer Chemistry* **2017**, 55, 1998-2003.

[41] T. S. Fischer, S. Spann, Q. An, B. Luy, M. Tsotsalas, J. Blinco, H. Mutlu, C. Barner-Kowollik, Self-reporting and refoldable profluorescent single-chain nanoparticles. *Chemical Science* **2018**, 9, 4696-4702.

[42] F. R. Bloesser, S. L. Walden, I. M. Irshadeen, L. C. Chambers, C. Barner-Kowollik, Chemiluminescent self-reported unfolding of single-chain nanoparticles. *Chemical Communications* **2021**, 57, 5203-5206.

[43] P. H. Maag, F. Feist, V. X. Truong, H. Frisch, P. W. Roesky, C. Barner-Kowollik, Visible-Light-Induced Control over Reversible Single-Chain Nanoparticle Folding. *Angewandte Chemie International Edition* **2023**, 62, e20230925.

[44] C. Stuckhardt, M. Wissing, A. Studer, Photo Click Reaction of Acylsilanes with Indoles. *Angewandte Chemie International Edition* **2021**, 60, 18605-18611.

[45] H. M. Staudinger, J. J. Meyer, Über neue organische Phosphorverbindungen III. Phosphinmethylenderivate und Phosphinimine. *Helvetica Chimica Acta* **1919**, 2, 635-646.

[46] E. Saxon, C. R. Bertozzi, Cell Surface Engineering by a Modified Staudinger Reaction. *Science* **2000**, 287, 2007-2010.

[47] M. Sundhoro, S. Jeon, J. Park, O. Ramstrom, M. D. Yan, Perfluoroaryl Azide Staudinger Reaction: A Fast and Bioorthogonal Reaction. *Angewandte Chemie International Edition* **2017**, 56, 12117-12121.

[48] J. Zhang, Y. Gao, X. Y. Kang, Z. T. Zhu, Z. Q. Wang, Z. Xi, L. Yi, o,o-Difluorination of aromatic azide yields a fast-response fluorescent probe for H_2S detection and for improved bioorthogonal reactions. *Organic & Biomolecular Chemistry* **2017**, 15, 4212-4217.

[49] Y. H. Xie, L. H. Cheng, Y. S. Gao, X. K. Cai, X. Yang, L. Yi, Z. Xi, Tetrafluorination of Aromatic Azide Yields a Highly Efficient Staudinger Reaction: Kinetics and Biolabeling. *Chemistry – An Asian Journal* **2018**, 13, 1791-1796.

[50] T. Meguro, N. Terashima, H. Ito, Y. Koike, I. Kii, S. Yoshida, T. Hosoya, Staudinger reaction using 2,6-dichlorophenyl azide derivatives for robust aza-ylide formation applicable to bioconjugation in living cells. *Chemical Communications* **2018**, 54, 7904-7907.

[51] M. Sundhoro, J. Park, B. Wu, M. D. Yan, Synthesis of Polyphosphazenes by a Fast Perfluoroaryl Azide-Mediated Staudinger Reaction. *Macromolecules* **2018**, 51, 4532-4540.

(52) W. A. Pryor, T.-L. Huang, The Kinetics of the Polymerization of Pentafluorostyrene. *Macromolecules* **1969**, 2, 70-77.

(53) J. F. W. Keana, S. X. Cai, New Reagents for Photoaffinity Labeling: Synthesis and Photolysis of Functionalized Perfluorophenyl Azides. *The Journal of Organic Chemistry* **1990**, 55, 3640-3647.

(54) J. M. Noy, Y. M. Li, W. Smolan, P. J. Roth, Azide-para-Fluoro Substitution on Polymers: Multipurpose Precursors for Efficient Sequential Postpolymerization Modification. *Macromolecules* **2019**, 52, 3083-3091.

(55) T. Kakuchi, Y. Chen, J. Kitakado, K. Mori, K. Fuchise, T. Satoh, Organic Superbase as an Efficient Catalyst for Group Transfer Polymerization of Methyl Methacrylate. *Macromolecules* **2011**, 44, 4641-4647.

(56) M. Jorge, A. W. Milne, M. C. Barrera, J. R. B. Gomes, New Force-Field for Organosilicon Molecules in the Liquid Phase. *ACS Physical Chemistry Au* **2021**, 1, 54-69.

(57) T. Borke, A. Korpi, F. Pooch, H. Tenhu, S. Hietala, Poly(glyc-eryl glycerol): A multi-functional hydrophilic polymer for labeling with boronic acids. *Journal of Polymer Science Part A: Polymer Chemistry* **2017**, 55, 1822-1830.

5. Toward Long-Term-Dispersible, Metal-Free Single-Chain Nanoparticles

5.1. Motivation

Single-chain polymer nanoparticles (SCNPs) synthesized *via* Cu(I)-catalyzed azide–alkyne cycloaddition (*i.e.,* "click" chemistry) often experience metal-induced aggregation issues during storage. Moreover, the presence of metal traces limits its use in a number of potential uses (e.g., "bio" and "electronic" applications). In this chapter, we report the synthesis of metal-free polystyrene (PS)-SCNPs without aggregation issues during storage, as demonstrated by small-angle X-ray scattering (SAXS) experiments, by using a special bifunctional cross-linker molecule with two highly strained and reactive alkyne bonds.

5.2. Introduction

Single-chain nanoparticles (SCNPs) are soft nano-object formed by the folding of a single chain of a polymer. These nanoparticles have a wide range of applications, as drug delivery, catalyst or sensing [1-9]. According to the nature of the intra-chain bonds that fold the chain, there are two types of SCNPs: permanent SCNPs and reversible SCNPs. While permanent SCNPs are result of covalent intra-chain bonds, reversible ones are conformed by non-covalent or dynamic covalent bonds [10-15]. Reversible SCNPs respond to external stimuli, like temperature or pH, so are used in enzyme mimicry and drug delivery applications [16-20], while permanent SCNPs are used to catalysis or all-polymer nanocomposites due to their long-term stability [21-25].

To synthesize SCNPs a polymer precursor is modified to create some functional groups along the chain that will react to create the intra-chain bonds that cause the collapse of the chain. There are reported different method to synthesize SCNP, but the more efficient ones are based in different click-reactions [26, 27]. One of the most used synthesize method is a click reaction discovered by Sharpless [28] and Meldal [29]: the copper (I)-catalyzed azide-alkyne cycloaddition (CuAAC) click-reaction [30-32]. In this reaction an azide group and an alkyne bond create a triazole group presence of copper (I) catalyst.

The copper (I)-catalyzed azide-alkyne cycloaddition (CuAAC) click-reaction is an efficient method to synthesize SCNPs with high yield and at room temperature. However, the resulting triazole group is prone to complex the copper ions from the catalyst, making significantly complicated to remove the metal traces. Consequently, those SCNP cannot be used in some applications due to the toxicity, coloration and stability issues [33, 34]. On the one hand, the Cu ions can interfere with many biological processes [35] and various electrical and optoelectronic phenomena [36]. On the other hand, some macromolecule-metal complexes have the tendency to aggregate due

to the electrostatic or dipole-dipole interactions of the metal ions [37]. So, these SCNP tend to an irreversible aggregation state during storage in the solid state [38].

In this chapter, a new method to synthesize SCNP is presented: to avoid the catalyst strain-promoted azide-alkyne cycloaddition (SPAAC) is used. SPAAC reaction that was developed by Bertozzi [39] is a catalyst-free equivalent of the CuAAC, where strained cyclooctynes that have a decreased activation energy to react with the azides without any catalyst. This type of metal-free click reactions has been applied in several field as dynamic in vivo imaging [40], cellulose modification [41] or functionalization of surfaces [42]. In this work, *sym*-dibenzo-1,5-cyclooctadiene-3,7-diyne (DIBOD) molecule (Figure 49) is used as cross-linker due to the presence of two highly strained alkyne bonds. This molecule was first synthesized by Sondheimer et al in 1974 [43] and has been used for fluorescence labeling of azido-glycoconjugates on cell surfaces [44] and for the efficient construction of rings [45] and cage-shaped polymers [46]. However, to the best of our knowledge, DIBOD has not yet been investigated as an intra-chain cross-linker for metal-free SCNP construction.

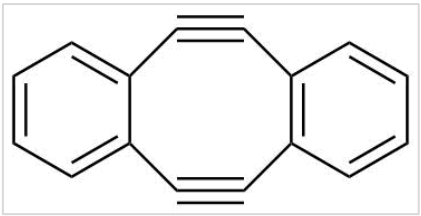

Figure 49. Scheme of the structure of sym-dibenzo-1,5-cyclooctadiene-3,7-diyne (DIBOD), the selected molecule as cross-linker.

To illustrate the utility of DIBOD as cross-linker for the synthesis of metal-free SCNPs via SPAAC, a poly(styrene-*co*-4-(Chloromethyl)styrene) (P(S-*co*-CMS)) copolymer has been synthesized and azided to create a polymer precursor with azide functional groups. DIBOD has been used as external bifunctional cross-linker to create the intra-chain bonds that fold the chain into SCNP. GPC and SAXS characterization techniques have been used to demonstrate that the metal-free SCNPs can be storage in solid state without significant aggregation issues. Remarkably, this new synthetic method is useful for the preparation of stable, metal-free SCNPs from potentially any polymer precursor decorated with azide functional groups.

Experimental procedures

5.2.1. Materials

Styrene (S, ≥99%), sodium azide (NaN_3, ≥99%), N,N-dimethylformamide (DMF, ≥99.9%) and 1,1'-azobis(cyclohexanecarbonitrile) (ACHN, ≥98%) were purchased from Sigma-Aldrich (Madrid,

Spain). Chloromethyl styrene (CMS, ≥90%) and sym-dibenzo-1,5-cyclooctadiene-3,7-diyne (DIBOD, >90%) were supplied by TCI Europe (Zwijndrecht, Belgium). Tetrahydrofuran (THF, GPC grade) and methanol (MeOH, analytical grade) were purchased from Scharlau (Barcelona, Spain). Benzyl azide (BzA, 94%) was purchased from Thermo Scientific (Eindhoven, Netherlands). S-cyanomethyl-S-dodecyltrithiocarbonate (CDTC, ≥97%) was purchased from Strem (Bischheim, France). Ethanol (EtOH, 96% v/v) was purchased from PanReac AppliChem (Barcelona, Spain). Deuterated chloroform ($CDCl_3$, 99.50%, 0.03% TMS v/v) was purchased from Eurisotop (Saint-Aubin, France). Unless otherwise specified, all reagents were used as received without further purification. To remove the inhibitor, S and CMS were purified by being passed through a column packed with activated basic alumina.

5.2.2. Techniques

- *Gel permeation chromatography (GPC)*

GPC measurements were performed at 25 ºC on an Agilent 1200 system equipped with PLgel 5 µm Guard and PLgel 5 µm MIXED-C columns, and triple detection: a differential refractive index (RI) detector (Optilab Rex, Wyatt, Toulouse, France), a multi-angle laser light scattering (MALS) detector (MiniDawn Treos, Wyatt, Toulouse, France), and a viscosimetric (VIS) detector (ViscoStar-II, Wyatt, Toulouse, France). Data analysis was performed using ASTRA Software (version 6.1) from Wyatt. THF was used as an eluent at a flow rate of 1 mL/min. A value of dn/dc = 0.186 was used for poly(S-*co*-CMS), poly(S-*co*-AMS) and the metal-free PS-SCNPs.

- *Dynamic light scattering (DLS)*

DLS measurements (number distribution) were taken at room temperature on a Malvern Zetasizer Nano ZS (Cambridge, United Kingdom) apparatus.

- *Small-angle X-ray scattering (SAXS)*

SAXS experiments were conducted on the Rigaku (Barcelona, Spain) 3-pinhole PSAXSL equipment of the Materials Physics Center, operating at 45 kV and 0.88 mA. The MicroMax-002+ X-ray Generator System is composed of a microfocus sealed tube source module and an integrated X-ray generator unit, which produces CuK_α transition photons of wavelength $\lambda = 1.54$ Å. The flight path and the sample chamber in this equipment are under vacuum. The scattered X-rays are detected on a two-dimensional multiwire X-ray Detector (Gabriel (Barcelona, Spain) design, 2D-200X) and converted to one-dimensional scattering curves by radial averaging. This gas-filled proportional type detector offers a 200 mm diameter active area with ca. 200-micron resolution. After radial integration, the scattered intensities were obtained as a function of

momentum transfer$Q = 4\pi\lambda^{-1} sin\ \theta$, where θ is half the scattering angle. Reciprocal space calibration was performed using silver behenate as standard. The sample-to-detector distance was 2 m, covering a Q-range between 0.008 and 0.20 $Å^{-1}$. The measurements were taken at r.t. on the THF solutions in boron-rich capillaries of 2 mm thickness, with counting times of 1 h. The concentration was 1 mg/mL in order to avoid interference effects between different macromolecules. The data were carefully corrected for background scattering (due to the capillary and solvent) and measured for each sample on the same capillary for the same time. Scattering cross-sections were obtained in absolute units using water as the calibration standard. The generalized Gaussian coil function [47] was employed for a precise determination of the values of the radius of gyration, R_g, and scaling exponent, ν.

- *Nuclear magnetic resonance (NMR)*

^1H NMR and ^{13}C NMR spectra were recorded at room temperature on Bruker (Madrid, Spain) spectrometers operating at 400 MHz, using $CDCl_3$ as solvent.

- *Fourier transform infrared spectroscopy (FTIR)*

FTIR spectra were recorded using ATR in a FT-IR JASCO 6360 (130-400K) infrared spectrometer at room temperature.

- *Elemental analysis (EA)*

The samples of this thesis were measured in an EA3000 elemental analyzer (CHNS).

- *Thermogravimetric analysis (TGA)*

TGA measurements were performed on a Q500-TA Instruments (Cerdanyola del Valles, Spain) apparatus at a heating rate of 10ºC/min under a nitrogen atmosphere.

5.2.3. Procedures

- *Synthesis of Poly(S-co-CMS)*

P(S-*co*-CMS) was prepared by RAFT polymerization [48] in bulk. S (2 mL, 17.4 mmol, 1 eq.), CMS (1.05 mL, 7.45 mmol, 0.43 eq.), ACHN as the initiators (2.6 mg, 6.12 x 10^{-4} eq.), and CDTC (5.1 mg, 9.23 x 10^{-4} eq.) as the RAFT agent were added to a 50 mL round bottom flask (Figure 50). The reaction was stirred at 65 ºC for 48 h. P(S-*co*-CMS) was obtained by precipitation in MeOH, isolated by filtration, and finally dried in a vacuum oven at 35 ºC overnight. Its parameter values were: yield = 40%; CMS content (^1H NMR) = 27 mol%; M_w (SEC/MALS) = 100.5 kDa; Đ (SEC) = 1.15; and R_h (SEC/VIS) = 8.2 nm.

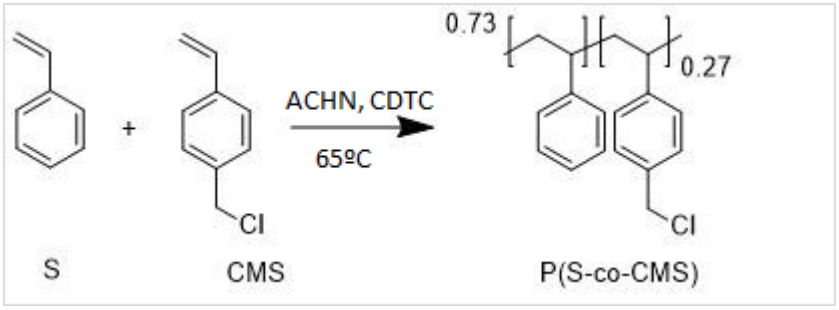

Figure 50. Synthetic scheme of the synthesis of Poly(S-co-CMS).

- *Synthesis of Poly(S-co-AMS)*

P(S-*co*-CMS) (2 g, 4.65 mmol of Cl, 1 eq.) and NaN_3 (0.604 g, 9.3 mmol, 2 eq.) were dissolved in DMF (80 mL) in a 100 mL round-bottom flask and the resulting mixture was stirred at 80 ºC for 24 h (Figure 51). P(S-*co*-AMS) was recovered by precipitation in a mixture of MeOH and water (1:1) and then filtered and dried at 35 ºC under vacuum overnight. ^{1}H and ^{13}C NMR spectroscopy were used to check that all the chlorine atoms in the original polymer were substituted with azide groups. Its parameter values were yield = 97%; azide content (^{1}H NMR) = 27 mol%; M_w (SEC/MALS) = 129.1 kDa; Đ (SEC) = 1.18; and R_h (SEC/VIS) = 9.2 nm.

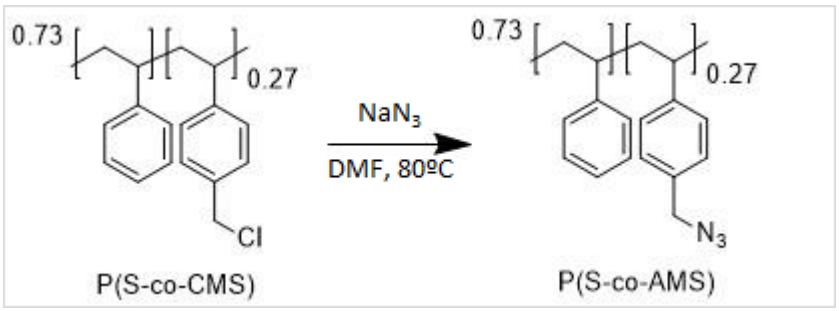

Figure 51. Synthetic scheme of the synthesis of Poly(S-co-AMS).

- *Synthesis of Metal-Free PS-SCNPs*

Poly(S-*co*-AMS) (50 mg, 0.106 mmol of N_3, 1 eq.) was dissolved in THF (25 mL) in a flask that was sealed and degassed. In a second flask that was also sealed, degassed, and protected from light with aluminum foil, DIBOD (12 mg, 0.53 eq.) was dissolved in 75 mL of THF. The solution containing poly(S-*co*-AMS) was injected into the DIBOD solution (both at r.t.) using an injection pump at an addition rate of 2.1 mL/h (Figure 52). The slow addition technique, first introduced by Hawker et al. [49] to avoid the creation of aggregates by bonds between different chains. After 24 h (12 h of injection + 12 h of additional stirring), BzA (20 µL, 1.6 eq.) was added and the solution was subjected to stirring at r.t. for an additional 24 h. The product was precipitated in

cold EtOH, filtrated, and dried at 35 ºC under a vacuum overnight. Its parameter values were yield = 89%; M_w (SEC/MALS) = 195.8 kDa; Đ (SEC) = 1.21; and R_h (SEC/VIS) = 6.9 nm.

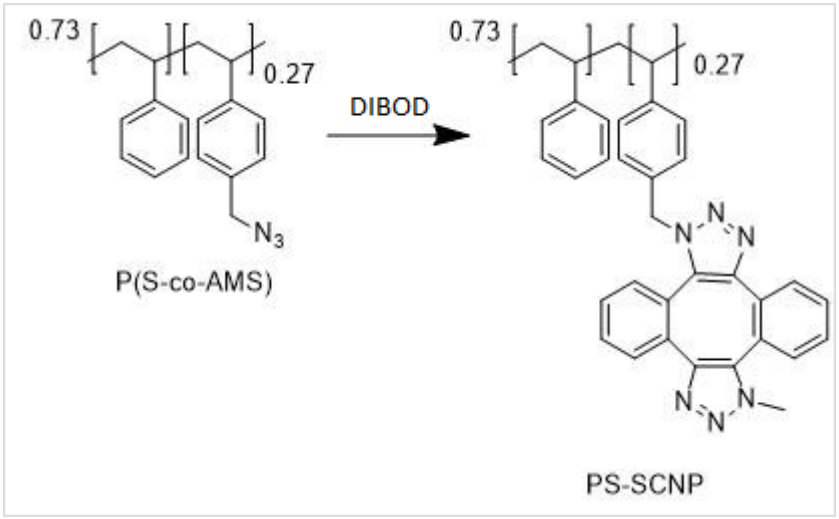

Figure 52. Synthetic scheme of the synthesis of PS-SCNPs.

5.3. Results and discussion

5.3.1. Synthesis of P(S-*co*-AMS)

The synthesized P(S-*co*-CMS) copolymer contains 27 mol% of CMS units, estimated by ^{1}H NMR (Figure 53), and has a weight-average molecular weight (M_w) of 100.5 kDa, polydispersity (Đ) of 1.15 and a hydrodynamic radius (R_h (VIS)) in THF of 8.2 nm, obtained by the GPC technique (Figure 55). The polymer was characterized by ^{13}C NMR too (Figure 54).

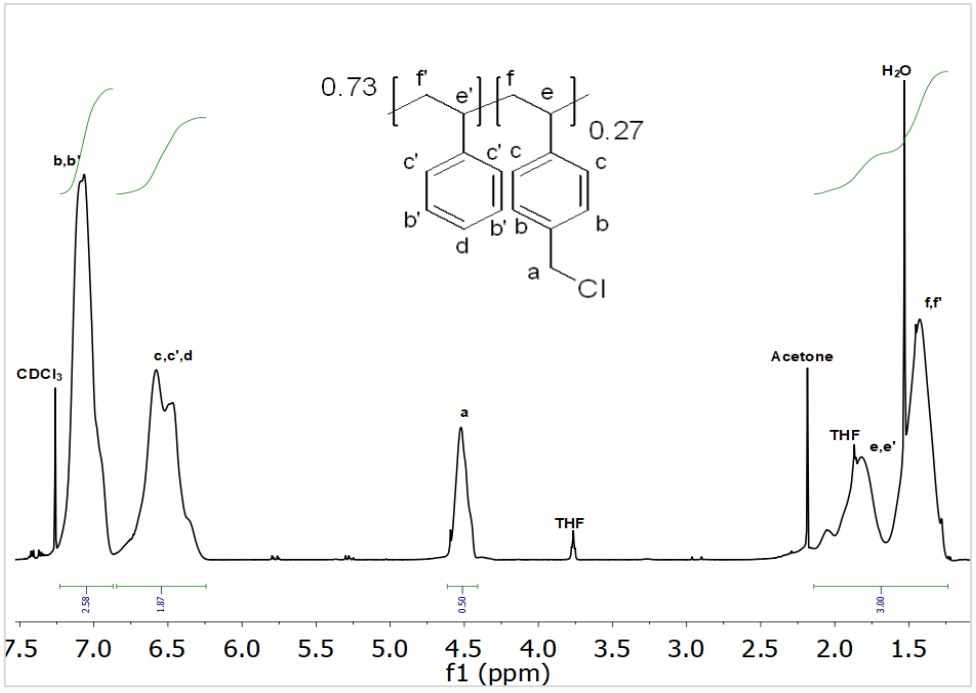

Figure 53. ^{1}H NMR spectrum of P(S-co-CMS).

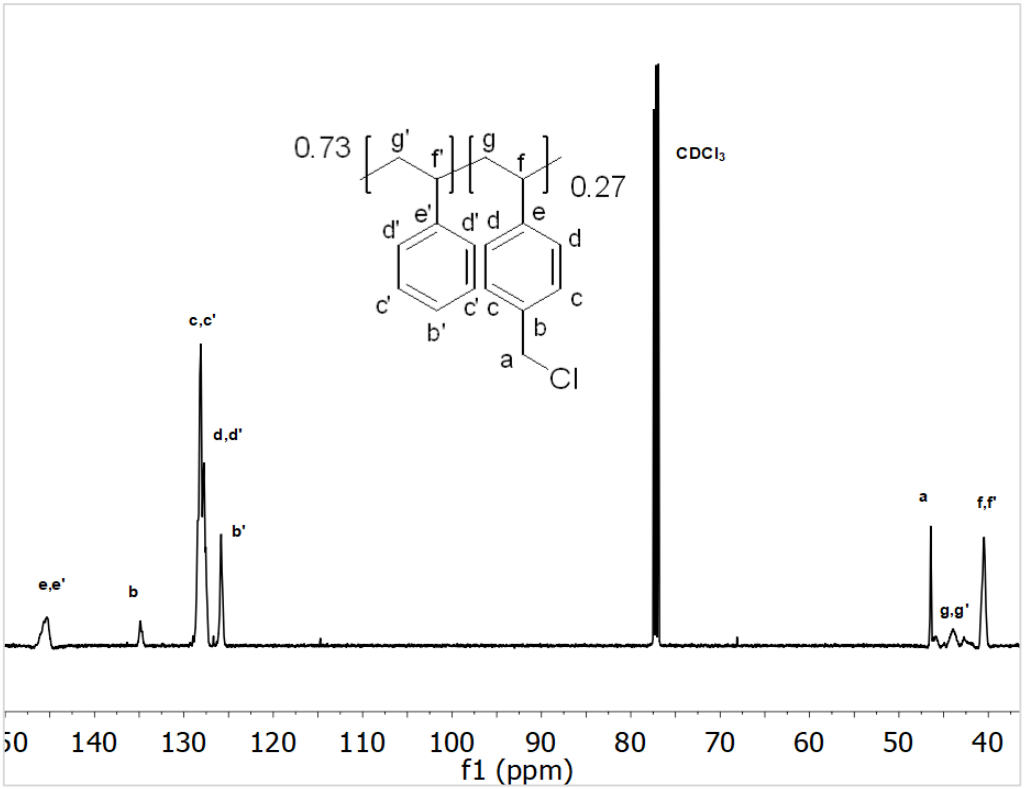

Figure 54. ^{13}C NMR spectrum of P(S-co-CMS).

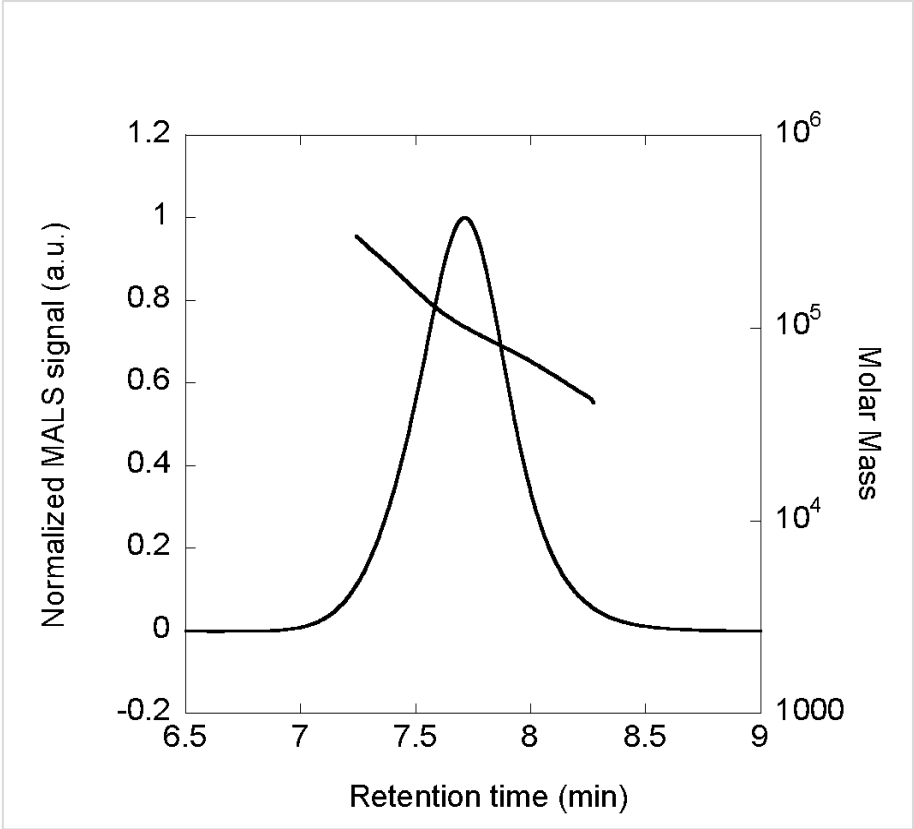

Figure 55. GPC chromatograph of P(S-co-CMS) (LS detector).

The azidation of the PS was checked by FTIR, observing the appearance of the characteristic peak of the azide group around 2100 nm. The total replacement of the Cl atoms with N_3 functional groups was confirmed by ^{1}H NMR and ^{13}C NMR techniques seeing the displacement of the signals related with the methyl group that is linked to the Cl and N_3 groups, Figures 56 and 57. As can check in the GPC characterization, Figure 58, the azidation reaction increase the polymer size, R_h (VIS) = 9.2 nm, and molecular mass, M_w = 129.1 kDa; but the polydispersity is approximately the same, Đ = 1.18.

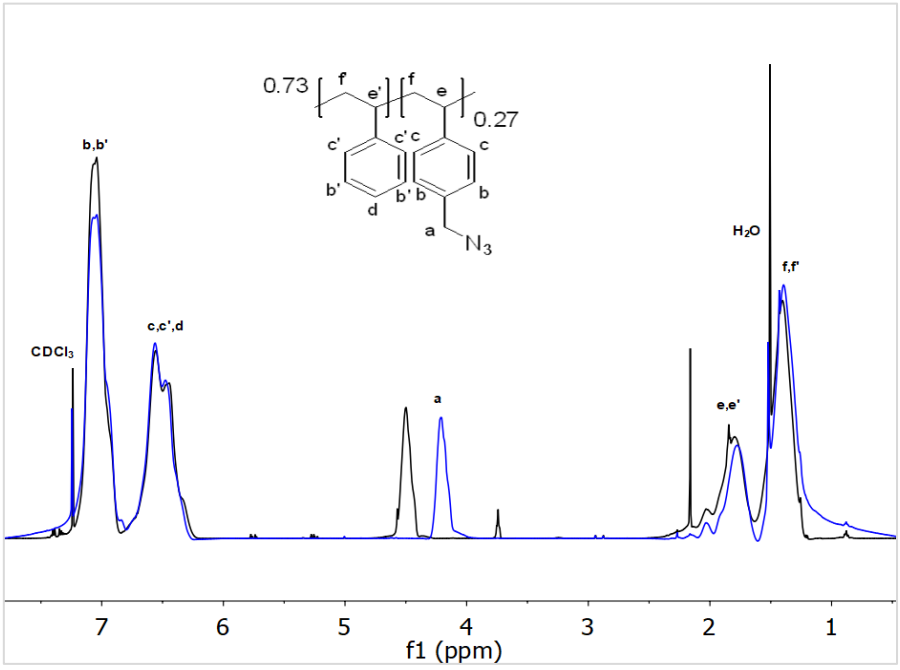

Figure 56. ^{1}H NMR spectra of P(S-co-CMS) (black) and P(S-co-AMS) (blue). The displacement of the peak a correspond to the replace of the Cl atoms with N_3 groups.

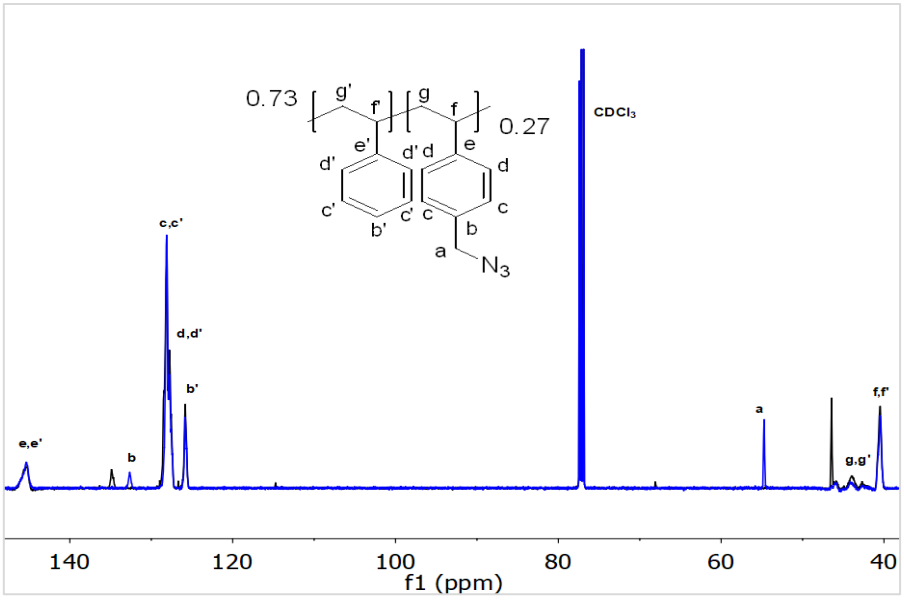

Figure 57. ^{13}C NMR of P(S-co-CMS) (black) and P(S-co-AMS) (blue). The displacement of the peak a correspond to the replace of the Cl atoms with N_3 groups.

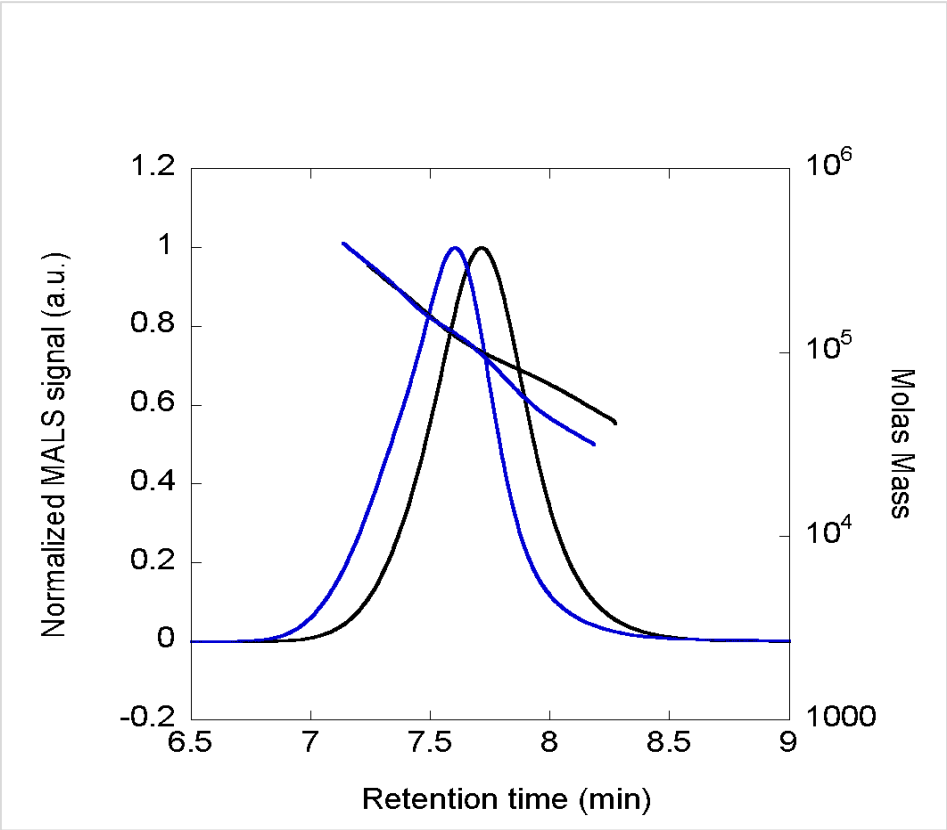

Figure 58. GPC chromatograph of P(S-co-CMS) (black) and P(S-co-AMS) (blue). Displacement for lower retention times shows an increase of size of the sample (LS detector).

5.3.2. Synthesis of PS-SCNPs

The size reduction of the SCNP compared with the azide polymer was checked by GPC, DLS and SAXS. Figure 59 shows the chromatograph of the precursor and the nanoparticles before and after the precipitation, showing that the SCNPs can be dried and re-dissolved without any aggregation problem. As was expected the peak of the SCNPs are displaced to larger retention times, that is related with the reduction of the size from R_h (VIS) (prec.) = 9.2 nm to R_h (VIS) (SCNP) = 6.9 nm. While the polydispersity is approximately the same, Đ = 1.21, the molar mass is increased, M_w = 195.8 kDa, due to the incorporation of the intra-chain cross-linker DIBOD. DLS technique (Figure 60) shows the size reduction too, from R_h (VIS) (prec.) = 10.1 nm to R_h (VIS) (SCNP) = 7.5 nm. While in the SAXS characterization (Figures 61) can be observe, in addition to the size reduction from R_g (prec.) = 14.1 nm to R_g (SCNP) = 9.1 nm, the reduction of the scaling factor that is reduced from ν = 0.59, that correspond to a value of a linear chain in good solvent, to a ν = 0.46 that is more similar to the value of a spherical particle (ν = 1/3).

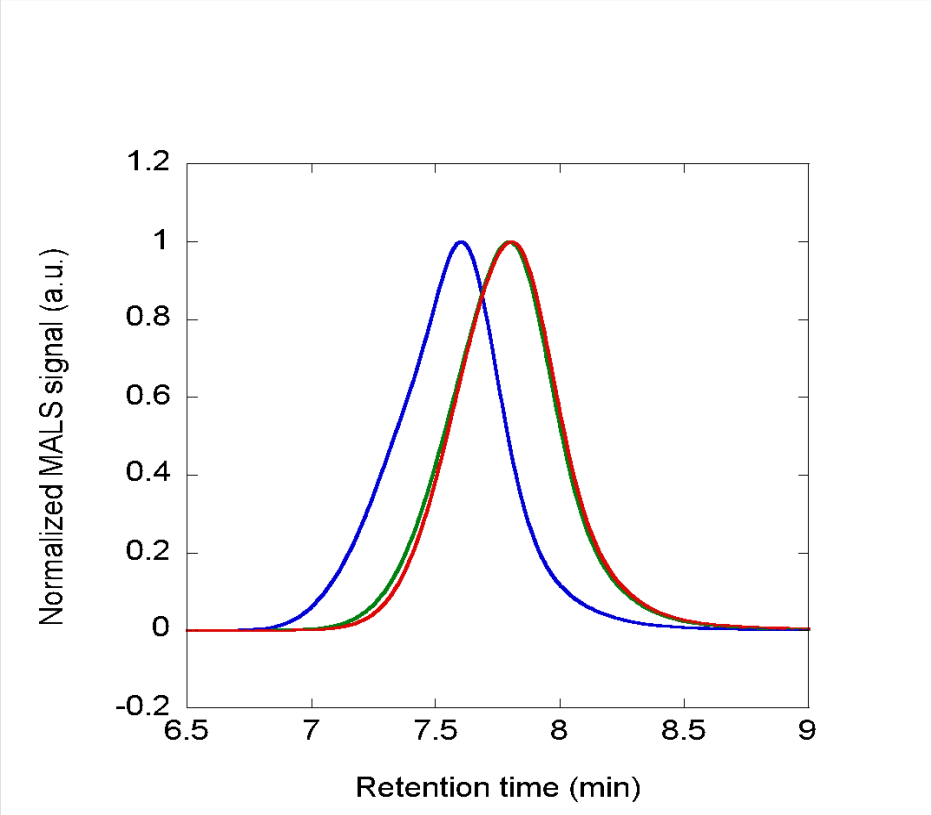

Figure 59. GPC chromatograph of P(S-co-AMS) (blue), PS-SCNPs crude (green) and PS-SCNPs dried (red) (LS detector). The displacement to higher retention times correspond to smaller size of the SCNPs. The SCNPs show no aggregation during the dry and redissolve process.

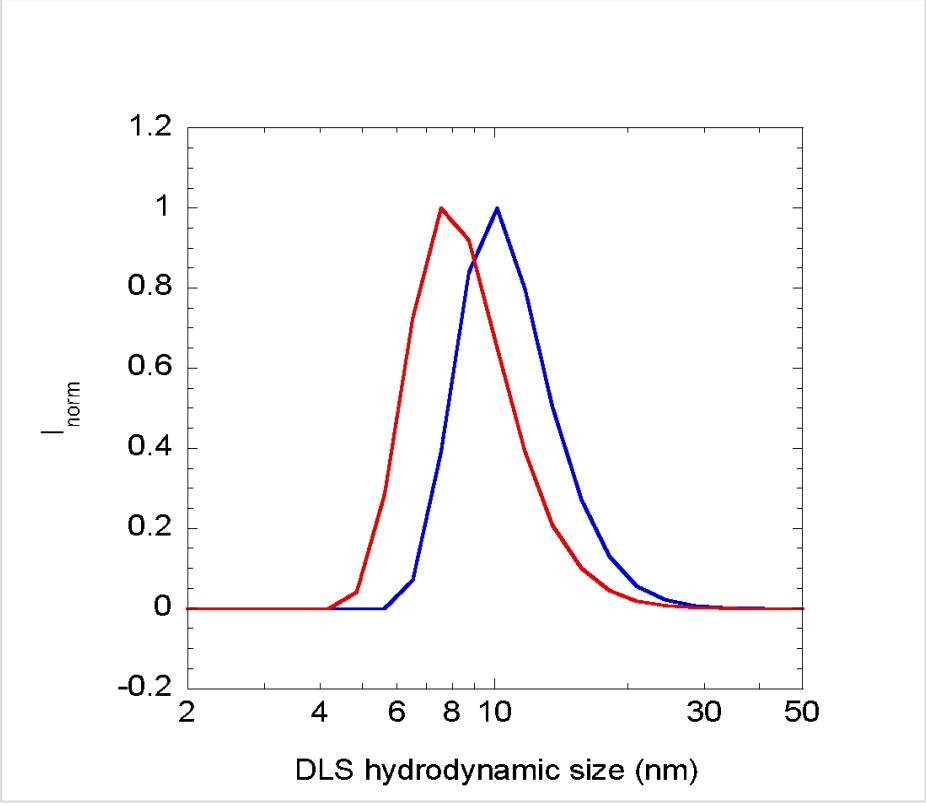

Figure 60. DLS measurement in THF of P(S-co-AMS) (blue) and PS-SCNPs dried (red). As expected the SCNPs have smaller size than the precursor.

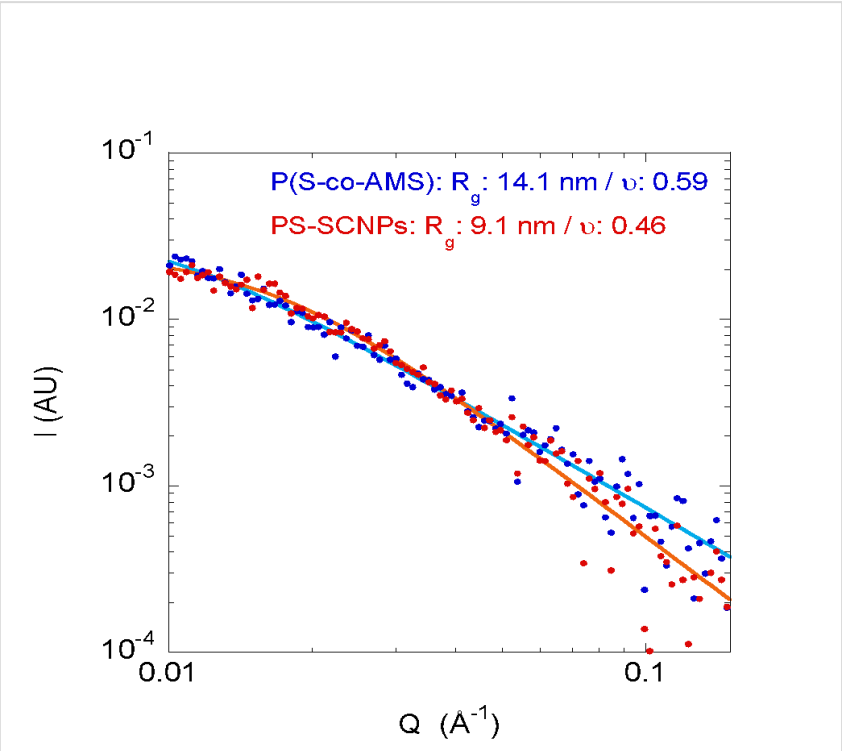

Figure 61. Experimental data (points) and fitting (line) of the SAXS characterization of P(S-co-AMS) (blue) and PS-SCNPs dried (red). Values of R_g and ν were obtained through fits of the experimental data to a generalized Gaussian coil function.

^{1}H NMR and ^{13}C NMR spectra (Figure 62 and 63) shows some peaks that correspond to the benzyl group of the cross linker, proving the correct incorporation of the DIBOD. It can be observed too in the FTIR spectra (Figure 64), where the reduction of the azide group peak around 2100 cm^{-1} of the FTIR spectra means that the reaction has been carried out correctly.

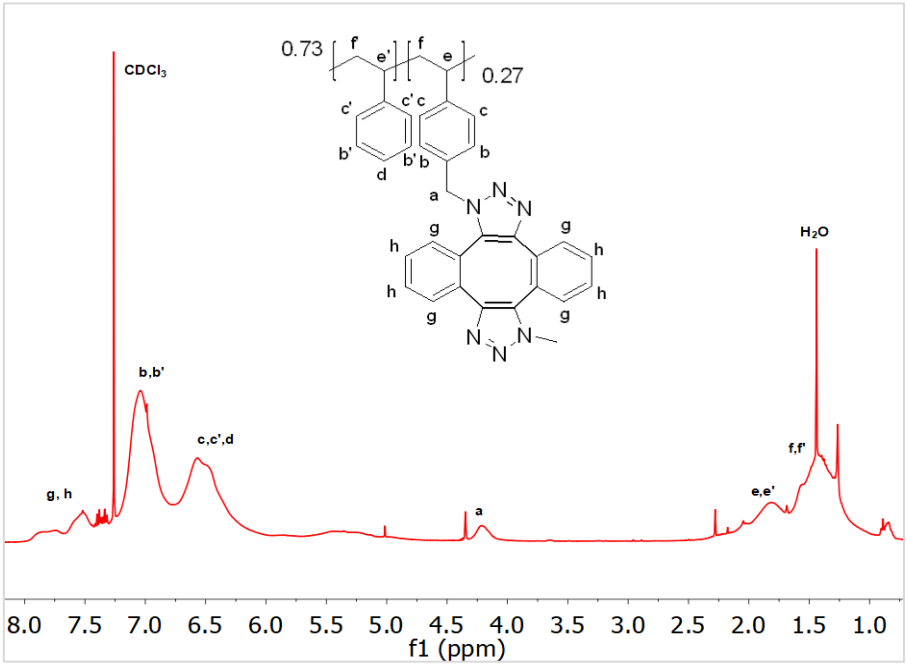

Figure 62. ^{1}H NMR spectrum of PS-SCNPs. The new peaks g and h correspond to the cross-linker.

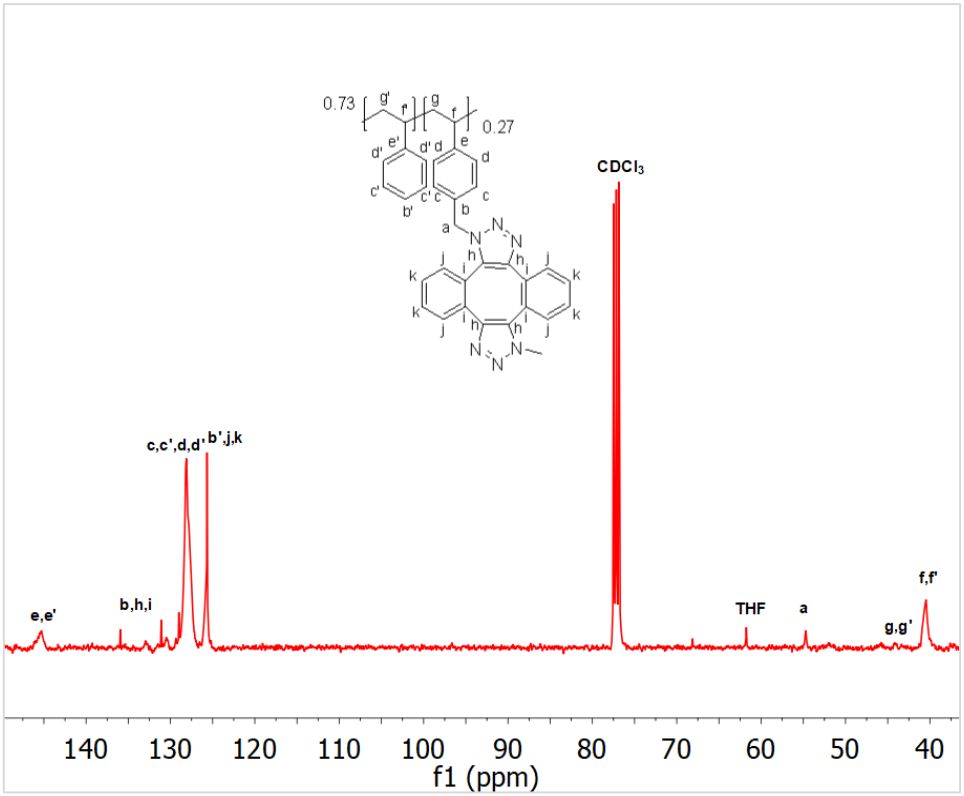

Figure 63. ^{13}C NMR of PS-SCNPs. The new peaks h, i, j and k correspond to the cross-linker.

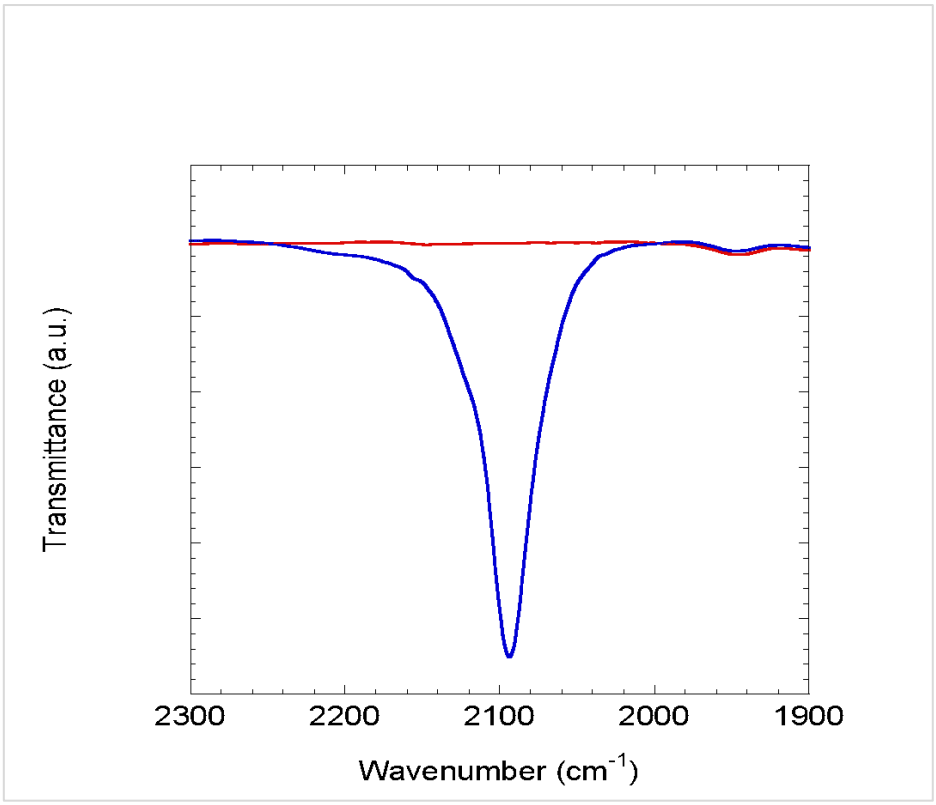

Figure 64. FTIR spectra of P(S-co-AMS) (blue) and PS-SCNPs (red). The total disappearance of the peak proof the total reaction of the azide groups.

In the Figure 65 can be observe the TGA characterization of the P(S-*co*-AMS) precursor and the PS-SCNPs. The degradation temperature of the precursor was 220 ºC that correspond to the liberation of dinitrogen molecules from azide group. SCNPs has a lower degradation temperature, 150 ºC, which is attributed to the lower thermal stability of the DIBOD cross-linker. Therefore, the SCNPs are stable material up to 150 ºC, without any weight loss.

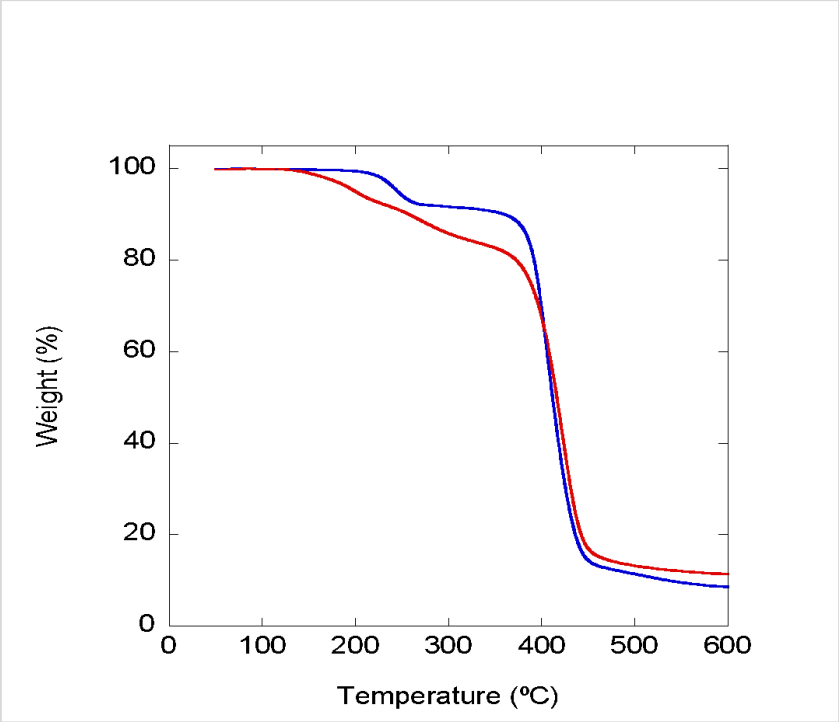

Figure 65. TGA result of P(S-co-AMS) (blue) and PS-SCNPs (red).

5.3.3. Long-term stability of Cu-free SCNPs.

The long-term stability against aggregation of the PS-SCNPs was investigated using SAXS characterization technique in THF. After the first characterization to check the reduction of size from the precursor, the SCNPs were storage 2 month in two different conditions: dissolved in THF and in solid state (Figure 66 (a) and (b)). The SAXS characterization was then repeated with these samples to check if it were aggregated. The nanoparticles before storage have characteristic of R_g (before) = 9.1 nm and ν (before) = 0.46. While the radius of gyration has no changed in the sample storage in THF solution (R_g (THF) = 8.7 nm), an increase is observed in the sample storage in solid state (R_g (solid) = 12.0 nm). Therefore, the size is smaller than the precursor's ones (R_g (precursor) = 14.1 nm), and the scaling factor were un-changed in the two cases (ν (THF) = 0.46 and ν (solid) = 0.47).

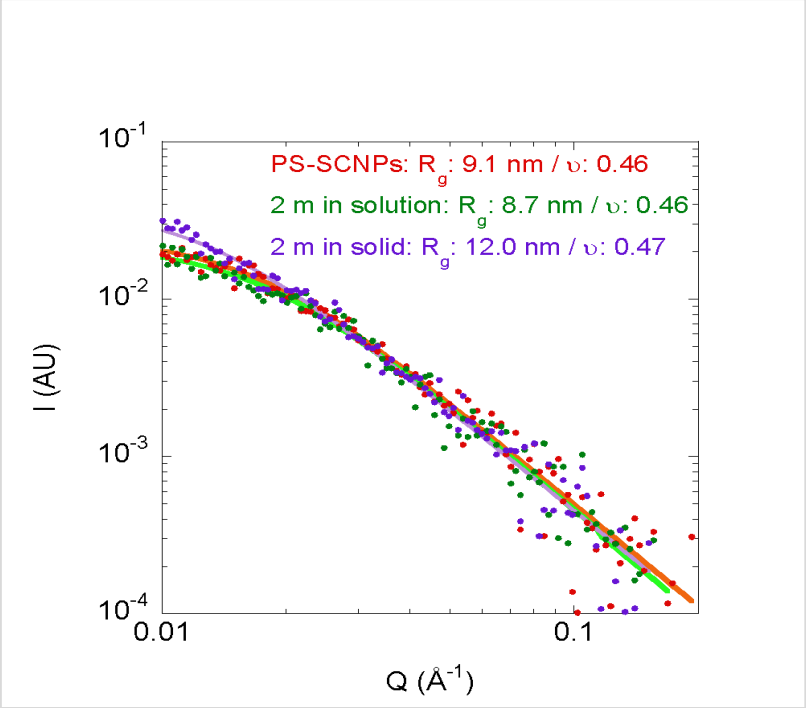

Figure 66. Fitting of the SAXS characterization of: PS-SCNPs before the storage (red), PS-SCNPs storage 2 months in THF solution (green) and (b) PS-SCNPs storage 2 months in solid state (orange).

5.4. Conclusion

We report on a new platform for the synthesis of stable, inert, dispersible, metal-free single-chain nanoparticles (SCNPs) via intramolecular metal-traceless azide–alkyne click chemistry at r.t. The use of the strain-promoted azide-alkyne cycloaddition (SPAAC) technique with sym-dibenzo-1,5-cyclooctadiene-3,7-diyne (DIBOD) as an external bifunctional cross-linker molecule, in combination with azide-containing polymeric precursors, provides a new method for synthesizing metal-free SCNPs through intramolecular folding/ collapse. We highlight the possibilities of this new synthesis technique by preparing metal-free polystyrene (PS) SCNPs from a copolymer precursor containing 27 mol% of azide functional groups. The successful formation of metal-free PS-SCNPs was confirmed through a powerful combination of techniques, including SEC with triple detection (RI, MALS, and VIS), ^{1}H and ^{13}C NMR spectroscopy, DLS, FTIR, TGA, and SAXS measurements. In addition to the advantages of these metal-free SCNPs, including their potential use in applications in which the total absence of metal traces is essential, the resulting nanoparticles exhibited significant long-term stability against irreversible aggregation. Finally, it is worth mentioning the potential versatility of this method for the synthesis of long-term-dispersible, metal-free SCNPs from any polymer precursor decorated with azide functional groups.

References

[1] *Single-Chain Polymer Nanoparticles: Synthesis, Characterization, Simulations, and Applications*; J. A. Pomposo, Ed.; John Wiley & Sons: Weinheim, Germany, 2017.

[2] M. A. M. Alqarni, C. Waldron, G. Yilmaz, C. R. Becer, Synthetic Routes to Single Chain Polymer Nanoparticles (SCNPs): Current Status and Perspectives. *Macromolecule rapid communication* **2021**, 42, 2100035.

[3] Y. Shao, Z. Yang, Progress in polymer single-chain based hybrid nanoparticles. *Progress in Polymer Science* **2022**, 133, 101593.

[4] A. Nitti, R. Carfora, G. Assanelli, M. Notari, D. Pasini, Single-Chain Polymer Nanoparticles for Addressing Morphologies and Functions at the Nanoscale: A Review. *ACS Applied Nano Materials* **2022**, 5, 13985–13997.

[5] R. Chen, E. B. Berda, 100th Anniversary of Macromolecular Science Viewpoint: Reexamining Single-Chain Nanoparticles. *ACS Macro Letters* **2020**, 9, 1836–1843.

[6] T. Terashima, Controlled Self-Assembly of Amphiphilic Random Copolymers into Folded Micelles and Nanostructure Materials. *Journal of Oleo Science* **2020**, 69, 529–538.

[7] A. R. A. Palmans, Chap. 25—Single-Chain Polymeric Nanoparticles: Toward In Vivo Imaging and Catalysis in Complex Media, in *Self-Assembling Biomaterials, Woodhead Publishing* **2018**.

[8] M. Gonzalez-Burgos, A. Latorre-Sanchez, J. A. Pomposo, Advances in Single Chain Technology. *Chemical Society Reviews* **2015**, 44, 6122–6142.

[9] C. K. Lyon, A. Prasher, A. M. Hanlon, B. T. Tuten, C. A. Tooley, P. G. Frank, E. B. Berda, A Brief User's Guide to Single-Chain Nanoparticles. *Polymer Chemistry* **2015**, 6, 181–197.

[10] S. Mavila, O. Eivgi, I. Berkovich, N. G. Lemcoff, Intramolecular Cross-Linking Methodologies for the Synthesis of Polymer Nanoparticles. *Chemical Reviews* **2016**, 116, 878–961.

[11] G. M. T. Huurne, A. R. A. Palmans, E. W. Meijer, Supramolecular Single-Chain Polymeric Nanoparticles. *CCS Chemistry* **2019**, 1, 64–82.

[12] O. Altintas, C. Barner-Kowollik, Single-Chain Folding of Synthetic Polymers: A Critical Update. *Macromolecule rapid communication* **2016**, 37, 29–46.

[13] A. Sanchez-Sanchez, J. A. Pomposo, Single-Chain Polymer Nanoparticles via Non-Covalent and Dynamic Covalent Bonds. *Particle & Particle Systems Characterization* **2014**, 31, 11–23.

[14] O. Altintas, C. Barner-Kowollik, Single Chain Folding of Synthetic Polymers by Covalent and Non-Covalent Interactions: Current Status and Future Perspectives. *Macromolecule rapid communication* **2012**, 33, 958–971.

[15] M. K. Aiertza, I. Odriozola, G. Cabañero, H.-J. Grande, I. Loinaz, Single-Chain Polymer Nanoparticles. *Cellular and Molecular Life Sciences* **2012**, 69, 337–346.

[16] N. M. Hamelmann, J. M. J. Paulusse, Single-chain polymer nanoparticles in biomedical applications. *Journal of Controlled Release* **2023**, 356, 26–42.

[17] M. H. Barbee, Z. M. Wright, B. P. Allen, H. F. Taylor, E. F. Patteson, A. S. Knight, Protein-Mimetic Self-Assembly with Synthetic Macromolecules. *Macromolecules* **2021**, 54, 3585–3612.

[18] J. Chen, E. S. Garcia, S. C. Zimmerman, Intramolecularly Cross-Linked Polymers: From Structure to Function with Applications as Artificial Antibodies and Artificial Enzymes. *Accounts of Chemical Research* **2020**, 53, 1244–1256.

[19] A. P. P. Kroger, J. M. J. Paulusse, Single-Chain Polymer Nanoparticles in Controlled Drug Delivery and Targeted Imaging. *Journal of Controlled Release* **2018**, 286, 326–347.

[20] A. Latorre-Sánchez, J. A. Pomposo, Recent bioinspired applications of single-chain nanoparticles. *Polymer International* **2016**, 65, 855–860.

[21] E. Verde-Sesto, A. Arbe, A. J. Moreno, D. Cangialosi, A. Alegria, J. Colmenero, J. A. Pomposo, Single-chain nanoparticles: Opportunities provided by internal and external confinement. *Materials Horizons* **2020**, 7, 2292–2313.

[22] H. Rothfuss, N. D. Knofel, P. W. Roesky, C. Barner-Kowollik, Single-Chain Nanoparticles as Catalytic Nanoreactors. *Journal of the American Chemical Society* **2018**, 140, 5875–5881.

[23] J. Rubio-Cervilla, E. González, J. A. Pomposo, Advances in Single-Chain Nanoparticles for Catalysis Applications. *Nanomaterials* **2017**, 7, 341.

[24] E. Blasco, B. T. Tuten, H. Frisch, A. Lederer, C. Barner-Kowollik, Characterizing Single Chain Nanoparticles (SCNPs): A Critical Survey. *Polymer Chemistry* **2017**, 8, 5845–5851.

[25] I. Perez-Baena, F. Barroso-Bujans, U. Gasser, A. Arbe, A. J. Moreno, J. Colmenero, J. A. Pomposo, Endowing Single-Chain Polymer Nanoparticles with Enzyme-Mimetic Activity. *ACS Macro Letters* **2013**, 2, 775–779.

[26] A. Sanchez-Sanchez, I. Pérez-Baena, J. A. Pomposo, Advances in Click Chemistry for Single-Chain Nanoparticle Construction. *Molecules* **2013**, 18, 3339–3355.

[27] H. C. Kolb, M. G. Finn, K. B. Sharpless, Click chemistry: Diverse chemical function from a few good reactions. *Angewandte Chemie International Edition* **2001**, 40, 2004–2021.

[28] V. V. Rostovtsev, L. G. Green, V. V. Fokin, K. B. Sharpless, A stepwise Huisgen cycloaddition process: Copper(I)-catalyzed regioselective "ligation" of azides and terminal alkynes. *Angewandte Chemie International Edition* **2002**, 41, 2596–2599.

[29] C. W. Tornøe, C. Christensen, M. Meldal, Peptidotriazoles on solid phase: [1,2,3]-triazoles by regiospecific copper(I)-catalyzed 1,3-dipolar cycloadditions of terminal alkynes to azides. *The Journal of Organic Chemistry* **2002**, 67, 3057–3064.

[30] A. Ruiz de Luzuriaga, N. Ormategui, H. J. Grande, I. Odriozola, J. A. Pomposo, I. Loinaz, Intramolecular click cycloaddition: An efficient room-temperature route towards bioconjugable polymeric nanoparticles. *Macromolecule rapid communication* **2008**, 29, 1156–1160.

[31] A. Ruiz de Luzuriaga, I. Perez-Baena, S. Montes, I. Loinaz, I. Odriozola, I. García, J. A. Pomposo, New route to polymeric nanoparticles by click chemistry using bifunctional cross-linkers. *Macromolecular Symposia* **2010**, 296, 303–310.

[32] L. Oria, R. Aguado, J. A. Pomposo, J. Colmenero, A versatile "click" chemistry precursor of functional polystyrene nanoparticles. *Advanced Materials* **2010**, 22, 3038–3041.

[33] N. Jasinski, A. Lauer, P. J. M. Stals, S. Behrens, S. Essig, A. Walther, A. S. Goldmann, C. Barner-Kowollik, Cleaning the Click: A Simple Electrochemical Avenue for Copper Removal from Strongly Coordinating Macromolecules. *ACS Macro Letters* **2015**, 4, 298–301.

[34] J. E. Macdonald, J. A. Kelly, J. G. Veinot, Iron/iron oxide nanoparticle sequestration of catalytic metal impurities from aqueous media and organic reaction products. *Langmuir* **2007**, 23, 9543–9545.

[35] J. Duguid, V. A. Bloomfield, J. Benevides, G. J. Thomas Jr., Raman spectroscopy of DNA-metal complexes. I. Interactions and conformational effects of the divalent cations: Mg, Ca, Sr, Ba, Mn, Co, Ni, Cu, Pd, and Cd. *Biophysical Journal* **1993**, 65, 1916–1928.

[36] Ö. Usluer, M. Abbas, G. Wantz, L. Vignau, L. Hirsch, E. Grana, C. Brochon, E. Cloutet, G. Hadziioannou, Metal Residues in Semiconducting Polymers: Impact on the Performance of Organic Electronic Devices. *ACS Macro Letters* **2014**, 3, 1134–1138.

[37] L. R. Middleton, K. I. Winey, Nanoscale Aggregation in Acid- and Ion-Containing Polymers. *Annual Review of Chemical and Biomolecular Engineering* **2017**, 8, 499–523.

[38] J. De-La-Cuesta, E. Verde-Sesto, A. Arbe, J. A. Pomposo, Self-Reporting of Folding and Aggregation by Orthogonal Hantzsch Luminophores within A Single Polymer Chain. *Angewandte Chemie International Edition* **2021**, 60, 3534–3539.

39. N. J. Agard, J. A. Prescher, C. R. Bertozzi, A Strain-Promoted [3+2] Azide-Alkyne Cycloaddition for Covalent Modification of Biomolecules in Living Systems. *Journal of the American Chemical Society* **2004**, 126, 15046–15047.

40. E. Kim, H. Koo, Biomedical applications of copper-free click chemistry: In vitro, in vivo, and ex vivo. *Chemical Science* **2019**, 10, 7835–7851.

41. A. M. Biyogo, L. Hespel, V. Humblot, L. Lebrun, F. Estour, Cellulose fibers modification through metal-free click chemistry for the elaboration of versatile functional surfaces. *European Polymer Journal* **2020**, 135, 109866.

[42] J. Escorihuela, A. T. M. Marcelis, H. Zuilhof, Metal-Free Click Chemistry Reactions on Surfaces. *Advanced Materials Interfaces* **2015**, 2, 1500135.

[43] H. N. C. Wong, P. J. Garratt, F. Sondheimer, Unsaturated eight-membered ring compounds. XI. Synthesis of sym-dibenzo-1,5-cyclooctadiene-3,7-diyne and sym-dibenzo-1,3,5-cyclooctatrien-7-yne, presumably planar conjugated eight-membered ring compounds. *Journal of the American Chemical Society* **1974**, 96, 5604–5605.

[44] I. Kii, A. Shiraishi, T. Hiramatsu, T. Matsushita, H. Uekusa, S. Yoshida, M. Yamamoto, A. Kudo, M. Hagiwara, T. Hosoya, Strain-promoted double-click reaction for chemical modification of azido-biomolecules. *Organic & Biomolecular Chemistry* **2010**, 8, 4051–4055.

[45] L. C. Zhang, Y. Wu, S. M. Li, Y. X. Zhang, K. Zhang, Scalable Bimolecular Ring-Closure Method for Cyclic Polymers. *Macromolecules* **2020**, 53, 8621–8630.

[46] Y. Zhang, Y. Wu, Y. Zhao, L. Zhang, K. Zhang, Versatile Bimolecular Ring-Closure Method for Cage-Shaped Polymers. *Macromolecules* **2021**, 54, 6901–6910.

[47] B. Hammouda, Small-Angle Scattering From Branched Polymers. *Macromolecular Theory and Simulations* **2012**, 21, 372–381.

[48] M. González-Burgos, A. Alegría, A. Arbe, J. Colmenero, J. A. Pomposo, An unexpected route to aldehyde-decorated single-chain nanoparticles from azides. *Polymer Chemistry* **2016**, 7, 6570–6574.

[49] E. Harth, B. V. Horn, V. Y. Lee, D. S. Germack, C. P. Gonzales, R. D. Miller, C. J. Hawker, A Facile Approach to Architecturally Defined Nanoparticles via Intramolecular Chain Collapse. Journal of the American Chemical Society **2002**, 124, 8653–8660.

6. Metamorphosis of a Commodity Plastic like PVC to Efficient Catalytic Single-Chain Nanoparticles

6.1. Motivation

Single-chain polymer nanoparticles (SCNPs) have always been synthesized from specialty polymeric precursors and not from waste of commodity plastics. Moreover, in the SCNPs field no significant attention has been paid to the replacement of common (toxic) organic solvents by "green" solvents. In this chapter, a complementary concept of polymeric waste valorization (upcycling) through metamorphosis in "green" media of an out-of-use piece of a daily life commodity plastic like polyvinyl chloride (PVC) to "valorized" PVC single-chain nanoparticles—useful as recyclable / metalloenzyme-mimetic catalyst for Cu(II)-catalyzed organic transformations—is introduced.

6.2. Introduction

In addition to recycling, waste valorization by converting polymeric waste materials into more useful products is attracting significant interest to mitigate plastic pollution issues. Polyvinyl chloride (PVC) is the third most widely produced synthetic polymer in the world after the most commonly used polyolefins, polyethylene (PE) and polypropylene (PP) [1]. Current global PVC production is estimated at ca. 40 million metric tons (Mt) per year. Around 6.5 Mt of PVC are annually manufactured in the European Union (EU) with ca. 2 Mt of post-consumer PVC waste Generated [2]. Mechanical recycling of rigid PVC from the construction and building sector (e.g., windows, pipes) is currently the main relevant recycling process in the EU for post-consumer

PVC waste. Recycling or valorization of flexible PVC waste from e.g. packaging, automotive and medical sectors is complicated by the difficulty to handle banned plasticizers (e.g., bis(2-ethylhexyl) phthalate) -still entering recycling streams- after isolation of neat PVC from flexible PVC waste. This seems to be the main cause of the closure in 2018 of the only plant in the EU established to recycle up to 10 000 t of flexible PVC waste a year [3]. Incineration and landfilling represent the main non-recycling treatment routes for PVC [2]. Non-conventional recycling processes like selective dissolution using green solvents could be an option to remove contaminants, plasticizers and/or metallic layers from PVC waste [4]. Currently, significant effort is devoted by many research groups on breaking PVC down to useful product. For instance, Jin, Yoshioka *et al.* introduced a new and green approach to achieve, in a single step, the complete dechlorination of PVC, as well the conversion of the hydrogen carbonate to form with nearly 100 % selectivity and 16 % yield [5]. Sun, Xie and coworkers have recently reported the first highly selective conversion of PVC waste into C_2 fuels by a universal photoinduced sequential C-C bond cleavage and coupling pathway under simulated natural environment conditions [6].

Tour *et al.* were able to convert a mixture of plastic wastes containing PVC into flash graphene via flash Joule heating [7]. Additionally, Yoshioka *et al.* have developed the Cl recovery process [8-10], which entails the dechlorination of PVC in NaOH / ethylene glycol (EG) solvent by ball-milling and treating the Cl ion dissolved in EG by electro-dialysis for the simultaneous recovery of NaCl and EG. In any case, alternative ways to reuse post-consumer PVC waste free from toxic plasticizers via waste valorization are certainly needed [11].

Herein, a new concept of polymeric waste valorization is introduced through metamorphosis of a commodity plastic like PVC to single-chain nanoparticles (SCNPs). Synthetic SCNPs are obtained through folding/collapse of discrete functionalized polymer chains by means of intra-chain (reversible/covalent) interactions [12]. Within the local compact domains of SCNPs active species as catalysts, drugs, or luminophores can be immobilized either reversibly or permanently [11-20]. These soft nanoparticles open a plethora of opportunities for the development of new drug delivery vehicles, highly efficient catalysts and improved sensing elements, among other ones [21-28]. For instance, Paulusse et al. developed a method for intracellular location of SCNPs by controlled surface modification with tertiary amines to improve intracellular targeting for biomedical applications [29]. Cheng et al. synthesized SCNPs loaded with the anticancer drug doxorubicin displaying selective cytotoxicity toward HeLa cancer cells, without affecting healthy NIH/3T3 cells [30]. Tang et al. showed polydopamine-coated surfaces containing SCNPs with excellent in vitro bactericidal activity against both Staphylococcus aureus and Escherichia coli with >99.9 % killing efficacy, excellent protein adsorption resistance, antibacterial adhesion and low cytotoxicity [31]. Recently, Yan et al. reported CO_2-folded SCNPs as recyclable, improved carboxylase mimics able to catalyze CO_2-insertion of C(sp3)-H and, even, C(sp2 and sp)-H substrates at room temperature (r.t.) [32]. Additionally, Tan et al. synthesized enzyme-mimetic SCNPs containing chiral Fe(II)-oxazoline complexes allowing efficient asymmetric sulfa-Michael addition of thiols to a wide range α,β-unsaturated ketones in water at r.t. without the need of any organic solvent or additional additives [33]. Remarkably, Collot et al. reported stealth and bright monomolecular fluorescent SCNPs as artificial analogues of fluorescent proteins, surpassing the latter >50-fold in terms of brightness [34]. More recently, a strategy for self-reporting both intra-molecular compaction and inter-molecular aggregation of SCNPs based on the installation of orthogonal luminophores via Hantzsch ester formation has been developed by our group [35]. However, SCNPs have always been synthesized from specialty polymeric precursors, and not from waste of commodity plastics.

As illustrated in Figure 67, we propose the metamorphosis of “PVC waste” to PVC-SCNPs in two steps: 1) partial azidation of discrete linear PVC chains via nucleophilic substitution to give PVC-

N_3 in which some of the chloride atoms are replaced by azide groups; and ii) intra-chain reaction of individual PVC-N_3 chains with the Sondheimer diyne [36] (5,6,11,12-tetradehydrodibenzo[a,e]cyclooctene, DIBOD), via metal-free strain-promoted double-click cycloaddition reaction to produce PVC-SCNPs. A constraint of the valorization strategy to produce PVC-SCNPs, however, is the requirement of using PVC waste free from banned plasticizers.

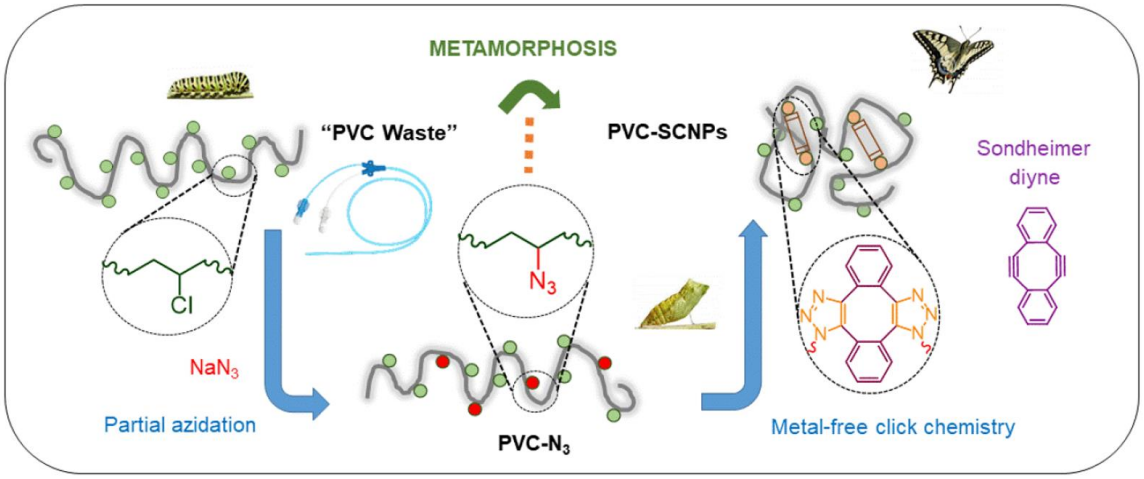

Figure 67. Metamorphosis of "PVC waste" to PVC single-chain nanoparticles (PVC-SCNPs) in two steps: i) partial azidation of PVC to PVC-N_3; and ii) intra-chain metal-free click chemistry at r.t. involving individual PVC-N_3 chains and the Sondheimer diyne (5,6,11,12-tetradehydrodibenzo[a,e]cyclooctene) to give PVC-SCNPs.

As a proof-of-concept, we initially started by performing the metamorphosis process using neat, commercial PVC and common (non-green) organic solvents. PVC chains can be functionalized by nucleophilic substitution of the chlorine atoms with a range of nucleophiles (e.g., azide, thiolates, and thiocyanate) through a SN_2 mechanism [37, 38]. We target partial azidation of PVC to give PVC-N_3 [39] as the right functionalization step for the subsequent intra-chain metal-free click chemistry procedure. In this sense, SCNPs are typically prepared from precursors containing between 10 and 30 mol% of functional groups [12]. To create the intra-chain bonds that collapse the chain to SCNPs, we use the strain-promoted double-click reaction, first introduced by Kii *et al.* [40], that allows to avoid the metal catalyst. Notably, the second cycloaddition reaction of the cross-linker was predicted by a density functional theory method, and confirmed experimentally with model compounds, to have a lower activation energy than the first one due to the resulting highly distorted alkyne bond [41, 42]. That increased kinetic of the second reaction, with the high dilution conditions, it is especially important to guarantee that no other PVC-N_3 reacts with the cross-linker, which is essential to avoid the aggregation caused by the inter-chain coupling. However, another condition is needed too: the continuous addition technique [43]. Adding the polymer slowly in solution to another solution of the cross-linker, we

optimized the conditions where small quantities of chains react with exceed of DIBOD to avoid intra-chain couplings. We use different techniques to characterize the formed SCNPs' size (as GPC or SAXS), chemical composition (as NMR and EA) and thermal behavior (TGA and DSC).

After optimization of the reaction conditions, the process was repeated with "PVC waste" and using only green and sustainable solvent [44]. As precursor we use polymer of two different commercial objects composed by PVC, one rigid PVC tube and one flexible PVC hose. Some different solvents were used to azide the PVC to compare the results, and N-butylpyrrolidinone (NBP) was selected as solvent for the rest of the process. NBP is a non-reproductively toxic substance (according to OECD 414 test method), non-mutagenic compound (OECD 471) and inherently biodegradable (OECD 302B) dipolar aprotic solvent, which is commercially available in industrial relevant quantities (Solvagreen™, TamiSolve™)[45]. Recently, NBP has been reported as the best green solvent candidate to replace reprotoxic DMF in solid-phase peptide synthesis [46].

The locally compact domains of SCNPs offer a plethora of opportunities for the development of recyclable, enzyme-mimetic catalysts by using the beneficial outer coordination sphere effect of the folded/collapsed chain [47-50]. In this sense we tried to load the vPVC-SCNPs with Cu(II) ions to investigate the SCNPs as recyclable / enzymemimetic catalyst for a variety of Cu(II)-catalyzed reactions. First, we selected the solvent-free alkyne homocoupling reaction [51-54] as a benchmark transformation to investigate the efficiency and recyclability of the resulting vPVC-SCNPs/Cu(II). Next, we performed a comparison of the vPVC-SCNPs/Cu(II) catalyst against $CuCl_2$ for the oxidation reaction of styrene to benzaldehyde in the presence of hydrogen peroxide [55]. Finally, we investigated the metalloenzyme-mimetic properties of vPVC-SCNPs/Cu(II) in the transformation of a o-diphenol model compound (3,5-di-tert-butylcatechol, DTBC) into a quinone product (3,5-di-tert-butyl-o-quinone, DTBQ).

6.3. Experimental procedures

6.3.1. Materials

Styrene (S, ≥99%), poly(vinyl chloride (PVC, M_w ≈ 43 kDa) sodium azide (NaN_3, ≥99%), N,N-dimethylformamide (DMF, ≥99.9%), dimethyl sulfoxide (DMSO, ≥99.5%), dihydrolevoglucosenone (Cyrene, ≥98.5%), 2-Methyltetrahydrofuran (2m-THF, ≥99.5%), γ-Valerolactane (GVL, 99%), 1-Butylpyrrolidin-2-one (NBP, ≥99.5%), copper(II) chloride ($CuCl_2$, anhydrous, ≥99.995%), propargyl acetate (PA, 98%), triethylamine (TEA, ≥99.5%), hexane (≥97.0%), acetonitrile (≥99.5%), 1,1,2,2-Tetrabromoethane (TBE, 98%) and 1,4-Dicyanobenzene (DCB, 98%) were purchased from Sigma-Aldrich (Madrid, Spain). Sym-dibenzo-1,5-

cyclooctadiene-3,7-diyne (DIBOD, >90%) was supplied by TCI Europe (Zwijndrecht, Belgium). Tetrahydrofuran (THF, GPC grade), methanol (MeOH, analytical grade) and diethyl ether (DE, EssentQ®) were purchased from Scharlau (Barcelona, Spain). Benzyl azide (BzA, 94%), propargyl propionate (PrPr, 98%) and hydrogen peroxide (H_2O_2, 35 wt%) were purchased from Thermo Scientific (Eindhoven, Netherlands). S-cyanomethyl-S-dodecyltrithiocarbonate (CDTC, ≥97%) was purchased from Strem (Bischheim, France). Ethanol (EtOH, 96% v/v) was purchased from PanReac AppliChem (Barcelona, Spain). 1-Ethynyl-4-fluorobenzene (FB, 98%) and 3,5-Di-tert-butylcatechol (3,5DTBCH_2, 95%) were purchased from BLDpharm (Kaiserslautern, Germany). Deuterated chloroform ($CDCl_3$, 99.50%, 0.03% TMS v/v) was purchased from Eurisotop (Saint-Aubin, France). Rigid and flexible PVC pipes were purchased from the OemClima and Kesote brands, respectably, via Amazon. Unless otherwise specified, all reagents were used as received without further purification.

6.3.2. Techniques

- *Gel permeation chromatography (GPC)*

GPC measurements were performed at 25 ºC on an Agilent 1200 system equipped with PLgel 5 µm Guard and PLgel 5 µm MIXED-C columns, and triple detection: a differential refractive index (RI) detector (Optilab Rex, Wyatt, Toulouse, France), a multi-angle laser light scattering (MALS) detector (MiniDawn Treos, Wyatt, Toulouse, France), and a viscosimetric (VIS) detector (ViscoStar-II, Wyatt, Toulouse, France). Data analysis was performed using ASTRA Software (version 6.1) from Wyatt. THF was used as an eluent at a flow rate of 1 mL/min. A value of dn/dc = 0.106 for PVC, PVC-N_3 and PVC-SCNPs.

- *Dynamic light scattering (DLS)*

DLS measurements (number distribution) were taken at room temperature on a Malvern Zetasizer Nano ZS (Cambridge, United Kingdom) apparatus.

- *Small-angle X-ray scattering (SAXS)*

SAXS experiments were conducted on the Rigaku (Barcelona, Spain) 3-pinhole PSAXSL equipment of the Materials Physics Center, operating at 45 kV and 0.88 mA. The MicroMax-002+ X-ray Generator System is composed of a microfocus sealed tube source module and an integrated X-ray generator unit, which produces CuK transition photons of wavelength λ = 1.54 Å. The flight path and the sample chamber in this equipment are under vacuum. The scattered X-rays are detected on a two-dimensional multiwire X-ray Detector (Gabriel (Barcelona, Spain) design, 2D-200X) and converted to one-dimensional scattering curves by radial averaging. This

gas-filled proportional type detector offers a 200 mm diameter active area with ca. 200-micron resolution. After radial integration, the scattered intensities were obtained as a function of momentum transfer $Q = 4\pi\lambda^{-1} sin\ \theta$, where θ is half the scattering angle. Reciprocal space calibration was performed using silver behenate as standard. The sample-to-detector distance was 2 m, covering a Q-range between 0.008 and 0.20 $Å^{-1}$. The measurements were taken at r.t. on the THF solutions in boron-rich capillaries of 2 mm thickness, with counting times of 1 h. The concentration was 1 mg/mL in order to avoid interference effects between different macromolecules. The data were carefully corrected for background scattering (due to the capillary and solvent) and measured for each sample on the same capillary for the same time. Scattering cross-sections were obtained in absolute units using water as the calibration standard. The generalized Gaussian coil function was employed for a precise determination of the values of the radius of gyration, R_g, and scaling exponent, ν.

- *Nuclear magnetic resonance (NMR)*

^1H NMR and ^{13}C NMR spectra were recorded at room temperature on Bruker (Madrid, Spain) spectrometers operating at 400 MHz, using $CDCl_3$ as solvent. The samples were dissolved in THF, precipitated in methanol and dried at vacuum to remove solvents traces in the spectra.

- *Fourier transform infrared spectroscopy (FTIR)*

FTIR spectra were recorded using ATR in a FT-IR JASCO 6360 (130-400K) infrared spectrometer at room temperature.

- *Elemental analysis (EA)*

The samples of this thesis were measured in an EA3000 elemental analyzer (CHNS).

- *Thermogravimetric analysis (TGA)*

TGA measurements were performed on a Q500-TA Instruments (Cerdanyola del Valles, Spain) apparatus at a heating rate of 10ºC/min under a nitrogen atmosphere.

- *Differential scanning calorimetry (DSC)*

The DSC measurements were carried out in a DSC Q2000 TMDSC instrument heating and cooling rate of 20ºC/min. The results are presented in “exo down” mode.

- *Ultraviolet-visible spectroscopy (UV-Vis)*

The UV-VIs were carried out in an Agilent 8453A UV-Vis spectrometer with Peltier thermostatic cell holder T-controller 89096A at 25ºC.

- *Inductively couple plasma mass spectrometry (ICP-MS)*

The ICP-MS were carried out in an LA-ICP-MS Agilent 7500 series.

6.3.3. Procedures

- *Purification of commercial PVC*

Polyvinyl chloride (PVC) (average M_w ≈ 43 kDa) was purified by a conventional solution-precipitation procedure using THF as solvent and cold MeOH as precipitant. This procedure was repeated twice and the resulting neat (commercial) PVC was dried at 50 ºC under vacuum overnight. *Yield (%):* 98.5. *M_w (SEC/MALS)*: 45.0 kDa. *Đ (SEC)*: 1.39

- *Synthesis of PVC-N3*

In a typical procedure, PVC (2 g, 32 mmol of Cl atoms) was dissolved in DMF (80 mL) in a 100 mL round-bottom flask. After addition of NaN_3 (2.08 g, 32 mmol of azide groups), the mixture was stirred at 80 ºC for 4 h (Figure 68). The product was precipitated in a large excess of a cold MeOH / H_2O (1 / 1 vol.) mixture, filtered, and re-dissolved in THF and precipitated in MeOH / H_2O (1 / 1 vol.) for three times. The material was dried at 50 ºC under vacuum overnight to give 1.92 g of PVC-N_3. Yield (%): 96.0. Azidation degree (EA): 12.2 mol%. M_w (SEC/MALS): 51.4 kDa. Đ (SEC): 1.35.

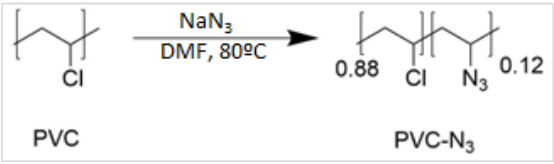

Figure 68. Synthetic scheme of the synthesis of PVC-N_3.

- *Synthesis of metal-free PVC-SCNPs*

PVC-N_3 (50 mg, 0.11 mmol of azide groups) was dissolved at r.t. in THF (25 mL) in a 50 mL round-bottom flask that was sealed with a septum and degassed with argon for 30 min. In a 100 mL flask, DIBOD (15 mg, 0.15 mmol of alkyne groups) was dissolved at r.t. in THF (75 mL). This second solution was sealed and degassed in the same way, and it was protected from light with aluminum foil. Then, the PVC-N_3 solution was injected into the 100 mL flask using an infusion pump (2.1 mL / h) (Figure 69). After 24 h (12 h of injection + 12 h of additional stirring), BAz (20 µL, 0.16 mmol of azide groups) was added, and stirring was maintained for 24 h at r.t. Finally, the product was precipitated in an excess of cold EtOH to remove potential traces of low molecular weight compounds. PVC-SCNPs (46 mg) were isolated as a white powder after filtration and further drying in vacuum at 50 ºC overnight. Yield (%): 92.0. Conversion (disappearance of azide IR vibration band): ≈95%. M_w (SEC/MALS): 92.1 kDa. Đ (SEC): 1.34.

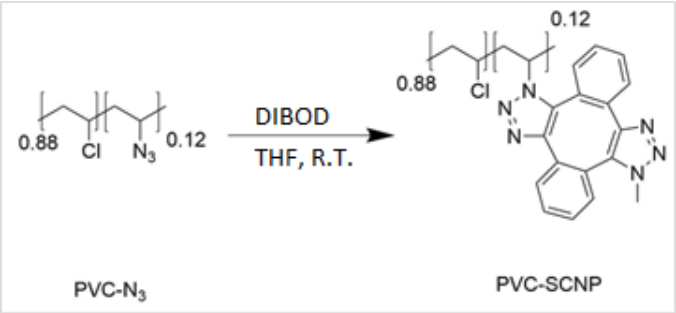

Figure 69. Synthetic scheme of the synthesis of *PVC-SCNPs.*

- *Screening of "green" solvents for the metamorphosis of "waste PVC" to valorized PVC single-chain nanoparticles (vPVC-SCNPs)*

We evaluated the full metamorphosis of "waste PVC" to vPVC-SCNPs (PVC isolation, PVC azidation and PVC-synthesis) in a variety of "green" solvents: dihydrolevoglucosenone (Cyrene), 2-methyltetrahydrofuran (2m-THF), gamma-valerolactone (GVL), dimethyl sulfoxide (DMSO), and N-butylpyrrolidinone (NBP). The azidation reaction was repeated in those solvents to compare the effect of each one. Only NBP was equivalent to DMF in the PVC azidation step without inducing aggregation phenomena during the synthesis of vPVC-SCNPs.

- *Purification of valorized PVC (vPVC)*

Flexible and rigid polyvinyl chloride (v-PVC (f) and v-PVC (r)) were cut into small pieces and dissolved in NBP at 80 ºC. After a filtration with paper filter, the samples were precipitated in cold MeOH / H2O (1 / 1 vol.). This procedure was repeated twice to isolate the valorized PVC (vPVC) from the "PVC waste". After this purification procedure, no difference was observed between v-PVC (f) and v-PVC (r) samples. Finally, vPVC was dried at 50 ºC under vacuum overnight. M_w (SEC/MALS): 104.9 kDa. Đ (SEC): 1.57.

- *Synthesis of vPVC-N_3*

vPVC (1 g, 16 mmol of Cl atoms) was dissolved in NBP (40 mL) in a 100 mL round-bottom flask. After addition of NaN_3 (1.04 g, 16 mmol of azide groups), the mixture was stirred at 80 ºC for 4 h (Figure 70). The product was precipitated in a large excess of a cold EtOH / H_2O (1 / 1 vol.) mixture and removed by filtration. After that, the polymer was dissolved and precipitated three times. Finally, the material was dried at 50 ºC in vacuum overnight to give 0.94 g of vPVC-N_3. Yield (%): 96.0. Azidation degree (EA): 16.0 mol%. M_w (SEC/MALS): 138.1 kDa. Đ (SEC): 1.52.

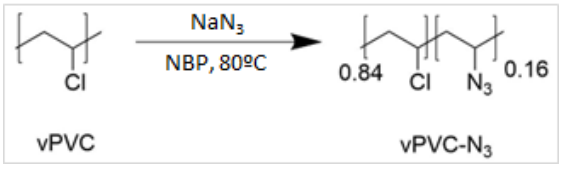

Figure 70. Synthetic scheme of the synthesis of vPVC-N_3.

- *Synthesis of metal-free PVC-SCNPs*

vPVC-N_3 (50 mg, 0.13 mmol of azide groups) was dissolved at r.t. in NBP (25 mL) in a 50 mL round-bottom flask that was sealed with a septum and degassed with argon for 30 min. In a 100 mL flask, 1 (18 mg, 0.18 mmol of alkyne groups) was dissolved at r.t. in NBP (75 mL). This second solution was sealed and degassed in the same way, and it was protected from light with aluminum foil. Then, the vPVC-N_3 solution was injected into the 100 mL flask using an infusion pump (2.1 mL / h) (Figure 71). After 24 h (12 h of injection + 12 h of additional stirring), BAz (25 µL, 0.2 mmol of azide groups) was added, and stirring was maintained for 24 h at r.t. Finally, the product was precipitated in an excess of cold EtOH to remove potential traces of low molecular weight compounds. vPVC-SCNPs (45.5 mg) were isolated as a white powder after filtration and further drying in vacuum at 50 ºC overnight. Yield (%): 91. Conversion (disappearance of azide IR vibration band): >98%. M_w (SEC/MALS): 183.8 kDa. Đ (SEC): 1.64.

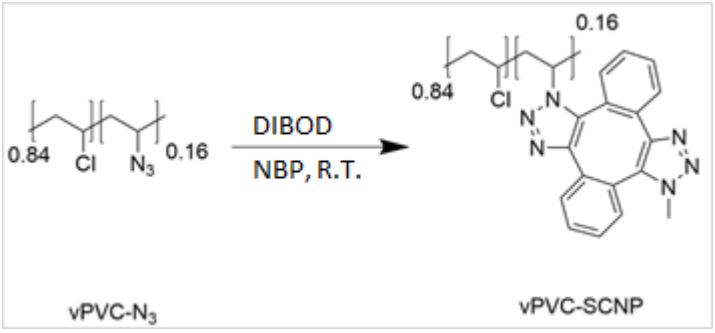

Figure 71. Synthetic scheme of the synthesis of vPVC-SCNPs.

- *Preparation of vPVC-Cu catalytic SCNPs*

In a typical procedure, 80 mg of vPVC-SCNPs (0.21 mmol of triazole groups) and 12.8 mg of $CuCl_2$ (0.095 mmol of Cu(II)) were dissolved in 80 ml of anhydrous THF (Figure 72). The solution was stirred for 48 hours at r.t. under N_2 atmosphere. Next, the solution was precipitated in H_2O to recover the vPVC-SCNPs/Cu(II) catalyst and to remove unreacted $CuCl_2$. The product was filtered and dried in a vacuum oven at 50 ºC overnight. ICP-MS characterization revealed a content of Cu ions of 7.3 mol% (1 µg of copper per mg of vPVC-SCNPs/Cu(II) catalyst).

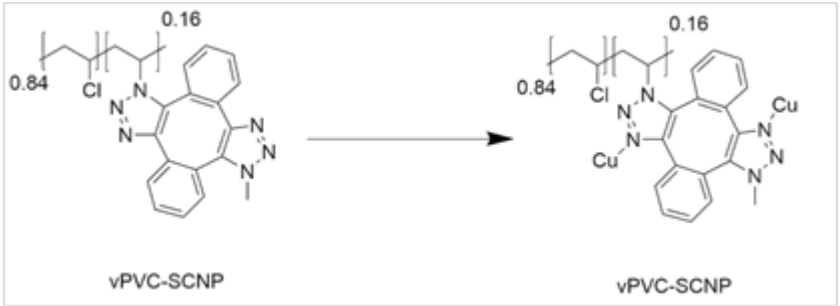

Figure 72. Synthetic scheme of the synthesis of vPVC-Cu SCNPs.

- *Applications of PVC-Cu SCNPS*

1,6-Diacetoxy-2,4-hexadiyne synthesis:

Model Reaction:

151 mg of propagyl acetate (1.54 mmol, 1 eq.), 5.3 mg of triethylamine (0.052 mmol, 0.03 eq.) and 10.3 mg of $CuCl_2$ catalyst (0.077 mmol, 0.05 eq.) were mixed in a 10 ml Schlenk flask (Figure 73). To measure the yield 2.7 mg of 1,4-dicyanobenzene was added too. To avoid the evaporation of the reactants, the Schlenk was closed with a septum with a globe with pressured air, because air presence is necessary to carry out the reaction. The mixture was stirred for 6 h at 60 ºC. After the reaction, the flask was washed with diethyl ether and water. The product was isolated extracting the organic phase, drying with magnesium sulfate and removing the solvent in a rotatory evaporator. Catalyst was recovered from aqueous phase removing the solvent too. The catalyst and the product were dried in a vacuum oven overnight.

Another model reaction was tried to carry out with recovered catalyst, but no product was obtained. So can concluded that the $CuCl_2$ is not reusable.

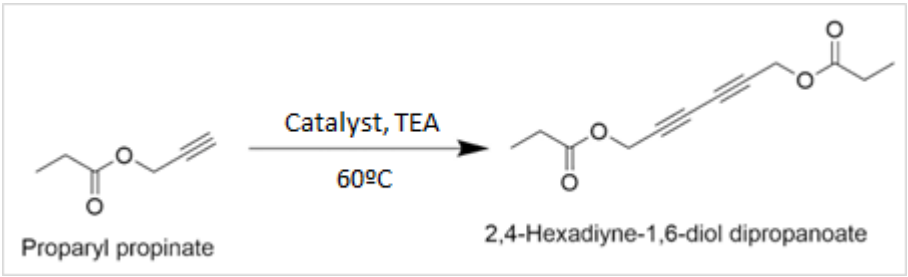

Figure 73. Synthetic scheme of the synthesis of 1,6-diacetoxy-2,4-hexadiyne.

PVC-Cu:

Cycle 1: 139 mg of propagyl acetate (1.42 mmol, 1 eq.), 6.5 mg of triethylamine (0.064 mmol, 0.04 eq.) and 50.9 mg of PVC-Cu catalyst ($8*10^{-4}$ mmol, $5*10^{-4}$ eq.) were mixed in a 10 ml Schlenk flask. To measure the yield 6.1 mg of 1,4-dicyanobenzene was added too. To avoid the evaporation of the reactants, the Schlenk was closed with a septum with a globe with pressured air, because air presence is necessary to carry out the reaction. The mixture was stirred for 6 h at 60 ºC. After the reaction, the flask was washed with diethyl ether and water. As the PVC is not soluble in those solvent the catalyst can be recovered easily. The product was isolated extracting the organic phase, drying with magnesium sulfate and removing the solvent in a rotatory evaporator. Catalyst and product were dried in a vacuum oven overnight.

Cycle 2: the same conditions of the Cycle 1 were used with 1.32 mmol of propagyl acetate, 0.05 mmol of trimethylamine, 43.3 mg of PVC-Cu (recycled from Cycle 1) and 5.2 mg of 1,4-dicyanobenzene.

Cycle 3: the same conditions of the Cycle 1 were used with 1.09 mmol of propagyl acetate, 0.05 mmol of trimethylamine, 43.0 mg of PVC-Cu (recycled from Cycle 2) and 2.3 mg of 1,4-dicyanobenzene.

Cycle 4: the same conditions of the Cycle 1 were used with 1.31 mmol of propagyl acetate, 0.05 mmol of trimethylamine, 41.8 mg of PVC-Cu (recycled from Cycle 3) and 2.1 mg of 1,4-dicyanobenzene.

Leaching experiment:

To check if the Cu was losing in each iteration of the reaction a leaching experiment was carried out. The experiment was equal to a previous catalyst reaction with 2.012 g (20.51 mmol) of propagyl acetate, 62.5 mg (0.62 mmol) of trimethylamine, 88.7 mg ($14.18*10^{-4}$ mmol, $7*10^{-5}$ eq.) of PVC-Cu and 17.3 mg of 1,4-dicyanobenzene. After 3 h, the PVC-Cu was removed from the reaction and a sample was recovered, extracted and dried to analyze with ^{1}H NMR. The reaction was carried out for another 3 hours. After the reaction, the product was isolated, dried and analyzed by NMR. Using the characteristic peak of the product yield was calculated: 45.24% for 3 h reaction and 48.53% for 6 h reaction, without the catalyst. As the yield has no a remarkable increase, can be concluded that there are not a remarkable loose of the Cu from PVC nanoparticles.

1,4-Bis(4-fluorophenyl)butadiyne synthesis:

Model reaction:

196.2 mg of 1-ethynyl-4-fluorobenzene (1.63 mmol, 1 eq.), 5.0 mg of triethylamine (0.05 mmol, 0.03 eq.) and 9.1 mg of $CuCl_2$ catalyst (0.07 mmol, 0.04 eq.) were mixed in a 10 ml Schlenk flask (Figure 74). To avoid the evaporation of the reactants, the Schlenk was closed with a septum with a globe with pressured air, because air presence is necessary to carry out the reaction. The mixture was stirred for 6 h at 60 ºC. After the reaction, the flask was washed with diethyl ether and water. As the PVC is not soluble in those solvent the catalyst can be recovered easily. The product was isolated extracting the organic phase, drying with magnesium sulfate and removing the solvent in a rotatory evaporator. Catalyst and product were dried in a vacuum oven overnight. To measure the yield 0.1 ml of 1,1,2,2-Tetrabromoethane was added.

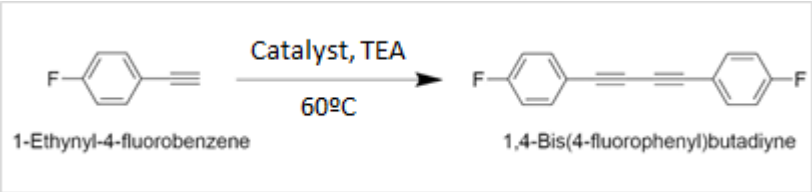

Figure 74. Synthetic scheme of the synthesis of *1,4bis(4-fluorophenyl)butadiyne*.

PVC-Cu:

320.2 mg of 1-ethynyl-4-fluorobenzene (2.67 mmol, 1 eq.), 8.1 mg of triethylamine (0.08 mmol, 0.03 eq.) and 53.6 mg of PVC-Cu catalyst ($8.4*10^{-4}$ mmol, $3*10^{-4}$ eq.) were mixed in a 10 ml Schlenk flask. To avoid the evaporation of the reactants, the Schlenk was closed with a septum with a globe with pressured air, because air presence is necessary to carry out the reaction. The mixture was stirred for 6 h at 60 ºC. After the reaction, the flask was washed with diethyl ether and water. As the PVC is not soluble in those solvent the catalyst can be recovered easily. The product was isolated extracting the organic phase, drying with magnesium sulfate and removing the solvent in a rotatory evaporator. Catalyst and product were dried in a vacuum oven overnight. To measure the yield 0.1 ml of 1,1,2,2-Tetrabromoethane was added.

2,4-Hexadiyne-1,6-diol, dipropanoate synthesis:

Model reaction:

115.6 mg of propargyl propionate (1.03 mmol, 1 eq.), 3.2 mg of triethylamine (0.03 mmol, 0.03 eq.) and 5.8 mg of $CuCl_2$ catalyst (0.04 mmol, 0.04 eq.) were mixed in a 10 ml Schlenk flask (Figure 75). To measure the yield 38.9 mg of 1,4-dicyanobenzene was added too. To avoid the evaporation of the reactants, the Schlenk was closed with a septum with a globe with pressured air, because air presence is necessary to carry out the reaction. The mixture was stirred for 6 h at 60 ºC. After the reaction, the flask was washed with diethyl ether and water. As the PVC is not soluble in those solvent the catalyst can be recovered easily. The product was isolated extracting the organic phase, drying with magnesium sulfate and removing the solvent in a rotatory evaporator. Catalyst and product were dried in a vacuum oven overnight.

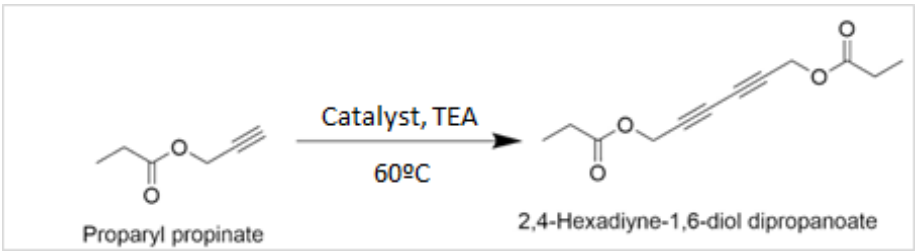

Figure 75. Synthetic scheme of the synthesis of 2,4-hexadiyne-1,6-diol dipropanoate.

PVC-Cu:

210.1 mg of 1-ethynyl-4-fluorobenzene (1.87 mmol, 1 eq.), 7.1 mg of triethylamine (0.07 mmol, 0.04 eq.) and 99.2 PVC-Cu catalyst ($15.5*10^{-4}$ mmol, $8.3*10^{-4}$ eq.) were mixed in a 10 ml Schlenk flask. To measure the yield 20.5 mg of 1,4-dicyanobenzene was added too. To avoid the evaporation of the reactants, the Schlenk was closed with a septum with a globe with pressured air, because air presence is necessary to carry out the reaction. The mixture was stirred for 6 h at 60 ºC. After the reaction, the flask was washed with diethyl ether and water. As the PVC is not soluble in those solvent the catalyst can be recovered easily. The product was isolated extracting the organic phase, drying with magnesium sulfate and removing the solvent in a rotatory evaporator. Catalyst and product were dried in a vacuum oven overnight.

Benzaldehyde synthesis:

Model Reaction:

6 ml of styrene (52.19 mmol, 1 eq.), 11 ml of hydrogen peroxide (30% w/w) (107.7 mmol, 2 eq.) and 72.2 mg of $CuCl_2$ catalyst (0.54 mmol, 0.01 eq.) were dissolved in 50 ml of acetonitrile in a 100 ml round-bottom flask (Figure 76). The mixture was heated to 90 ºC and irradiated with microwave (15 W) for 30 min. After the reaction, the flask was washed with diethyl ether and water and the organic phase was extracted. The product was isolated by chromatographic column using hexane/diethyl ether (7/3) as eluent. To measure the yield 50 µL of 1,1,2,2-Tetrabromoethane was added.

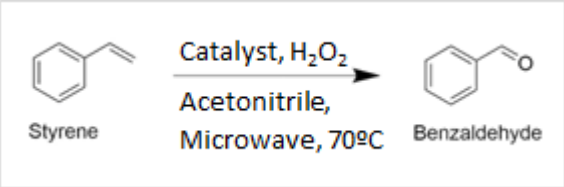

Figure 76. Synthetic scheme of the synthesis of benzaldehyde.

PVC-Cu:

6 ml of styrene (52.19 mmol, 1 eq.), 11 ml of hydrogen peroxide (35% w/w) (107.6mmol, 2 eq.) and 96 mg of PVC-Cu catalyst ($1.5*10^{-3}$ mmol, $3*10^{-5}$ eq.) were dissolved in 50 ml of acetonitrile in a 100 ml round-bottom flask. The mixture was heated to 90 ºC and irradiated with microwave (15 W) for 30 min. After the reaction, the flask was washed with diethyl ether and water and the organic phase was extracted. The PVC-Cu catalyst was recovered in solid form. The product was isolated by chromatographic column using hexane/diethyl ether (7/3) as eluent. To measure the yield 50 µl of 1,1,2,2-Tetrabromoethane was added.

3,5-Di-t-butyl-o-quinone synthesis:

Model Reaction:

34.3 mg of 3,5-Di-tert-butylcatechol (0.15 mmol) was dissolved in 3 ml of methanol. Another dissolution was prepared with 1.3 mg $CuCl_2$ ($9.67*10^{-3}$ mmol) in 50 ml of DMF and 1 ml of this dissolution was diluted with another 19 ml of DMF to obtain a dissolution of 1.3 µg $CuCl_2$ in 20 ml of DMF. 0.125 ml of each dissolution and 0.875 ml of DMF and methanol were mixed in a 1 cm path length optical cell, obtaining a dissolution with 0.163 µg $CuCl_2$ ($1.21*10^{-6}$ mmol of Cu) and 1.43 mg of 3,5-Di-tert-butylcatechol in 1 ml DMF and 1 ml methanol (Figure 77). The reaction was monitored measuring the UV-Vis absorbance spectrum each 30 min for 3 hours.

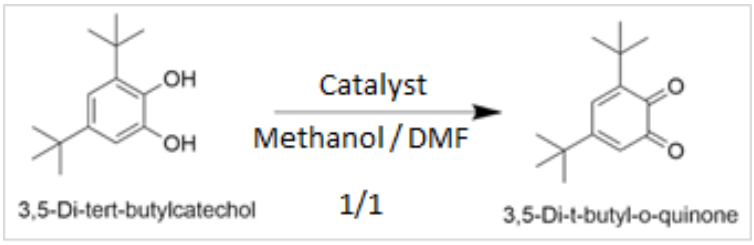

Figure 77. Synthetic scheme of the synthesis of 3,5-di-t-butyl-o-quinone synthesis.

PVC-Cu:

34.3 mg of 3,5-Di-tert-butylcatechol (0.15 mmol) was dissolved in 3 ml of methanol. Another dissolution was prepared with 12.6 mg PVC-Cu (12.6 µg Cu) in 20 ml of DMF. 0.125 ml of each dissolution and 0.875 ml of DMF and methanol were mixed in a 1 cm path length optical cell, obtaining a dissolution with 78.75 µg PVC-Cu ($1.24*10^{-6}$ mmol of Cu) and 1.43 mg of 3,5-Di-tert-butylcatechol in 1 ml DMF and 1 ml methanol. The reaction was monitored measuring the UV-Vis absorbance spectrum each 30 min for 3 hours.

Kinetic investigation of the 3,5-Di-t-butyl-o-quinone synthesis:

3,5-Di-t-butyl-o-quinone synthesis was characterized according with Michaels-Menten kinetic, using the value 2200 $L*mol^{-1}*cm^{-1}$ as extinction coefficient (ε) of 3,5-Di-t-butyl-o-quinone [37, 38]. The reaction was repeated for 1 hour with different concentrations of the 3,5-Di-tert-butylcatechol ($0.5*10^{-3}$ M, $1*10^{-3}$ M, $2*10^{-3}$ M, $3*10^{-3}$ M, $4*10^{-3}$ M, $5*10^{-3}$ M, $6*10^{-3}$ M, $7*10^{-3}$ M and $8*10^{-3}$ M) and the same concentration of the catalyst ($4.83*10^{-6}$ M for $CuCl_2$ and $4.96*10^{-6}$ M for PVC-Cu).

6.4. Results and discussion

6.4.1. Azidation of PVC

Elemental analysis (EA) data of PVC-N_3 Table 2 shows a substitution of 12.2 mol% by performing the azidation reaction with sodium azide. PVC-N_3 was subsequently characterized by proton (^{1}H) and carbon (^{13}C) nuclear magnetic resonance (NMR) spectroscopy, size exclusion chromatography (SEC) and infra-red (IR) spectroscopy.

Table 2. EA of the commercial PVC.

EA Comercial PVC					
Theoretical			Experimental		
PVC	C%	38.40	PVC	C%	39.11
	H%	4.80		H%	4.88
	N%	0.00		N%	<1.6
PVC-N_3 (12.2%)	C%	37.92	PVC-N_3	C%	38.29
	H%	4.74		H%	4.89
	N%	8.10		N%	8.13

The ^{1}H NMR spectrum of commercial PVC (weight average molecular weight, $M_{w\ (MALS)}$ = 46.5 kDa; dispersity, Đ = 1.35) shows tacticity features in both the methine (Cl-C**H**-CH_2-) and methylene (Cl-CH-C**H_2**-) protons placed at 4.06 – 4.60 and 1.85 – 2.39 ppm, respectively [39]. Upon partial azidation, new bands appear in the ^{1}H NMR spectrum of PVC-N_3 located at 4.05 – 4.18 and 1.85 ppm that can be attributed, respectively, to N_3-C**H**-CH_2- methine and N_3-CH-C**H_2**- methylene protons (Figure 78 a)). Similarly, in the ^{13}C NMR spectrum of PVC-N_3 new signals from N_3-**C**H-CH_2- methine and N_3-CH-**C**H_2- methylene carbons are clearly visible at 55.8 and 42.0 – 43.3 ppm, respectively, when compared to the signals of neat PVC (Figure 78 b)). The weight average molecular weight and dispersity of PVC-N_3 ($M_{w\ (MALS)}$ = 51.4 kDa, Đ = 1.35) were found to be very similar to those of the starting PVC material, as determined by SEC (Figure 79 a)). Complementary, the IR spectrum of PVC-N_3 showed an intense band centered at ca. 2110 cm-1 corresponding to the stretching vibration of the azide moiety (Figure 79 b)). Taken together, these results support the successful (partial) functionalization of PVC chains in DMF with a number of azide pendants. Partial azidation of PVC to PVC-N_3 decreased by around 100 ºC the degradation temperature (from $T_{d\ (PVC)}$ = 275 ºC to $T_{d\ (PVC\text{-}N3)}$ = 170 ºC) (Figure 80 a)); and 10 ºC the glass transition temperature (from $T_{g\ (PVC)}$ = 80 ºC to $T_{g\ (PVC\text{-}N3)}$ = 70 ºC) due to an increase in

free volume introduced by the azide pendants, when compared to the chlorine moieties (Figure 80 b)).

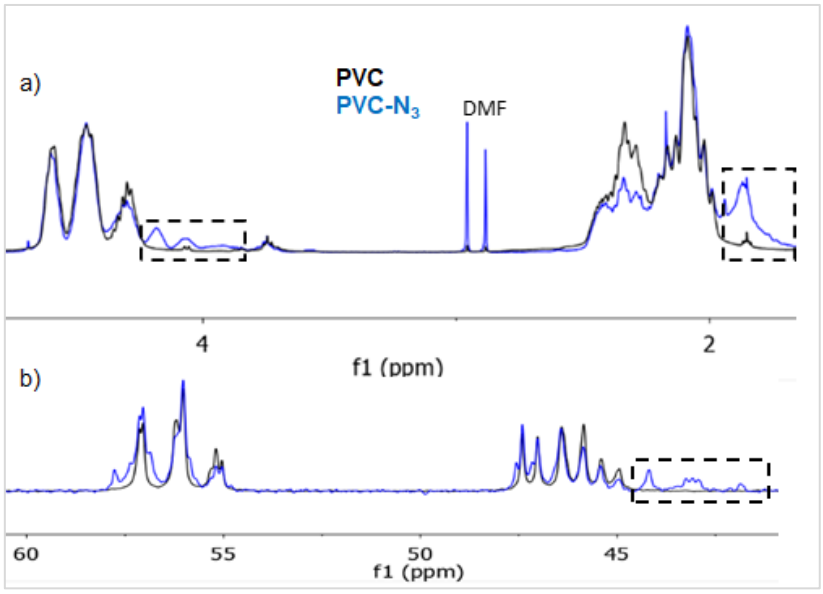

Figure 78. a) ^{1}H NMR and b) ^{13}C NMR spectra of PVC (black) and PVC-N_3 (blue). In the black boxes are marked the new bands associated to PVC-N_3.

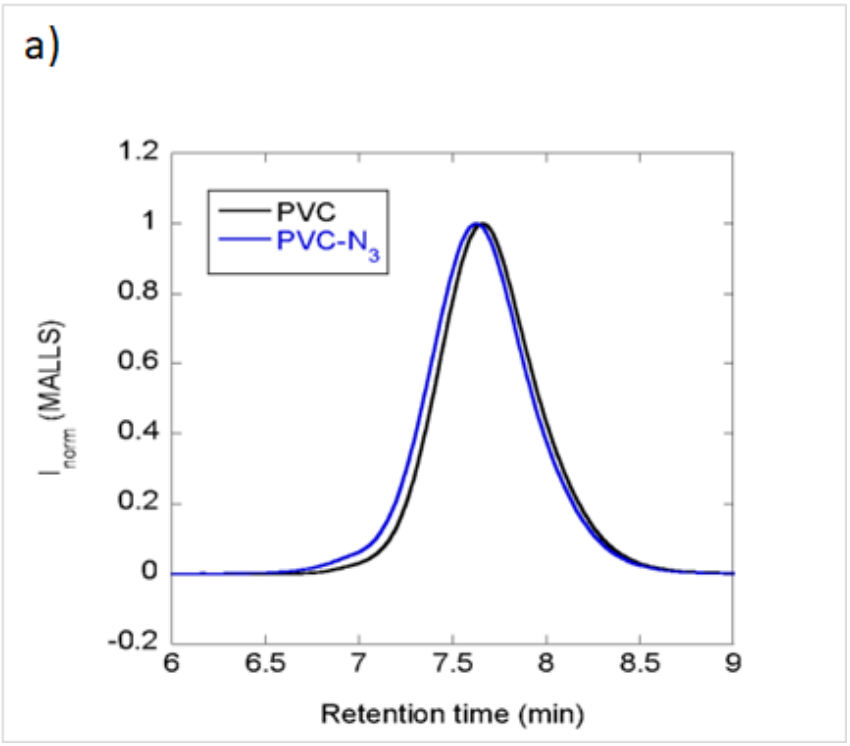

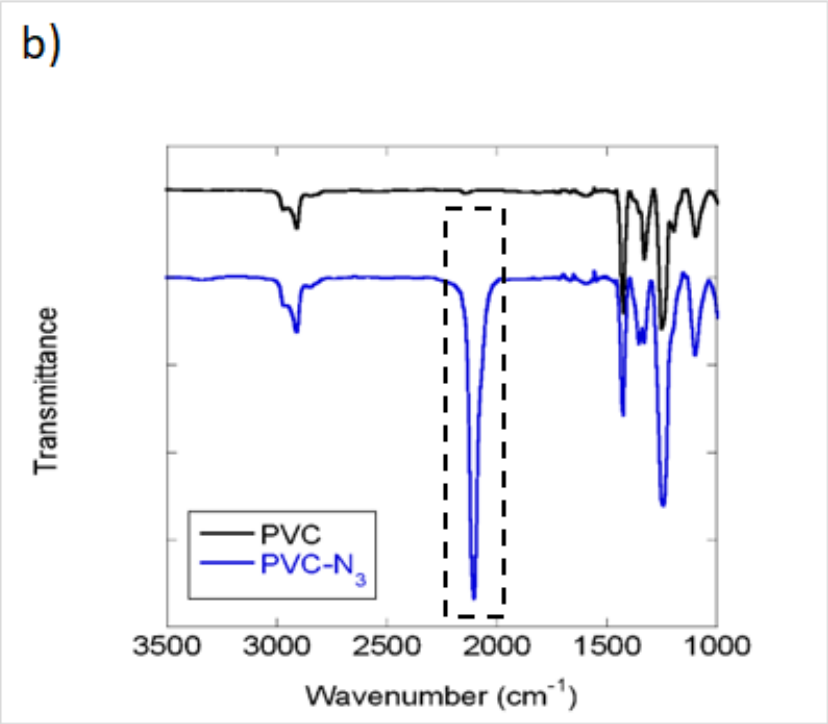

Figure 79. a) GPC chromatogram (LS detector) and b) FTIR spectra. PVC in black and PVC-N_3 in blue. The new peak associated with the azide group is marked with the black box.

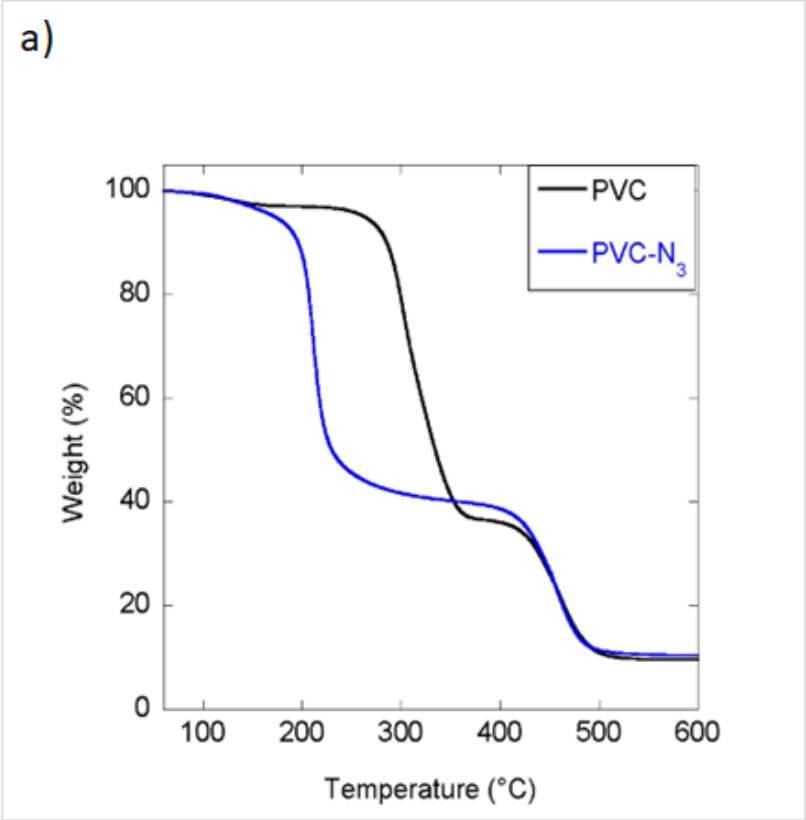

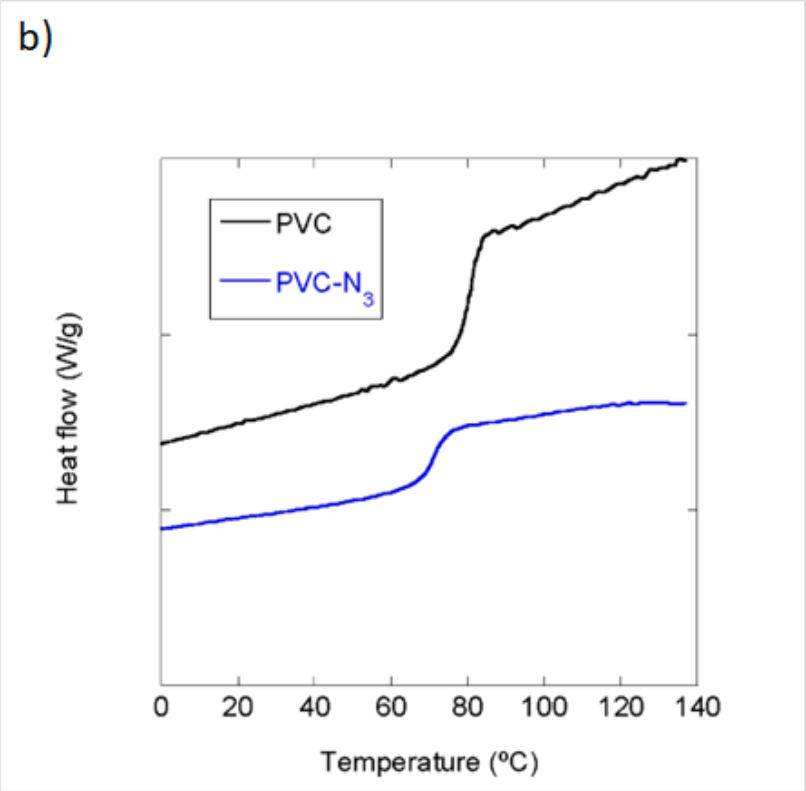

Figure 80. a) TGA and b) DSC traces of PVC (black) and PVC-N_3 (blue). The DSC traces have been downshifted for clarity. Both, degradation and glass-transition temperature are decreased after azidation.

6.4.2. Synthesize of PVC-SCNPs

Figure 81 shows the ^{1}H and ^{13}C NMR spectra of the PVC-SCNPs. The most notorious features are the presence of new bands in the ^{1}H and ^{13}C NMR spectra of the PVC-SCNPs coming from the incorporation of the intra-chain cross-linker and the disappearance of the bands from N_3-C**H**-CH_2- and N_3-CH-C**H_2**- protons as well as N_3-**C**H-CH_2- and N_3-CH-**C**H_2- carbons when compared, respectively, to the ^{1}H and ^{13}C NMR spectra of PVC-N_3. It can be observed too in the FTIR spectra (Figure 82), where the reduction of the azide group peak around 2100 cm^{-1} of the FTIR spectra means that the reaction has been carried out correctly.

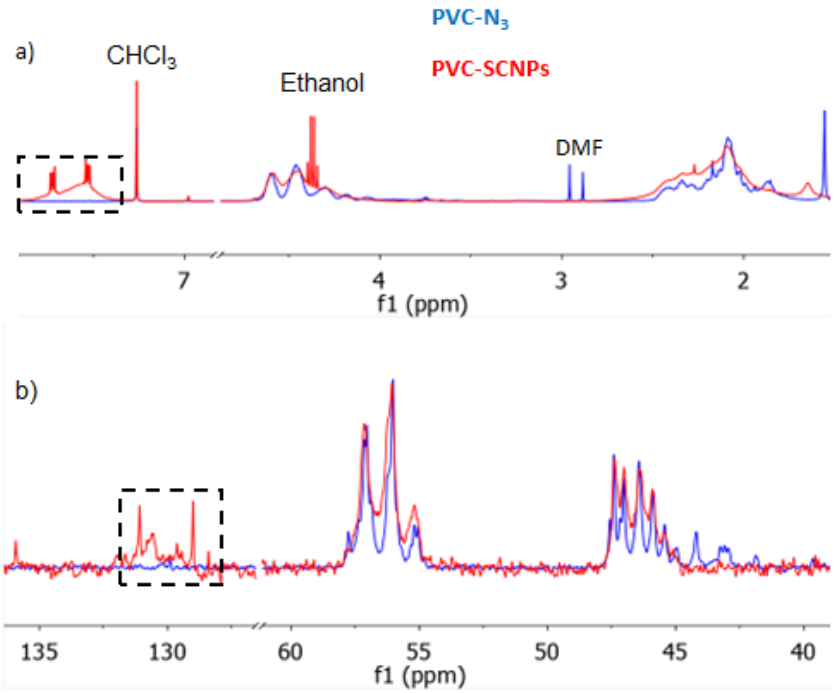

Figure 81. a) ^{1}H NMR and b) ^{13}C NMR of PVC-N_3 (blue) and PVC-SCNP (red). In the black box are marked the new bands associated to cross linker.

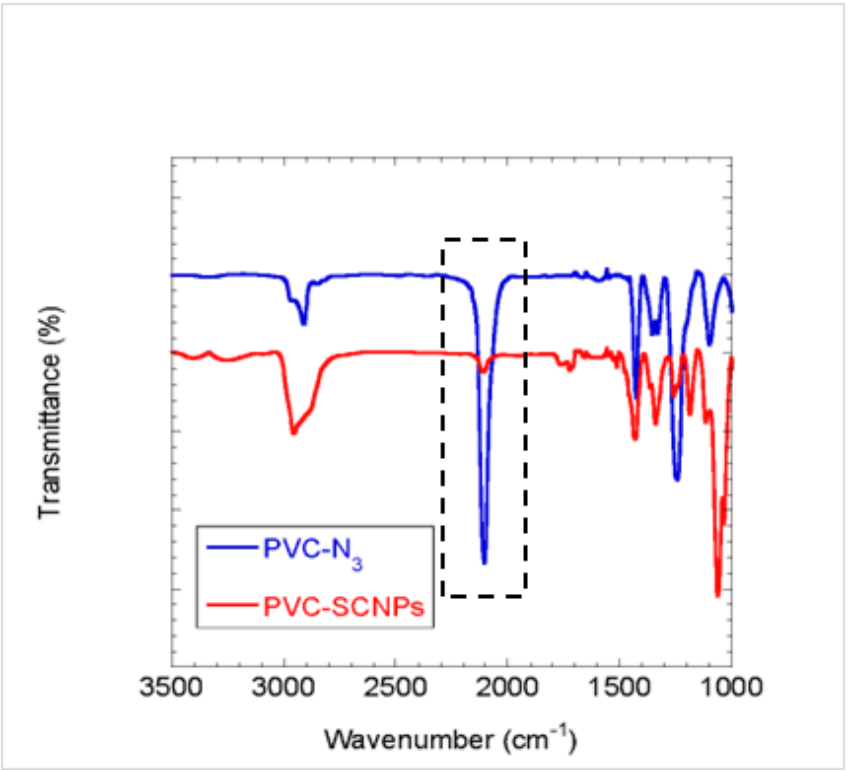

Figure 82. FTIR spectra of PVC-N_3 (blue) and PVC-SCNP (red). In the black box is marked the peak associated to the azide group.

SEC provided a solid confirmation of efficient formation of PVC-SCNPs. A shift towards longer SEC retention time and, hence, a reduction in average hydrodynamic size was clearly observed upon PVC-SCNPs formation (Figure 83 a)). Simultaneously, the weight average molecular weight

and dispersity of PVC-SCNPs ($M_{w\,(MALS)}$ = 92.1 kDa, Đ = 1.34) were consistent with the expected behavior upon incorporation of DIBOD as intra-chain cross-linker. Dynamic light scattering (DLS) measurements in THF (Figure 83 b)) confirmed a reduction in average hydrodynamic radius from 10.1 nm (PVC-N_3) to 6.5 nm (PVC-SCNPs). Complementarily, we determined the radius of gyration (R_g) and size-scaling exponent (ν) of PVC-N_3 and PVC-SCNPs by means of small-angle X-ray scattering (SAXS) measurements (Figure 83 c)). PVC-N_3 showed $R_{g\,(PVC\text{-}N3)}$ =14.7 nm and $\nu_{(PVC\text{-}N3)}$ = 0.59; the typical value for linear polymer chains in good solvent conditions. As expected, PVC-SCNPs showed a significant reduction in both R_g and ν: $R_{g\,(PVC\text{-}SCNPs)}$ = 6.7 nm, $\nu_{(PVC\text{-}SCNPs)}$ = 0.46. A reduction in R_g and ν is commonly observed upon intrachain folding of isolated chains to produce SCNPs [12, 35]. Specifically, the lower value of ν in the case of PVC-SCNPs when compared to $\nu_{(PVC\text{-}N3)}$ = 0.59 is a clear indication of a higher level of chain compaction. More importantly, no significant changes were detected when the PVC-SCNPs were subjected to SAXS experiments after 2 months of storage in the solid state, or when stored in THF solution for 2 months (Figure 83 d)). These experimental findings shows that the PVC-SCNPs are highly stable during storage and no significant interchain aggregation processes were involved either in solution or in the solid state for months. We attribute this stability to the final end-capping procedure with benzyl azide that is able to limit the number of residual reactive functional groups. In addition, the absence of any metallic catalyst in the intra-chain cross-linking step contributes -presumably- to the stability of the PVC-SCNPs.

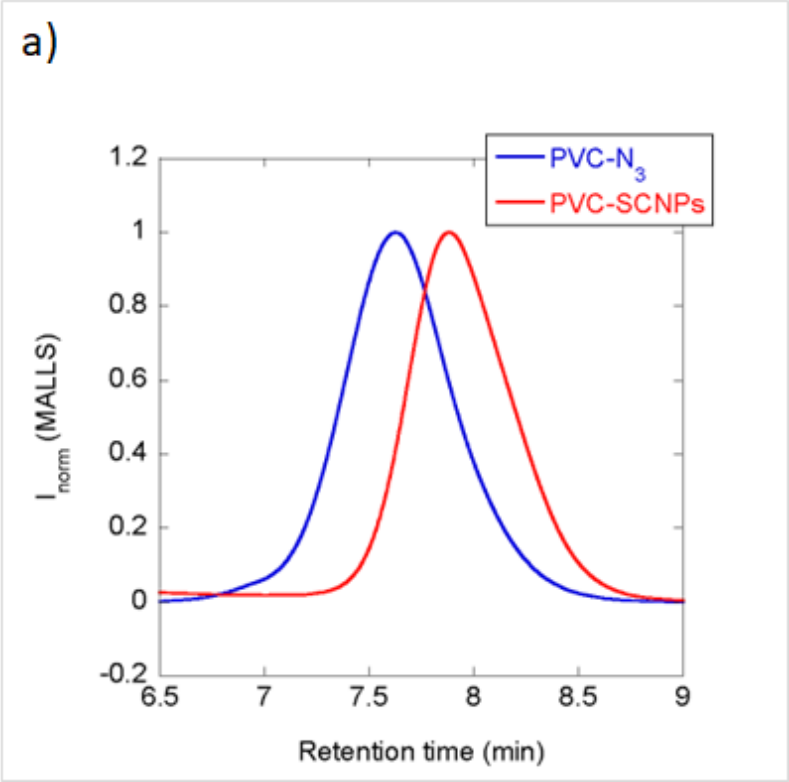

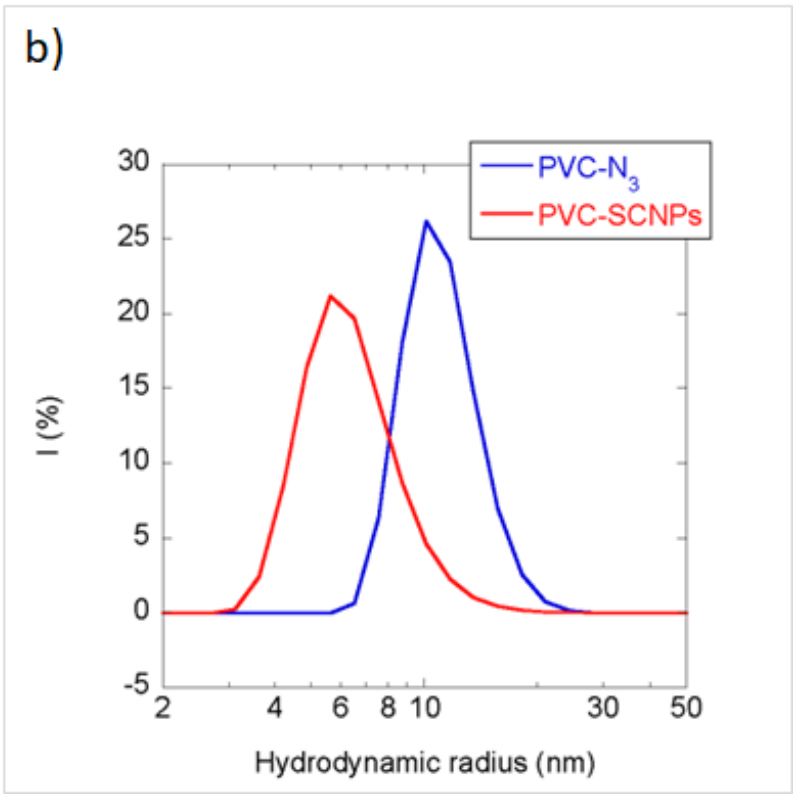
b)
PVC-N3
PVC-SCNPs
I (%)
30
25
20
15
10
5
0
-5
2
4
6
8
10
30
50
Hydrodynamic radius (nm)

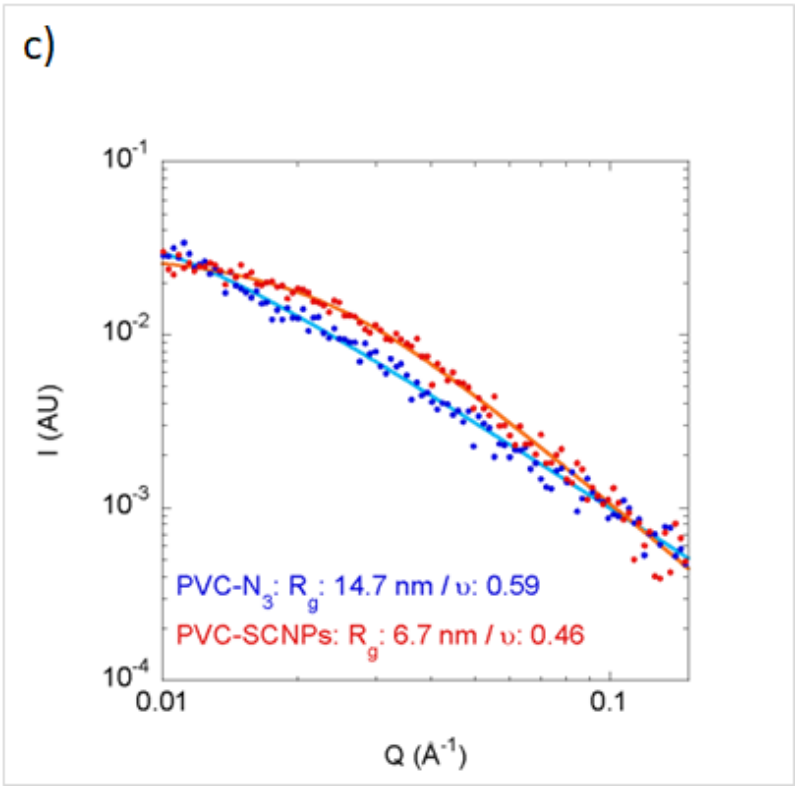
c)
I (AU)
10-1
10-2
10-3
10-4
0.01
0.1
Q (Å-1)
PVC-N3: Rg: 14.7 nm / υ: 0.59
PVC-SCNPs: Rg: 6.7 nm / υ: 0.46

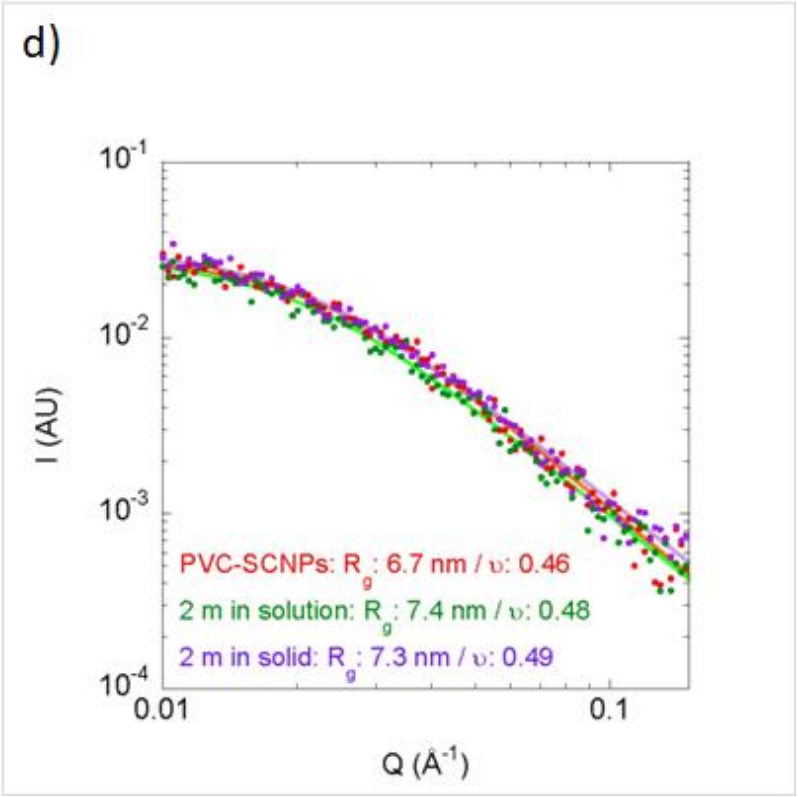

Figure 83. a) GPC chromatogram (LS detector), b) DLS size distribution in THF and SAXS result of the SCNPs after synthesis (c)) and after 2 months of storage (d)). PVC-N_3 in blue, SCNPs after synthesis in red, SCNPs after 2 months of storage in solution in green and SCNPs stored in solid in pink.

Folding of individual PVC-N_3 chains to PVC-SCNPs resulted, additionally, in a modification of the thermal properties of the bulk material as illustrated in Figure 84 a) and b). While the degradation temperature was not modified ($T_{d\ (PVC\text{-}N3)}$ = 170 ºC to $T_{d\ (PVC\text{-}SCNPs)}$ = 175 ºC), the glass transition temperature increased by 15 ºC upon PVC-SCNPs formation ($T_{g\ (PVC\text{-}SCNPs)}$ = 85 ºC) as a consequence of the reduced segmental mobility caused by the intra-chain cross-links. All the above results support the successful formation of stable, well-defined PVC-SCNPs via intra-chain metal-free click chemistry at r.t. from commercial PVC and common organic solvents.

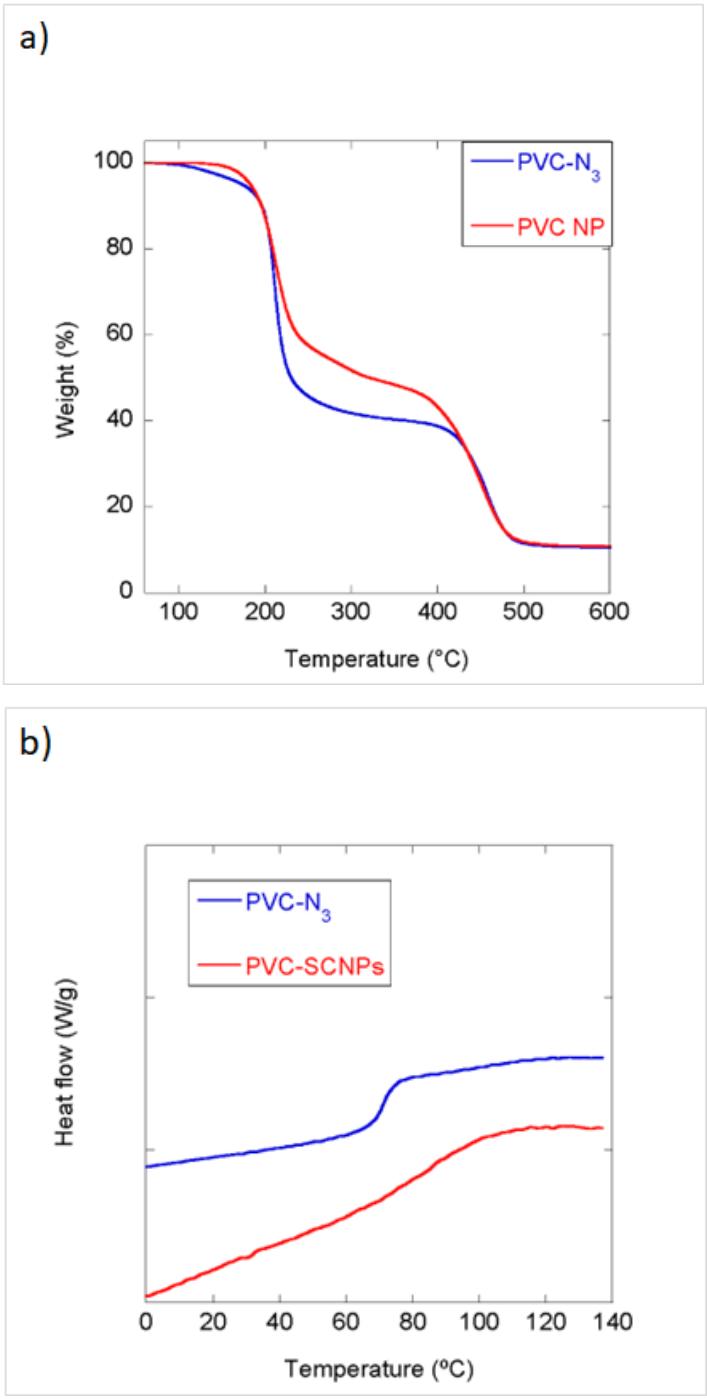

Figure 84. a) TGA and b) DSC traces of PVC-N_3 (blue) and PVC-SCNPs (Red). The DSC traces have been downshifted for clarity. The increase of Tg is related with the reduction of segmental mobility caused by the intra-chain cross-links.

6.4.3. Green solvent election

As can be seen in the Figure 85 many of the solvents cannot carry out the azidation the sample correctly. DMSO and NBP shows an as good result as DMF, but other samples show a drastically smaller peak related with the azide. According to these results, NBP was chosen as solvent for the rest of the chapter experiments. DMSO shows good result too, but NBP is better considerer as green solvent, so this last was the chosen one.

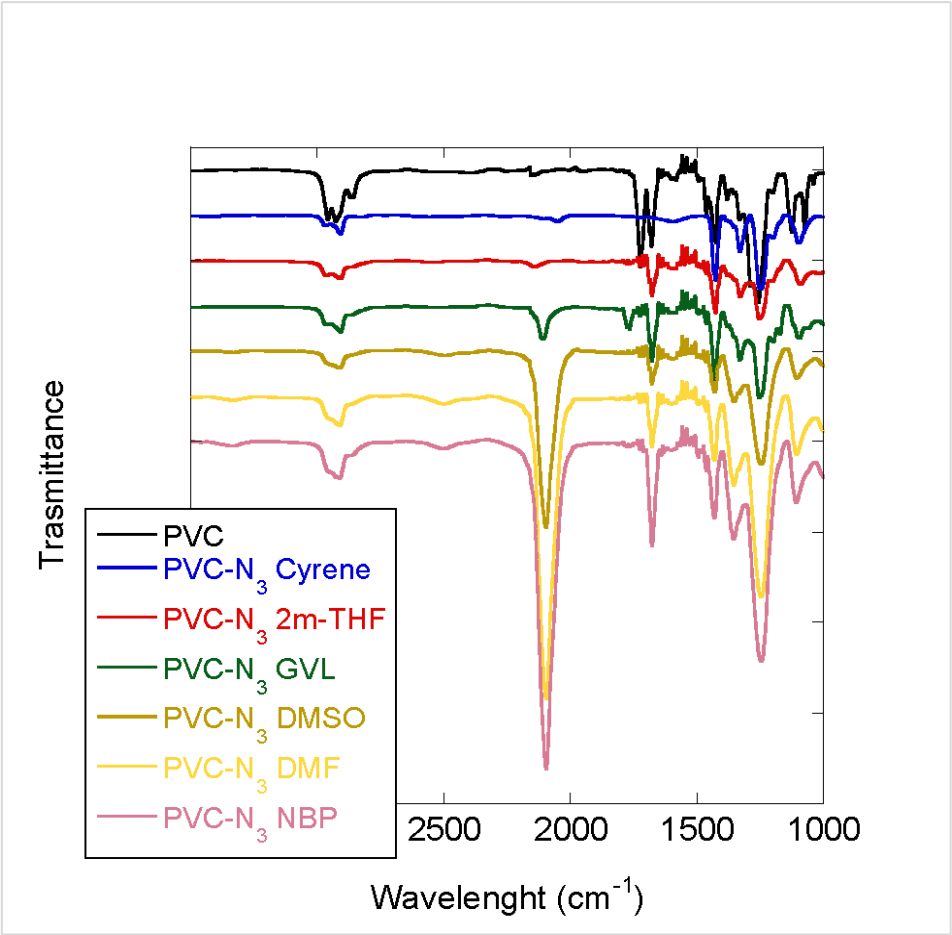

Figure 85. IR spectra of PVC (black) and PVC-N_3 synthesized in different solvents. The azidation reaction was carried out at same conditions in cyrene (blue), 2m-THF (red), GVL (green), DMSO (bronze), DMF (yellow) and NBP (pink).

6.4.4. Purification of vPVC

We selected an out-of-use piece of clear flexible PVC hose and a rigid PVC tube (Figure 86 a) and b)) for valorization to PVC-SCNPs. After the purification the two samples shows the same result in the GPC characterization (Figure 87 a)), and were same that the commercial PVC in the ^{1}H NMR characterization (Figure 87 b)). The vPVC, from flexible PVC hose, ($M_{w\,(MALS)}$ = 104.9 kDa, Đ = 1.57) has a higher molar mass than the commercial PVC, but a good dispersity value.

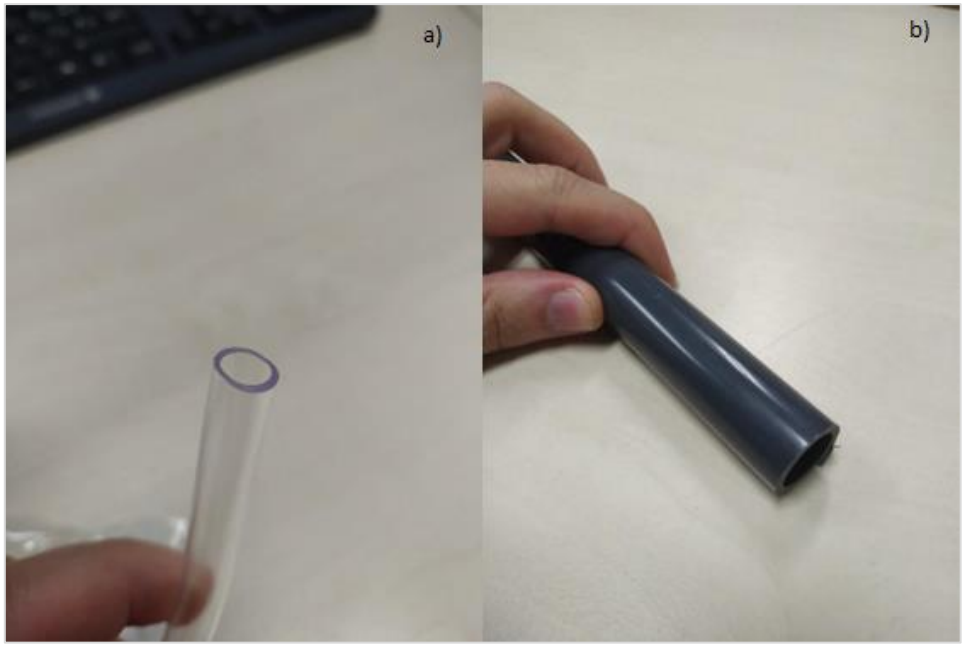

Figure 86. Picture of the polymers to be valorized: a) clear flexible PVC hose and b) rigid PVC tube.

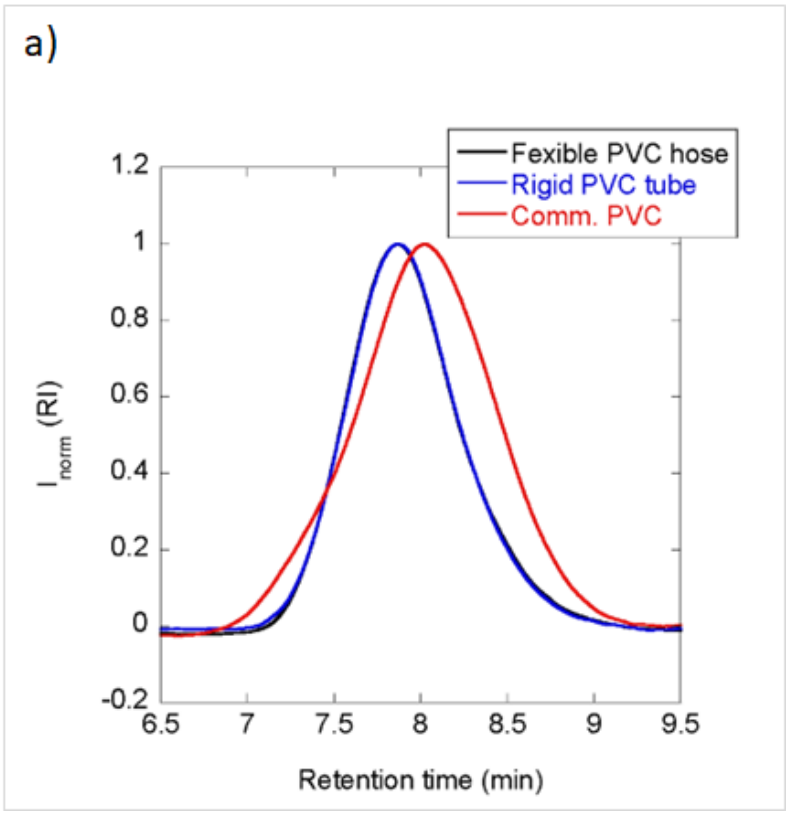

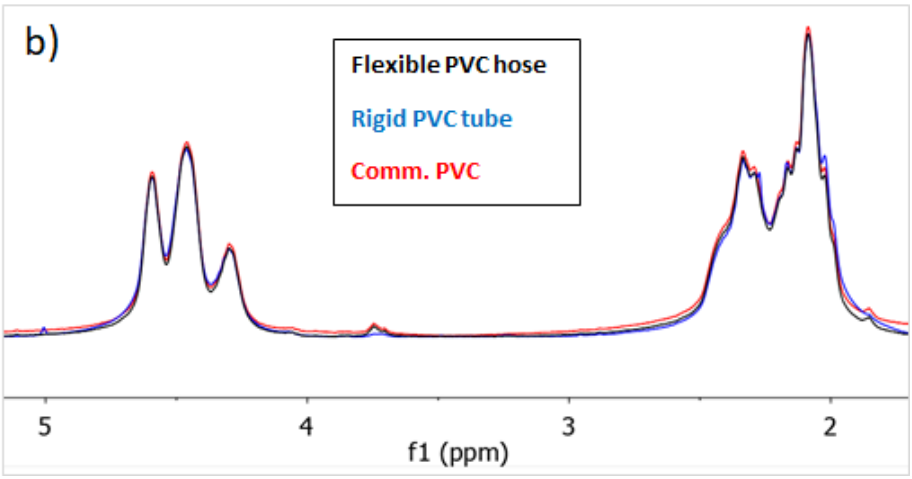

Figure 87. a) GPC chromatograph (RI detector) and b) ^{1}H NMR spectra of the valorized and commercial PVC. PVC from flexible hose in black, from rigid tube in blue and commercial in red. After the purification all the PVC samples were identical.

6.4.5. Azidation of vPVC

Successful partial azidation of vPVC in NBP to give vPVC-N_3 was confirmed by the same characterization techniques previously employed for the azidation of neat, commercial PVC. Specifically, the degree of chlorine substitution of vPVC in NBP was found to be 16.0 mol%, as determined by EA (Table 3). As with the commercial one, new bands are visible in the NMR spectra (Figure 88 a) and b)). The stretching vibration of the azide moiety at ca. 2110 cm^{-1} was clearly visible in the IR spectrum of vPVC-N_3 too (Figure 89) whereas no relevant changes in both M_w and Đ were found by SEC after azidation of vPVC in NBP ($M_{w\,(MALS)}$ = 138.1 kDa, Đ = 1.52). As can see in the Figure 90 a) and b), the thermal behavior was almost identical that the behavior of the commercial PVC samples (TGA: $T_{d\,(vPVC)}$ = 280 ºC and $T_{d\,(vPVC\text{-}N3)}$ = 220 ºC / DSC: $T_{g\,(vPVC)}$ = 70 ºC, $T_{g\,(PVC\text{-}N3)}$ = 60 ºC).

Table 3. EA of the vPVC.

EA					
Theoretical			Experimental		
vPVC	C%	38.40	vPVC	C%	38.17
	H%	4.80		H%	4.82
	N%	0.00		N%	<1.6
vPVC-N_3 (16%)	C%	37.77	vPVC-N_3	C%	37.78
	H%	4.72		H%	5.07
	N%	10.58		N%	10.61

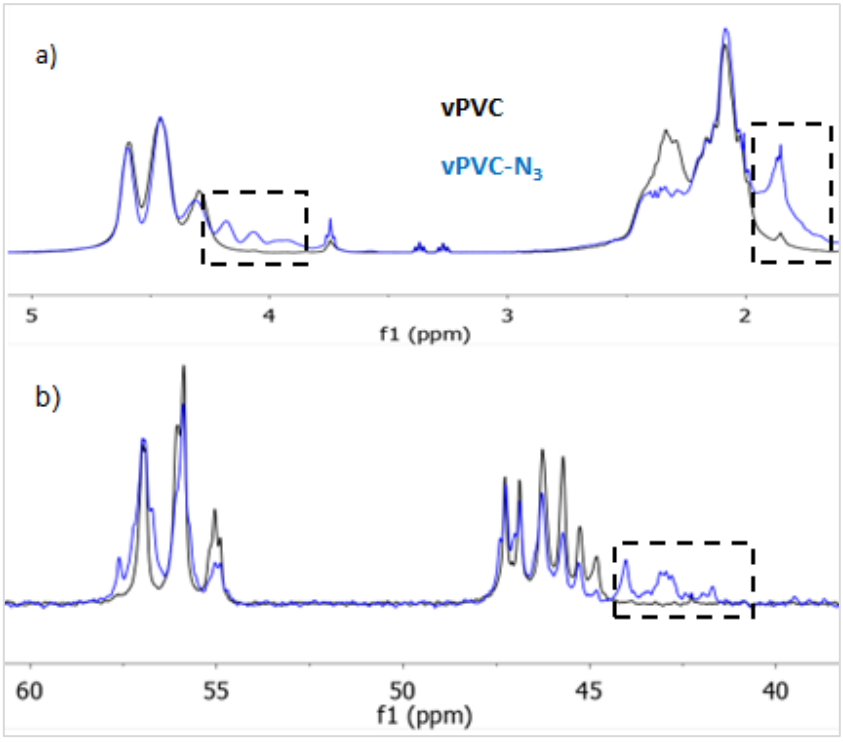

Figure 88. a) ^{1}H NMR and b) ^{13}C NMR spectra of vPVC (black) and vPVC-N_3 (blue). In the black boxes are marked the new bands associated to vPVC-N_3.

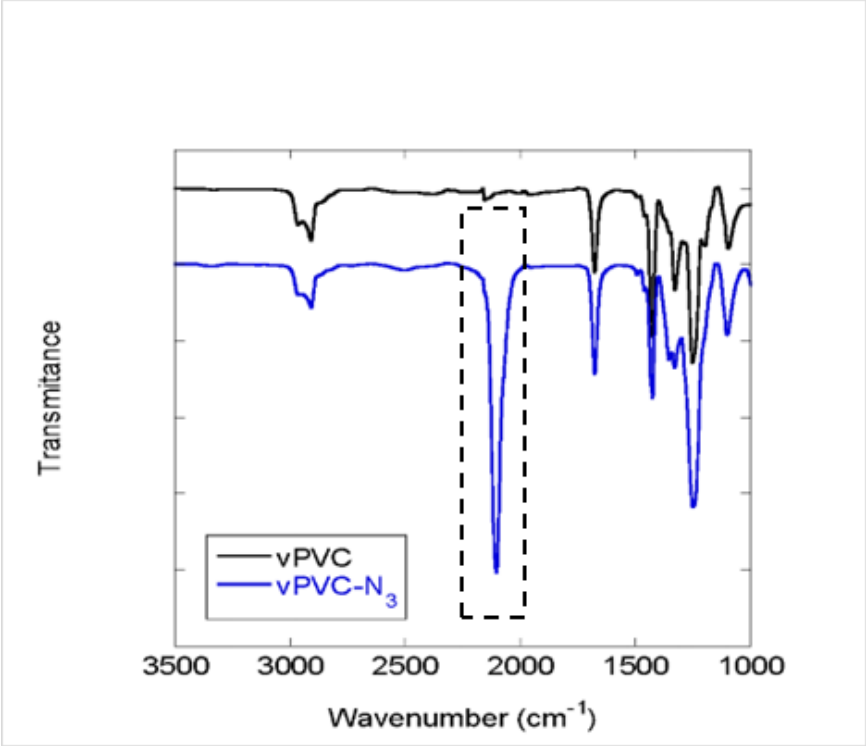

Figure 89. FTIR spectra of vPVC in black and vPVC-N_3 in blue. The new peak associated with the azide group is marked with the black box.

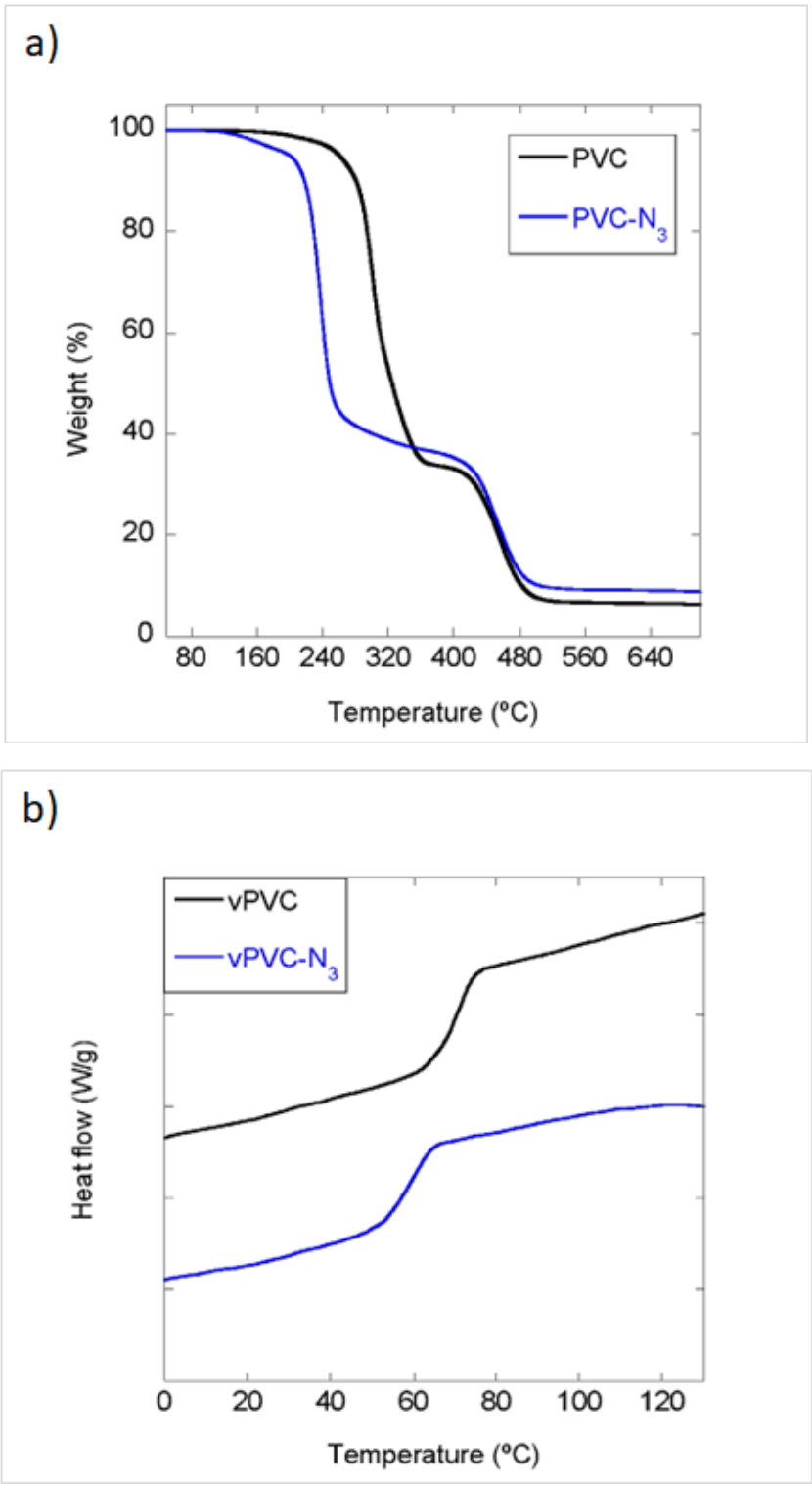

Figure 90. a) TGA and b) DSC traces of vPVC (black) and vPVC-N_3 (blue). The DSC traces have been downshifted for clarity. Both, degradation and glass-transition temperature are decreased after azidation.

6.4.6. Synthesize of vPVC-SCNP

Figure 91 shows that the ^{1}H and ^{13}C NMR spectra of the vPVC-SCNPs have the same peaks of the cross-linker, like the PVC-SCNPs. The Figure 92 shows that all the azide groups reacted, so the characteristic peak have been disappeared in the FTIR spectra.

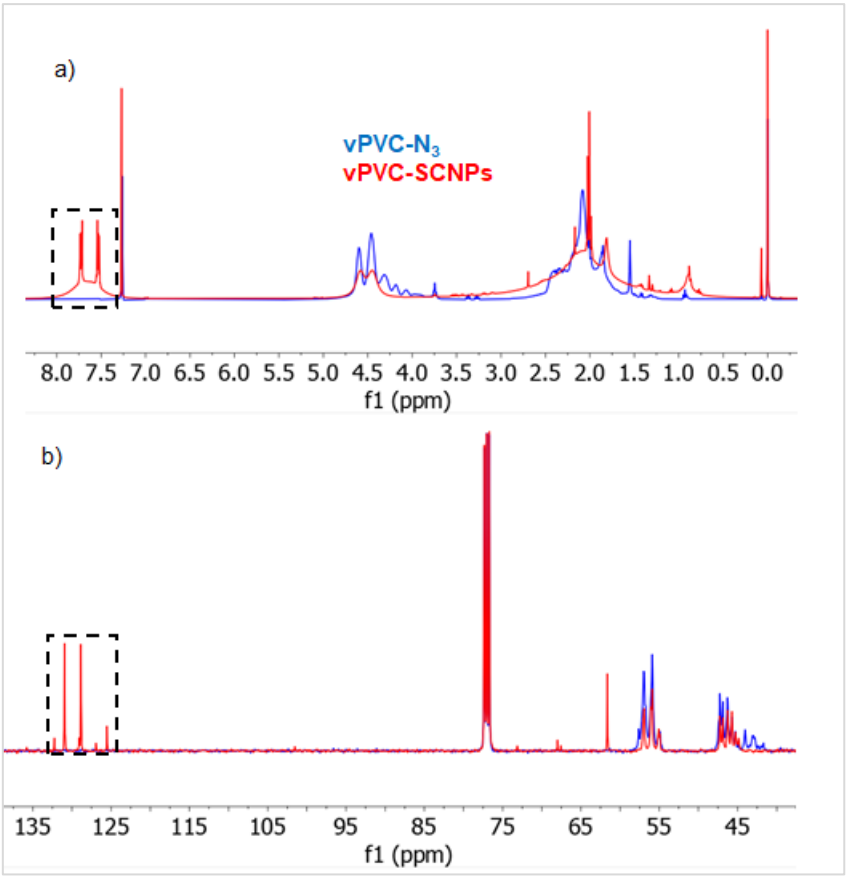

Figure 91. a) ^{1}H NMR and b) ^{13}C NMR spectra of vPVC-N_3 (blue) and vPVC-SCNP (red). In the black box are marked the new bands associated to cross linker.

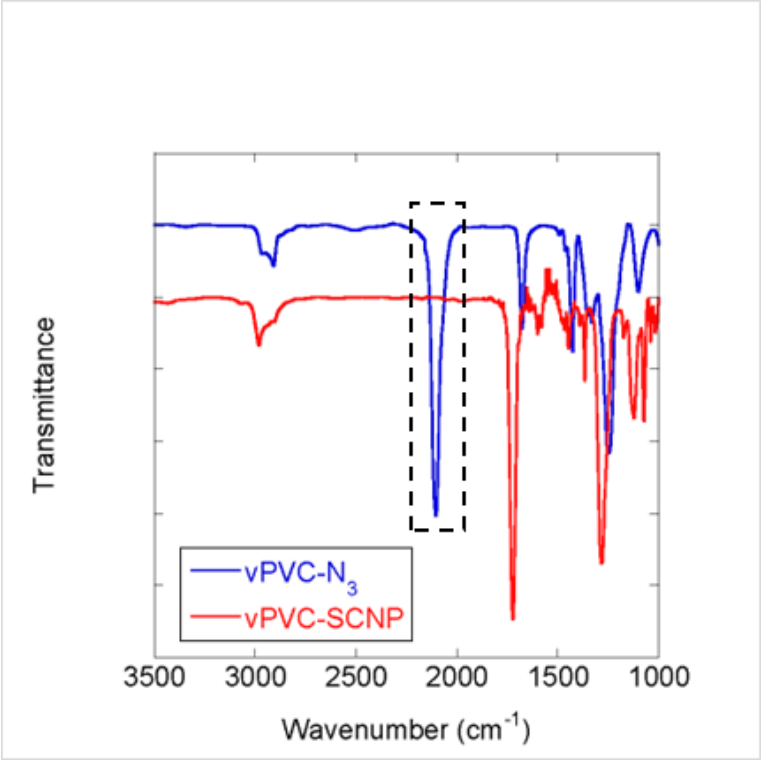

Figure 92. FTIR spectra of vPVC-N_3 (blue) and vPVC-SCNP (red). In the black box is marked the peak associated to the azide group.

Figure 93 a) shows a comparison of the SEC traces of vPVC-N_3 and valorized PVC-SCNPs (vPVC-SCNPs) prepared using only NBP as green solvent, and a cold mixture of EtOH / H_2O (1/1 vol.) as non-solvent. vPVC-SCNPs showed a clear shift towards longer SEC retention time, as a consequence of reduced hydrodynamic size when compared to vPVC-N_3. Complementary, size reduction upon vPVC-SCNPs formation was also determined by DLS and SAXS measurements (Figure 93 b) and Figure 93 c)). Moreover, as illustrated in Figure 94 a) and b), the thermal behavior of vPVC-SCNPs was similar to that recorded for nanoparticles of the commercial PVC (TGA: $T_{d\ (vPVC\text{-}SCNPs)}$ = 225 ºC / DSC: $T_{g\ (vPVC\text{-}SCNPs)}$ = 75 ºC). Taken together, the above results confirm the successful metamorphosis of an out-of-use piece of clear flexible PVC hose to vPVC-SCNPs in “green” media involving only NBP, EtOH and H_2O.

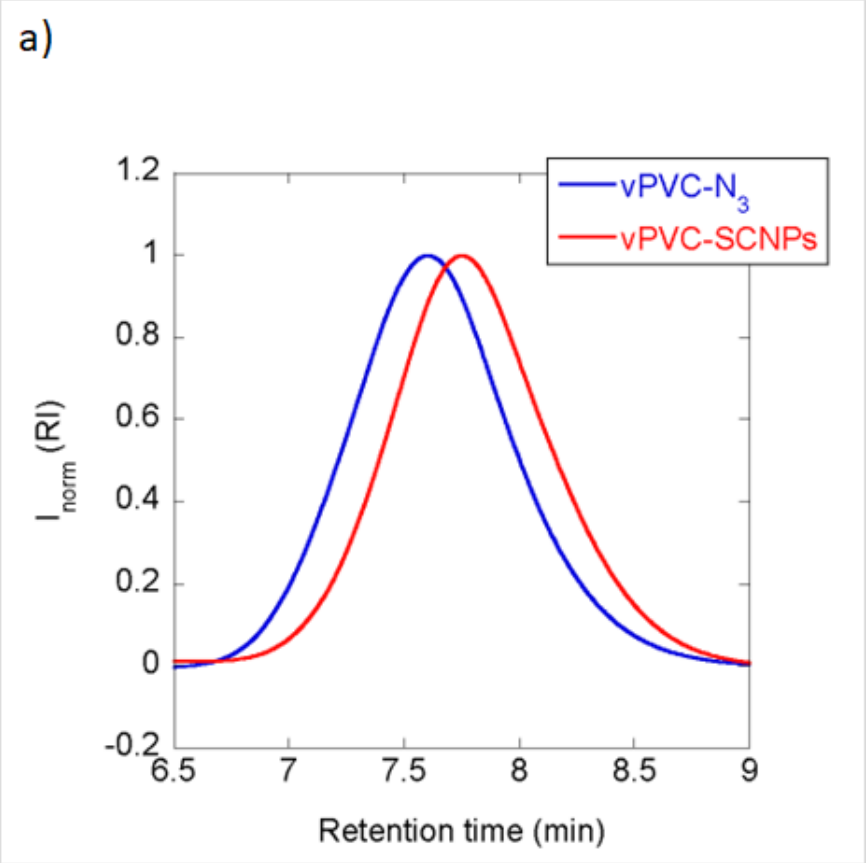

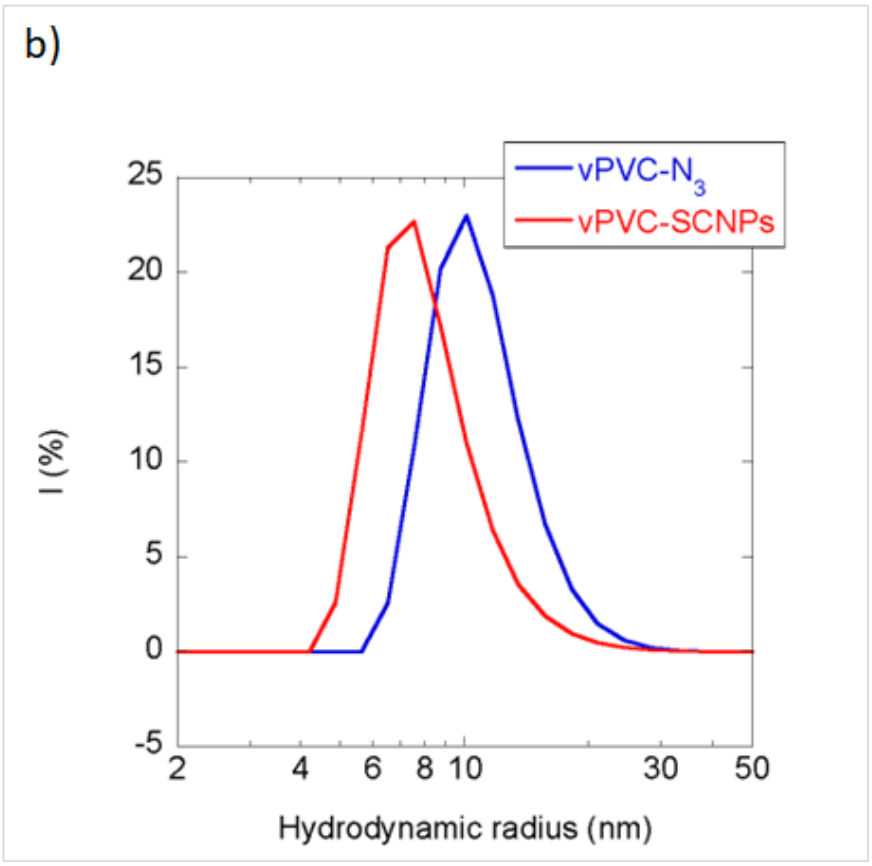

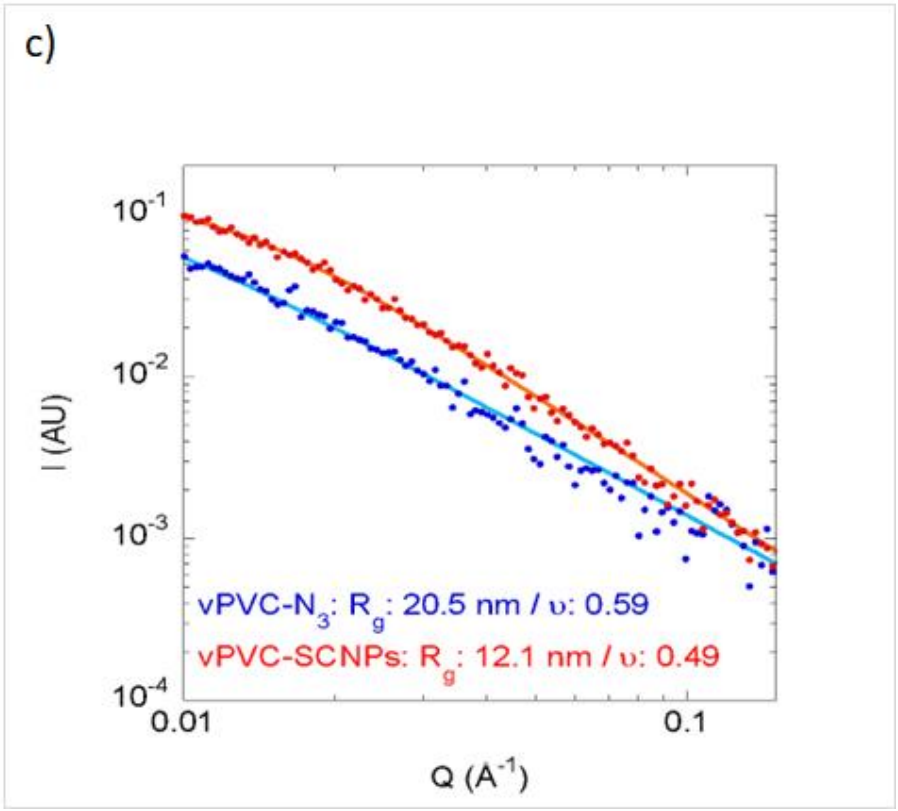

Figure 93. a) GPC chromatogram (RI detector), b) DLS size distribution in THF, c) SAXS result of vPVC-N_3 in blue and vPVC-SCNPs red. All results correspond to a correct collapse of the SCNPs.

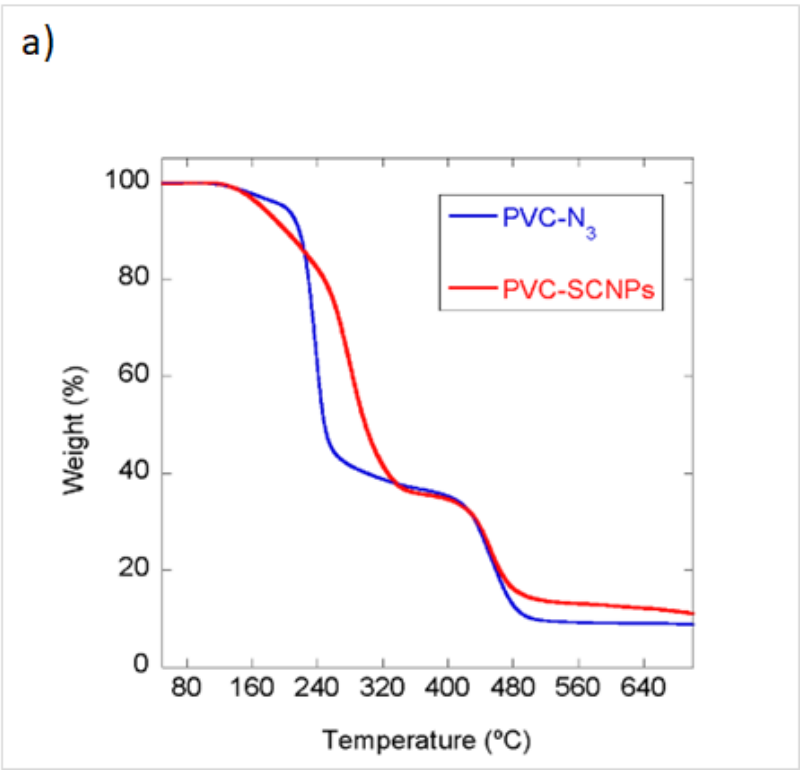

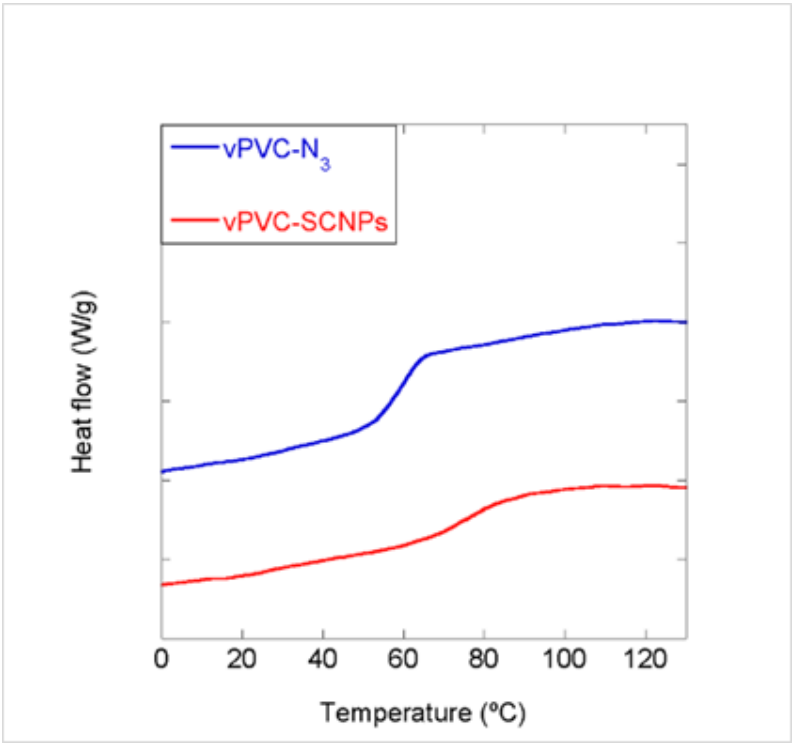

Figure 94. a) TGA and b) DSC traces of vPVC-N_3 in blue and vPVC-SCNPs red. The DSC traces have been downshifted in b) for clarity. The increase of Tg is related with the reduction of segmental mobility caused by the intra-chain cross-links.

6.4.7. Preparation of vPVC-Cu catalytic SCNP

ICP-MS characterization revealed a content of Cu ions of 7.3 mol% (1 µg of copper per mg of vPVC-SCNPs/Cu(II) catalyst).

6.4.8. Catalytic reactions

- **Alkyne homocoupling reactions**

The vPVC-SCNPs/Cu(II) catalyst combined with neat propargyl acetate (^{1}H NMR in the Figure 95) provided hexa-2,4- diyne-1,6-diyl diacetate (Figure 97 a), b), c) and d)) in very good yield (93%), similar to the model reaction with $CuCl_2$ as catalyst (86%) (Figure 96). Interestingly, vPVC-SCNPs/Cu(II) can be easily recycled two times without losing catalytic activity, but the yield is abruptly reduced in the 4th cycle (see Figure 98). Neither acidic nor thermal treatment was required, only filtration followed by drying in a vacuum oven overnight. The leeching experiment reaction has a yield of 45% at 3h and 49% at 6h (Figure 99 a) and b)), demonstrating that the copper is nor released from the vPVC-SCNPs during the reaction. A monitoring of the size of the vPVC-SCNPs/Cu(II), via DLS (Figure 100), showed that they begin to aggregate during the reactions to the point of becoming partially insoluble after 3 reactions, which is why it is interpreted that it is no longer an efficient catalyst.

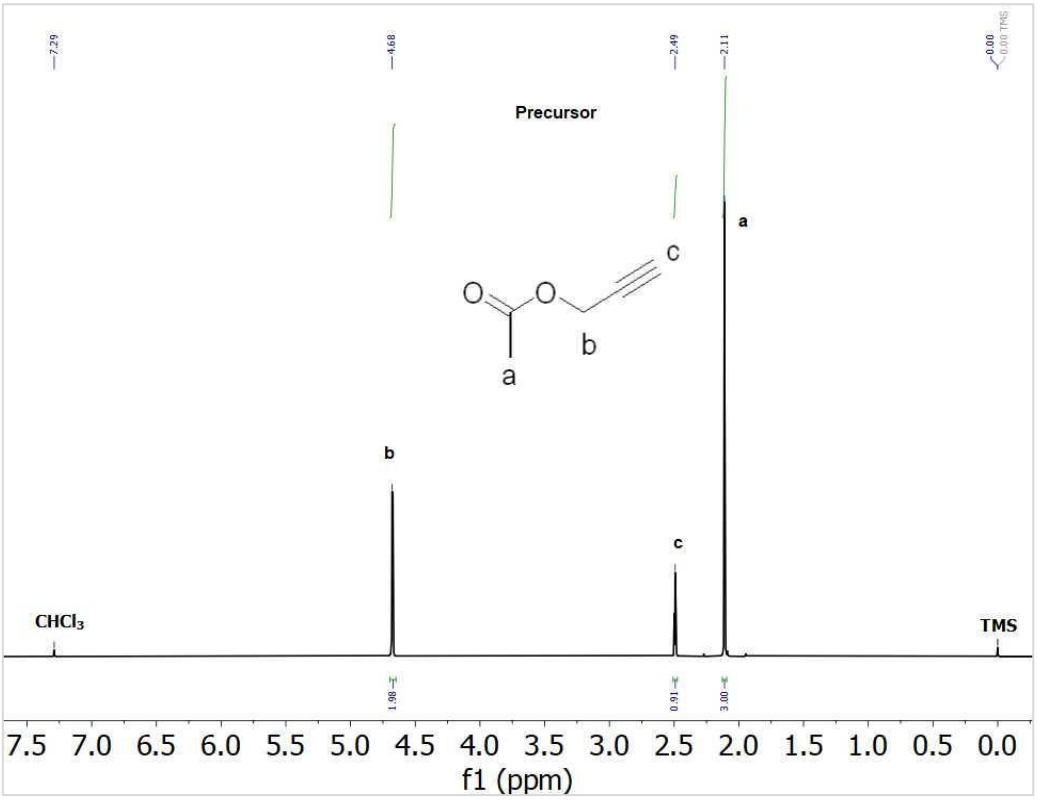

Figure 95. ^{1}H NMR spectra of propargyl acetate, the reagent of the reaction.

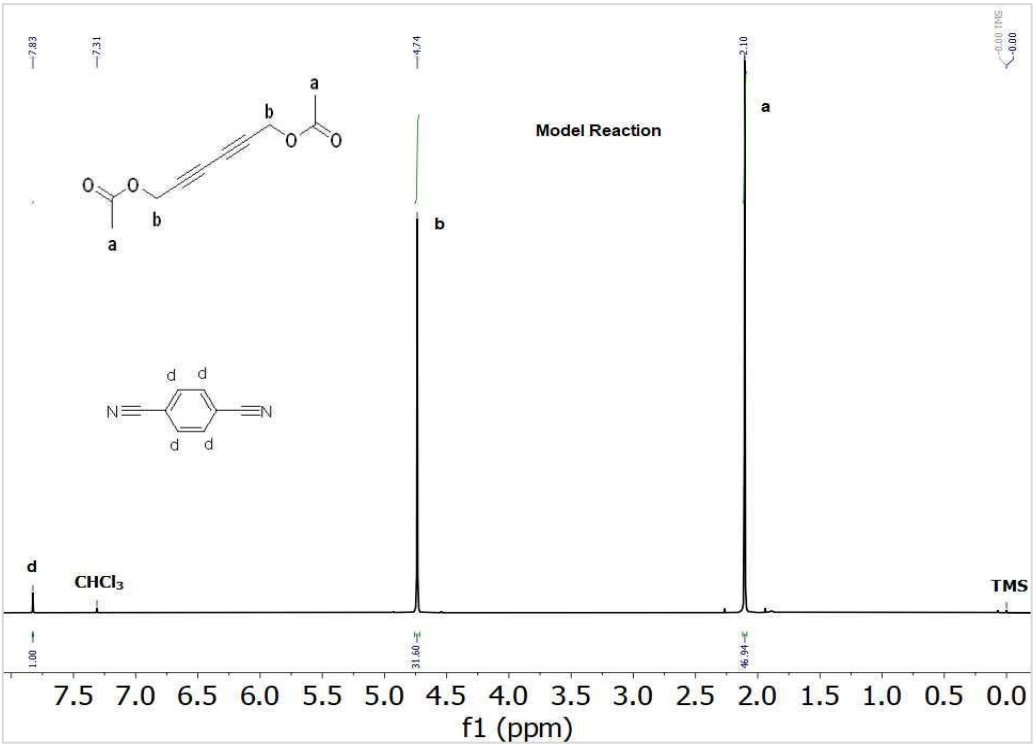

Figure 96. ^{1}H NMR spectra of the hexa-2,4-diyine-1-6diyl diacetate synthesized, as a model reaction, with $CuCl_2$.

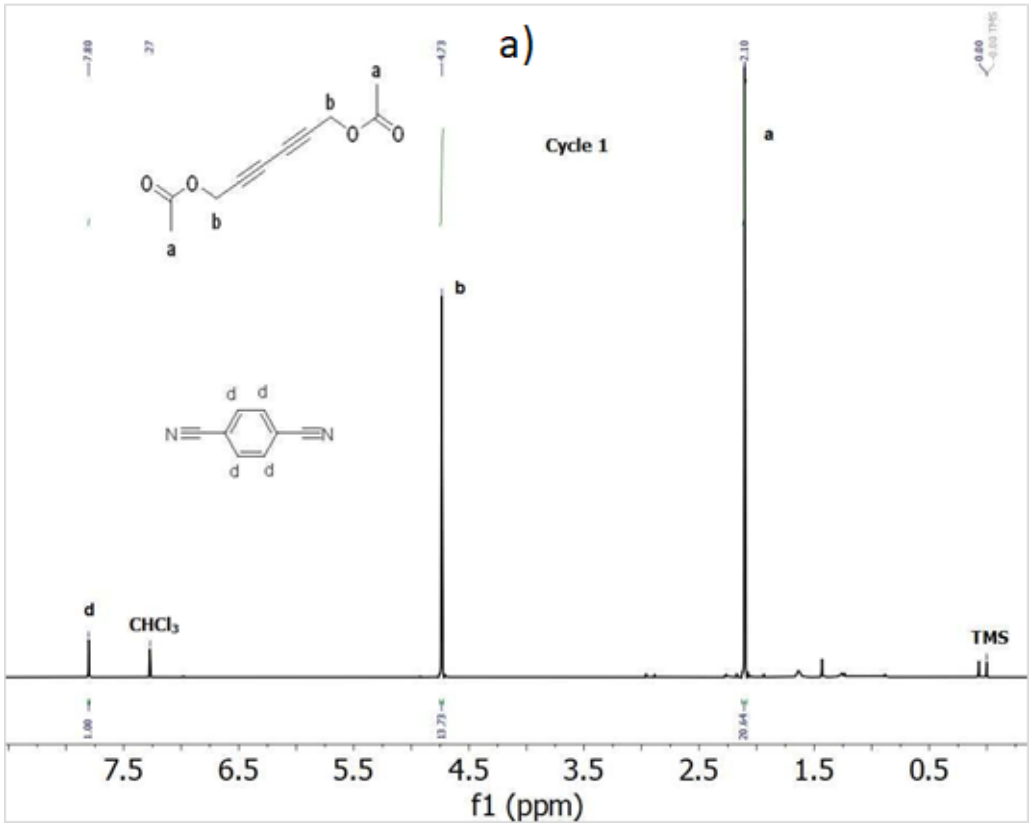

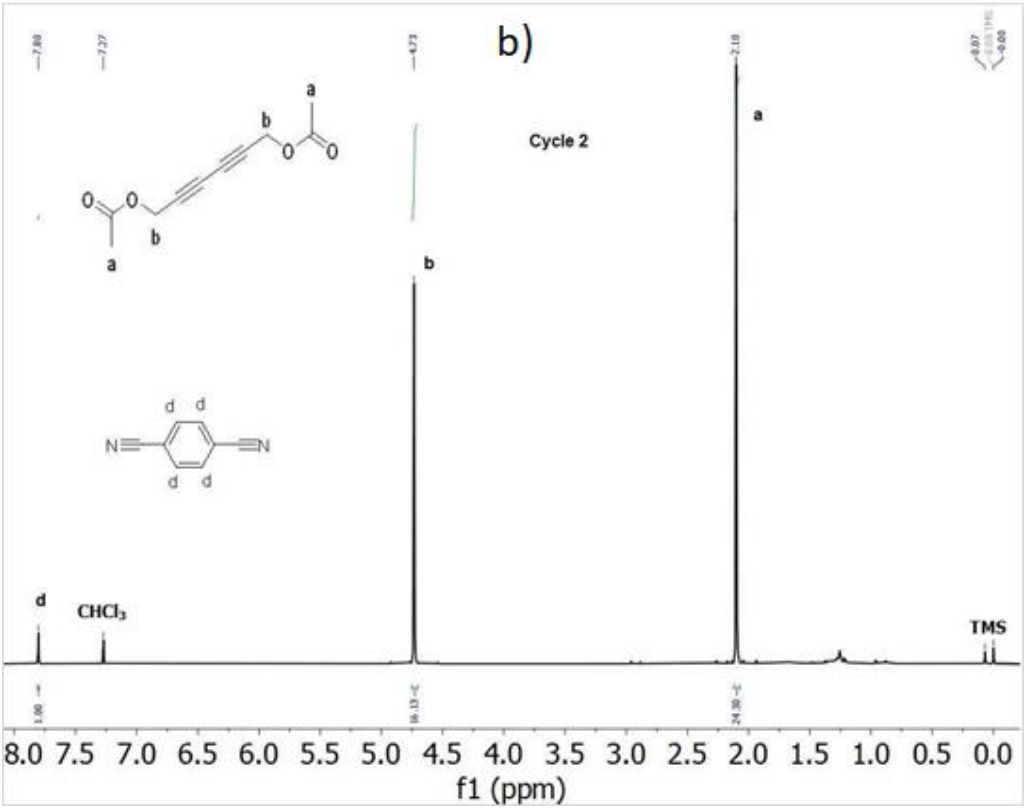
b)
Cycle 2
a
b
d
CHCl3
TMS
8.0 7.5 7.0 6.5 6.0 5.5 5.0 4.5 4.0 3.5 3.0 2.5 2.0 1.5 1.0 0.5 0.0
f1 (ppm)

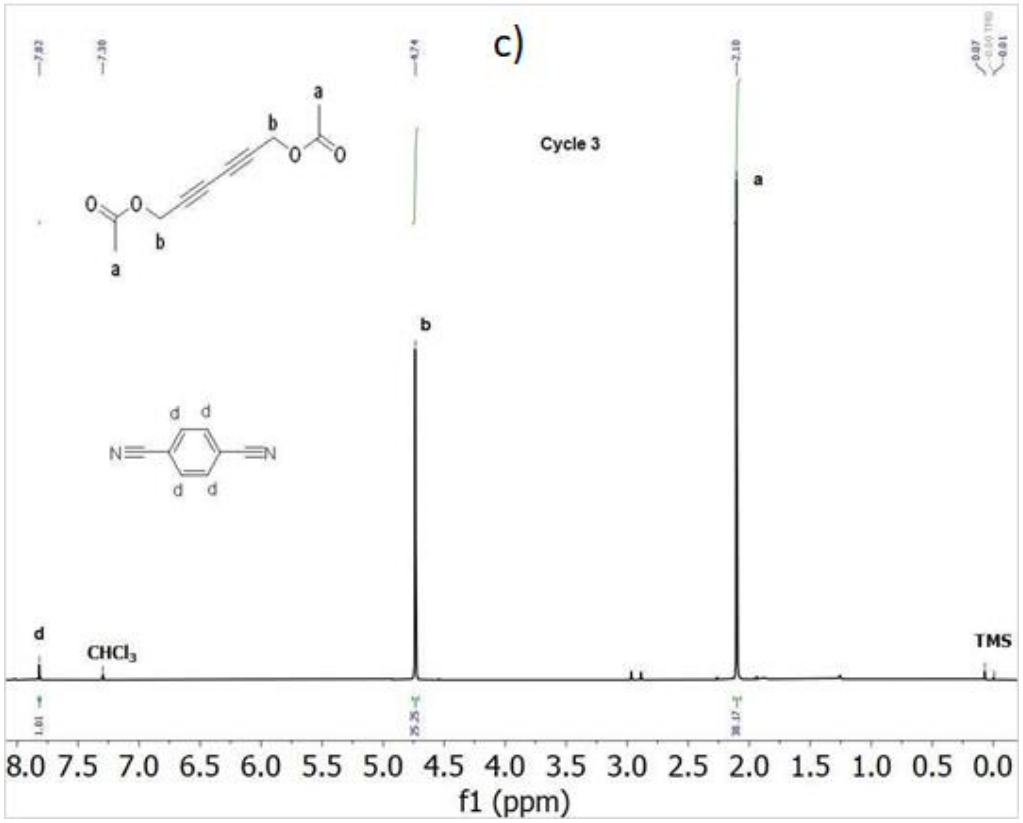
c)
Cycle 3
a
b
d
CHCl3
TMS
8.0 7.5 7.0 6.5 6.0 5.5 5.0 4.5 4.0 3.5 3.0 2.5 2.0 1.5 1.0 0.5 0.0
f1 (ppm)

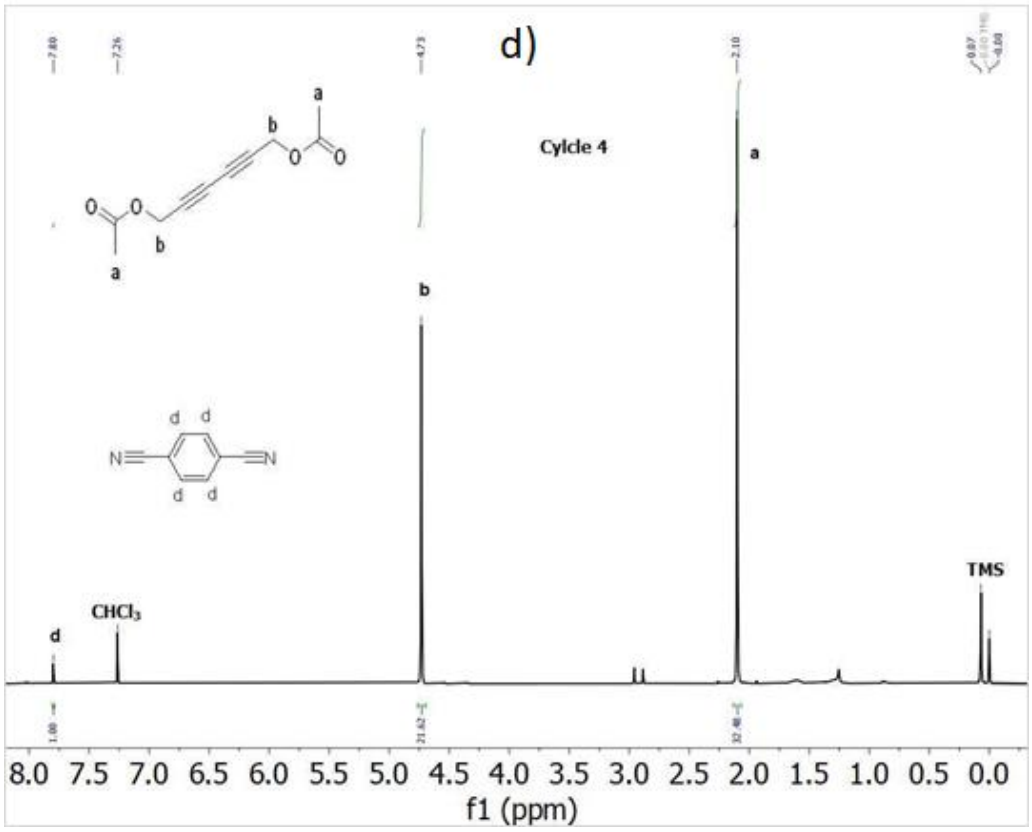

Figure 97. ^{1}H NMR spectra of the hexa-2,4-diyine-1-6diyl diacetate synthesized with vPVC-SCNPs/Cu(II) at a) first cycle, b) second cycle, c) third cycle and d) fourth cycle.

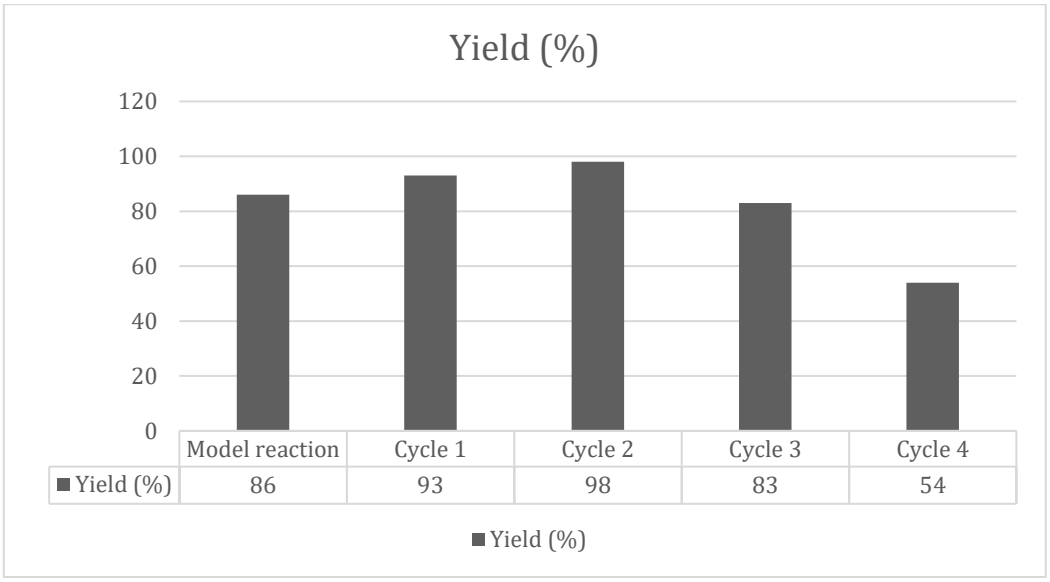

Figure 98. Graph of the yields of the hexa-2,4-diyine-1-6diyl diacetate synthesis reactions showing the comparison between model reaction and each cycle reaction with PVC-Cu SCNPs.

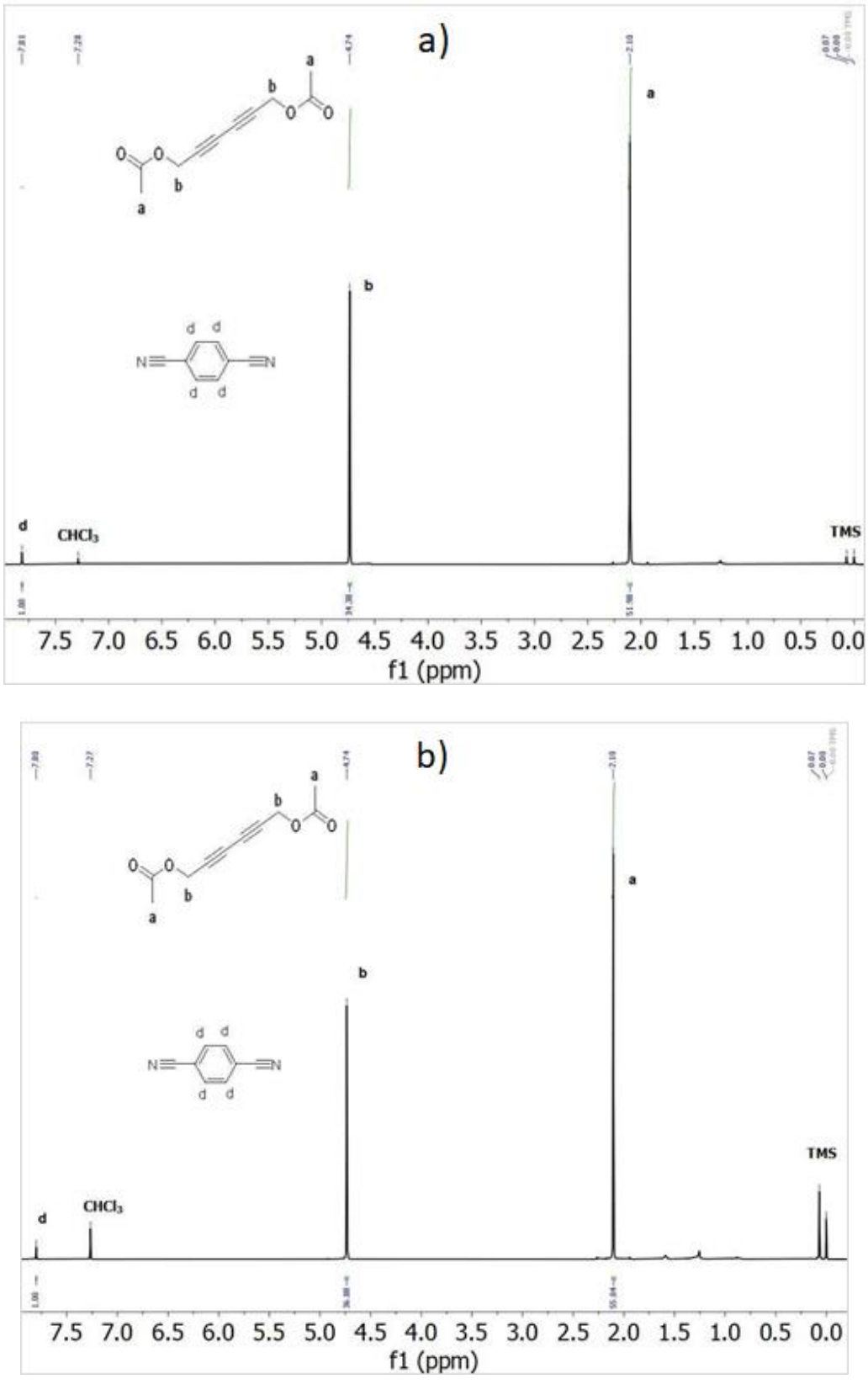

Figure 99. Leaching experiment. ^{1}H NMR spectra of the hexa-2,4-diyine-1-6diyl diacetate synthesized with vPVC-SCNPs/Cu(II) a) for 3 hours and b) for another additional 3 hours after remove the vPVC-SCNPs/Cu(II) catalyst .

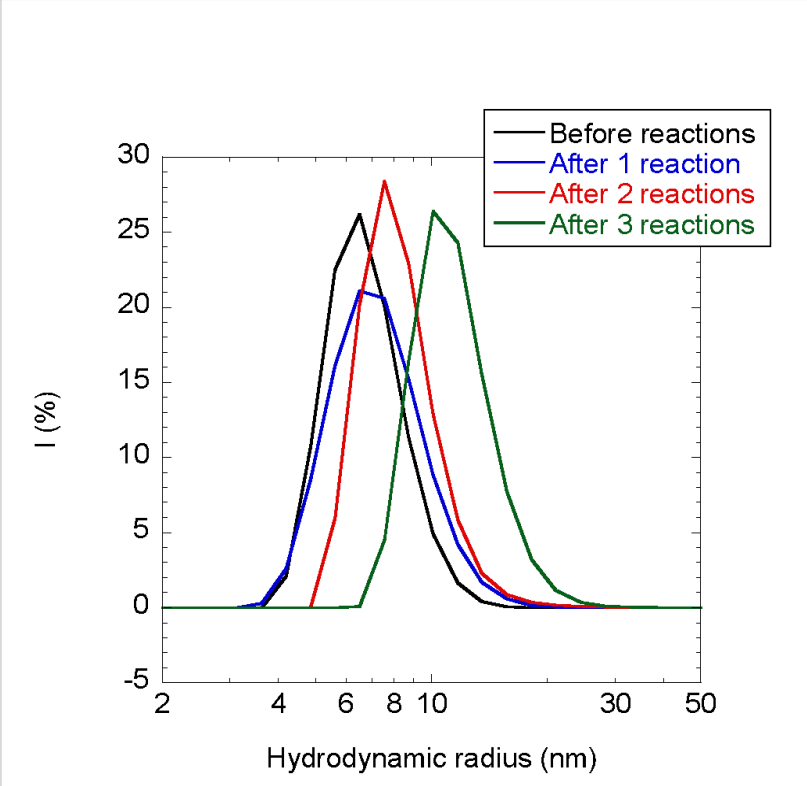

Figure 100. DLS size distribution in THF of vPVC-SCNPs/Cu(II) before the catalysis reactions (black) and after 1 (blue), 2 (red) and 3 (green) reactions. As "after 3 reactions" sample was partially insoluble, the showed signal is for the soluble part after a filtration.

Synthesis of 2,4-hexadiyne-1,6-diol dipropanoate from propagyl propionate and 1,4-bis(4-fluorophenyl)butadiyne from 1-ethynyl-4-fluorobenzene were carried out with good yields too (91% and 98% respectively) (Figure 101 c) and Figure 102 c)).

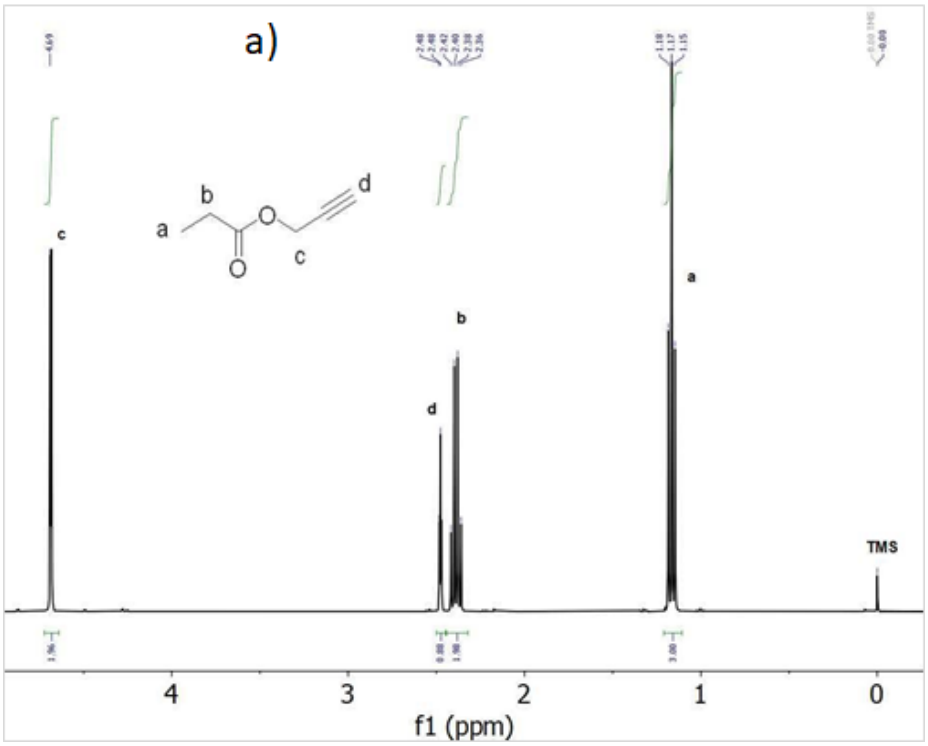

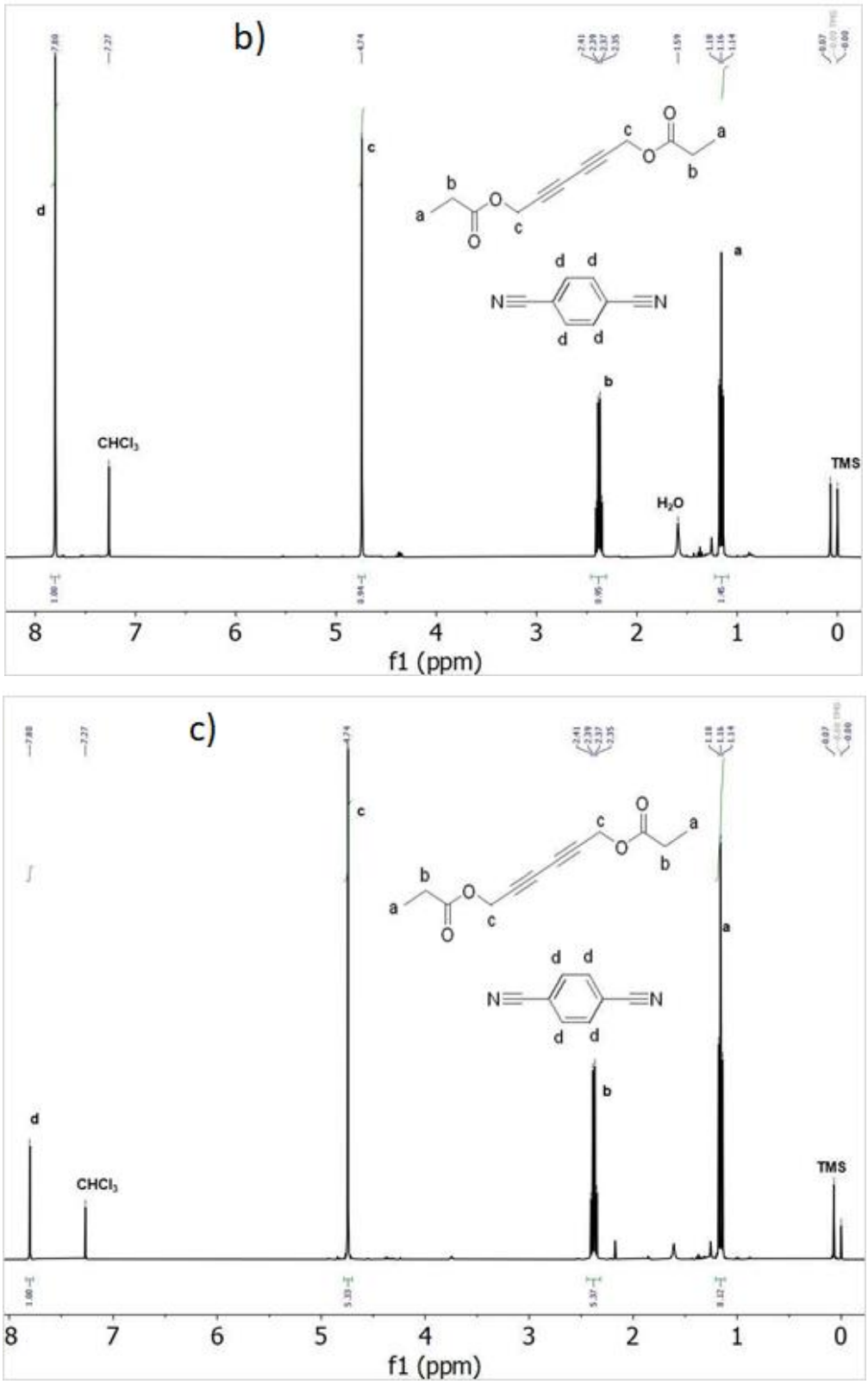

Figure 101. ^{1}H NMR spectra of a) propargyl propionate (the reagent), b) 2,4-hexadiyne-1,6-diol dipropanoate synthesized with $CuCl_2$ (the model reaction) and c) 2,4-hexadiyne-1,6-diol dipropanoate synthesized with vPVC-SCNPs/Cu(II).

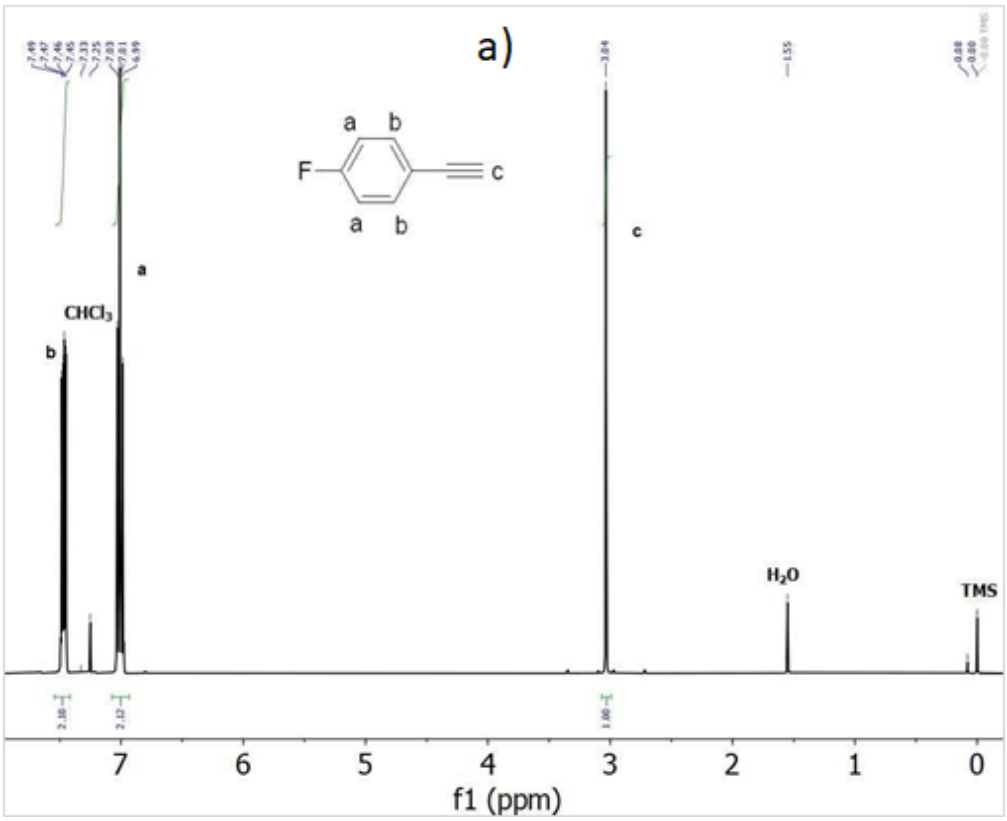
a)
a b
F
c
a b
a
c
CHCl3
b
H2O
TMS
7 6 5 4 3 2 1 0
f1 (ppm)

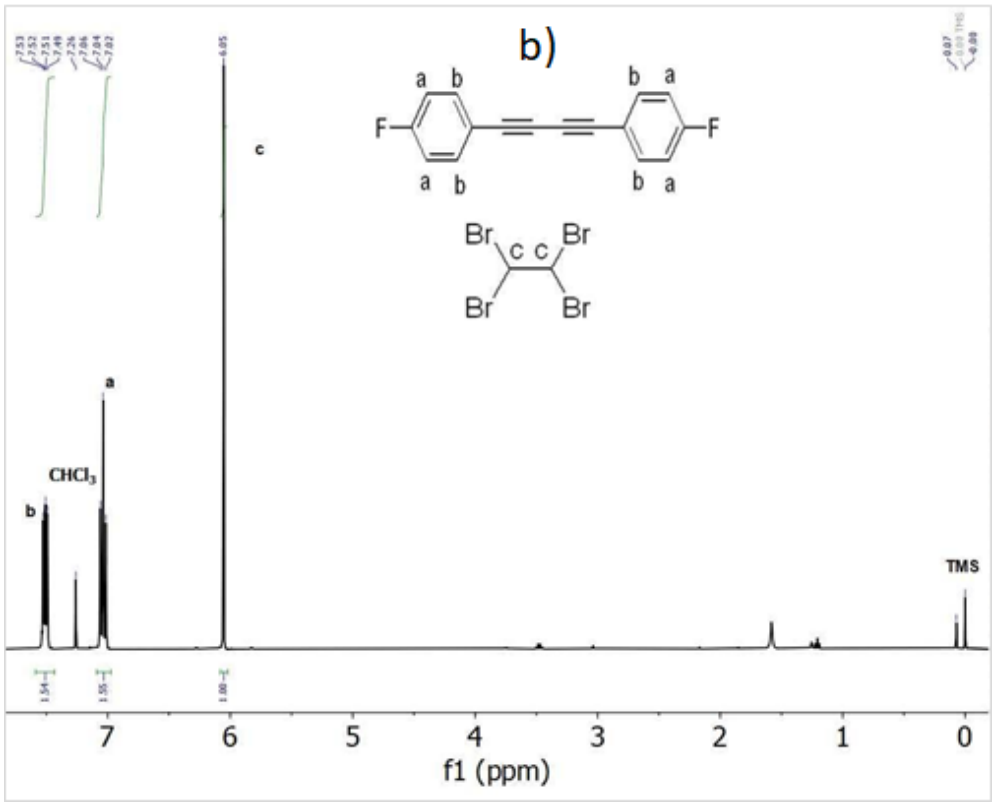
b)
a b
b a
F
F
a b
b a
Br
c c
Br
Br
Br
c
a
CHCl3
b
TMS
7 6 5 4 3 2 1 0
f1 (ppm)

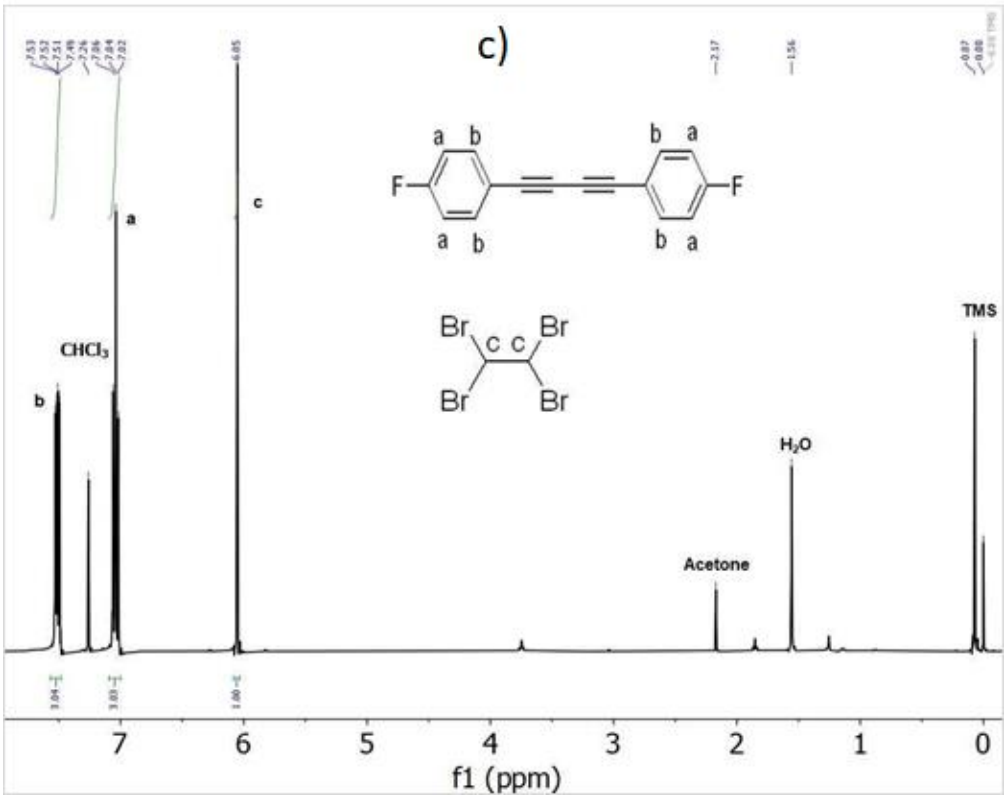

Figure 102. ^{1}H NMR spectra of a) 1-ethynyl-4-fluorobenzene (the reagent), b) 1,4-bis(4-fluorophenyl)butadiyne synthesized with $CuCl_2$ (the model reaction) and c) 2,4-hexadiyne-1,6-diol dipropanoate synthesized with vPVC-SCNPs/Cu(II).

- **Benzaldehyde synthesis from styrene**

Oxidation of the styrene was carried out, and a higher yield was obtained with the PVC-Cu that the model reaction with $CuCl_2$ (66% and 28% respectively) (Figure 103 b) and c)). vPVC-SCNPs/Cu(II) in acetonitrile provided benzaldehyde in higher yield that the homologous inorganic catalyst even at a higher concentration of Cu(II) in the latter case. The turnover frequency (moles of product per mole of catalyst per unit of time, TOF) of the vPVC-SCNPs/Cu(II) catalyst in this reaction was 4.9×10^4 h^{-1}, higher than that reported for Cu(II)-triazole complexes (TOF = 1.2×10^2 h^{-1}) [55].

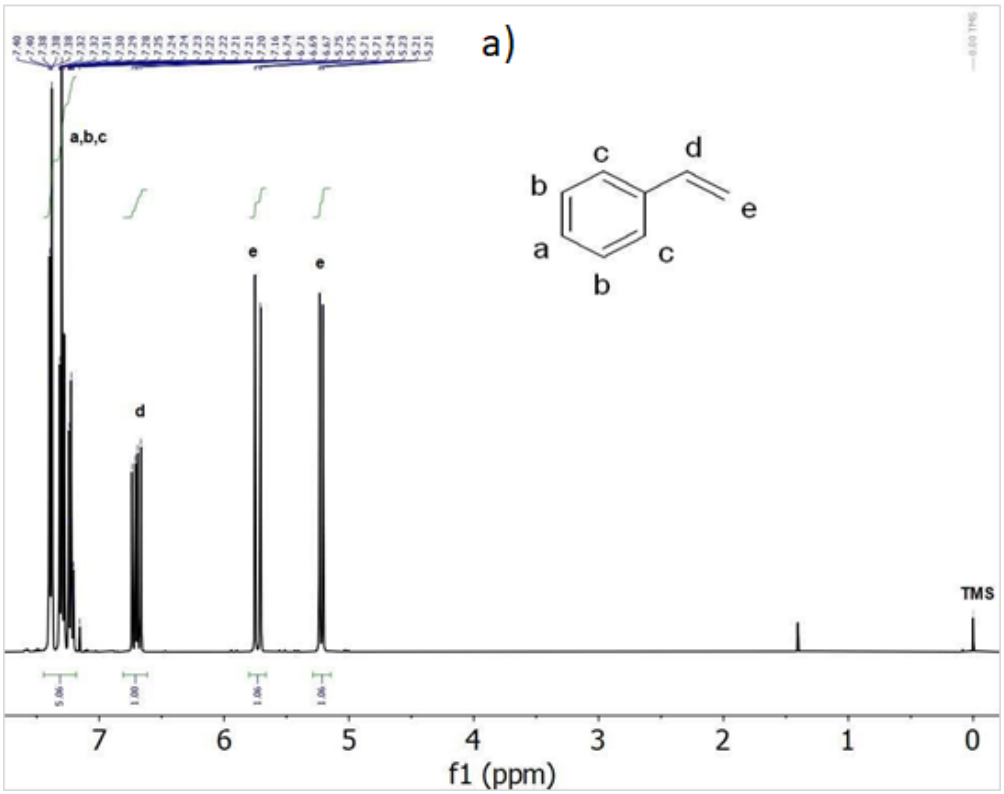
a)
a,b,c
d
e
e
TMS
c
d
b
e
a
c
b
7
6
5
4
3
2
1
0
f1 (ppm)

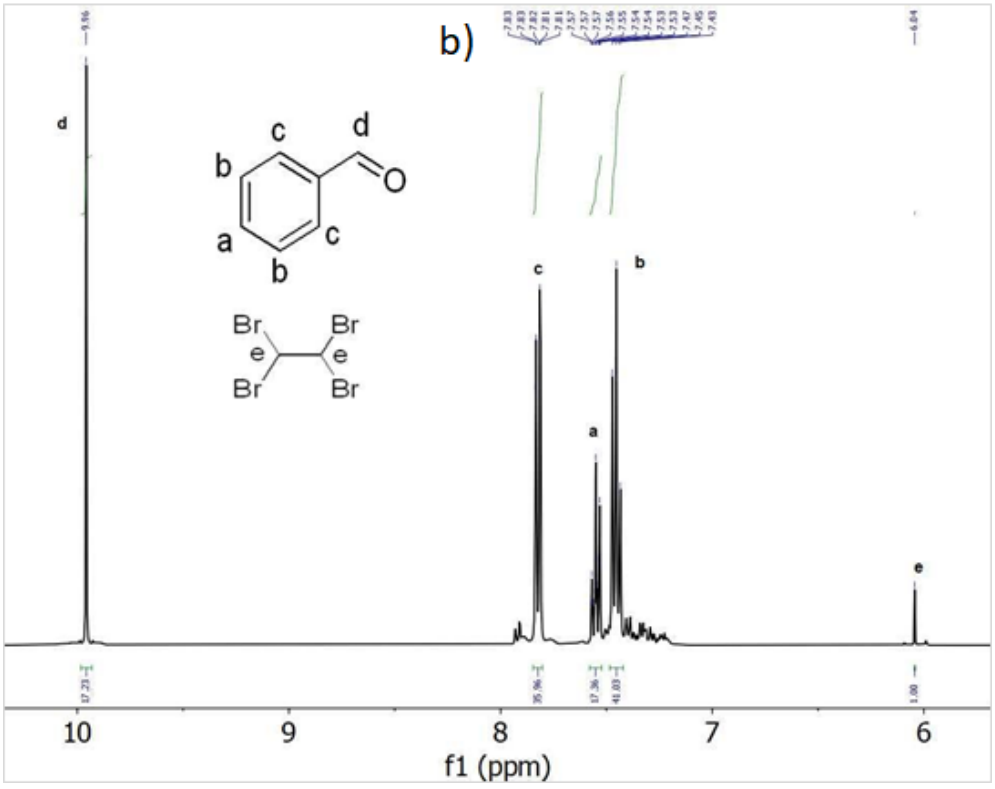
b)
d
c
d
b
O
a
c
b
Br
Br
e
e
Br
Br
c
b
a
e
10
9
8
7
6
f1 (ppm)

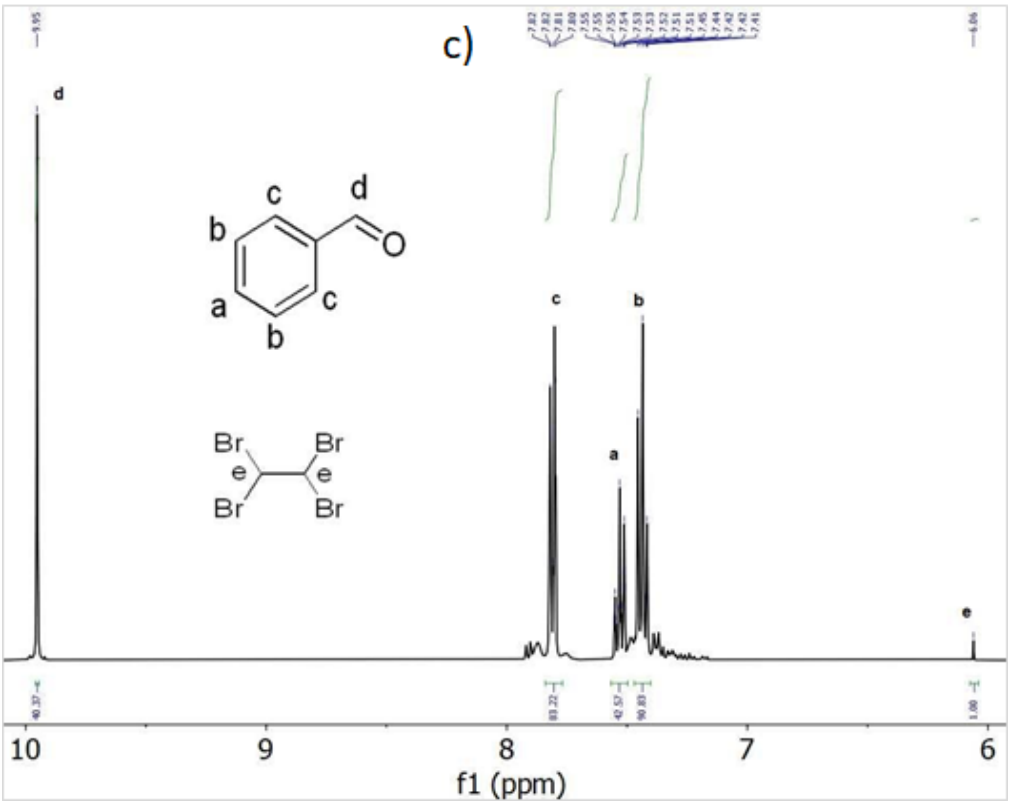

Figure 103. ^{1}H NMR spectra of a) styrene (the reactive), b) benzaldehyde synthesized with $CuCl_2$ (the model reaction) and c) benzaldehyde synthesized with vPVC-SCNPs/Cu(II).

- **3,5-Di-t-butyl-o-quinone synthesis**

3,5-Di-t-butyl-o-quinone synthesis was successfully carried out with vPVC-SCNPs/Cu(II) catalyst, as can see in the UV-Vis spectra (Figure 104 a), b) and c)) observing the increase of the absorbance at 400 nm caused by the increase of the concentration of the product. At constant concentration of the vPVC-SCNPs/Cu(II) catalyst, a kinetic saturation pattern was found at high substrate concentration resembling enzyme-like behavior [56]. Analysis of the data in Figure 105 (created with the kinetics study with different concentrations presented at Figure 106 from a) to h)) provided an apparent Michaelis–Menten constant ($K_{M,app}$) of 2.33 mM and an apparent catalytic constant ($k_{cat,app}$) of 1.98 x 10^2 h^{-1} (Table 5). Notably, the catalytic activity of vPVC-SCNPs/Cu(II) is similar to that reported for some model copper complexes of the catechol oxidase metalloenzyme [57], as well as to the catalytic activity of aldolase enzyme-mimetic SCNPs reported by Huerta *et al.* [58] ($K_{M,app}$ = 5.36 mM, $k_{cat,app}$ = 1.91 x 10^2 h^{-1}).

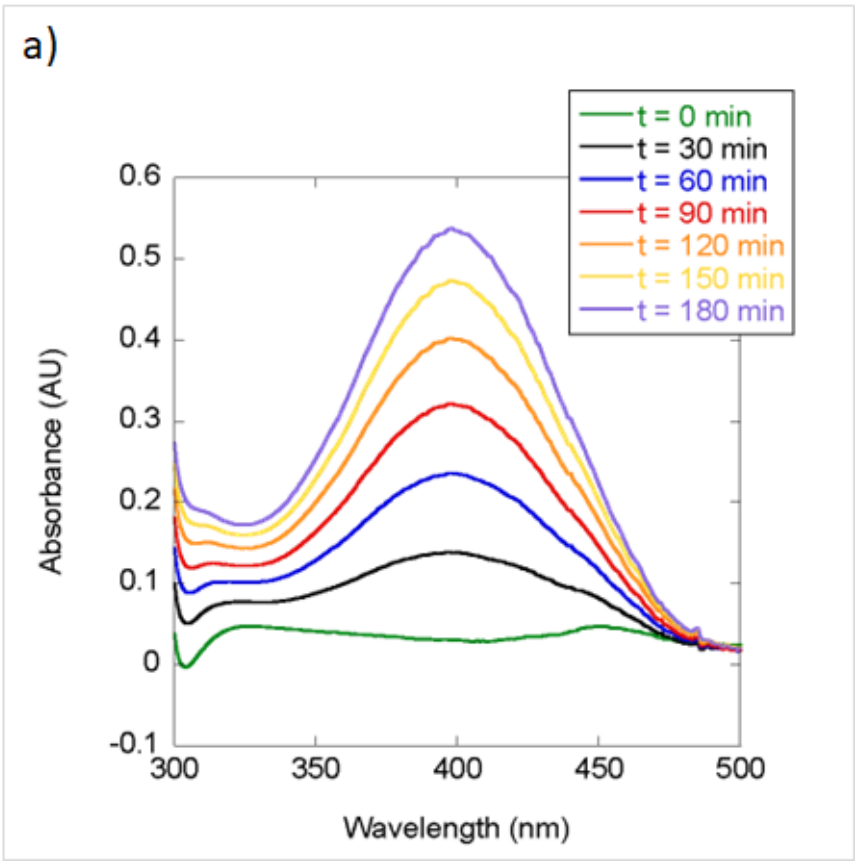
a)
t = 0 min
t = 30 min
t = 60 min
t = 90 min
t = 120 min
t = 150 min
t = 180 min
Absorbance (AU)
0.6
0.5
0.4
0.3
0.2
0.1
0
-0.1
300
350
400
450
500
Wavelength (nm)

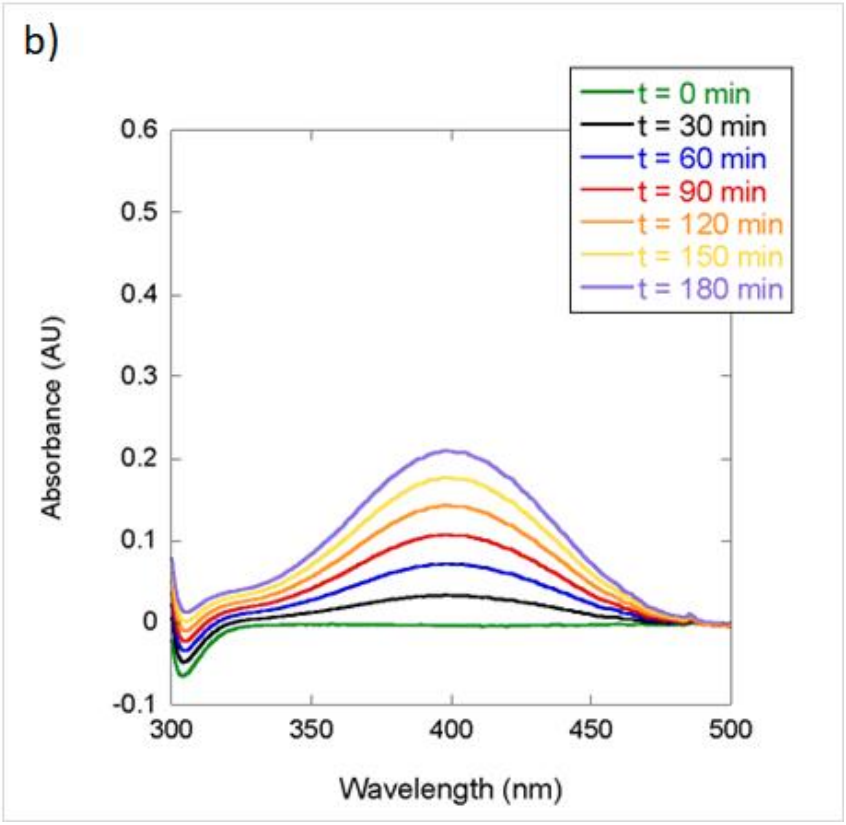
b)
t = 0 min
t = 30 min
t = 60 min
t = 90 min
t = 120 min
t = 150 min
t = 180 min
Absorbance (AU)
0.6
0.5
0.4
0.3
0.2
0.1
0
-0.1
300
350
400
450
500
Wavelength (nm)

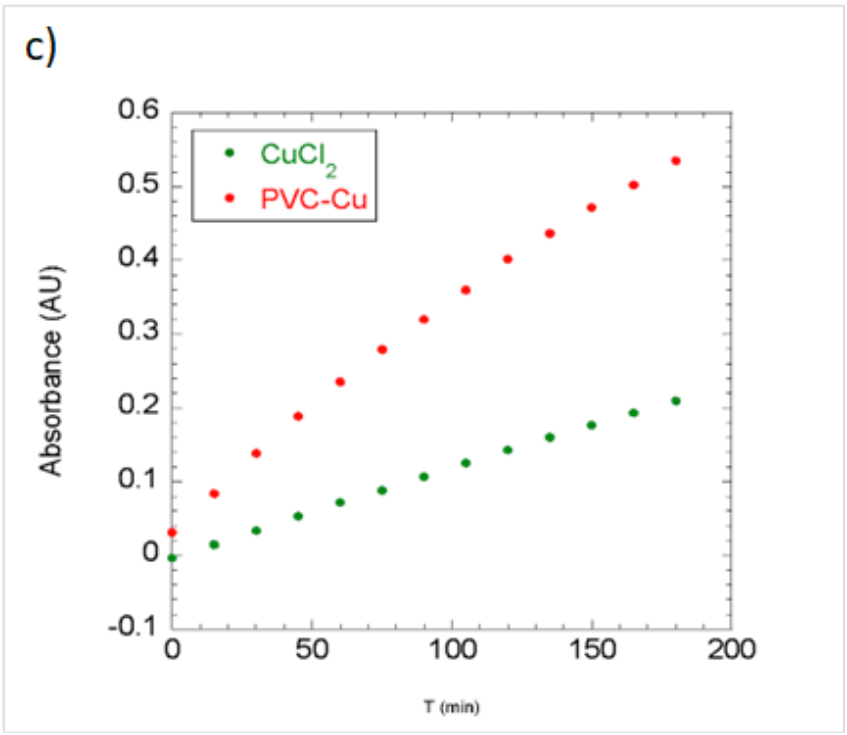

Figure 104. a) UV-Vis spectra and of the 3,5-di-butyl-o-quinone synthesis with vPVC-SCNPs/Cu(II) as catalyst (model reaction), a) UV-Vis spectra and of the 3,5-di-butyl-o-quinone synthesis with $CuCl_2$ as catalyst and c) comparison of the absorbance at 400 nm synthesis with $CuCl_2$ (green) and vPVC-SCNPs/Cu(II) (red) as catalyst.

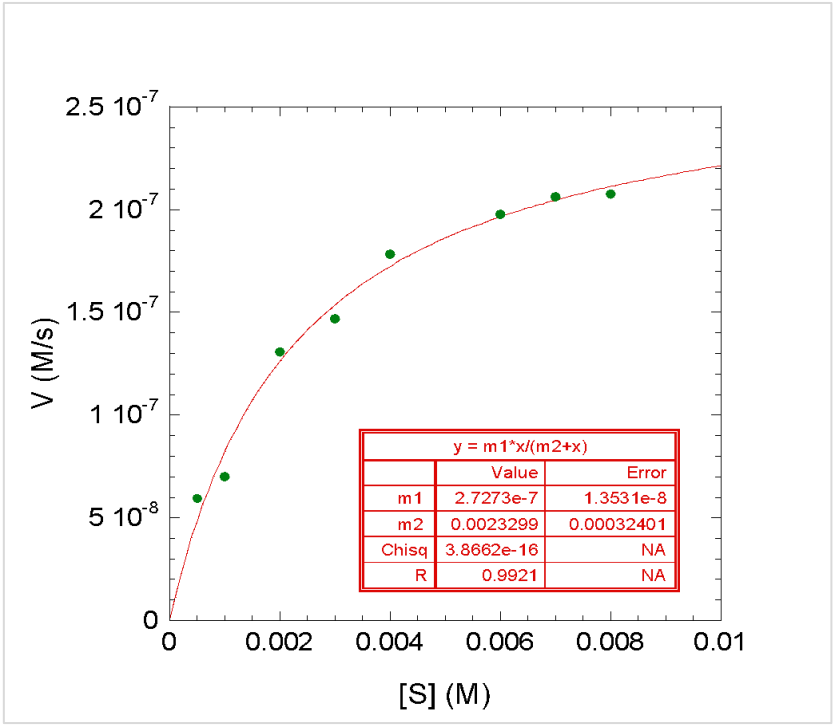

Figure 105. Michaelis-Menten study for a) model reaction, with $CuCl_2$ as catalyst, and b) reaction vPVC-SCNPs/Cu(II) as catalyst. Reaction where repeated with different precursor concentrations for the same catalyst concentration.

Table 4. Michaelis-Menten parameters for the 3,5-di-t-butyl-o-quinone synthesis with vPVC-SCNPs/Cu(II) as catalyst.

Reaction	V_{max} (M/min)	K_M (M)	k_{cat} (h^{-1})	K_{cat}/K_M ($M^{-1}h^{-1}$)
vPVC-SCNPs/Cu(II)	$16.4*10^{-6}$	$2.3*10^{-3}$	198.0	$85.0*10^{3}$

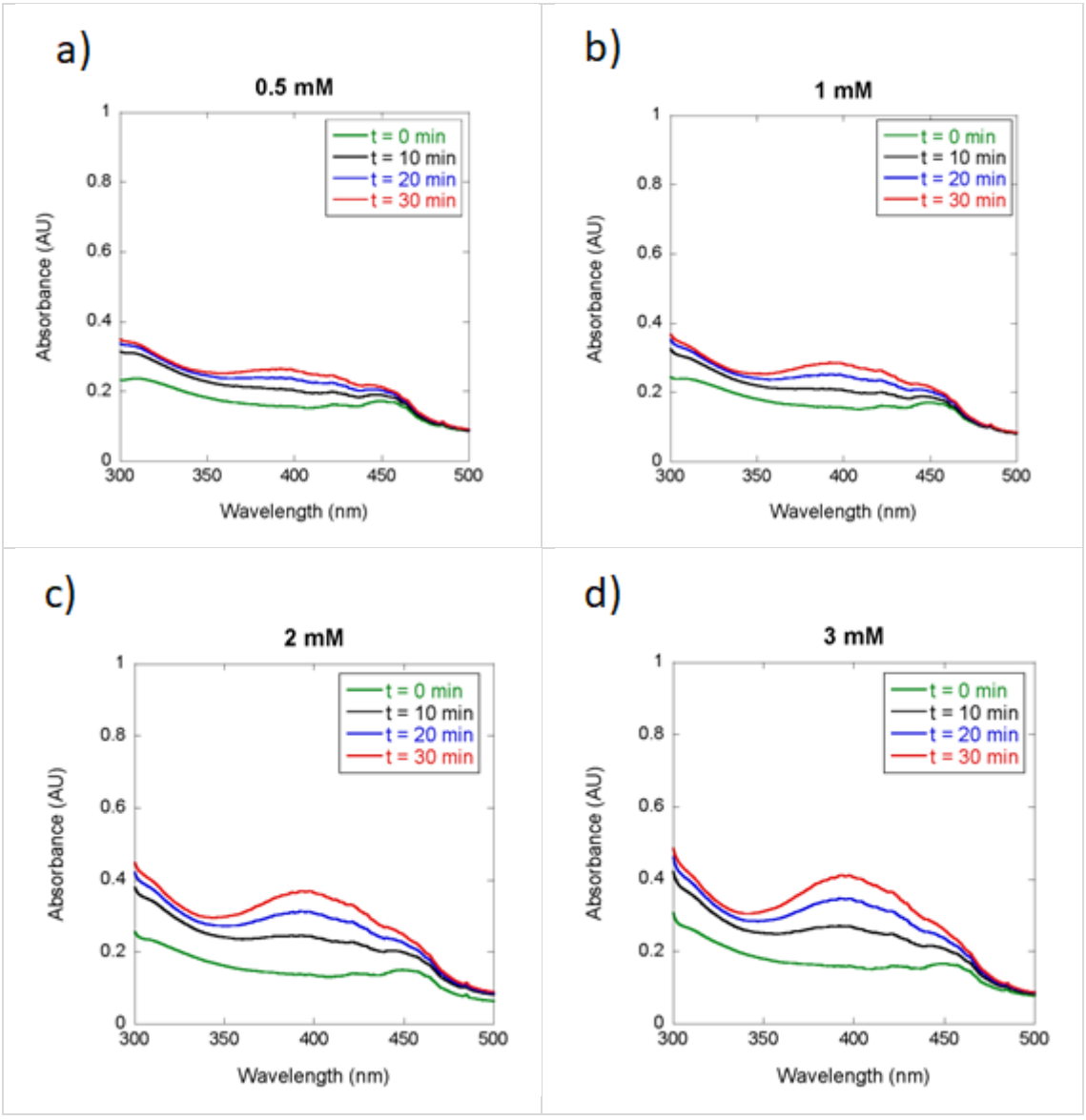

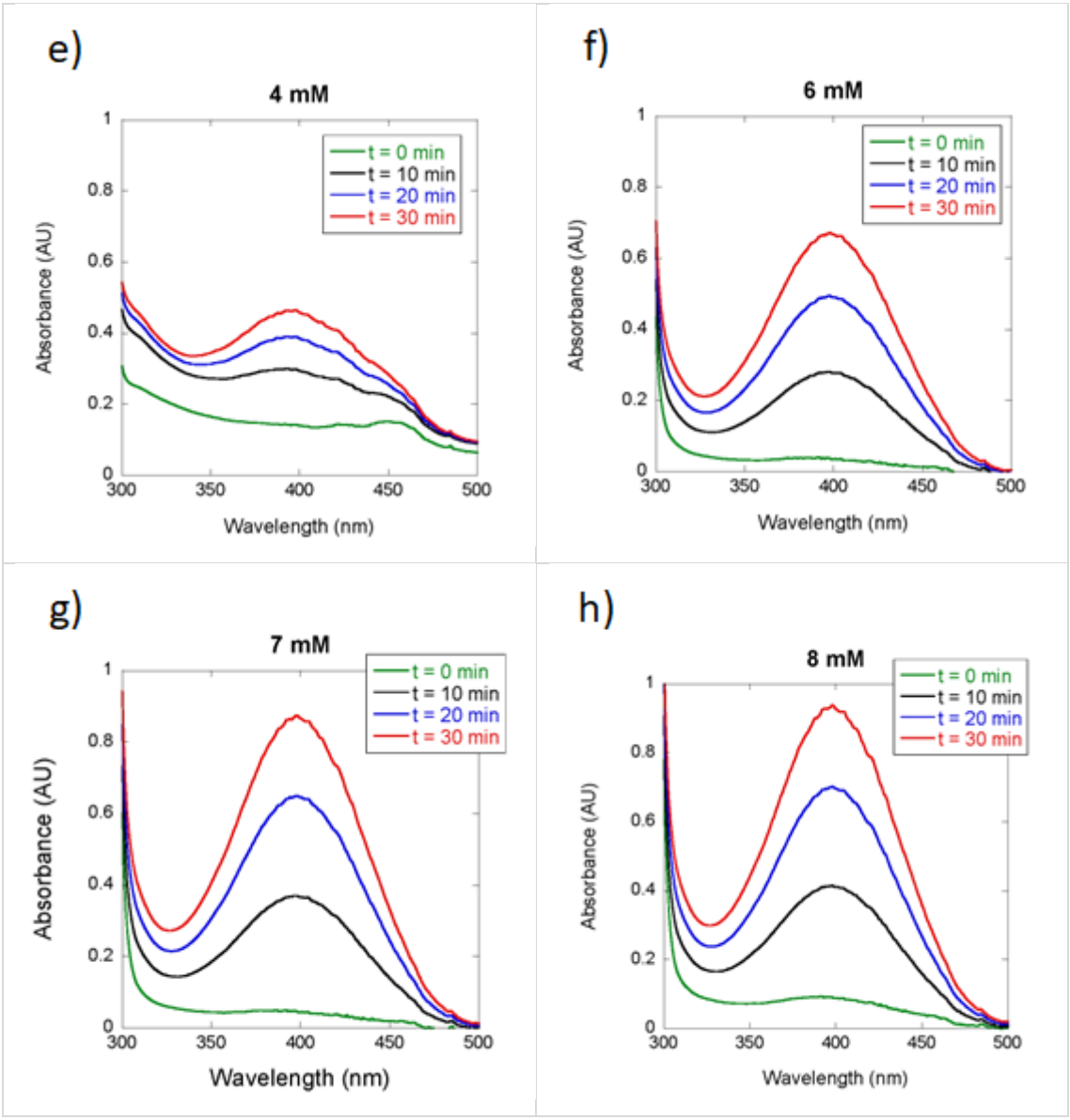

Figure 106. Kinetics experiments to asses for Michaelis–Menten behavior of vPVC-SCNPs/Cu(II) in the oxidation of DTBC to DTBQ with substrate concentrations ranging from 0.5 mM to 8 mM and identical concentration of vPVC-SCNPs/Cu(II) catalyst ([Cu(II)] = 4.8 µM).

6.5. Conclusion

In conclusion, we disclose an innovative concept of polymeric waste upcycling by metamorphosis of a commodity plastic of common use in dairy life like polyvinyl chloride (PVC) to "valorized" PVC single-chain nanoparticles (vPVC-SCNPs). The full valorization process (PVC isolation, PVC azidation, vPVC-SCNPs synthesis) can be run in a green, dipolar aprotic solvent like NBP and involving, when required, a simple mixture of EtOH and H_2O (1/1 vol.) as non-solvent. We show that the metamorphosis process when carried out via metal-free click chemistry by means of the Sondheimer diyne as intra-chain cross linker plus a specific end-capping procedure with benzyl azide leads to well-defined, uniform vPVC-SCNPs that are stable during storage in the solid state for months. We demonstrate that vPVC-SCNPs when loaded with 7.3 mol% of Cu(II) ions -to give vPVC-SCNPs/Cu(II)- become an efficient and recyclable catalyst in a benchmark transformation such as some alkyne homocoupling reactions, styrene oxidation and 3,5-Di-t-butyl-o-quinone synthesis. We envision the use of vPVC-SCNPs/Cu(II) as recyclable catalyst in other Cu(II)-catalyzed organic transformations like cyclopropanation, Chan-Lam coupling or the Henry reaction, among other ones. Notably, this new concept is amenable for the valorization of other commodity plastics in which it is feasible to install azide functional groups along their linear polymer chains.

References

[1] OECD. Global Plastics Outlook: Economic Drivers, Environmental Impacts and Policy Options, OECD Publishing, Paris **2022**. https://doi.org/10.1787/de747aef-en

[2] European Commission, Directorate-General for Environment, The use of PVC (poly vinyl chloride) in the context of a non-toxic environment: final report **2022**. https://data.europa.eu/doi/10.2779/375357

[3] J. Sherwood, Closed-Loop Recycling of Polymers Using Solvents : Remaking plastics for a circular economy, *Johnson Matthey Technology Review* **2020**, 64, 4-15.

[4] J. Nieminen, I. Anugwom, M. Kallioinen, M. Mänttäri, Green solvents in recovery of aluminium and plastic from waste pharmaceutical blister packaging, *Waste Management* **2020**, 107, 20-27.

[5] L. Lu, H. Zhong, T. Wang, J. Wu, F. Jin, T. Yoshioka, A new strategy for CO_2 utilization with waste plastics: conversion of hydrogen carbonate into formate using polyvinyl chloride in water, *Green Chemistry* **2020**, 22, 352-358.

[6] X. Jiao, K. Zheng, Q. Chen, X. Li, Y. Li, W. Shao, J. Xu, J. Zhu, Y. Pan, Y. Sun, Y. Xie, Photocatalytic Conversion of Waste Plastics into C_2 Fuels under Simulated Natural Environment Conditions *Angewandte Chemie International Edition* **2020**, 59, 15497-15501.

[7] W. A. Algozeeb, P. E. Savas, D. X. Luong, W. Chen, C. Kittrell, M. Bhat, R.Shahsavari, J. M. Tour, Flash Graphene from Plastic Waste, *ACS Nano* **2020**, 14, 15595-15604.

[8] J. Lu, S. Kumagai, Y. Fukushima, H. Ohno, S. Borjigin, T. Kameda, Y. Saito, T. Yoshioka, Sustainable Advance of Cl Recovery from Polyvinyl Chloride Waste Based on Experiment, Simulation, and Ex Ante Life-Cycle Assessment, *ACS Sustainable Chemistry & Engineering* **2021**, 9, 14112-14123.

[9] T. Kameda, H. Ohno, G. Grause, T. Mizoguchi, T. Yoshioka, Ball Mill-Assisted Dechlorination of Flexible and Rigid Poly(vinyl chloride) in NaOH/EG Solution, *Industrial & Engineering Chemistry Research* **2008**, 47, 8619-8624.

[10] T. Kameda, S. Fukushima, C. Shoji, G. Grause, T. Yoshioka, Electrodialysis for NaCl/EG solution using ion-exchange membranes, *Journal of Material Cycles and Waste Management* **2013**, 15, 111-114.

[11] H. Zhou, Y. Wang, Y. Ren, Z. Li, X. Kong, M. Shao, H. Duan, Plastic Waste Valorization by Leveraging Multidisciplinary Catalytic Technologies, *ACS Catalysis* **2022**, 12, 9307-9324.

[12] J. A. Pomposo, Single-Chain Polymer Nanoparticles: Synthesis, Characterization, Simulations, and Applications, *Wiley-VCH, Weinheim* **2017**.

[13] H. Frisch, B. T. Tuten, C. Barner-Kowollik, Macromolecular Superstructures: A Future Beyond Single Chain Nanoparticles, *Israel Journal of Chemistry* **2020**, 60, 86-99.

[14] J. Chen, E. S. Garcia, S. C. Zimmerman, Intramolecularly Cross-Linked Polymers: From Structure to Function with Applications as Artificial Antibodies and Artificial Enzymes, *Accounts of Chemical Research* **2020**, 53, 1244-1256.

[15] R. Chen, E. B. Berda, 100th Anniversary of Macromolecular Science Viewpoint: Re-examining Single-Chain Nanoparticles, *ACS Macro Letters* **2020**, 9, 1836- 1843.

[16] E. Verde-Sesto, A. Arbe, A. Moreno, D. Cangialosi, A. Alegría, J. Colmenero, J. A. Pomposo, Single-chain nanoparticles: opportunities provided by internal and external confinement, *Materials Horizons* **2020**, 7, 2292-2313.

[17] G. M. ter Huurne, A. R. A. Palmans, E. W. Meijer, Supramolecular Single-Chain Polymeric Nanoparticles, *CCS Chemistry* **2019**, 1, 64- 82.

[18] S. Mavila, O. Eivgi, I. Berkovich, N. G. Lemcoff, Intramolecular Cross-Linking Methodologies for the Synthesis of Polymer Nanoparticles, *Chemical Reviews* **2016**, 116, 878-961.

[19] C. K. Lyon, A. Prasher, A. M. Hanlon, B. T. Tuten, C. A. Tooley, P. G. Frank, E. B. Berda, A brief user's guide to single-chain nanoparticles, *Polymer Chemistry* **2015**, 6, 181-197.

[20] M. Gonzalez-Burgos, A. Latorre-Sanchez, J. A. Pomposo, Advances in single chain technology, *Chemical Society Reviews* **2015**, 44, 6122-6142.

[21] J. F. Hoffmann, A. H. Roos, F.-J. Schmitt, D. Hinderberger, W. H. Binder, Fluorescent and Water Dispersible Single-Chain Nanoparticles: Core–Shell Structured Compartmentatio, *Angewandte Chemie International Edition* **2021**, 60, 7820-7827.

[22] C. Stuckhardt, M. Wissing, A. Studer, Photo Click Reaction of Acylsilanes with Indoles, *Angewandte Chemie International Edition* **2021**, 60, 18605-18611.

[23] M. A. M. Alqarni, C. Waldron, G. Yilmaz, C. R. Becer, Synthetic Routes to Single Chain Polymer Nanoparticles (SCNPs): Current Status and Perspectives, *Macromolecule rapid communication* **2021**, 42, 2100035.

[24] M. H. Barbee, Z. M. Wright, B. P. Allen, H. F. Taylor, E. F. Patteson, A. S. Knight, Protein-Mimetic Self-Assembly with Synthetic Macromolecules, *Macromolecules* **2021**, 54, 3585-3612.

[25] E. S. Garcia, T. M. Xiong, A. Lifschitz, S. C. Zimmerman, Tandem catalysis using an enzyme and a polymeric ruthenium-based artificial metalloenzyme, *Polymer Chemistry* **2021**, 12, 675-6760.

[26] S. Liao, L. Wei, L. A. Abriata, F. Stellacci, Control and Characterization of the Compactness of Single-Chain Nanoparticles, *Macromolecules* **2021**, 54, 11459-11467.

[27] J. J. Piane, L. E. Chamberlain, S. Huss, L. T. Alameda, A. C. Hoover, E. Elacqua, Organic Photoredox-Catalyzed Cycloadditions Under Single-Chain Polymer Confinement, *ACS Catalysis* **2020**, 10, 13251-13256.

[28] F. Eisenreich, E. W. Meijer, A. R. A. Palmans, Amphiphilic Polymeric Nanoparticles for Photoredox Catalysis in Water, *Chemistry – A European Journal* **2020**, 26, 10355-10361.

[29] N. M. Hamelmann, J.-W. D. Paats, J. M. J. Paulusse, Single-Chain Polymer Nanoparticles in Controlled Drug Delivery *ACS Macro Letters* **2021**, 10, 1443-1449.

[30] C.-C. Cheng, S.-Y. Huang, W.-L. Fan, A.-W. Lee, C.-W. Chiu, D.-J. Lee, J.-Y. Lai, Water-Soluble Single-Chain Polymeric Nanoparticles for Highly Selective Cancer Chemotherapy, *ACS Applied Polymer Materials* **2021**, 3, 474−484.

[31] X. Tian, R. Xue, F. Yang, L. Yin, S. Luan, H. Tang, Single-Chain Nanoparticle-Based Coatings with Improved Bactericidal Activity and Antifouling Properties, *Biomacromolecules* **2021**, 22, 4306-4315.

[32] R. Zeng, L. Chen, Q. Yan, CO_2-Folded Single-Chain Nanoparticles as Recyclable, Improved Carboxylase Mimics, *Angewandte Chemie International Edition* **2020**, 59, 18418-18422.

[33] W. Wang, J. Wang, S. Li, C. Li, R. Tan, D. Yin, Iron(II)-folded single-chain nanoparticles: a metalloenzyme mimicking sustainable catalyst for highly enantioselective sulfa-Michael addition in water, *Green Chemistry* **2020**, 22, 4645-4655.

[34] M. Collot, J. Schild, K. T. Fam, R. Bouchaala, A. S. Klymchenko, Stealth and Bright Monomolecular Fluorescent Organic Nanoparticles Based on Folded Amphiphilic Polymer, *ACS Nano* **2020**, 14, 13924-13937.

[35] J. De-La-Cuesta, E. Verde-Sesto, A. Arbe, J. A. Pomposo, Self-Reporting of Folding and Aggregation by Orthogonal Hantzsch Luminophores Within a Single Polymer Chain, *Angewandte Chemie International Edition* **2021**, 60, 3534-3539.

[36] H. N. C. Wong, P. J. Garratt, F. Sondheimer, Unsaturated eight-membered ring compounds. XI. Synthesis of sym-dibenzo-1,5-cyclooctadiene-3,7-diyne and sym-dibenzo-1,3,5-cyclooctatrien-7-yne, presumably planar conjugated eight-membered ring compounds, *Journal of the American Chemical Society* **1974**, 96, 5604-5605.

[37] S. Marian, G. Levin, Modification of polyvinylchloride in solution or suspension by nucleophilic substitution, *Journal of Applied Polymer Science* **1981**, 26, 3295-3304.

[38] M. Takeishi, M. Okawara, Synthesis and reaction of poly(vinyl chloride) containing azide groups, *Journal of Polymer Science Part B: Polymer Letters* **1969**, 7, 201-203.

[39] A. Earla, R. Braslau, Covalently Linked Plasticizers: Triazole Analogues of Phthalate Plasticizers Prepared by Mild Copper-Free "Click" Reactions with Azide-Functionalized PVC, *Macromolecule rapid communication* **2014**, 35, 666-671.

[40] I. Kii, A. Shiraishi, T. Hiramatsu, T. Matsushita, H. Uekusa, S. Yoshida, M. Yamamoto, A. Kudo, M. Hagiwara, T. Hosoya, Strain-promoted double-click reaction for chemical modification of azido-biomolecules, *Organic & Biomolecular Chemistry* **2010**, 8, 4051-4055.

[41] S. Yoshida, A. Shiraishi, K. Kanno, T. Matsushita, K. Johmoto, H. Uekusa, T. Hosoya, Enhanced clickability of doubly sterically-hindered aryl azides, *Scientific Reports* **2011**, 1, 82.

[42] P. Sun, J. Chen, J. Liu, K. Zhang, Self-Accelerating Click Reaction for Cyclic Polymer, *Macromolecules* **2017**, 50, 1463−1472.

[43] E. Harth, B. V. Horn, V. Y. Lee, D. S. Germack, C. P. Gonzales, R. D. Miller, C. J. Hawker, A Facile Approach to Architecturally Defined Nanoparticles via Intramolecular Chain Collapse, *Journal of the American Chemical Society* **2002**, 124, 8653-8660.

[44] A. Jordan, C. G. J. Hall, L. R; Thorp, H. F. Sneddon, Replacement of Less-Preferred Dipolar Aprotic and Ethereal Solvents in Synthetic Organic Chemistry with More Sustainable Alternatives, *Chemical Reviews* **2022**, 122, 6749-6794.

[45] J. Sherwood, H. L. Parker, K. Moonen, T. J. Farmera, A. J. Hunt, N-Butylpyrrolidinone as a dipolar aprotic solvent for organic synthesis, *Green Chemistry* **2016**, 18, 3990-3996.

[46] A. Kumar, M. Alhassan, J. Lopez, F. Albericio, B. G. de la Torre, N-Butylpyrrolidinone for Solid-Phase Peptide Synthesis is Environmentally Friendlier and Synthetically Better than DMF, *ChemSusChem* **2020**, 13, 5288-5294.

[47] S. Thanneeru, J. K. Nganga, A. S. Amin, B. Liu, L. Jin, A. M. Angeles-Boza, J. He, "Enzymatic" Photoreduction of Carbon Dioxide using Polymeric Metallofoldamers Containing Nickel–Thiolate Cofactors, *ChemCatChem* **2017**, 9, 1157-1162.

[48] H. Rothfuss, N. D. Knöfel, P. W. Roesky, C. Barner-Kowollik, Single-Chain Nanoparticles as Catalytic Nanoreactors, *Journal of the American Chemical Society* **2018**, 140, 5875-5881.

[49] J. Rubio-Cervilla, E. González, J. A. Pomposo, Advances in Single-Chain Nanoparticles for Catalysis Applications, *Nanomaterials* **2017**, 7, 341.

[50] C. A. Tooley, S. Pazicni, E. B. Berda, Toward a tunable synthetic [FeFe] hydrogenase mimic: single-chain nanoparticles functionalized with a single diiron cluster, *Polymer Chemistry***2015**, 6, 7646-7651.

[51] C. Glaser, Untersuchungen über einige Derivate der Zimmtsäure, *Liebigs Annalen* **1870**, 154, 137-171.

[52] A. S. Hay, Oxidative Coupling of Acetylenes. II[1], *The Journal of Organic Chemistry* **1962**, 27, 3320-3321.

[53] D. Wang, J. Li, N. Li, T. Gao, S. Hou, B. Chen, An efficient approach to homocoupling of terminal alkynes: Solvent-free synthesis of 1,3-diynes using catalytic Cu(II) and base, *Green Chemistry* **2010**, 12, 45-48.

[54] P. Siemsen, R. C. Livingston, F. Diederich, Acetylenic Coupling: A Powerful Tool in Molecular Construction, *Angewandte Chemie International Edition* **2000**, 39, 2632-2657.

[55] Y. P. Petrenko, K. Piasta, D. M. Khomenko, R. O. Doroshchuk, S. Shova, G.Novitchi, Y. Toporivska, E. Gumienna-Kontecka, L.M. D. R. S. Martins, R. D. Lampeka, An investigation of two copper(II) complexes with a triazole derivative as a ligand: magnetic and catalytic properties, *RSC Advances* **2021**, 11, 23442-23449.

[56] K. S. Banu, T. Chattopadhyay, A. Banerjee, S. Bhattacharya, E. Suresh, M. Nethaji, E. Zangrando, D. Das, Catechol Oxidase Activity of a Series of New Dinuclear Copper(II) Complexes with 3,5-DTBC and TCC as Substrates: Syntheses, X-ray Crystal Structures, Spectroscopic Characterization of the Adducts and Kinetic Studies, *Inorganic Chemistry* **2008**, 47, 7083-7093.

[57] S. K. Dey, A. Mukherjee, Catechol oxidase and phenoxazinone synthase: Biomimetic functional models and mechanistic studies, *Coordination Chemistry Reviews* **2016**, 310, 80-115.

[58] E. Huerta, P. J. M. Stals, E. W. Meijer, A. R. A. Palmans, Consequences of Folding a Water-Soluble Polymer Around an Organocatalyst, *Angewandte Chemie International Edition* **2013**, 52, 2906-2910.

7. Conclusions

In conclusion, we present two novel metal-free methods for synthesizing single-chain nanoparticles (SCNPs), both yielding stable nanoparticles that can be stored in solid form and redissolved without any sign of aggregation.

The first method involves the synthesis of stable, inert, dispersible, metal-free SCNPs through the intramolecular Staudinger reaction of a copolymer, poly(styrene-2,3,4,5,6-pentafluorostyrene) (P(S-co-PFS)). The incorporation of 4-azido-2,3,5,6-tetrafluorostyrene monomers results in stable bonds that resist hydrolysis by water. Using a biphosphino molecule, such as 1,3-bis(diphenylphosphino)propane, strong intra-chain bonds are formed through a simple and metal-free reaction at room temperature. The successful formation of metal-free P(S-co-PFS)-SCNPs is confirmed through various techniques, including SEC with triple detection (RI, MALS, and VIS), ^{1}H, ^{19}F, ^{31}P, and ^{13}C NMR spectroscopy, DLS, FTIR, and TGA measurements. These "Staudinger" SCNPs exhibit thermal stability up to 150 °C and resist strong acids like TFA and standard reagents for azaylides. Interestingly, their cross-linking N=P bonds react efficiently with a reagent containing the "electropositive" silicon atom and weak acidity like TMS, enabling the selective unfolding of these otherwise robust SCNPs. This expands the toolbox for unfolding covalently bonded SCNPs.

The second method is employed for synthesizing stable, inert, dispersible, metal-free single-chain SCNPs through intramolecular metal-traceless azide–alkyne click chemistry at room temperature. Utilizing the strain-promoted azide-alkyne cycloaddition (SPAAC) technique with sym-dibenzo-1,5-cyclooctadiene-3,7-diyne (DIBOD) as an external bifunctional cross-linker molecule, in conjunction with azide-containing polymeric precursors, offers a new method for metal-free SCNP synthesis through intramolecular folding/collapse. This method is applied to produce metal-free SCNPs from polystyrene (PS), commercial polyvinyl chloride (PVC), and "valorized" PVC from pieces of pipes. Confirmation of metal-free PS-SCNPs formation is achieved through a combination of techniques, including SEC with triple detection (RI, MALS, and VIS), ^{1}H and ^{13}C NMR spectroscopy, DLS, FTIR, TGA, and SAXS measurements. These SCNPs, in addition to their metal-free advantage, exhibit significant long-term stability, lasting at least two months, against irreversible aggregation.

Finally, the SPAAC method is used to introduce an innovative concept of polymeric waste upcycling, transforming common-use commodity plastic such as polyvinyl chloride (PVC) into "valorized" PVC single-chain nanoparticles (vPVC-SCNPs). The entire valorization process, including PVC isolation, PVC azidation, and vPVC-SCNPs synthesis, can be conducted in a green, dipolar aprotic solvent like NBP, with a simple mixture of EtOH and H_2O (1/1 vol.) as a non-

solvent if required. vPVC-SCNPs loaded with 7.3 mol% of Cu(II) ions, denoted as vPVC-SCNPs/Cu(II), prove to be an efficient and recyclable catalyst in various benchmark transformations, including alkyne homocoupling reactions, styrene oxidation, and 3,5-di-t-butyl-o-quinone synthesis. This concept can potentially extend to the valorization of other commodity plastics capable of incorporating azide functional groups along their linear polymer chains.

APPENDIX

Publications

This thesis has contributed to the following publications:

- A. Blázquez-Martín, S. Bonardd, E. Verde-Sesto, A. Arbe, J. A. Pomposo, Trimethylsilanol Cleaves Stable Azaylides as Revealed by Unfolding of Robust "Staudinger" Single-Chain Nanoparticles, *ACS Polymers Au* **2024**. doi.org/10.1021/acspolymersau.3c00046
- A. Blazquez-Martín, E. Verde-Sesto, A. Arbe, J. A. Pomposo, Metamorphosis of a Commodity Plastic like PVC to Efficient Catalytic Single-Chain Nanoparticles. *Angewandte Chemie International Edition* **2023**, e202313502.
- A. Blázquez-Martín, A. Ruiz-Bardillo, E. Verde-Sesto, A. Iturrospe, A. Arbe, J.A. Pomposo, Toward Long-Term-Dispersible, Metal-Free Single-Chain Nanoparticles, *Nanomaterials* **2023**, 13.
- A. Blazquez-Martín, E. Verde-Sesto, A.J. Moreno, A. Arbe, J. Colmenero, J.A. Pomposo, Advances in the Multi-Orthogonal Folding of Single Polymer Chains into Single-Chain Nanoparticles, *Polymers* **2021**, 13.
- E. Verde-Sesto, A. Blázquez-Martín, J.A. Pomposo, Advances in the Phototriggered Synthesis of Single-Chain Polymer Nanoparticles, *Polymers* **2019**, 11, 1903.

Table of figures

Table of tables

Table of equations

Table of abbreviations

2m-THF	2-Methyltetrahydrofuran	EG	Ethylene glycol
3,5DTBCH$_2$	3,5-Di-tert-butylcatechol	EtOH	Ethanol
ACHN	1,1'-azobis(cyclohexanecarbonitrile)	EU	European Union
AIBN	2,2'-Azobis(2-methylpropionitrile)	f	Frequency
ATFS	4-Azide-2,3,5,6-tetraflourostyrene	f_0	Reference frequency
ATR	Attenuated total reflection	FB	1-Ethynyl-4-fluorobenzene
BzA	Benzyl azide	FTIR	Fourier transform infrared spectroscopy
c	concentration	GPC	Gel permeation chromatography
$CDCl_3$	Deuterated chloroform	GVL	γ-Valerolactane
CDTC	S-cyanomethyl-S-dodecyltrithiocarbonate	H_2O	Water
CMDTC	Cyanomethyl dodecyl carbonotrithioate	H_2O_2	Hydrogen peroxide
CMS	Chloromethyl styrene	HB	Hydrogen bond
CO_2	Carbon dioxide	HETCOR	Heteronuclear Correlation Spectroscopy
CS_2	Carbon disulphide	HOMO	Highest Occupied Molecular Orbital
CTA	Chain transfer agent	I	Transmitted light
CuAAC	Copper(I)-catalyzed azide-alkyne cycloaddition	I(q)	intensity of the scattered beams
$CuCl_2$	Copper(II) chloride	I_0	Incident light
D	Diffusion coefficient	ICP-MS	Inductively couple plasma mass spectrometry
Đ	Polydispersity	I_{LS}	Intensity of the MALS detector signal
DCB	1,4-Dicyanobenzene	IR	Infrared spectroscopy
DE	Diethyl ether	I_{RI}	Intensity of the RI detector signal
DIBOD	*Sym*-dibenzo-1,5-cyclooctadiene-3,7-diyne	I_{VI}	Intensity of the VI detector signal
DLS	Dynamic light scattering	k_B	Boltzmann's constant
DMF	N,N-dimethylformamide	L	Path length
DMSO	Dimethyl sulfoxide	LUMO	Lowest Unoccupied Molecular Orbital
DOSY	Diffusion-Ordered NMR Spectroscopy	MALS	Multi-angle light scattering
DPPP	1,3-Bis(diphenylphosphino)propane	mCPBA	meta-chloroperbenzoic acid
DSC	Differential scanning calorimetry	MeOH	Methanol
EA	Elemental analysis	Me_3SiOH	Trimethylsilanol

M_n	Number averaged molecular mass	r.t.	Temperature
MS	Mass spectrometry	RAFT	Reversible addition fragmentation chain transfer
M_w	Mass averaged molecular mass	R_g	Radius of gyration
n	Reflective index	R_h	Hydrodynamic radius
N_2	Nitrogen gas	RI	Refractive index
N_A	Avogadro's number	S	Styrene
NaCl	Sodium chloride	S(q)	Structure factor
NaN_3	Sodium azide	SAXS	Small-angle X-ray
NaOH	Sodium hidroxide	SCNP	Single-chain nanoparticle
NBP	1-Butylpyrrolidin-2-one	SEC	Size exclusion chromatography
NIR	Near infra-red	SPAAC	Strain-promoted azide-alkyne cycloaddition
NMR	Nuclear magnetic resonance	TBE	1,1,2,2-Tetrabromoethane
NPs	Nanoparticles	TEA	Triethylamine
P(q)	Form factor	TFA	Trifluoroacetic acid
P(S-co-AMS)	Poly(styrene-co-4-(azidemethyl)styrene)	TGA	Thermogravimetric analysis
P(S-co-ATFS)	Poly(styrene-co-4-azide-2,3,5,6-tetrafluorostyrene)	THF	Tetrahydrofuran
P(S-co-CMS)	Poly(styrene-co-4-(Chloromethyl)styrene)	TMS	Trimethylsilanol
P(S-co-NTFS)	Unfolded SCNPs of Poly(styrene-co-2,3,4,5,6-pentafluorostyrene)	UV-Vis	Ultraviolet-visible spectroscopy
P(S-co-PFS)	Poly(styrene-co-2,3,4,5,6-pentafluorostyrene)	VI	Viscometer
PA	Propargyl acetate	vPVC	Valorized PVC
PE	Polyethylene	vPVC-Cu	Copper-polymeric complex from vPVC-SCNPs
PFS	2,3,4,5,6-Pentaflourostyrene	vPVC-N_3	Azided vPVC
pH	Potential of hydrogen	TOF	Moles of product per mole of catalyst per unit of time, TOF
PP	Polypropylene	δ	Chemical shift
PrPr	propargyl propionate	ε	Extinction coefficient
PS	Polystyrene	θ	Half of the scattering angle
PVC	Polyvinyl chloride	λ	Wavelength
PVC-N_3	Azided PVC	ν	Flory exponent
q	Scattering vector	μ	Intrinsic viscosity
R	End-to-end distance vector		

Agradecimientos

En primer lugar, me gustaría agradecer al Prof. Juan Colmenero por darme la oportunidad de unirme al grupo de "Polymers and Soft Matter", así como Centro de Física de Materiales (CFM) por la concesión de la beca y a la Universidad del País Vasco (UPV/EHU) por aceptarme en este programa de doctorado. Sin ellos no habría tenido la posibilidad de vivir esta experiencia que, sin duda, quedará en mi memoria para siempre como un hito de mi vida.

Me gustaría agradecer especialmente a mis directores de tesis, Prof. José A. Pomposo y Dra. María Ester Verde, por su guía a lo largo de este largo camino. Sin su constante dedicación y apoyo no habría podido llevar a cabo este trabajo. Siempre que lo he necesitado han estado disponibles y dispuestos a ayudarme, y durante todo este proceso he recibido sus consejos que me han ayudado a mejorar como científico y a madurar como persona.

También me gustaría mostrar mi agradecimiento a todos los integrantes del grupo de "Polymers and Soft Matter" que me han acogido como un más y sin quienes no habría podido concluir este trabajo. Especialmente a Isabel, quien me enseñó a desenvolverme en el laboratorio como pez en el agua y quien siempre ha estado dispuesta a echarme un mano cuando lo necesitaba. Al profesor Ángel Alegría, por su ayuda en todos los trámites relacionados con el doctorado. A la Prof. Arantxa Arbe y a Amaia, por su ayuda como las medidas de caracterización SAXS. A Jon y a Sebastián, por ayudarme con la caracterización térmica y dieléctrica. Y también a todos aquellos con los que he tenido el honor de compartir estos años: Julen, Jokin, Davide, Ainara, Pelayo, Baltasar…

También me gustaría agradecer a todo el personal del Centro de Física de Materiales con quienes he trabajado y convivido. Así como a los Servicios Generales de Investigación (SGIker) de la Universidad del País Vasco que me han permitido el acceso a equipos y técnicas que ha resultado indispensables en este trabajo, especialmente al Dr. José Ignacio Miranda, Dr. Luis Bartolomé y Dra. Alicia Sánchez.

He de agradecer también a mi familia; especialmente mis padres Ángel y Maribel y mi hermana Ainara; y mis amigos; Beñat, Mai, Olatz, Sergio, Unai y Xabi. Quienes me han acompañado estos años, los cuales me han dado ánimos en los momentos más complicados y me han aguantado cuando estaba más irascible.

Por último, quiero agradecer especialmente a mi abuela, Manuela Guerra. Este trabajo te lo dedico a ti.